GLOBAL AND LOCAL STRUCTURAL ANALYSIS OF THE SULFHEME COMPLEX: A ROLE IN THE DECREASE OF MYOGLOBIN FUNCTIONALITY

by

Elddie Marie Román-Morales

A dissertation submitted in partial fulfillment of the requirements for the degree of
DOCTOR IN PHILOSOPHY

in

APPLIED CHEMISTRY
(Biophysics)
UNIVERSITY OF PUERTO RICO
MAYAGUEZ CAMPUS
2016

Approved by:

_____	_____
Juan López-Garriga, PhD President, Graduate Committee	Date
_____	_____
Carmen Amaralis Vega, PhD Member, Graduate Committee	Date
_____	_____
Samuel Hernández-Rivera, PhD Member, Graduate Committee	Date
_____	_____
Nilka Rivera-Portalatin, PhD Member, Graduate Committee	Date
_____	_____
Jorge Almodovar, PhD Representative, Graduate Studies Office	Date
_____	_____
Enrique Melendez, PhD Chairperson of the Chemistry Department	Date

ABSTRACT

When the human body is exposed to high concentration of hydrogen sulfide (H_2S, recently identified as a signaling gas), a rare type of anemia called sulfhemoglobinemia is developed. This condition is triggered by the increase of the physiological concentration of sulfheme complex. Proteins bearing a His distal residue with an adequate orientation, as in Myoglobin (Mb) and Hemoglobin (Hb), form this complex. The sulfur atom is incorporated across the β-β double bond of the pyrrole "B", reducing the protein's oxygen (O_2) affinity. This change in affinity is attributed to the heme group distortion and the electron withdrawing forces induce by the sulfur atom. However, other aspects may also contribute to the decrease in protein affinity, e.g. conformational change and final bound heme Fe-ligand. Our intention was to analyze the contribution of these global and local structural features with those previously reported and relate them to the changes in protein functionality. Therefore, this research was directed to further comprehend the reactivity and action mode of H_2S in the human body, specifically Mb. In this project we: (1) evaluated the possible significant changes in protein conformation that may affect the protein-O_2 interaction, and (2) identified the Sulfmyoglobin-Ligand (SMb-L) complexes that naturally take place as products during the SMb complex formation, and hence, serve as physiological competitors for the binding of O_2 to the heme-Fe.

To answer these inquiries, Small angle X-ray scattering (SAXS) and Electron Paramagnetic Resonance (EPR) were used to analyze the SMb complex, along with control protein HbI from *Lucina pectinata that does not form the sulfheme complex*. The EPR data showed that the possible final products of the SMb complex formation are H_2O-SMb (2.49, 2.26, and 1.84 g values), O_2-SMb (loss of signal), ferrous (loss of signal) and ferric H_2S-SMb (2.36, 2.26 and 1.91 g values). In order for O_2 to bind to the sulfheme-Fe, it will have to compete with

H_2O and H_2S ligands, in addition to the ferric heme-Fe oxidation state, which contributes to the loss of O_2-protein interaction.

Finally, the SAXS results showed that SMb formation induces a change in the protein conformation; where its envelope forms a very small cleft and the protein is more flexible, less rigid and compact. Theoretical scattering curve of SMb crystal structure suggest that the global conformational change and internal structural fluctuations are hampered by the crystal packing forces; thus, limiting the range of conformational motion accessible to the protein. Based on the direct relationship between Mb's structural conformation and its functionality, we suggest that the conformational change observed upon SMb formation plays a role and contribute to the protein decrease in O_2 affinity and, therefore, on its functionality.

RESUMEN

Cuando el cuerpo humano se expone a altas concentraciones de sulfuro de hidrógeno (H_2S), se desarrolla un tipo de anemia rara llamada sulfhemoglobinemia. Esta condición es provocada por el aumento en la concentración fisiológica del complejo sulfhemo. Las proteínas que forman este complejo son aquellas que tienen una histidina distal con una orientación apropiada, como mioglobina (Mb) y hemoglobina (Hb). El átomo de azufre se incorpora a través del doble enlace β-β del pirol "B", reduciendo la afinidad de la proteína por oxígeno (O_2). Esta disminución en afinidad se le atribuye a la distorsión del grupo hemo y la capacidad de azufre para atraer electrones. Sin embargo, otros aspectos pueden contribuir a la disminución de la afinidad, por ejemplo: un cambio conformacional y el ligando enlazado al hierro (Fe) en el grupo hemo como producto "final". Nuestra intención era analizar la contribución de las características estructurales globales y locales, que en combinación con lo reportado anteriormente, se relacionan con los cambios en la funcionalidad de la proteína. Por tanto, esta investigación estaba dirigida a comprender aún mejor la reactividad y el modo de acción de H_2S en el cuerpo humano, en especial su interacción con mioglobina. En este proyecto se: (1) evaluó los posibles cambios conformacionales significativos que pueden afectar la interacción entre proteína-O_2; y (2) identificó los complejos Sulfmioglobina-ligando (SMb-L), que naturalmente se forman como productos en la reacción de formación del complejo SMb, y por consiguiente, sirven como competidores fisiológicos del enlace de O_2 con el Fe del grupo hemo.

Para contestar estas preguntas, se utilizaron las técnicas de Dispersión de Rayos-X en Ángulos Pequeños (SAXS) y Resonancia Paramagnética Electrónica (EPR) para analizar el complejo de SMb, utilizando como control la proteína HbI de la almeja *Lucina pectinata*. Los resultados de EPR demostraron que los posibles productos finales de la formación del complejo

SMb son: H_2O-SMb (2.49, 2.26, y 1.84), O_2-SMb (pérdida de señal), ferroso (pérdida de señal) and férrico H_2S-SMb (2.36, 2.26 y 1.91). En adición a la baja afinidad que tiene el O_2 por el estado de oxidación férrico del hemo, este para lograr enlazarse al Fe del grupo sulfhemo tendría que competir con los ligandos H_2O y H_2S que son más afín con el estado férrico del Fe. Estas desventajas contribuyen a la perdida de interacción entre el O_2 y la proteína.

Finalmente, los resultados de SAXS demuestran que la formación de SMb induce un cambio en la conformación de la proteína, donde la envoltura de la proteína forma una pequeña hendedura y la proteína pasa a ser más flexible, menos rígida y compacta. La curva de dispersión teórica de la estructura cristalina de SMb sugiere que los cambios conformacionales y las fluctuaciones estructurales internas son obstaculizadas por las fuerzas de empaque del cristal, limitando los rangos de los movimientos conformacionales accesibles a la proteina. En base a la relación directa entre la estructura conformacional de la proteína y su funcionalidad, sugerimos que los cambios conformacionales observados a causa de la formación del complejo SMb juegan un papel y contribuyen a la disminución de la afinidad por O_2, y por consiguiente, en la funcionalidad de la proteína.

Copyright© Elddie Marie Román-Morales 2016

Dedication

In life,

what sometimes appears to be the end,

is really a new beginning.

To my family and husband,

You are my rock, love, happiness, strength and peace.

Acknowledgement

I thank God, my husband Edgardo Jesús Quiñones Cruz and my family: Freddie H. Román Avilés & Elba Iris Morales Medina, Fredito, Humbertito, Iris, Elbita, Hortensia, Blanca, Freddie Alejandro, Laura Isabel, Olivia Ximena, and Dario Humberto for their indescribable and unconditional love and support. To my friends, you are the true definition of friendship.

I wish to thank my mentor, Dr. Juan López-Garriga, for guidance and support. I also wish to thank my thesis committee members Dr. Samuel Hernández-Rivera, Dra. Carmen Amaralis Vega and Dra. Nilka Rivera-Portalatin for their guidance and kindness. To Dr. Gary Gerfen for his indescribable attention and support. My special appreciation to Dra. Ruth Pietri for her knowledge, guidance, kindness and attention. To the Chemistry Department of the University of Puerto Rico in Mayagüez, and my partners from the laboratory and the Science on Wheels Educational Center. I am very grateful to all of these persons who helped me put together this work. I really appreciate the time and effort that each one spent into the multiple aspects of this research.

This work was supported in part by funds from the NSF (Grant 0843608), and fellowships from NIH-RISE2Best (Grant R25GM088023), and Alfred P. Sloan (NACME Grant 2010-3-02).I thank Dr. Lisa Miller, Mr. Vito Graziano, and Dr. Mark Allaire for the X9-SAXS/WAXS facilities at NSLS. This research used resources of beamline X9 of the National Synchrotron Light Source, a U.S. Department of Energy (DOE) Office of Science User Facility operated for the DOE Office of Science by Brookhaven National Laboratory under Contract No. DE-AC02-98CH10886.

List of Tables

List of Figures

List of Symbols and Abbreviations

H_2S	hydrogen sulfide
HbI	hemoglobin I
Mb	myoglobin
Hb	hemoglobin
°C	Celsius
%	per cent
pKa	acid dissociation constant
g	gram
mL	milliliter
µL	microliter
mmol	millimol
L	liter
CcO	cytochrome c oxidase
CBS	cystathione β-synthase
CSE	cystathione γ-lyase
3-MST	3-mercapto pyruvate sulftransferase
β	beta
β	Bohr magneton
α	alpha
γ	gamma
NO	nitric oxide
CO	carbon monoxide
nM	nanoMolar

μ	micro
O_2	oxygen
Fe	iron
Heme-Fe	heme iron
Fe^{II}	ferrous iron
Fe^{III}	ferric iron
Xe	Xenon
Xe_1-Xe_4	Xenon pockets
H_2O	water
H_2O_2	hydrogen peroxide
SMb	sulfmyoglobin
SHb	sulfhemoglobin
dL	deciliter
Comp I	compound I
Comp II	compound II
Mb^{IV}	Mb with oxidation state of IV
Mb^{III}	Mb with oxidation state of III
Mb^{II}	Mb with oxidation state of II
R-SH	donating thiol
HS•	thiol radical
Na_2S	sodium sulfide
^{35}S	sulfur isotope
$(NH_4)_2S$	ammonium sulfide
CN	cyanide

N_3	azide
C_α	alpha carbon
N-Fe	bond between nitrogen and iron
C-Fe	bond between carbon and iron
L-Fe	bond between ligand and iron
M-L	bond between metal and ligand
D_{4h}	symmetry
C_{2v}	symmetry
nm	nanometer
υ^4	oxidation state marker
^{1}H-NMR	proton nuclear magnetic resonance
ppm	parts per million
π	pi
SMb_A	SMb isomer A
SMb_B	SMb isomer B
SMb_C	SMb isomer C
His	histidine
HisE7	histidine in the E7 position
Val E11	valine in the E11 position
Ile99	isoleucine in the 99 position
Gln64	glutamine in the 64 position
His64	histidine in the 64 position
δ	delta
met	metaquo, water bound to iron

oxy	oxygen bound to iron
$p^{1/2}$	pressure were half protein saturation occur
mmHg	milliliter of mercury
Fe^{III}-$OO^{\bullet-}$	ferric superoxide
~	approximately
υ	frequency
IR	infrared spectroscopy
cm^{-1}	wavenumber
SO_2	sulfur dioxide
SO_3^{-2}	sulfite
SO_4^{-2}	sulfate
$Hg(OAc)_2$	mercury (II) acetate
$HgCl_2$	mercury (II) chloride
HCl	hydrogen chloride
Hg^{2+}	mercury ion
H	hydrogen or proton
rHbI	recombinant HbI
w/v	weight per volume
µg	microgram
M	Molarity
IPTG	isopropyl thiogalactoside
KH_2PO_4	potassium dihydrogen phosphate
K_2HPO_4	potassium hydrogen phosphate
Tb	terrific broth

μm	micrometer
rpm	revolutions per minute
OD	optical density
NBB	native binding buffer
UV-vis	Ultraviolet-Visible spectroscopy
CV	column volume
FPLC	fast performance liquid chromatography
MPa	megapascal
SDS-Page	sodiumdodecyl sulfphate polyacrinamide gel electrophoresis
Tris-HCl	2-amino-2-(hydroxymethyl)propane-1,3-diol hydrochloride
mA	milliampere
V	voltage
EDTA	ethylenediaminetetraacetic acid
A	absorbance
b	cuvette pathlength
c	concentration
c	scaling factor
ε	absorption coefficient
$Na_2S_2O_4$	sodium hydrosulfite
SAX	small angle x-ray scattering
WAX	wide angle x-ray scattering
mg	milligram
EPR	electron paramagnetic resonance spectroscopy
GHz	gigahertz

mW	milliwatts
s	second
K	kelvin
q	momentum transfer vector
sin	sine
θ	angle
λ	wavelength
d	real space distance
Å-1	angstrom
I	intensity
Rg	radius of gyration
ln	natura logarithm
I(0)	Intensity at cero angle
P(r)	pair distribution function
Dmax	maximum dimension
Vp	hydrated particle volume
Q	Porod Invariant
X2	discrepancy
Icalc(q)	computational profile
σ(q)	experimental error of the measured profile
N	number of points in the profile
PDB	Protein Data Bank
1MBO	oxyMb crystal structure
1YMC	SMb crystal structure

Bo	applied magnetic field
μ	magnetic moment
ms	electron spin
g	g-factor
L	orbital angular momentum
ΔE	change in energy
h	planck constant

Table of Contents

Chapter 1: Introduction

CHAPTER 1: INTRODUCTION

This research is focused in understanding the interaction of Hydrogen Sulfide (H_2S), a gasotransmitter, with Myoglobin (Mb) that leads to the sulfheme complex formation, which can produce a condition known as sulfhemoglobinemia.

1.1 Hydrogen Sulfide

Hydrogen Sulfide (H_2S) was present since the beginning of Earth, approximately 4.6 billion years ago. The abundance and versatility of H_2S in prebiotic Earth implicates its role as the primordial energy source in the origin Earth's life [1, 2]. Eukaryotes first appeared in euxinic environment (anoxic and sulfidic) [2]. H_2S generation is still observed in different ecosystems like volcanoes, bacteria, and thermal vents, among others. H_2S is a well-known poisonous gas whose cytotoxic effects have been studied for more than 300 years [3]. Under physiological conditions (7.4 pH and 37°C), approximately 18.5% of H_2S is undissociated and 81.5% is dissociated to hydrosulfide ion (pKa of 6.9), see Figure 1-1 [2, 4]. The term ''H_2S'' is generally used since it has not been possible to determine the bioactive form. Hence, H_2S refers to the combination of the undissociated species and the hydrosulfide anion. H_2S is a lipophilic weak acid that is also soluble in water and plasma (1 g in 242 ml at 20°C; 80 mmol/L at 37°C) and it can penetrate cells of all types by simple diffusion [2, 4-6].

$$H_2S \xrightarrow[pKa_1 = 6.9]{} HS^- + H^+ \xrightarrow[pKa_2 = 19]{} S^{2-} + H^+$$

Figure 1-1. Hydrogen sulfide dissociation

Some of the cytotoxic outcomes of H_2S are: the disruption of the respiratory process by cytochrome c oxidase (CcO) inhibition, mitochondrial dysfunction, generation of endogenous free radical/oxidant species, and the production of a rare blood condition known as

sulfhemoglobinemia [7]. Interestingly, the discovery that the human body naturally produces H_2S has dramatically changed the reputation of this gas from a toxic pollutant to a biologically relevant molecule. At the moment, there are six enzymes responsible for the physiological production of H_2S [8, 9]. Figure 1-2 shows the three enzymes most studied in the H_2S physiological production: cystathionine β-synthase (CBS), cystathionine γ-lyase (CSE) and 3-mercaptopyruvate sulftransferase (3-MST) expressed predominantly in central nervous system, cardiovascular system, and kidney/liver, respectively [1, 2, 4, 5, 7-13]. H_2S is now considered to be an important physiological mediator with a wide variety of roles: anti-inflamatory, anti-tumor, ion channel regulation, cardiovascular protection, antioxidation and, neuromodulation [1, 2, 4, 5, 7]. However, H_2S physiological role depends on specific circumstances, interplay with other signaling gases (NO and CO), and on H_2S concentration. H_2S is known to have a physiological hormetic effect, where beneficial effects are observed at low concentration (nM to μM) and toxic effects at high concentrations (μM to mM) [1, 2, 4, 5]. H_2S has been considered as a therapeutic tool. Three general classes of H_2S pro-drugs have been develop: natural products, hydrolysis based, and controlled released. Some of the challenges ahead for these H_2S-donors are: good tissue specificity, target delivery, slow/controlled release mimicking physiological release, determination of the right H_2S concentration depending on the tissue or target, and better protective effects with lower toxicity. To acquire this, the H_2S biological mechanism, pathways, and effects need to be further evaluated for safe use of H_2S.

1.2 Myoglobin and Hemoglobin

Myoglobin (Mb) and Hemoglobin (Hb) are globular vertebrate heme proteins whose principal function involves the binding of oxygen (O_2) to the ferrous iron (Fe^{II}) of the heme group (protoporphyrin IX), seen in Figure 1-3. Hb is a tetrameric protein (two α subunits and two

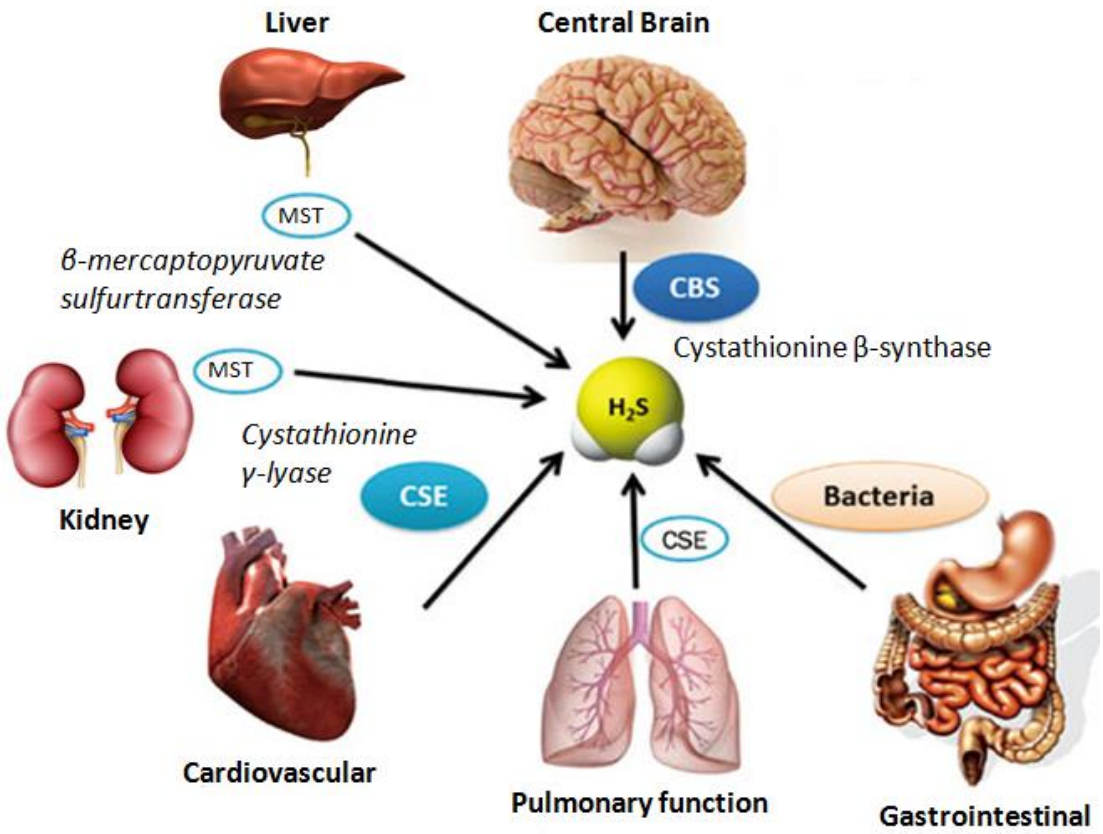

Figure 1-2. Widespread distribution of H_2S-synthesizing enzyme (Image taken, modified and reprinted from publication: Hydrogen Sulfide and Translational Medicine; Wei Guo, Ze-yu Cheng, and Yi-zhun Zhu; *Acta Pharmacologica Sinica* (2013) 34: 1284–1291 DOI: 10.1038/aps.2013.127 with permission from Nature Publishing Group)

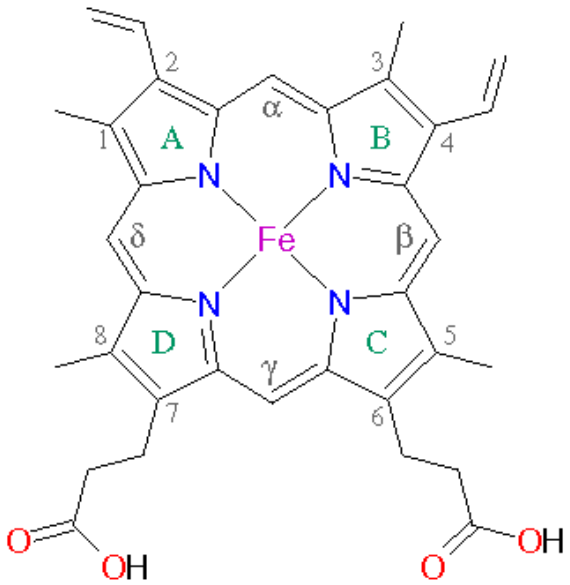

Figure 1-3. Structure of the Protoporphyrin IX

β subunits) that transports O_2, with cooperative structure fluctuations, from lungs to muscles, see Figure 1-4. However, Mb is a monomeric protein with O_2 storage character in the muscles and transport character to the mitochondria. Mb has been through the years a popular model system to evaluate concepts and theories of protein structure, function, dynamics, and evolution [14, 15].

It is widely accepted that the biological function of many proteins is controlled by conformational changes at different magnitudes [14, 15]. It was shown that the packing of the Mb is essential and directly relates to the protein functionality. The protein conformation has what are called the Xenon pockets (Xe_1, Xe_2, Xe_3, and Xe_4), which are packing imperfections or cavities that the ligand occupies on its migration toward the active site; see Figure 1-5 and Figure 1-6 [14, 16, 17]. The ligand migration in the cavity produces a structural expansion of the cavity itself follow-on by gating motions of the surrounding residues that leads to a self opening of the migrating channel [17]. The cavity comes back to its original volume once the ligand has left the cavity, mimicking a breathing motion. The final channel is created by the rotating motion of the distal His opening the gate toward the active heme site [17]. These cavities have been demonstrated to play a crucial role in the protein functionality. Any change in the size and shape of these pockets directly affects the Mb function, which implicate in significant physiological effects [15-17]. Olson *et al*. performed experiments where changes in the cavities size and shape were acquired by Mb's mutants [16]. They concluded that a decrease in the size of the cavity produced a more rigid and compact packing. As a result, it lowers the rate of ligand capture by making it difficult for the ligand to arrive to the active site. However, if the ligand is able to arrive to the active site, dissociation is even more difficult since the ligand is "trap" in the active site, leading to an overall increase in O_2 affinity [16].

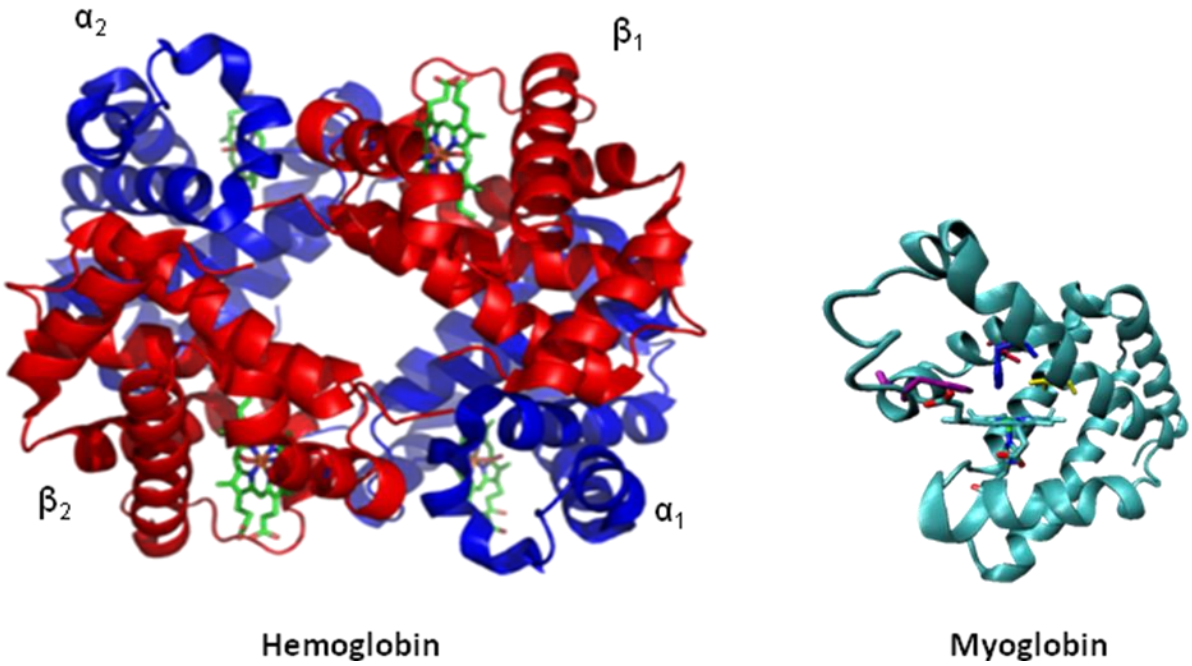

Figure 1-4. Myoglobin (1MBO) and Hemoglobin (image obtained from wikipedia)

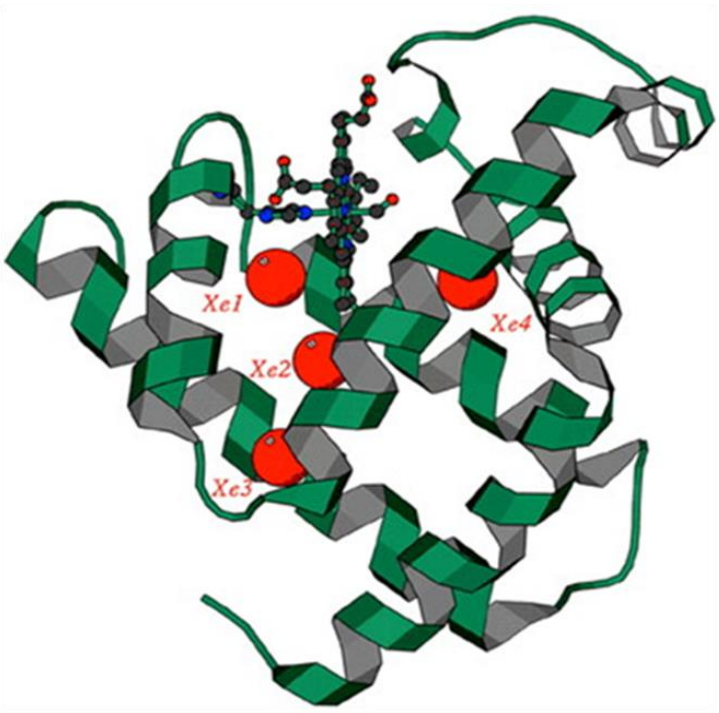

Figure 1-5. Myoglobin Xenon Cavities represented in red spheres (Image obtained and reprinted from publication: Cavities and Packing Defects in the Structural Dynamics of Myoglobin; Maurizio Brunori and Quentin H. Gibson; *EMBO Reports* (2001) 2: 674-679 DOI: 10.1093/embo-reports/kve159 with permission 4002460328568 from publisher John Wiley and Sons)

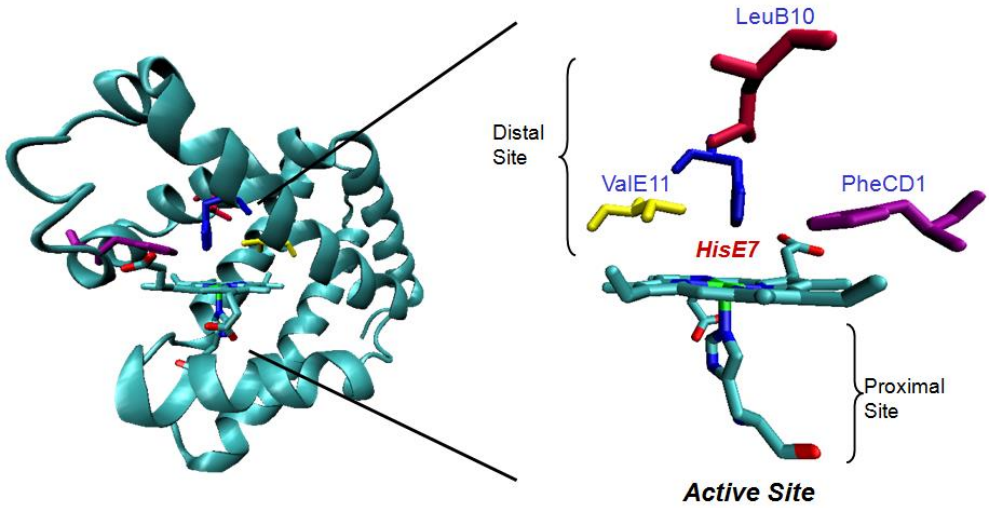

Figure 1-6. Active Site of myoglobin (1MBO) and hemoglobin.

Furthermore, in addition to the heme-Fe ligand transport, it has been suggested that the conformational cavities are capable of carrying additional ligands, such as NO, giving Mb further physiological roles [14-16]. As a result, a role of ligand (eg. CO) scavenger has been suggested for Mb in addition to transport and storage of other ligands (eg. NO), apart from O_2 [14-16]. Moreover, depending on O_2 affinity and occupancy, Mb could bear additional O_2, resulting in a higher than (1:1) O_2 stoichiometry and carrying capacity. Suggesting than even with Fe oxidation, Mb may still contain O_2 in its cavities [17] as long as no structural alteration of the cavity occurs. In addition to CO and NO, H_2O occupancy within the protein packing has been also suggested [18].

Both of them, Mb and Hb, are capable of binding H_2S to the heme-ferric iron (heme-Fe^{III}), however, with low affinity. This interaction produces a fast reduction of the heme-Fe by observation of the deoxy Fe^{II} and/or oxy Fe^{II} complex formation, facilitated by the histidine in the distal site of the heme cavity, seen in Figure 1-7 [19, 20]. Furthermore, their H_2S interaction in the presence of O_2 or hydrogen peroxide (H_2O_2) can modify the heme group by forming sulfheme proteins (sulfmyoglobin [SMb] and sulfhemoglobin [SHb], see Figure 1-8) inducing sulfhemoglobinemia blood condition [20-22].

1.3 Sulfhemoglobinemia

The sulfheme complex has lower affinity towards O_2 than native Mb. High levels of sulfheme proteins can be poisonous since it alters the protein O_2 transport or storage functionality, causing a cyanosis known as sulfhemoglobinemia [21]. The most common reported cases are due to drugs ingestion. Depending on the specific situation, the treatment involves O_2 exposure, blood transfusion, and stomach/gastric lavage. Normal physiological SHb blood concentrations are below 5.7 μM (0.037 g/dL) [23]; where only 0.3% of the functional Hb

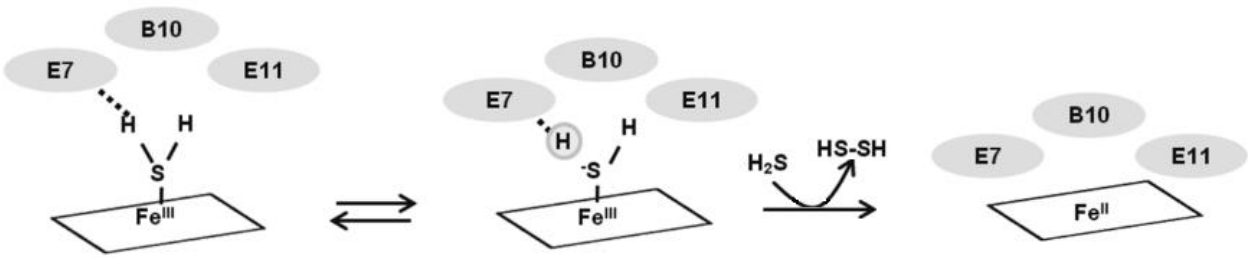

Figure 1-7. Generalized reactions for H_2S reactivity with hemeproteins. (Image taken, modified and reprinted from publication: Hydrogen Sulfide and Hemeproteins: Knowledge and Mysteries; Ruth Piertri, Elddie Román-Morales, and Juan López Garriga; *Antioxidant and Redox Signaling* (2011) 15: 393-404 DOI: 10.1089/ars.2010.3698 with permission from publisher Mary Ann Liebert, Inc.)

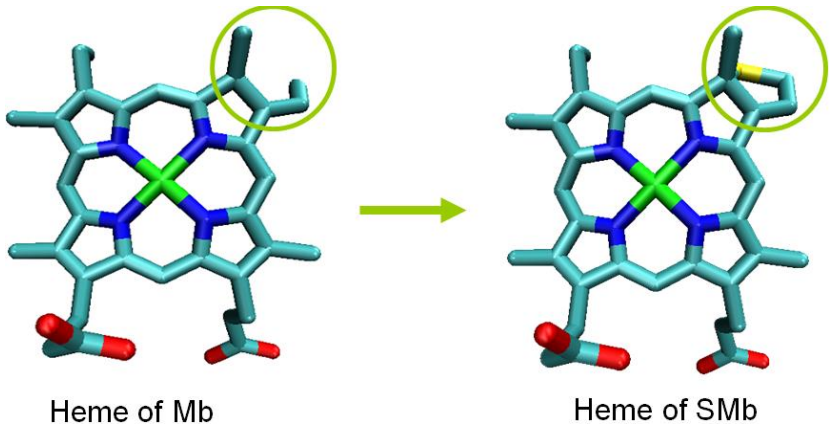

Figure 1-8. Heme modification upon SMb complex formation (PDB: 1MBO and 1YMC). (Image taken, modified, and reprinted from publication: Sulfmyoglobin Conformational Change: A Role in the Decrease of Oxy-myoglobin Functionality; Elddie Román-Morales, Erika López-Alfonzo, Ruth Pietri, and Juan López-Garriga; *Biochemistry and Biophysics Reports* (2016) 7: 386-393 DOI: 10.1016/j.bbrep.2016.07.002 with permission from publisher Elsevier)

is converted to SHb (considering an Hb concentration of 12g/dL). Thus, at physiological conditions, sulfHb is constantly present in small concentrations. However, in order to be clinically detectable with cytotoxic effects, the SHb blood concentration should be more than 78 μM (0.5 g/dL) leading to 4% of the functional Hb. In a clinical case, a sulfHb blood concentration of 117 μM (0.754 g/dL) was reported [23, 24]. The highest accepted H_2S physiological concentration is approximately 300 μM [1, 25]. Therefore, the physiological concentration ratio between [sulfHb:H_2S], under normal conditions, is [1:52.6] while in clinically detectable sulfhemoglobinemia is [1:3.8]. The sulfheme protein cannot be reverted to the normal functional protein by natural mechanism in the red cells. However, the body can bear low concentration of the sulfheme complex by spontaneous and natural destruction of the red cells.

1.4 Sulfmyoglobin and Sulfhemoglobin

In order to understand the functional abnormality produce by the sulfheme complex, the structural alteration of the native protein during the formation of the sulfheme complex must be further study since; it is well known that protein functionality is directly related to the protein structure. The sulfheme proteins are define as compounds formed by analogous reactions of several protoheme proteins and H_2S, which includes the sulfhemoglobin (SHb) and sulfmyoglobin (SMb) derivates [26]. When Mb and Hb are exposed to H_2S in the presence of O_2 or H_2O_2, a sulfur atom incorporates across the β-β double bond of the pyrrole B, as shown in Figure 1-9. This was defined by many scientists that invested time through years in determining the different aspects of the sulfheme protein complex that leads to the decrease in O_2 affinity.

1.4.1 General Aspects of sulfhemoglobin and sulfmyoglobin

The first person who observed the sulfheme complex was Hoppe-Seyler in 1866 when he formed a green product when O_2-Hb interacted with H_2S, see Figure 1-10. He called this green

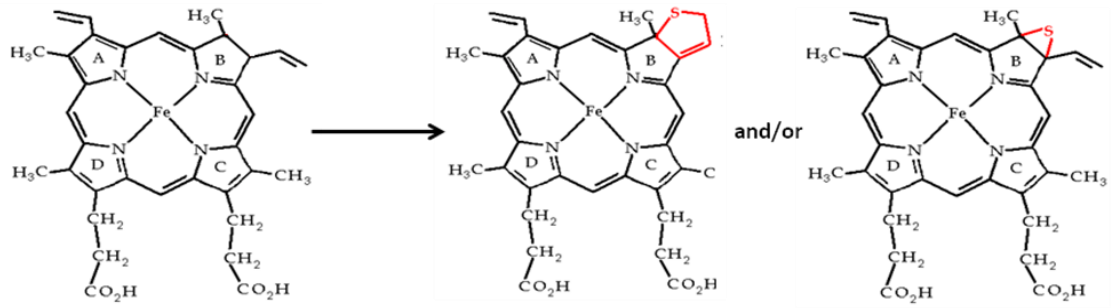

Figure 1-9. Sulfur atom incorporates across the β-β double bond of the pyrrole B upon sulfheme formation.

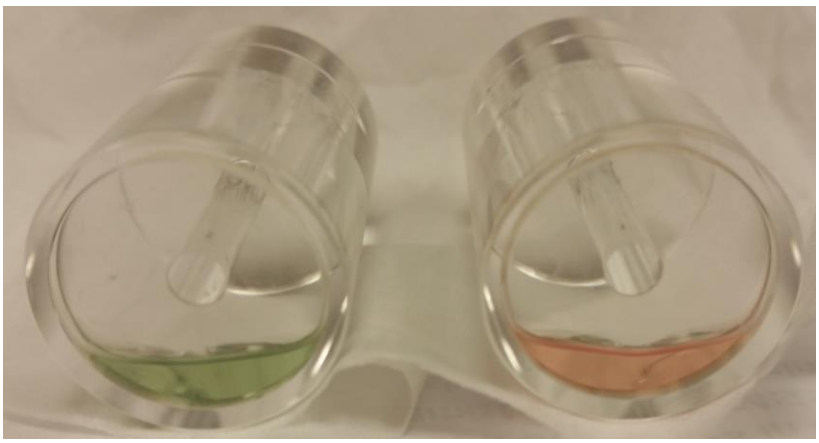

Figure 1-10. SMb (green, left) and oxyMb (red, right).

product sulfhemoglobin. Figure 1-11 shows the characteristic absorption band of the sulfheme complex around 620 nm for ferrous-SMb and around 720 nm for ferric-SMb [26-35]. The mechanism for sulfheme complexes formation is still unknown. However, it was suggested that the formation of SMb depends on the presence of oxo-ferryl intermediates known as Compound I (Fe^{IV}=O Por $^{\bullet+}$) and Compound II (Fe^{IV}=O), produced by the heme protein interaction with peroxides source (ie. O_2 and H_2O_2). Figure 1-12 shows the generalized interaction of ferric Mb with H_2O_2; where Compound II and cation radical Compound I are formed. When Compound I acquires an electron from the protein, then Compound II is formed. Further on, a turn over may occur were met-Mb is reacquired. Which oxy-ferryl intermediate is involved in the sulfheme complex formation is not known [21].

It was demonstrated over the years that a thiol compound is also necessary for the sulfheme formation. Since the pK_1 of the H_2S molecule is 6.9 and many of the sulfheme experiments have been perform at a pH of 8, where the predominant species in the H_2S equilibrium is HS^-, it was suggested that the active sulfur specie in the sulfheme formation was HS^- [36]. However, thiyl radical's products have been observed from the interaction of Mb^{IV} with thiols. Therefore, it must also be taken into consideration the possibility that the sulfur specie that forms the sulfheme complex could be a thiyl radical [37-39]. Moreover, the requirement of a proton donating thiol (R-SH) for the sulfheme complex formation was suggested since the sulfheme complex is not observed with thiols that do not have a H to donate [22]. This is an important aspect to consider during the mechanism for the formation of the sulfheme complex given that it was recently demonstrated a direct relationship between pH and the formation rate of the 620 nm characteristic sulfheme band. It was observed, with a decreasing pH, an increase in the rate formation of the sulfheme complex. Consequently, pH

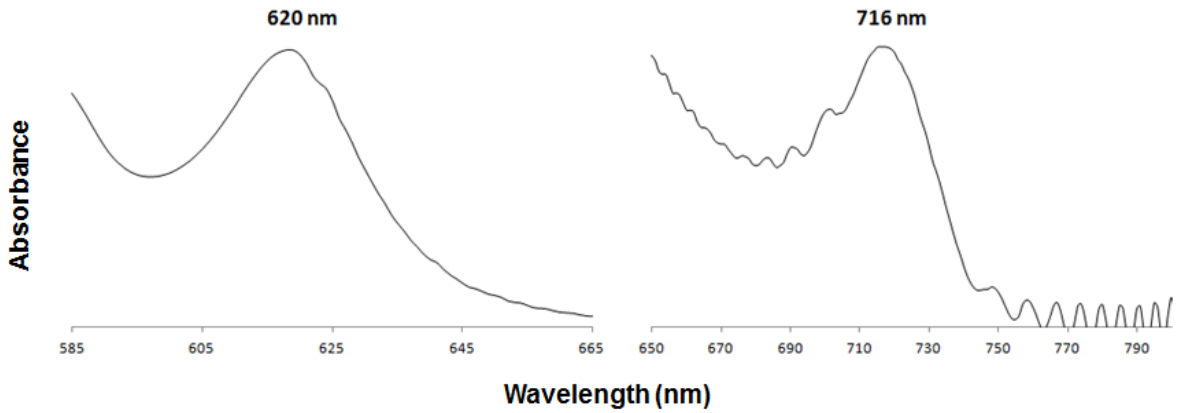

Figure 1-11. Characteristic absorption band of ferrous-SMb (620 nm) and ferric-SMb (716 nm) (The wiggles in the spectra line around 675-700 nm and 750-800 nm regions are due to instrumental noise).

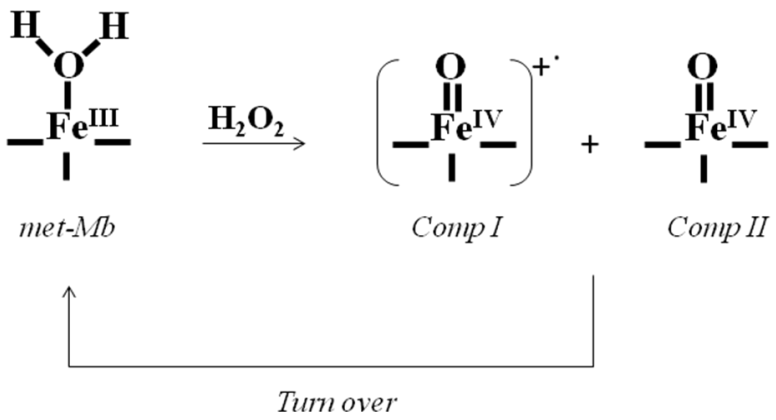

Figure 1-12. Oxy-ferryl intermediates; Compound I (Comp I) and Compound II (Comp II).

dependence for the ferrous sulfheme complex formation was established [37]. This indicates a proton donation participation in the mechanism for the formation of the sulfheme complex, suggesting HS• involvement in the sulfheme derivate development. If in fact HS• is the sulfur component of the sulfheme specie, this would provide an antioxidant/reducing agent functionality to the H_2S specie in the sulfheme complex formation.

The chemical nature and concentration of the thiol and peroxide species can influence the reaction route and final product [38]. Nicholls, *et al*. observed that the addition of 1 mole of H_2S per heme produced ferric SMb, which could then be reduced to ferrous SMb by H_2S excess [38]. This data suggested that the ferric SMb is formed first, and that further ferrous SMb formation depends on the H_2S concentration [26]. Since there was initially a 2.4 fold excess of Mb^{IV} over added Na_2S, the ferric SMb found can be attributed to oxidation of the initial ferrous SMb product by excess of Mb^{IV} to produce ferric Mb and ferric SMb. To verify this, ferrous SMb to an equimolar quantity of Mb^{IV} was prepared under identical conditions. It led to immediate oxidation of the ferrous SMb to ferric SMb with production at the same time of ferric Mb from the reduction of Mb^{IV} [36]. In the process of trying to understand the H_2S interaction with hemeproteins, optical spectra analysis and EPR studies were performed on the higher oxidation state of Mb (eg. Mb^{IV}) in the presence of various thiols [37]. Depending on the physicochemical properties of the thiol, two reaction processes could occur. The first one is a direct electron transfer from the thiol to Mb^{IV} forming Mb^{III} and a thiyl radical. Only dihydrolipoic acid (that has two –SH group in its structure) was able to further interact with Mb^{III} on a second redox reaction producing O_2-Mb^{II}. Disulfides with S-S bond within their structure were not able to produce either redox reaction with Mb due to a high activation energy of the S-S bond cleavage [39], in addition to a possible steric coverage of the S-S bond [21]. The second route involves the

electron transfer reduction of the heme-iron followed by the 620 nm characteristic sulfheme band formation [39]. In the presence of catalase that removes the excess of H_2O_2, only dihydrolipoic acid was capable of performing iron reduction process in combination to the formation of the sulfheme complex. While in the absence of catalase, all thiols were capable of performing iron reduction process in addition to the sulfheme derivate formation with higher thiyl radical concentration detection. Regarding this, it is evident that not only the physico-chemical properties of the thiol, but also the thiol and H_2O_2 concentration are important during sulfheme complex formation and stability [39].

1.4.2 Sulfheme Protein Structure Characterization

One of the first questions that needed to be answered was the quantity and location of sulfur atoms that produce the structural modification of the protein and thus, affecting the protein functionality. Michel *et. al* in 1938, analyzed a solution mixture of SHb and Hb, and determined that SHb, compared to Hb, contain one additional sulfur atom per heme [40]. Later, Morell *et al.* used ^{35}S in the preparation of the sulfheme protein with a 100 fold excess of labeled ^{35}S $(NH_4)_2S$ [41]. Since their sulfheme protein purity was of approximately 70%, it suggested 1.5-2 g atoms of ^{35}S per mole of heme [26]. Berzofsky *et al.* optimized the SMb formation process to 90% purity (the 10% impurity is unreacted native Mb) and re-examined the incorporation of the ^{35}S in SMb using only 1.67 fold excess of radioactive sulfide. They determine that only one atom of ^{35}S was incorporated per prosthetic group [36]. It was later confirm by Timkovich, *et. al* through High Resolution Mass Spectra [42]. The extraction of the prosthetic group of ^{35}S labeled SMb demonstrated that 85% of the ^{35}S co-extracted with the prosthetic group, therefore, the S atom most have been incorporated in the heme group [36].

Many theories about the location of the sulfur atom and its structure were discussed through the years. Some suggestions of the structure were a: thiohistidine on the proximal histidine ligand, chlorine episulfide, thiomethene carbon, and thiochlorin [26, 29-35, 38, 41]. The possibility that the S was incorporated as a ligand bound to the heme-Fe was discarded since it was demonstrated that ligands like CO, CN, N_3, H_2O, and O_2 bind to the heme-Fe of the sulfheme complex demonstrating that heme-Fe site is available for interaction [26-35, 38]. The option of a thiohistidine was eliminated by Berzofsky *et al*. [26] since attempts to insert a sulfur atom to the C_α of the N-Fe bond in the proximal heme histidine, using space-filling Corey-Pauling-Koltun models, demonstrated that the atomic volume of sulfide is significantly large and it could not happen without immense strain.

It was suggested that the sulfheme structure of the prosthetic group is a chlorin (see Figure 1-13). The symmetry of Mb and Hb prosthetic group is D_{4h}, corresponding to a metallo-porphyrin. However, when the symmetry of a porphyrin is reduced to a C_{2v}, corresponding to a metallo-chlorin, an increase in degeneracy of the electronic transitions occurs. These changes are observed in the optical spectrum of the formation of sulfheme proteins where the visible absorption bands split. This means that the sulfheme complex formation, which involves the incorporation of a sulfur atom, decreases the symmetry of the heme group from a porphyrin to that of a chlorin, increasing the degeneracy of the electronic transitions. This structural modification is observed in the optical spectrum when the two visible absorption bands characteristic of a porphyrin change to four visible absoption bands, characteristic of a chlorin. In addition to this, the decrease in symmetry permits an increase in intensity of the electronic transitions at higher wavelength, observed in sulfheme protein optical spectrum as "sulfheme band" (approximately around 620 nm and/or 720 nm, see Figure 10). All of these changes are

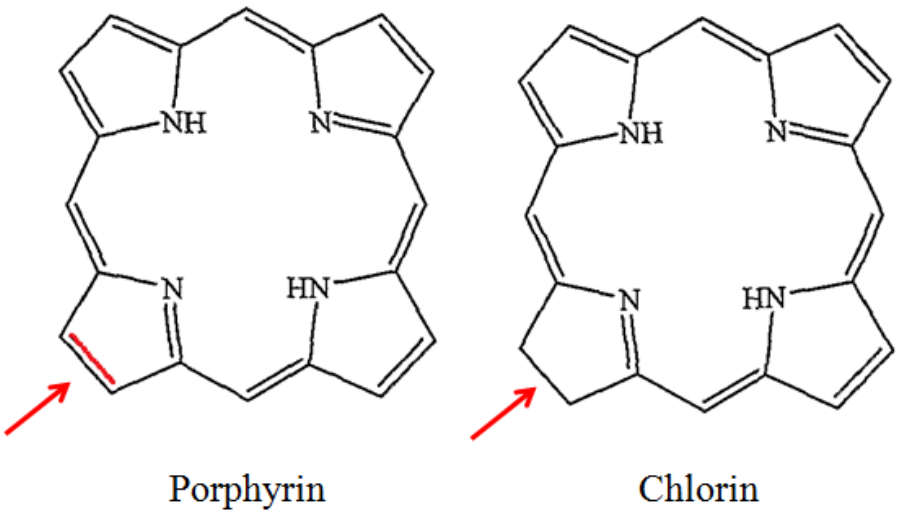

Figure 1-13. Difference between the porphyrin (left) and chlorin (right) structures.

characteristic of chlorin and are observed in the optical spectrum of the CO-SMb at low temperatures. Therefore, it suggest that the sulfur atom must be incorporated to the heme group, thus, affecting the symmetry of the porphyrin [26-28].

Also, resonance Raman Spectroscopy shows additional evidence for an iron-chlorin prosthetic group in the SMb formation [22, 43]. The first evidence was an increase in the relative spectral intensity patterns and depolarization ratios. Furthermore, new bands are observed in the resonance Raman spectra of SMb (specially the satellite bands around the oxidation state marker ν_4) as a consequence of the polarized modes of the sulfheme complex produced by the S incorporation to the heme group, see Figure 1-14 [22]. These spectral characteristics can be observed in the Raman spectra of chlorins. The spectral characteristics between SMb and metallo-chlorins are complementary. These strongly suggest that the prosthetic group of SMb is a chlorin produced by the incorporation of a sulfur atom to the heme group [22, 43].

Therefore, it is clear that the incorporation of the S involves disruption of the ring conjugation. Since the sulfheme structure involves ring conjugation perturbation, the suggestion that the sulfheme complex has a methene sulfur structure was proved wrong, given that, it involves no disruption of the ring conjugation [26]. Moreover, the performed Corey-Paulin-Koltun space filling models proved that the sulfur addition to a methene carbon was impossible without disruption of the structure [26]. Proton NMR Spectroscopy of SMb evaluated the sulfur atom position by analyzing the chemical shifts of the heme 1,3,5,8-methyls substitution [42]. Timkovich and Vavra suggested that the protein perturbation should be only local and in the heme group since the SMb spectrum was comparable to that of native Mb with general homology in the aromatic resonance region. Regarding this, in a saturated ring the methyl

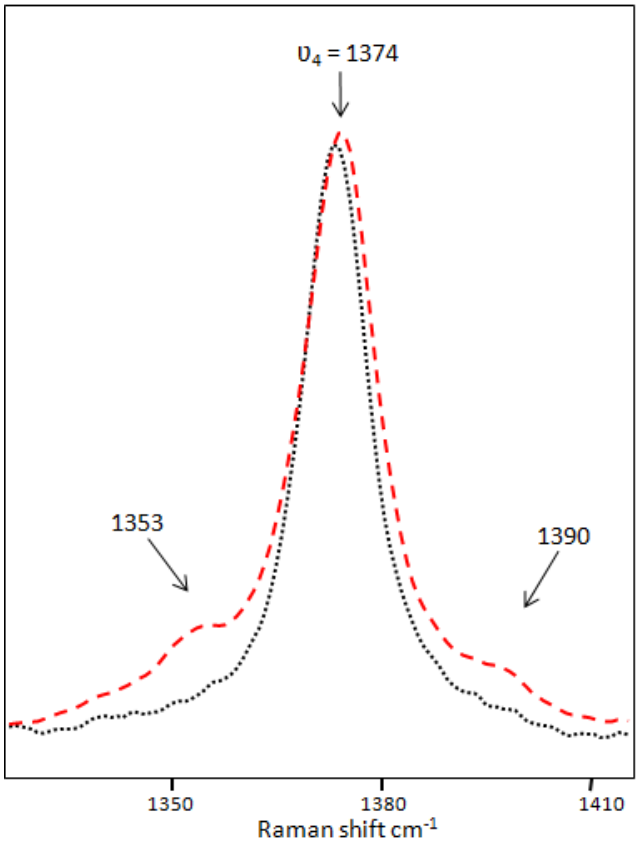

Figure 1-14. Resonance Raman spectra of Mb and HbI (control, does not form the sulfheme complex) shows the adjacent modes to ν_4 of metMb (red-dashed line) and metHbI (black-dotted line), in the presence of H_2O_2 and H_2S. (Image taken, modified and reprinted from publication: Structural Determinants for the Formation of Sulfhemeprotein Complexes; Elddie Román-Morales, Ruth Pietri, Brenda Ramos-Santana, Serge N. Vinogradov, Ariel Lewis-Ballester, and Juan López-Garriga; *Biochemical and Biophysical Research Communications* (2010) 400: 489–492 DOI: 10.1016/j.bbrc.2010.08.068 with permission 4002210450839 from publisher Elsevier)

protons are found upfield while in an unsaturated ring they are downfield. The SMb ^{1}H NMR spectra showed that the 5,8-methyls shifts were similar to native Mb, thus, the pyrrole rings C and D do not suffer any significant modification upon sulfheme complex formation. As a result, the possibility of the sulfur incorporation on pyrrole C and D was eliminated. However, 1-methyl showed a 10ppm downfield shift characteristic of a saturated ring [42]. They were not able to identify the 3-methyl shift do to a significant band displacement towards the crowded diamagnetic envelope due to the sulfur atom incorporation in the pyrrole B [32, 35, 42]. This has been seen in other derivates where a chemical reaction perturbs the π conjugation of a pyrrole [32]. The evidence of the incorporation of the sulfur atom to the heme pyrrole B gave support to the episulfide and thiochlorine sulfheme structure.

Proton NMR of metaquo (H_2O-SMb) and cyano SMb (CN-SMb) complexes revealed the presence of three isomeric forms A, B, and C of the sulfmyoglobin complex, see Figure 1-15 [30, 31, 33]. These isomers cannot be distinguished through optical spectroscopy [30, 31, 33]. Each sulfheme isomer proved to have different chemical properties since they have different reactivity and stability [30, 31, 33]. SMbB showed different reactivity from SMbA when a mixture of SMbA and B were exposed to CN, SMbB showed preferential binding interaction to CN than SMbA. CN-SMbC showed different stability from the CN-SMbA and CN-SMbB isomers since the SMbC isomer maintain stable through days while CN-SMbA underwent rapid conversion to Fe^{III} protoporphyrin IX. The SMbC isomer is the most stable of the three [30, 31, 33].

Chatfield *et al*. suggested that the probable cause for difference in reactivity and stability between the sulfheme isomers should reside in the porphyrin peripherary alterations, where the incorporated sulfur lays, since all 3 isomers where observed at different pH, temperature, protein concentration, presence/absence of catalase, and storage [30, 31, 33]. In contrast to the native

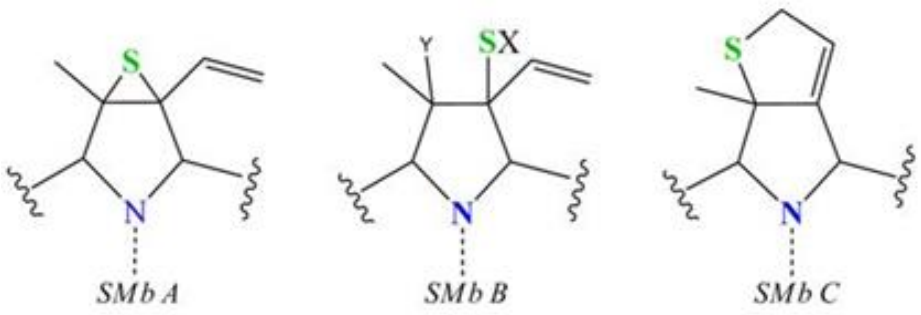

Figure 1-15. Sulfheme isoform were identified as sulfMbA an episulfide, sulfMbB a ring opened episulfide and sulfMbC a thiochlorin. (Image taken, modified, and reprinted from publication: Hydrogen Sulfide Activation in Hemeproteins: The Sulfheme Scenario; Bessie B. Ríos-González, Elddie M. Román-Morales, Ruth Pietri, and Juan López-Garriga; *Journal of Inorganic Biochemistry* (2014) 133: 78–86 DOI: 10.1016/j.jinorgbio.2014.01.013 with permission 4002201234177 from publisher Elsevier)

Mb and the 2-vinyl from SMbC, the 4-$H_{\beta's}$ vinyls from SMbC have a larger coupling corresponding to geminal coupling of a saturated methylene pair. This means that the $4C_{\alpha}H$-$C_{\beta}H_2$ no longer has a double bond. Isotope labeling at the vinyl positions showed that the 4-vinyl group is without a doubt involved in the SMbC formation. Therefore, the sulfur incorporation in SMbC is in the pyrrole B [30, 31, 33]. The localized and selective perturbation on the saturated pyrrole is due to direct attenuation of transferred spin density to the affected pyrrole, reducing the effective transfer [34, 35]. In H_2O-SMbC, the pyrroles A and C, adjacent to pyrrole B, demonstrate similar shifts. However, pyrrole D, trans to pyrrole B, has a major shift indicative of an increase in spin transfer on pyrrole D [34, 35]. The 3 isomers have attenuation of the 3-methyl shift and shift enhancement of the 8-methyl. The ^{1}H NMR Spectral pattern of the 3 sulfheme isomers is so similar that it suggests the same pyrrole involvement during the sulfheme complex formation with difference in substituent's functionalities [30, 31, 33-35]. The reaction is specific to pyrrole B because if there were fluctuations of the incorporation of the sulfur atom from pyrrole B to pyrrole A more band multiplicity would have been observed [30, 31, 33, 42]. This indicates that vinyl groups are not necessary part of the complex formation; they just affect the type of sulfheme isomer that can be formed [30, 31, 33]. Hence, SMbC can only be observed in hemes with vinyl substituents [30, 31, 33]. The evidence of a chlorine type structure for all sulfheme isomers can be indirectly identify through NMR spectroscopy [32]. The reduced current shift for ValE11 δ-methyl in all SMb species have been previously observed in chlorophyll spectra. It is consistent with a pyrrole saturation. The H-meso upfield shift, compare to the native Mb, is more similar to the ones observed in chlorines. SMbA and SMbB have similar optical spectra that differ from SMbC where red shift of 5-18nm is observed, see Table 1-

1. This red shift has been observed in chlorine models where there is an ethylidene group in the 4^{th} position [32].

In general, the NMR spectrum shows a symmetry reduction of the prosthetic group and an alteration of the π conjugation of at least one pyrrole [32]. The SMbA structure is an episulfide structure across the β-β bond [32]. This episulfide structure leads to a rapid reversion to the protoheme when extracted from the heme group [42]. The SMbB structure is a "ring opened episulfide" while the SMbC structure is a thiochlorine [32]. It has been observed that SMbA → SMbB and SMbA →SMbC, but no conversion occurs from SMbB→SMbC. The SMbB→SMbC isomerization could be difficult if the sulfur atom is bound to the 4-C instead of the 3-C of the pyrrole B. This conversions show that SMbA is the precursor and SMbB/SMbC are both end products [32].

SHb does not go through the isomeric interconversion [42]. SHb structure is very similar to unstable sulfheme isomer SMbA with a 10% of the SMbB [32]. The sulfur ring modification in SHb only occurs in 1-2 of the Hb subunits leaving 2-3 intact [44].

There exists a great dependence in the possible sulfheme isomer formed with respect to the experimental conditions [32]. The type of isomer form is dependent to pH [32, 42]. SMbB formation is enhanced in acidic pH and favors high spin complexes (met > deoxy > CN > CO). On the other hand, the SMbC formation is enhanced at alkaline pH and it is observed in all oxidation states and ligands (CO > CN > H_2O), except for deoxy complex [32]. Each sulfheme isomer has a different chemical reactivity in respect to ligand affinity and complex stability. It can be generalize as C > B > A, and should be taken into account when analyzing the sulfheme protein affinity towards O_2 [32].

Oxidation and Ligation State	SAMb	SBMb	SCMb
Deoxy	618	618	636
	420	420	416
Carbonmonoxy	612	612	626
	412	412	412
Met-aquo	718	720	736
	594	598	600
	408	408	406
Met-cyano	594	594	596
	412	412	412

Table 1-1. Sulfheme isoforms characteristic absorption bands.

To further comprehend the mechanism for the sulfheme complex formation, it was important to determine if the S attack came from the distal area that is more open or from the proximal site [45]. Determination of the 3-methyl chirality provided insights to the answer of this inquiry, and was determined through analysis of dipolar connectivity of the 3-methyl with the protein moiety. The Ile99 was used since it has a satisfactory interaction with pyrroles B and C that promotes a high dipolar shift and takes its signal out of the diamagnetic envelope. The 3-methyl in the sulfheme complex was out of the heme plane pointing towards the proximal area and increasing its distance from Ile99, which suggested that the S attack came from the distal site. The same 3-methyl chirality was observed in the SMbA and SMbC complexes, retaining the chirality through the isomerization [45]. All NMR spectra of the sulfheme protein have projected the same sulfheme characteristic pattern with the prosthetic group alone (extracted from the protein) and with the prosthetic group within the protein moiety.

Also, it was suggested that the formation of the sulfderivate does not significantly alter the proximal-axial interaction since the native Mb and SMbA/C showed similar labile ring proton of the 7-propionate and proximal histidyl imidazole contact shifts [34, 35]. Given that, it was inferred that the general cavity structure and the protein tertiary structure of SMb was similar to native Mb, and did not suffer a considerable modification [32].

1.4.3 Sulfheme Protein Implications

As with the native proteins, SMb and SHb bind numerous ligands at distal site of the heme iron. Spontaneous autoxidation as well as oxidation state interconversion with different reducing and oxidating reagents are also maintained in these sulfheme derivatives without disturbing the sulfur ring [32]. However, O_2 affinity is substantially reduced in both SMb (2500 fold) and SHb (135 fold). In this section we evaluate O_2 binding in SMb and SHb and the factors

that may influence O_2 affinity in these proteins. Reconversion of the native proteins from the sulfheme derivatives and the possible physiological implications of SMb and SHb are also discussed. Two aspects of sulfheme reactivity have been evaluated: ligand reversibility and sulfheme reversibility.

1.4.3.1 Ligand Reversibility

The O_2 affinity of SMb has been carefully studied for it physiological relevance. When deoxy SMb was exposed to O_2, an optical shift from 616 nm to 624 nm was observed, with same symmetry and intensity (deoxy SMb $\rightarrow$ oxy SMb). The Soret band also shifted from 424 nm (deoxy SMb) to 408 nm (oxy SMb). Optical spectra analysis criteria of the absorption intensity and Q/Soret bands displacements of the O_2-SMb and deoxy-SMb complexes have suggested that the O_2-SMb complex is a 6-coordinated low spin ferric species while the deoxy SMb complex is a 5-coordinated high spin ferrous species [28]. The completely reverse effect was observed when the same sample was exposed to Argon (oxy SMb $\rightarrow$ deoxy SMb).

The SMb O_2 binding curve is a rectangular hyperbolic structure as with native Mb, representative of a reversible protein-ligand interaction (ligand association and dissociation) affected by significant changes in O_2 concentration [28]. From the binding curve, one can obtain the $p^{1/2}$ define as the ligand concentration at which half of the available protein binding sites are occupied by the ligand (in this case O_2), which gives information about the ligand affinity towards the protein. However, the $p^{1/2}$ of SMb is 530 mmHg while Mb is 0.21 mmHg, at the same temperature (5 °C). It led them to conclude that SMb was in fact able to bind O_2 reversibly in a concentration dependent manner. SMb needs a higher O_2 concentration in order to have half of its available binding sites interact with O_2, therefore, SMb has a lower O_2 affinity. This represents a decrease in O_2 affinity of 2,500 fold in comparison with native Mb [28].

In addition to O_2, it has been observed the ligand reversibility of CO-SMb (Soret 413 nm, Q 612 nm) towards the deoxy-SMb complex when the sample is purge with Argon, and an optical shift toward 424 nm and 616 nm is observed. The opposite effect is observed when CO is purge to the same sample. The CO SMb binding curve has a rectangular hyperbolic shape with a $p^{1/2}$ of 9.2 mmHg. The decrease in CO affinity of SMb is of 1500 fold [27].

SHb interaction with O_2 was also studied by Carrico *et al*. in 1978 [46]. When the deoxy SHb complex was exposed to O_2, the ferrous SHb band at 619 nm moved to 623 nm. Based on the spectral similarities between SHb and SMb, the authors assigned the 623 nm band to the oxy SHb derivative (SHb-O_2). As observed with native Hb, SHb O_2 binding curve was found to have sigmoidal shape, suggesting that SHb was able to reversibly bind O_2. The sigmoidal shape, characteristic of cooperative behavior, indicated that SHb retained some cooperative character of the native protein, and is affected by small changes in O_2 concentration. The $p^{1/2}$ of SHb was 63 mmHg while that of native Hb was 0.46 mmHg, under similar conditions. It indicates that SHb needs a higher O_2 concentration in order to have half of its available binding sites interact with O_2, therefore, SHb has a lower O_2 affinity. On this bases, it was concluded that the affinity of SHb for O_2 was 135 lower that the native protein.

The substantial decrease in O_2 affinity, in both SMb and SHb, has been attributed to the electron withdrawing character of the heme-chlorine structure [27, 28]. Incorporation of the sulfur atom to the β-β double bond of the pyrrole B removes electron density from the iron towards the periphery of the chlorin ring, reducing the ability of the iron to donate electron density back to bound ligand and as a consequence iron affinity for O_2 decreases. It is well known that when O_2 binds to the ferrous heme in Mb and Hb, it donates two electrons to the heme iron, increasing in turn the electron density on the Fe. To stabilize the complex, the Fe

donates electron density to the π orbital of the O_2, producing ferric superoxide (Fe^{III}-$OO^{\bullet -}$) [27, 28]. Hence, the inability of SMb and SHb to effectively transfer electron density to O_2, destabilize the complex and lower their affinity for O_2. Overall, the electro withdrawing capacity of the S atom removes electron density of the Fe, reducing its electron retro alimentation capacity of the Fe to the ligand, affecting the Fe-ligand interaction and weakening their bond and as a consequence reducing the Fe affinity towards the ligand [27].

Although this interpretation shed light into the reduced affinity of SMb and SHb for O_2, it does not explain the differences of O_2 affinity between SMb and SHb. As described above, SMb was shown to be ~2500-fold lower, whereas binding in SHb was reduced by a factor of ~135 [27, 28, 46]. The higher affinity of SHb for O_2, as opposed to SMb can be rationalized by the fact that in the former only two of the four hemes are modified by H_2S leaving the other two hemes available for normal O_2 binding. In addition, the episulfide structure of the SHb isoform (SHbA), which is more flexible than the thiochlorin of SMb, may reduce the withdrawing character of the heme-chlorin, increasing the affinity of SHb for O_2 [21, 44].

It was demonstrated how the use of electron donating or withdrawing substituents in the 2,4 heme positions affect the Fe electronic density, hence, affecting the ligand affinity [27]. When using substituents with electro withdrawing capacity, it is observed an increase in ν C-O bond that is representative of an increase in bond energy, bond order and bond strength. The opposite occurs at the same time in the Fe-C bond whereas the Fe-Ligand interaction is weakened. When comparing the IR stretching ν of CO in the CO-Mb complex (1943 cm^{-1}) versus SMb-CO (1953 cm^{-1}), an increase in C-O stretching ν is observed as a consequence of the sulfur atom incorporation [27]. It indicates that the presence of the sulfur atom in the heme group removes electronic density of the Fe. Hence, the electron transfer capacity of the Fe towards the

ligand is decrease, affecting the metal-lingand π bonding, and the affinity of the Fe for the ligand. In addition, the decrease in the Fe electron density also decreases its basicity property affecting the Fe contribution towards the M-L π bonding and weakening this bond. This is also favored by the rupture of the heme group conjugation produced by the heme distortion as a result of the sulfur ring incorporation. Regarding this, the observed decrease in ligand affinity should be produce by electronic effects [27]. However, they suggested that a 0.5 cm^{-1} shift corresponds to a decrease in O_2 affinity by a factor of 10, which indicates that this local chemical structural change contributes to only a 200 fold decrease in O_2 affinity [28], representing only 8% of the total decrease in affinity (2,500 folds) determined by the O_2 binding curve. Thus, there are other significant changes occurring in the protein as a consequence of the sulfheme complex formation that also contribute to the decrease in protein functionality.

1.4.3.2 Sulfheme Reversibility

The reconversion of the sulfheme products to the native functional proteins has been studied for many years. In 1961, Nicholls was the first to observe the reconversion of SMb to native Mb, when he exposed the SMb sample to H_2O_2. Similar results were obtained when he exposed SMb to dithionite in the presence of O_2 or cyanide (CN-), which also produces H_2O_2) [38]. Photo-excitation of the SMb-CO complex also induced reconversion of the sulfheme complex to the normal Mb-CO derivative. Berzofsky et al. observed that when a SMb-CO sample was exposed to successive periods of irradiation, the Soret band shifted from 413 nm, typical of the sulf-CO complex, to 422 nm with a progressive disappearance of the 612 nm [27]. The results were explained in terms of the differences in activation energy, both in the ground and excite state of the chlorine structure. In the ground state, large activation energy is required to release the bound sulfur and unsaturated the pyrrole ring. During photo-excitation, the chlorin

structure reaches an electronic excited state that reduces this activation energy, resulting in a thermodynamically favored reconversion of the native Mb-CO complex [27]. Further reagents used for protein reconversions were azide and CN [27].

In order to understand the possible functionality of the sulfheme protein, it was crucial to determine the decomposition species of the sulfheme complex and its kinetics, under various conditions. This knowledge would give further insights on the feasible reversibility of the sulfheme derivate to the native protein. Studies of the decomposition of the extracted sulfheme complex prosthetic group, "sulfhemin", were done by Berzofsky in 1972 [36]. The sulfhemin was found to be unstable once extracted from the protein and no matter the initial oxidation state of the protein, the extracted prosthetic sulfhemin group would be found in the ferric state. The decomposition showed the production hemin species, and a mixture of sulfur molecules where H_2S, SO_2, SO_3^{-2}, and elemental sulfur could be excluded (were not detected). The sulfur mixture was 50% of SO_4^{-2}, however, the experimental condition provided abundant peroxides and O_2 in the solvent that could react with the initial sulfur decomposition product to generate the observed SO_4^{-2} [36]. Peroxides, $Hg(OAc)_2$, and $HgCl_2$ with excess of HCl decomposed the sulfhemin. The Hg^{2+} has been suggested to act directly on the sulfur and promote its removal living the hemin behind [36].

Although reversion of the sulfheme products to the native derivatives has been observed under several experimental conditions, the analogous processes have not been detected *in vivo*. This implies that the only mechanism of SHb and SMb removal in our body is through the natural decomposition of these molecules in tissues and cells. Curiously, it was demonstrated recently that H_2S diffuses rapidly across the red blood cell, acting as a sink for endogenous H_2S [47]. Thus, it is plausible that oxy Hb interacts with H_2S to form SHb, which is then eliminated

by the natural destruction of red blood cells. Furthermore, the normal life span of an erythrocyte is approximately 100-120 days, which suggests that SHb can be easily detect and that indeed, it can be used as a biomarker for H_2S generation in cells.

1.4.3.3 Histidine Role

Interaction of H_2S with hemeproteins have been studied through the years in invertebrate systems that serve as outstanding models in the effort of trying to understand the physiological roles and reactions of H_2S. An excellent model has been the Hemoglobin I (HbI) from the clam *Lucina pectinata* that leaves mangroves with high H_2S concentration and O_2 presence. The clam lacks a mouth/gut and lives in sulfide-rich mangroves where its nutritional needs are met by a symbiotic relationship with sulfide oxidizing bacteria. Bacteria living inside the gill oxidize H_2S in the presence of oxygen (O_2) and this energy is utilized to synthesize organic nutrients for the invertebrate. The protein responsible for delivering H_2S to the bacteria is HbI [48], which binds H_2S in the ferric heme iron with very high affinity. Interestingly, this hemeprotein (HbI) lives in a high H_2S environment in the presence of O_2 but, it does not form the sulfheme complex. This led attention towards the role of the distal surroundings in the sulfheme complex inhibition. In other words, how the nature of the heme pocket defines or changes the reaction of H_2S with hemeproteins. In an attempt to answer this inquiry, HbI mutants that mimic the distal site of Mb were exposed to H_2S in the presence of H_2O_2. Sulfheme formation was monitored by the characteristic sulfheme optical band, and by resonance Raman following the structural changes in heme distortion, 4-vinyl sustituent, and porphyrin $\rightarrow$ chlorin [22]. When glutamine in the 64 position of the protein (Gln64) was changed to histidine (His64), an optical band at 624 nm was observed. None of the other mutants produce the characteristic sulfheme band, not even the His68 mutant or Arg64. An increase in number of band and their intensity was observed in the

resonance Raman spectra of the HbI-His64 mutant. The formation of satellites band (1353 cm^{-1} and 1390 cm^{-1}) around the oxidation state marker ν^4, not present on the native HbI, were observed (see Figure 1-16). These two previous observations are characteristic of a chlorine structure and heme distortion. Deconvolution realized on the 4-vinyl band (1620 and 1626 cm^{-1}) revealed the absence of one of the H-vinyl (1626 cm^{-1}), representative of pyrrole saturation by the sulfur atom incorporation. All of these data suggested that histidine in the distal site plays a crucial role in the sulfheme protein formation, but it needs to be in an appropriate orientation for an adequate interaction. To confirm this, hemeproteins with very different conformation and volume to Mb, but containing a histidine in their distal site (the giants Hbs from the worms *Macrobdella decora* and *Lumbricus terrestris*), were evaluated (see Figure 1-17). The formation of optical spectra at 624 nm was also observed. These supported the requirement of a properly orientated histidine in the distal site in order for the sulfheme complex to form [22].

Therefore, it was hypothesize that after heme reduction facilitated by histidine, as previously reported [19], the O_2 coordination to the heme-Fe occurs, followed by histidine stabilization of the peroxo or oxo-ferryl intermediates that in the presence of H_2S stimulates the sulfheme formation [22]. Regarding this, hemeproteins with histidine residue at the ligand binding distal site, low Zinc ion sites, and low free cysteine residue will form the sulfheme derivate. However, hemeproteins with histidine residue at the distal site, abundant zinc ion sites, and/or free cysteine residue will not form the sulfheme complex since the H_2S molecule, while diffusing through the protein, will encounter alternative binding sites that will limit its access to the heme cavity reducing the possibility of protein functional abnormality or toxicity.

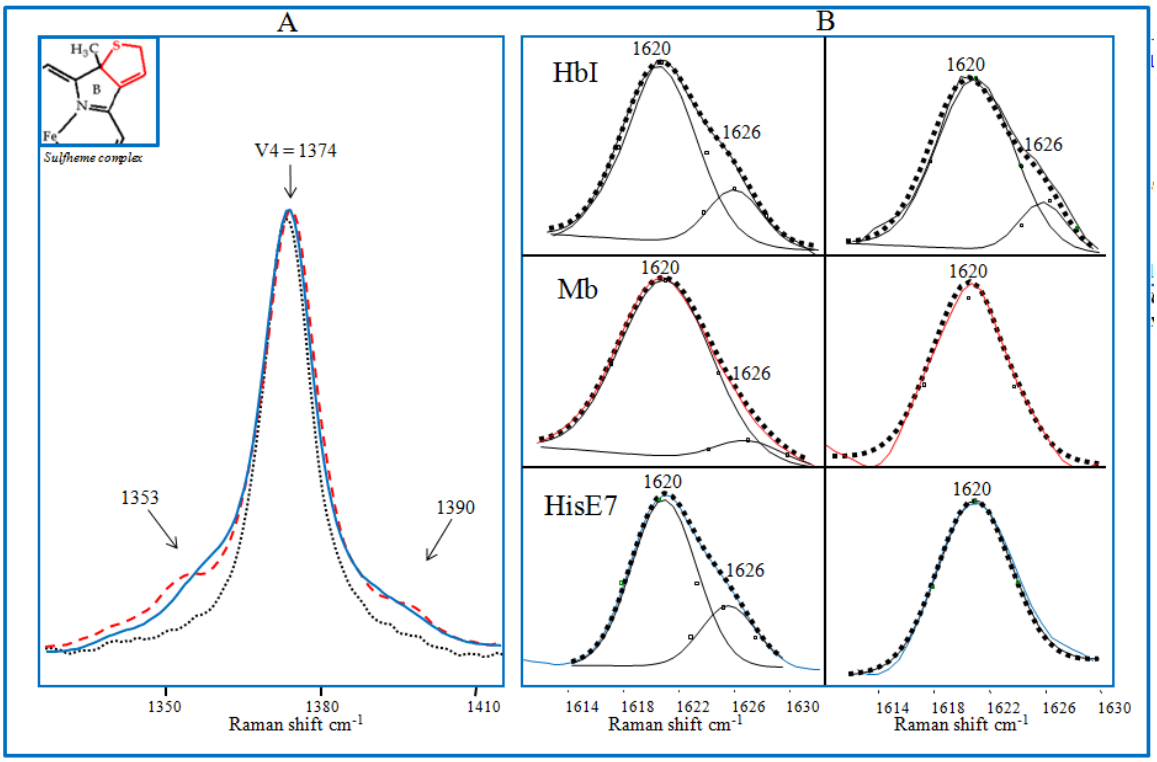

Figure 1-16. Resonance Raman spectra of Mb, HbI, and the HbI GlnE7His mutant. **A** shows the adjacent modes to ν^4 of metMb (dashed line), metHbI (dotted line), and HbI GlnE7His (solid line), in the presence of H_2O_2 and H_2S. **B** illustrates the decomposition of the vinyl bands. The left panel shows the met complexes while the right panel demonstrates heme proteins in the presence of H_2O_2 and H_2S. The filled squared lines are the fit after deconvolution. (Image taken and reprinted from publication: Structural Determinants for the Formation of Sulfhemeprotein Complexes; Elddie Román-Morales, Ruth Pietri, Brenda Ramos-Santana, Serge N. Vinogradov, Ariel Lewis-Ballester, and Juan López-Garriga; *Biochemical and Biophysical Research Communications* (2010) 400: 489–492 DOI: 10.1016/j.bbrc.2010.08.068 with permission 4002210450839 from publisher Elsevier)

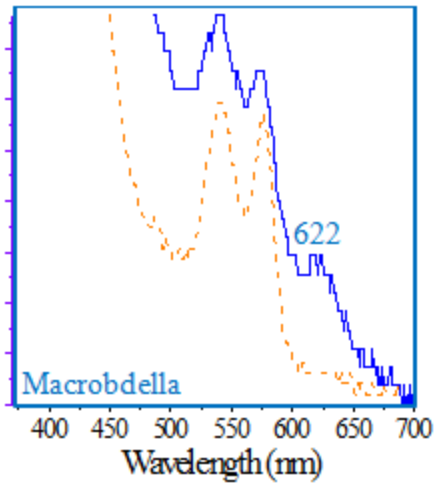

Figure 1-17. Optical spectra of *Macrobdella* Hb interaction with with H_2O_2 (orange-dashed line) and H_2S (blue-solid line) that leads to the sulfheme formation (622 nm). (Image taken, modified and reprinted from publication: Structural Determinants for the Formation of Sulfhemeprotein Complexes; Elddie Román-Morales, Ruth Pietri, Brenda Ramos-Santana, Serge N. Vinogradov, Ariel Lewis-Ballester, and Juan López-Garriga; *Biochemical and Biophysical Research Communications* (2010) 400: 489–492 DOI: 10.1016/j.bbrc.2010.08.068 with permission 4002210450839 from publisher Elsevier)

Nonetheless, this theory is still under controversy [20]. The importance of the protein distal environment is evident, since it defines the H_2S chemical reaction route and functions. Keeping this in mind, it should be taken into account the part that could have played the distal histidine in the thiyl radical formation observed during the reaction of Mb^{IV} with H_2S that also leads to the sulfheme formation. These observations and the tautomeric nature [49, 50] and orientation of distal His, which can behave as an acid-base catalyst, allows suggesting the general mechanisms shown in Figure 1-18. Due to the cyclic nature of the reaction between hemeproteins and H_2O_2, it is difficult to assign the initial peroxide adduct (ferric hydroperoxide or compound II) responsible for sulfheme formation. Assuming that in the presence of an H_2O_2 scavenger the end product of the reaction is compound II, then the predominant reaction can be summarized as shown in Figure 18a. On the other hand if the cyclic reaction is operative, the reaction can be described as demonstrated in Figure 18b. In both scenarios the SH• appears to be the reactive species that attack the double β-β bond of pyrrole B heme [21, 51].

It is clear that much remains to be investigated of the sulfheme proteins. The fact that this complex is also produced in heme-peroxidases and catalases, suggests that this derivative can also be generated in other heme-containing enzymes involved in O_2 chemistry. Some key issues that require further attention are: *(a)* the final sulfheme product (heme-iron oxidation state and ligand) that is the competition/limitation of O_2 interaction and *(b)* in addition to the sulfur electro withdrawing capacity and heme distortion, what other chemical changes contribute to the decrease in O_2 affinity, ex. conformational changes. Insights into these issues will help in the determination of the sulfheme proteins role in H_2S metabolism, detection and physiology, as well as, much needed knowledge of the physiological H_2S-protein interaction when developing H_2S therapeutic drugs and procedures.

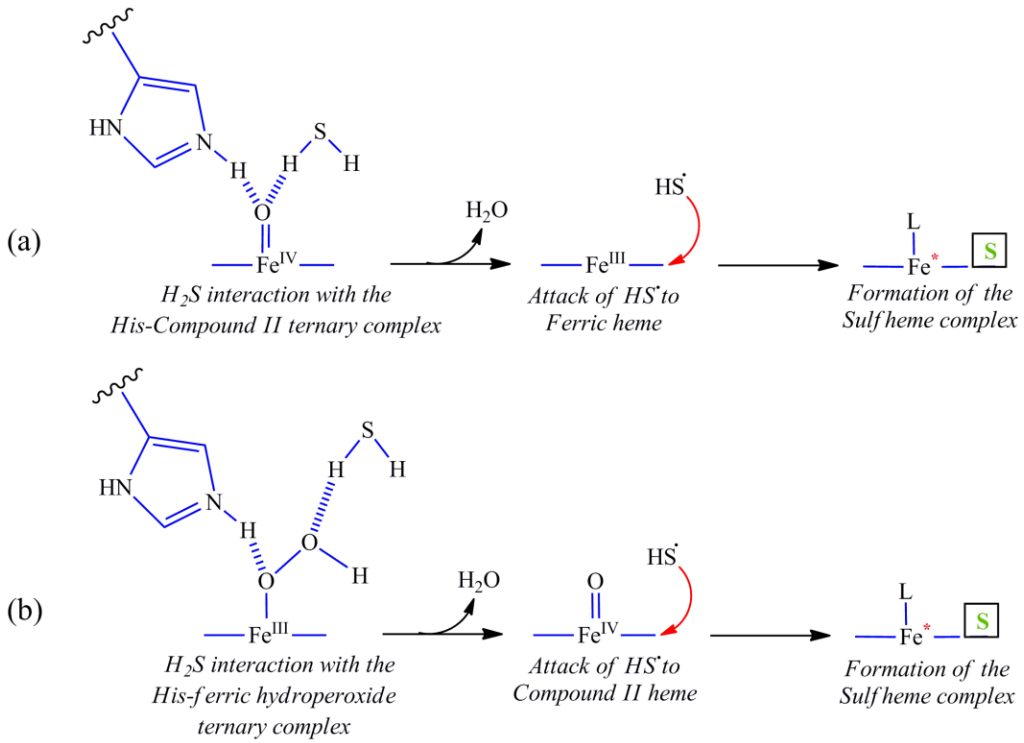

Figure 1-18. Proposed mechanism for sulfheme protein formation. (Image taken and reprinted from publication: Hydrogen Sulfide Activation in Hemeproteins: The Sulfheme Scenario; Bessie B. Ríos-González, Elddie M. Román-Morales, Ruth Pietri, and Juan López-Garriga; *Journal of Inorganic Biochemistry* (2014) 133: 78–86 DOI: 10.1016/j.jinorgbio.2014.01.013 with permission 4002201234177 from publisher Elsevier)

Chapter 2: Material and Methods

CHAPTER 2: MATERIAL AND METHODS

2.1 Sample Acquisition

The hemeproteins used for the study were horse heart Mb and recombinant HbI (rHbI) from the clam *Lucina Pectinata*, which is considered an experimental control. Horse heart Mb was purchased from Sigma-Aldrich and used without further purification. One way to preserve living organisms without affecting the scientific advances and research is through the use of mutant bacterial cell growth for sample acquisition. The desired rHbI was obtained by procedures described in the literature [48, 52]. The procedure basically consists of four steps: cloning, large-scale expression, lysis, and purification. Recombinant HbI (rHbI) was used and considered as the control throughout the study. The creation of the rHbI mutant was produced according to Leon et al., 2004 [53]. The biomolecular laboratory of Dr. Carmen Cadilla, at the University of Puerto Rico-Medical School Campus, provided the E. coli Bli5 competent cells with the plasmid of the specific HbI mutant. To assure their lifetime, cultures were prepared immediately and stored in frozen stocks at - 80˚C in a 50% sterile glycerol.

2.2 Large Scale Expression of the rHbI mutant

The procedures for the Large Scale Expression were applied as reported in the literature [53, 54], with slight modifications. The solutions used for the fermentation were: 300 mL of 50% w/v glucose, 500 mL of 1.5 monobasic potassium phosphate, 500 mL of 30% w/v ammonium hydroxide, 5 mL of 1 mM IPTG, 500 mL of Terrific Broth (TB) Medium with 30 µg/mL of chloroamphenical and 70 µg/mL of kanamycin, and a solution of 0.17 M KH_2PO_4 with 0.72 M K_2HPO_4. All solutions, except the ammonium solution, were sterilized at a temperature of 120˚C for 20 minutes. For the fermentation process a Bioflo 110 Modular Benchtop Fermentator was used and prepared with 4 L of Tb medium and 15 mL of glycerol. The vessel was sealed with the

exception of an exhaust to avoid an explosion. The exhaust had at the end, a 0.20 µm autoclavable millex vent filter unit from Millipore covered with foil paper to limit the possibility of contamination. After filling the vessel jacket with water, the vessel was placed in a Sanyo Labo Autoclave for sterilization at 121˚C for 1 hour. The glassware and equipment used during this process were cleaned and also sterilized for 20 minutes at 121˚C using a Market Forge Sterilmatic.

The selected frozen stock cells of the rHbI were transferred 24 hours before the fermentation to a 50 mL TB medium and incubated at 120-150 rpm in a Precision Reciprocal Shaking Bath from Precision Scientific, at 37˚C for 12 hours. After the first 12 hour of incubation, the 50 mL cell culture was transferred to 450 mL TB medium and incubated for another 12 hours under the same conditions. Prior to the fermentation, the vessel was not removed from the autoclave to avoid possible contamination.

Five hundred mL of phosphate solution, 30 µg/mL chloramphenicol, 70 µg/mL kanamycin, 500 µL antifoam solution and 75 mL of 50% w/v glucose were added to the vessel when the temperature reached 37˚C. Subsequently, the pH and dissolved oxygen sensors were placed and calibrated according to the Fermentator manual. The software was programmed to maintain a pH of 7.0 and 100% of oxygen in the media. Then 25 mL of the media were collected to be use as a blank and solvent for the evaluation of cell growth every 30 minutes during the fermentation process by measuring the optical density at 600 nm. The 450 mL cell culture of the last 12 overnight hours was added to the vessel media to inoculate. Immediately, 3 mL aliquot of the inoculated media was collected and an OD_{600} was taken. Another 75 mL of the 50% w/v glucose solution were added after inoculation. When bacterial growth reached the lag phase as indicated by measurements of constant growth, 5 mL of 1M IPTG were added to induce the

protein expression. The solution of 33mg/mL hemin chloride in ammonium hydroxide was also added as needed. The extraction process of the culture from the vessel was initiated when the measurements of the bacterial growth were constant and oxygen consumption was low, known as the lag phase. The culture was collected in a 500 mL Beckman bottle and centrifuged at 4˚C and 4000 rpm for 20 minutes, using a Beckman J2-HS Centrifuge. The supernatant was decanted and discarded; the remaining pellet was store.

2.3 Lysis of the cell

After the large scale expression process, the desired protein was separated from the cytoplasm of the bacteria by lysis or cell breakage. The sterilized buffer used to resuspend the pellet was Native Binding Buffer (NBB), consisting of 58 mM dibasic sodium phosphate, 17mM monobasic sodium phosphate and 68mM sodium chloride. The quantity of NBB necessary to re-suspend the pellet depended on the weight of the pellet; for every 1 g of cells, 1 mL of NBB were added. In addition, 1 mg of Chicken Egg White Lysozyme was added for every gram of bacteria cell, and incubated for 45 minutes on ice with sporadic stirring. For every 100 mL of NBB, 20 µL of protease inhibitor were added to minimize the degradation of the protein. Periods of 75 seconds of 25% intensity sonification, with 45 resting seconds, were applied to break the cell membrane. The lysate was centrifuged at 15000 rpm for 1 hour at 4˚C. The pellet was discarded and the supernatant stored.

2.4 Purification of the rHbI mutant

The techniques used for the protein purification are based one of size and ionic properties differences, as described in the literature [48, 55], utilizing an AKTA Fast Performance Liquid Chromatography Instrument from Amersham Bioscience. The FPLC was equipped with an UV-Vis lamp and a Frac-950 collector. To separate the desired HbI mutant from other proteins

produced by the bacteria, two chromatographic processes were conducted: affinity and size exclusion chromatography. The previously describe purification process was applied.

2.4.1 Affinity Chromatography

The affinity method used for the purification of the HbI mutant was based on the interaction between the protein mutants with a metal affinity resin, BV TalonTM from Clonetech. This resin involves a tetradentate chelator of Cobalt (II) in a sepharose bead. This metal is polyhistidine-tagged selective, therefore binding to the polyhistidine-tagged HbI mutant, thus separating the mutant from other proteins.

A Tricorn 10/100 column from Amersham was utilized for the process. The column was filled with 8-10 mL of resin, which made 1 column volume (CV) of the total column. Following the instruction manual, the column was equilibrated at a 5.0 mL/min flow. It contained 10 CV of the 7.0 pH equilibrating buffer (50 mM sodium phosphate and 300 mM sodium chloride).

To assure the removal of impurities before the column purification, the lysate was centrifuged again at 4˚C and 15,000 rpm for 30 minutes and filtered using a 0.45 µm syringe filter. To start the purification process, 20 mL of the lysate at a 1.0 mL/min flow were injected into the column. A wash buffer was used for the removal of all weakly attached proteins in the resin column. This 7.0 pH wash buffer consisted of 50 mM sodium phosphate, 300 mM sodium chloride and 10 mM imidazole. To elude the mutant species from the column, an elution buffer of 50 mM sodium phosphate, 300 mM sodium chloride and 150 mM imidazole at a pH of 7.0 was used. Photometric chromatograms at 280 nm wavelength were obtained using an UV-Vis lamp in the FPLC instrument, which monitored the presence of all the proteins.

Protein fraction selection and collection were made using the Unicorn 4.0 Software chromatogram, which monitors all molecules by their absorbance and conductivity. The figure 2-

1 demonstrates the elution profile by Metal Affinity Chromatography at 280 nm for the separation of HbI mutant from impurities, where one can observe the elution of the impurities was observed first followed by the desired protein.

The sample was concentrated and washed with deionized water at 4˚C, by pressure filtration using Nitrogen as the pressure gas and a YM-10 membrane with a molecular range of 10000 in an AMICON ultrafiltration cell. This procedure assured the functionality of the protein by eliminating the imidazole remaining in the sample from the purification buffers. All the mutants with the exception of the HbIGlnE7His mutant, which aggregates in the absence of salts, were washed with 7.0 pH 0.1 M sodium phosphate buffer to maintain the functionality and stability of the mutant. The sample was stored.

2.4.2 *Size Exclusion Chromatography*

The size exclusion method was conducted for the removal of impurities that may have still been present in the sample. Five mL of the bright reddish filtered protein mixture were passed through a Size Exclusion Chromatography HiLoadTM 26/60 SuperdexTM 200 pre grade column from Amersham Bioscience with a matrix of dextran, covalently bound to highly cross-linked agarose. The proteins are separated by their differences in molecular size when passed through the gel filtration column, using a 50 mM sodium phosphate and 300 mM sodium chloride with pH of 7.0 at a flow rate of 1.5 mL/min under 0.3 MPa pressure.

Figure 2-2 shows the elution profile by Size Exclusion Chromatography at 280 nm for the separation of HbI mutant from imidazole and salts impurities; where the elution of the impurities was first observed followed by the elution of the desired protein. In order to determine and select the best protein fractions, photometric chromatogram at 280 nm wavelength was done using a UV-Vis lamp in the FPLC instrument, monitoring the presence of all the proteins. All the FPLC

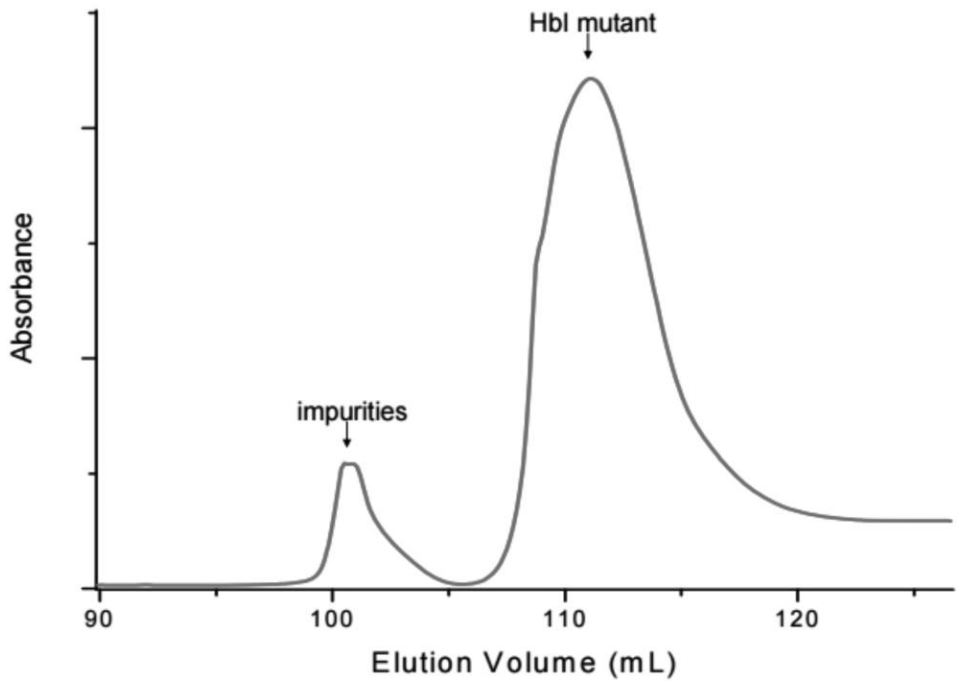

Figure 2-1. Metal Affinity Chromatography at 280 nm of the separation of HbI mutant from impurities.

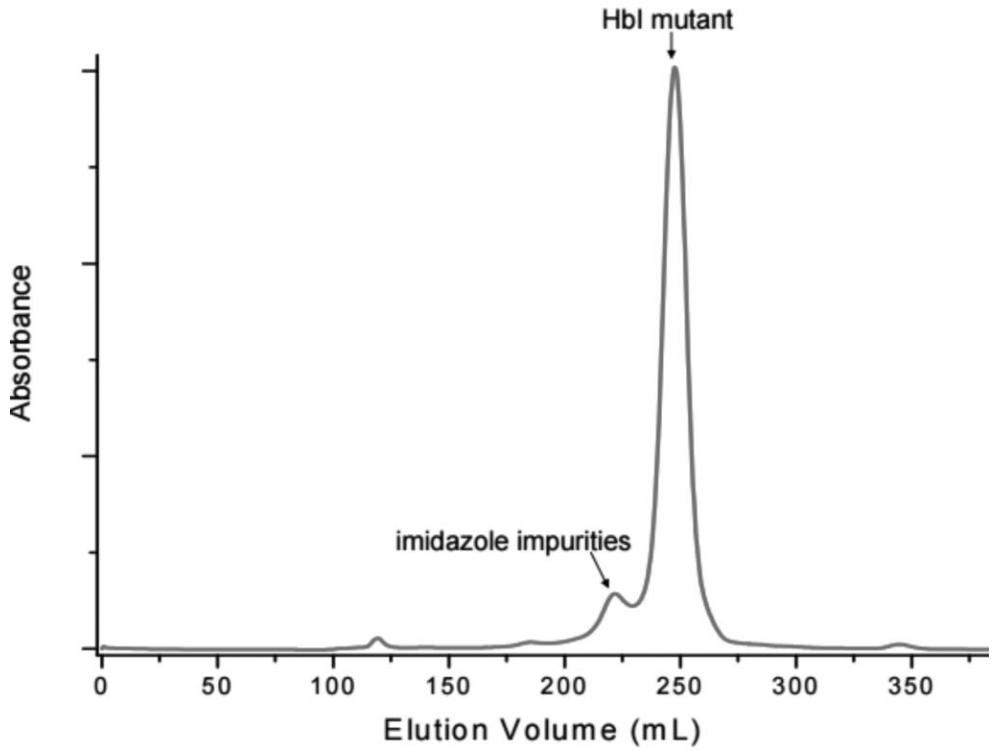

Figure 2-2. Elution profile of the Size Exclusion Chromatography at 280 nm for the separation of the HbI mutant from imidazole and salts impurities.

procedures and chromatograms visualizations were controlled using a Unicorn 4.0 Software installed in the FPLC Computer. After all the eluted fractions were collected in the Frac-950 collector, the selection of the desired fraction of protein was made using the Unicorn 4.0 Software chromatogram which monitors all the molecules by their absorbance and conductivity. The desired protein was concentrated and the solvent changed to 7.0 pH 0.1 M sodium phosphate buffer by pressure filtration at 4˚C, using Nitrogen as the pressure gas and a YM-10 membrane, with a molecular range of 10000 in an AMICON ultrafiltration cell. It was stored at approximately 50˚C to assure the stability and lifetime of the rHbI mutant.

2.5 Verification of Sample Purity

The method used for determining the purity of HbI was sodiumdodecyl sulphate-polyacrylamide gel electrophoresis (SDS-PAGE). It is a qualitative method based on the different rates of migration of proteins with different molecular weight represented by the bands when an electric field is applied. This electrophoresis uses a polyacrylamide gel as a support medium and an anionic denaturalizing detergent that binds to the proteins increasing their solubility and imparts a negative net charge to them. This net charge facilitates the migration of the molecules through the gel when the electric field is applied, separating them according to their molecular weight. The migration profile provides the heavier molecules on top of the gel (slow migration) and the lighter molecules on the bottom of the gel (more migration).

For a simple evaluation of the purification process and estimation of the proteins molecular weight, the resulting bands were compared to these of a SDS-PAGE standard from Bio-Rad with a molecular range from 6,900 to 194,239 Daltons. The electrophoresis analysis was made using an 8-16% Tris-HCl Ready Gel from Bio-Rad. The samples were prepared by mixing in a Vortex, 20 µL of the protein and 10 µL of the running buffer solution, which

consisted of 0.5 M Tris-HCl at a 6.8 pH, 10% SDS, 1% bromophenol blue as dye marker, Glycerol and β-mercaptoethanol. The mixtures were heated for 5 minutes using a sand bath at 95˚C. Immediately, 16 µL of the heated mixture were transferred to the wells in the gel. For the preparation of the standard, 20 µL of the SDS-Page Standard were heated in a sand bath for 1 minute at 32˚C. Then, immediately injected into the first well. The ready gels were previously placed in the vertical trays of the ready gel electrophoresis cell from Bio-Rad, which was filled with running buffer. The migration of the proteins through the gel was initiated by applying a current of 114 mA and a voltage of 150 V for 45 minutes, using a power supply PAC 3000 from BioRad. The migrations of the samples were stopped by discontinuing the applied potential. Then, the gel was carefully removed and stained for 15 minutes with Coomasie Blue G-250, which was then removed by washing with acetic acid solution three times and left in deionized water for a period of 24 hours. After all this procedure, one can clearly observe the presence of bands and determine the purity and absence of contaminant in the protein sample.

2.6 Ultraviolet-Visible Spectroscopy and Complexes formation

The UV-Vis spectroscopy gave information about the concentration, complex formation, and purity of the protein sample based on the heme group, using an Agilent 8453 UV-Vis spectrophotometer. To determine the concentration of the sample, the protein was converted to metaquo-Mb complex (see Figure 2-3) through potassium ferrocyanide titration. The metaquo complex formation was monitored through the formation of its characteristic absorption bands at 407, 505, and 633 nm. In order to eliminate the excess of potassium ferrocyanide and change the solvent of the sample to100 mM succinic acid, 100 mM potassium phosphate dibasic and 1mM EDTA solution at a pH of 6.5 or 7.4, a centricon centrifugal filter device with a YM-10 membranes from Amicon were used and centrifuge for periods of 10 minutes in a JA-20 rotor at

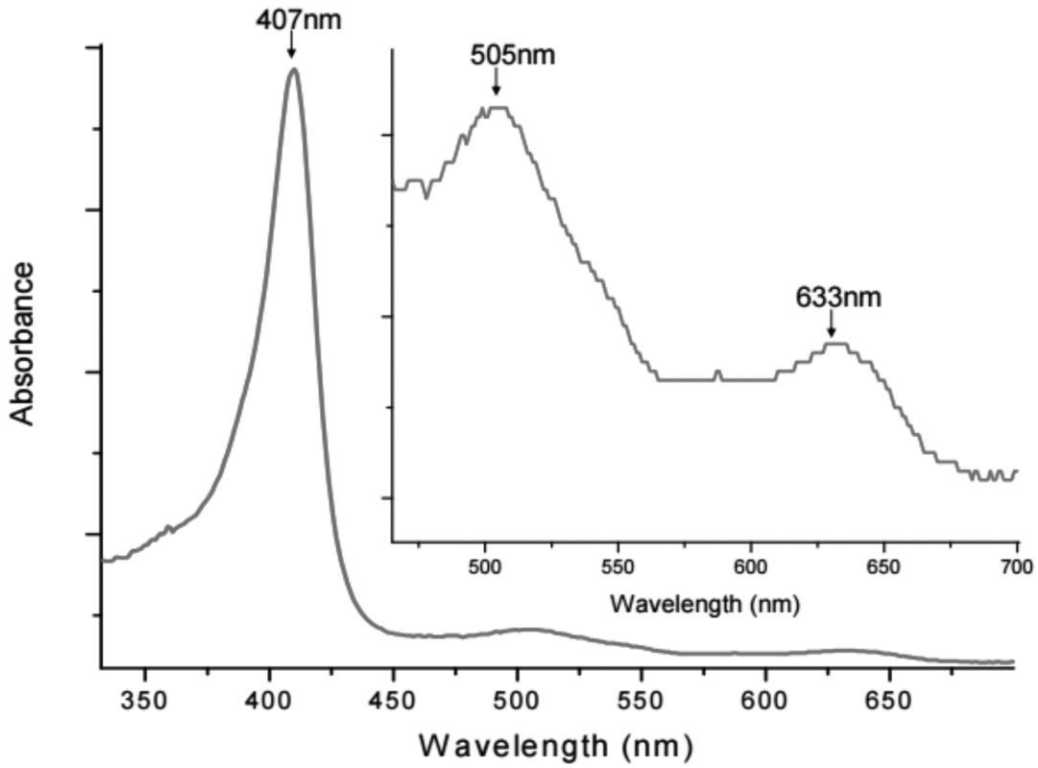

Figure 2-3. Metaquo complex formation was monitored through the formation of its characteristic absorption bands at 407, 505, and 633 nm.

8000 rpm and 4˚C. This procedure was performed until all the yellow residue of the potassium ferrocyanide was eliminated and the desired concentration obtained. The sample concentration was determined at the maximum absorption wavelength of the Soret band applying the Beer-Lambert Law: A = εbc, where A is the maximum absorbance, b is the cuvette pathlength, c is the concentration and ε is the absorptivity coefficient reported in the literature [48].

The protein sample, buffer, hydrogen peroxide solution, Na_2S salt, and $Na_2S_2O_4$ salt were each transferred to a small vials (ranging from 300 μL to 1.5 mL) and tightly sealed with a rubber septum. They were degassed and then, purged for 15 minutes with 99.0% nitrogen gas (N_2; from Linde), to remove the oxygen present in the sample. Syringes used for the transferation of buffer to the vials with Na_2S and $Na_2S_2O_4$ to acquire the H_2S and $Na_2S_2O_4$ solution were also purged with N_2 gas. Syringes used for the addition of specific aliquots of H_2O_2, H_2S, and/or $Na_2S_2O_4$ solution, in addition to sample transfer, were also purged with N_2 gas.

2.6.1 Sulfheme complex formation with H_2O_2

The protein experimental concentration was 2 mM. The [protein:H_2O_2:H_2S] concentration ratio used in the EPR experiments were [1:1:1], [1:5:3], and [1:5:90]. The H_2O_2 was added to the metaquo protein to form the ferryl species (at approximately 540 and 582 nm) with subsequent addition of H_2S to form the sulfheme specie, all performed in anaerobic conditions. The sulfheme protein formation was monitored by evaluating the characteristic sulfheme absorption bands at 620 and 720 nm. The reaction at 1, 10, and 30 minutes was hand-quenched by transferring the sample into 4-mm quartz EPR tubes and immediately immersed in liquid nitrogen.

2.6.2 Sulfheme complex formation with O_2

The oxy-derivatives (seen in Figure 2-4 at approximately 416, 541, and 576 nm) were prepared by adding [1:15] concentration ratio of [met-protein:sodium dithionite] under anaerobic conditions to form the deoxy-complex (at approximately 550 nm) followed by O_2 purging [19]. The sulfheme complex was acquired by adding H_2S to the oxyMb complex in a [1:70] concentration ratio of [oxy-protein:H_2S] that provides the highest intensity and stability of the 620 nm characteristic band. The sulfheme complex formation was monitored through its characteristic 620 nm band by UV-Vis spectroscopy using an Agilent 8453 spectrophotometer.

2.7 SAX/WAX data acquisition and processing

SAXS/WAXS data were recorded on oxyMb and oxyHbI in the absence and presence of H_2S. The 620 nm band was monitored before and after data acquisition for both proteins. The band was only detected in oxyMb after addition of H_2S since oxyHbI does not form the sulfheme derivative. The 100 mM succinic acid, 100 mM potassium dihydrogen phosphate, and 1mM EDTA buffer was used as a background. In the absence of H_2S, the scattering data of oxyMb were first collected at 5, 6, 10, and 11 mg/mL. The optimal protein concentration was found to be 11 mg/mL and the scattering data in the presence of H_2S were therefore collected at this concentration. For HbI the final protein concentration was 6.7 mg/mL. The SAXS/WAXS data was collected simultaneously at the X-9 Beamline of the National Synchrotron Light Source at Brookhaven National Laboratory using a PILATUS 300k SAXS detector and a Photonic Science CCD WAXS detector [56]. For triplicated data acquisition, 20 μL of sample was continuously flowed through a 1-mm diameter capillary where it was exposed to the x-ray beam for 30 s. Initial data processing was performed using the pyXS-v2 software package developed at X9.

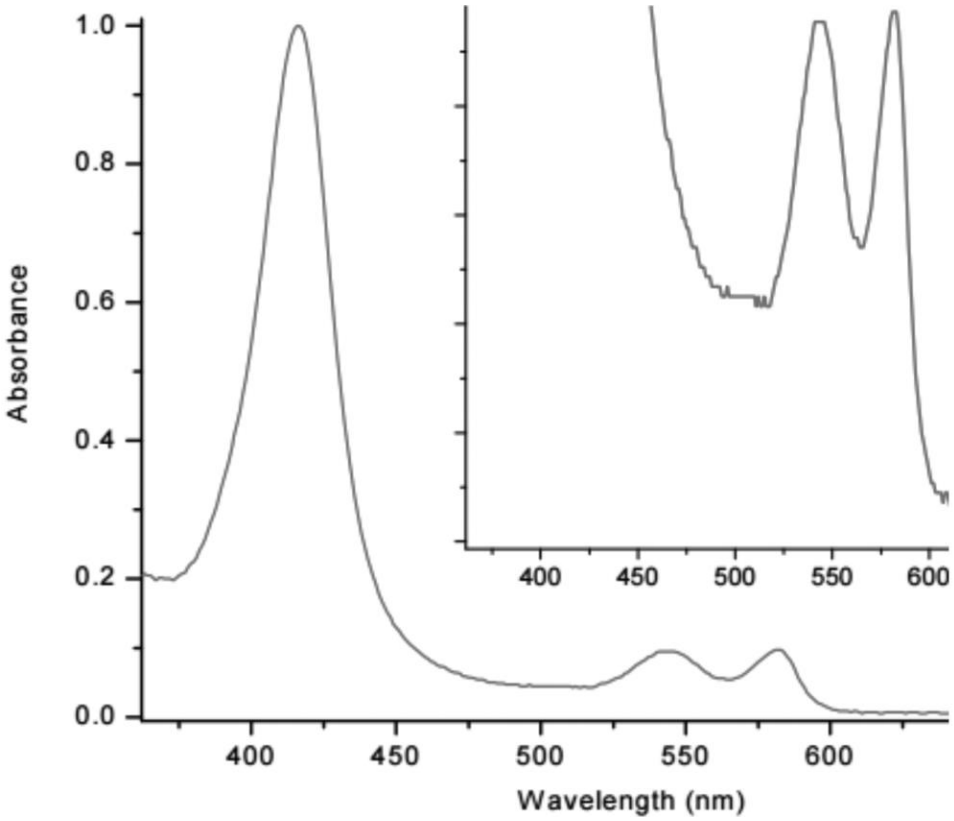

Figure 2-4. The oxy complex formation was monitored through the formation of its characteristic absorption bands at 416, 541, and 576 nm.

The program converted the two-dimensional scattering patterns recorded on the SAXS/WAXS detectors into one-dimensional scattering profiles. Three scattering patterns of each sample were obtained, averaged, and buffer (background) subtracted. Further SAXS/WAXS data processing and analysis were performed using 2.5.2 ATSAS Package [57, 58]. Guinier, Kratky and Porod [59] analyses were conducted using Primus [60]. The pair distribution functions were evaluated using GNOM [61]. 3-D surfaces were generated using DAMMIN [62] , averaged using DAMAVER [63], and superimposed using SUPCOMB [64]. The theoretical scattering profiles of oxyMb and SMb atomic models were evaluated using CRYSOL [65]. Pymol was used for graphical visualization and figure generation.

2.8 EPR data acquisition and processing

Electron paramagnetic resonance (EPR) data were obtained with a Varian E112 X-Band model spectrometer using a TE102 resonator, Gunn diode as the microwave source and a liquid nitrogen finger Dewar vessel. The parameters for EPR were as follows: center field of 3,000 and 1,200 G; sweep width of 2,000 and 1,600 G, microwave frequency of 9.1 GHz, microwave power of 1.0 mW, time constant of 0.5 s, gain of 1250, scan number of 4, scan point of 2,000 and temperature of 77 K. Baseline correction was performed using an Origin Pro 9.0 Program.

Chapter 3: Results and Discussion

CHAPTER 3: RESULTS AND DISCUSSION

3.1 Global Structure Evaluation

Characterization of oxyMb and oxyHbI with and without H_2S was conducted using their overall dimensions and shapes, as well as their internal structural features derived from SAXS and WAXS scattering data, respectively.

3.1.1 Scattering Curve and Guinier Plot

In SAXS/WAXS, the intensity of the scattered X-ray beam is measured as a function of the momentum transfer vector q, ($q = 4\pi sin\theta)/\lambda$), where θ is the scattering angle and λ is the beam wavelength [58, 66]. The transfer vector q is inversely related to the real space distance between scattering centers d within the particle ($q = 2\pi/d$) [58, 66], see Figure 3-1. Thus, the low q region in the scattering pattern (~0.01-0.05 $Å^{-1}$) represents vectors of length ~600 to 100 Å and differences in the intensity within this region would reflect changes in the overall shape of the molecule. Conversely, at higher q, the length space distance d between centers become smaller and changes in this region suggest fluctuations in internal structural features [67, 68]. Overall, it can be generalized that an increase in protein fluctuations or mobility is illustrated by a decrease in the definition or sharpness of peaks, in the high q region of the scattering curve of the protein [67-70].

Figuree 3-2 shows the scattering curves ($I(q)$ vs q) of the oxyHbI complex in the absence (black line) and presence of H_2S (red line). The HbI scattering curves maintain the same scattering central maxima in the presence or absence of H_2S. This indicates that the overall shape and internal structure of the protein remain unchanged in the presence of H_2S. Figure 3-3 illustrates the scattering curves of oxyMb (black line) in the presence of H_2S, which leads to the formation of the SMb complex (red line). In addition to an evident increase in protein mobility

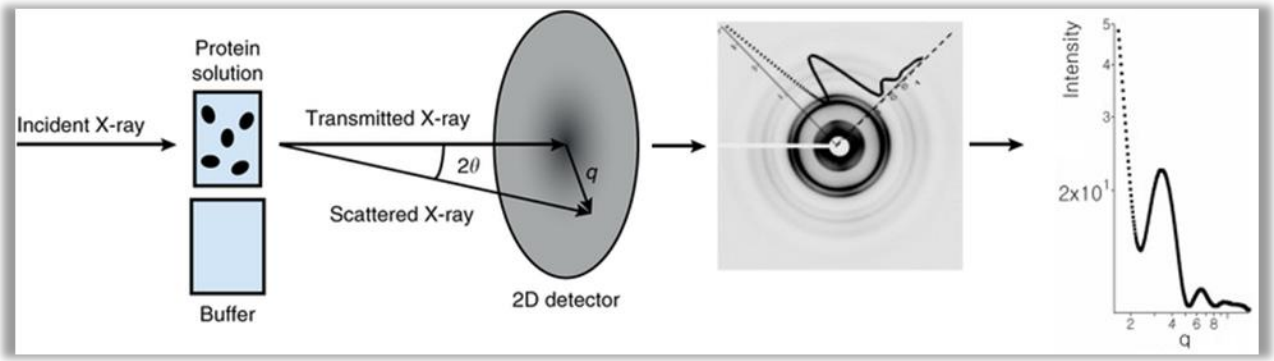

Figure 3-1. In SAXS/WAXS, the intensity of the scattered X-ray beam is measured as a function of the momentum transfer vector q, ($q = 4\pi\sin\theta/\lambda$), where θ is the scattering angle and λ is the beam wavelength. The transfer vector q is inversely related to the real space distance between scattering centers d within the particle ($q = 2\pi/d$) . (Image taken, modified, and reprinted from http://www.mrl.ucsb.edu/~safinyaweb/XRD.htm and publication: Synchrotron-based Small-angle X-ray Scattering of Proteins in Solution; Soren Skou, Richard E. Gillilan, and Nozomi Ando; *Nature Protocols* (2014) 9: 1727-1739 DOI: 10.1038/nprot.2014.116 with permission 4002470340618 from Nature Publishing Group)

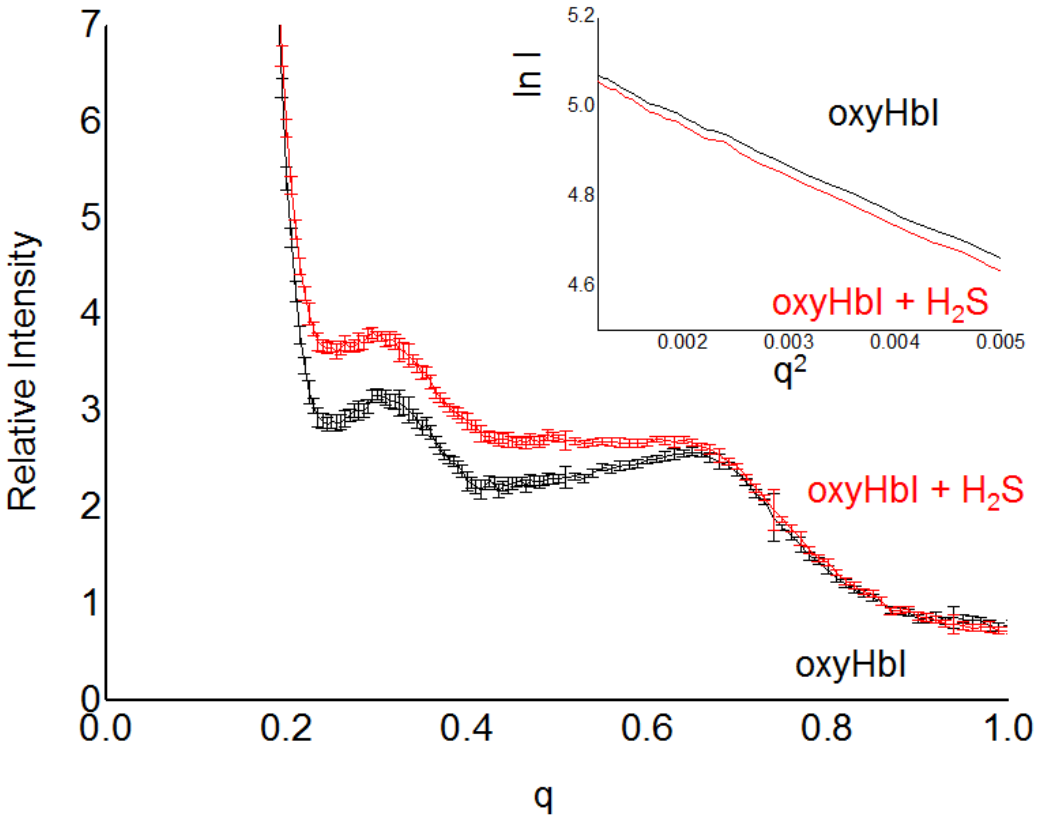

Figure 3-2. SAXS/WAXS scattering curves (showing *q* range of 0.19-1.0 $Å^{-1}$), with their corresponding Guinier Plot of oxyHbI in the absence (black line) and presence of H_2S (red line) (inset; *q* range = 0.030-0.072 $Å^{-1}$ for HbI). (Image taken, modified, and reprinted from publication: Sulfmyoglobin Conformational Change: A Role in the Decrease of Oxy-myoglobin Functionality; Elddie Román-Morales, Erika López-Alfonzo, Ruth Pietri, and Juan López-Garriga; *Biochemistry and Biophysics Reports* (2016) 7: 386-393 DOI: 10.1016/j.bbrep.2016.07.002 with permission from publisher Elsevier)

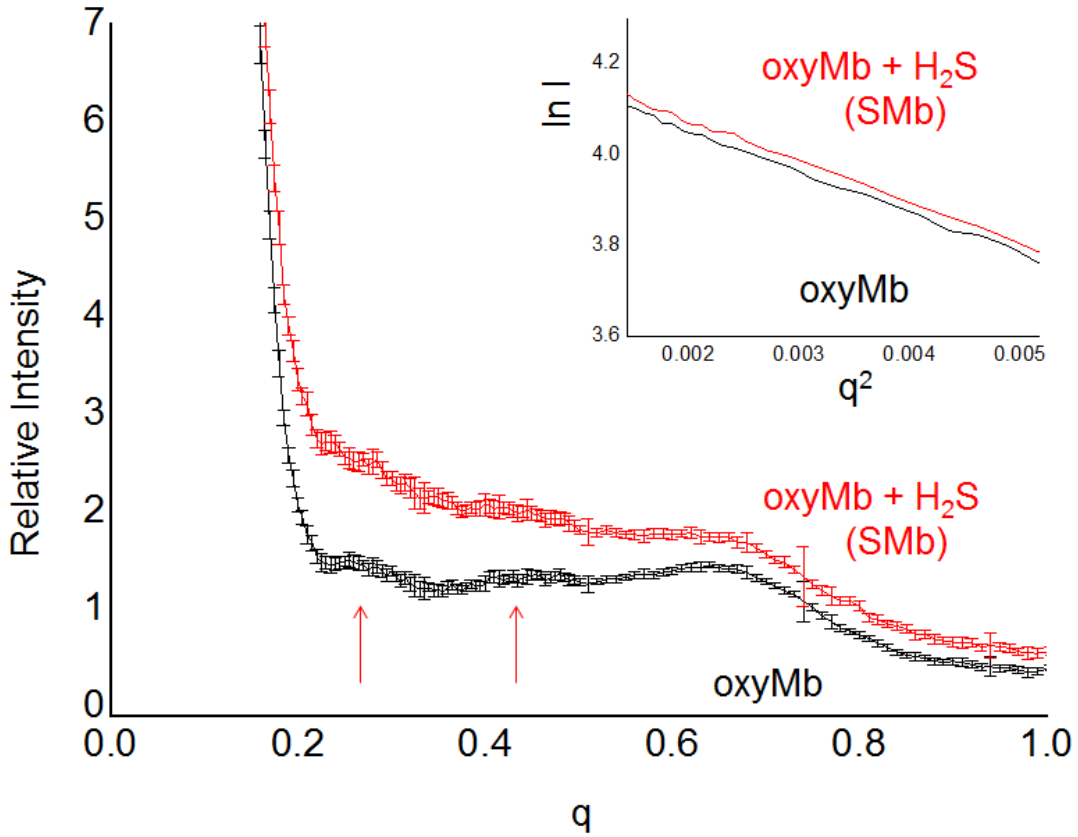

Figure 3-3. SAXS/WAXS scattering curves (showing *q* range of 0.19-1.0 $Å^{-1}$), with their corresponding Guinier Plot (inset; *q* range = 0.038-0.072 $Å^{-1}$ for Mb) of oxyMb (black line) and SMb (red line, product of oxyMb and H_2S interaction). (Image taken, modified, and reprinted from publication: Sulfmyoglobin Conformational Change: A Role in the Decrease of Oxymyoglobin Functionality; Elddie Román-Morales, Erika López-Alfonzo, Ruth Pietri, and Juan López-Garriga; *Biochemistry and Biophysics Reports* (2016) 7: 386-393 DOI: 10.1016/j.bbrep.2016.07.002 with permission from publisher Elsevier)

and fluctuations characterized by a decrease in peak definition and sharpness, a noticeable fading of the scattering peaks at ~0.27 and 0.43 $Å^{-1}$ was observed upon SMb complex formation. When comparing the scattering curves of Mb and HbI after addition of H_2S, the scattering pattern with the greatest degree of change is that observed for Mb (e.g. *q* region at 0.27-0.43 $Å^{-1}$) as a result of SMb complex formation. It is important to mention that oxyHbI reacts with H_2S to form ferric hemoglobin sulfide in which H_2S coordinates to the ferric heme iron (Fe^{III}-H_2S) most probably by nucleophilic displacement of the bound superoxide [48]. In contrast, reaction of oxyMb with H_2S modifies the heme active center producing SMb [21, 22]. Thus, the data indicate that H_2S binding to the ferric heme in oxyHbI does not induces significant global and internal structural changes, while modification of the heme macrocycle in oxyMb produces internal structural fluctuations. Overall, SMb shows greater variation of structural conformational changes upon interaction with H_2S, as evidence by the loss of scattering peaks. The structural distances that were present in oxyMb (represented by the scattering peaks at 0.27 and 0.43 $Å^{-1}$or *d* space of ~23-15 Å) are no longer the most abundant as a consequence of the structural conformational change associated to the SMb complex. Interestingly, time resolved X-ray scattering data on Mb-CO showed that the disappearance of the peaks in these regions was due to tertiary structural relaxation, specifically to displacement of the E and F helices [71]. It is therefore plausible that SMb induce changes in these helices as well.

One parameter that can be determined directly from the SAXS data in the low *q* region (~0.01-0.05 $Å^{-1}$) is the radius of gyration or R_g, using the Guinier approximation. The R_g is the root mean square distance of an object from its center of mass and provides a measure of the overall size of the protein. According to the Guinier approximation, at very small *q* ($q<1.3/R_g$) a plot of ln $I(q)$ versus q^2 should be linear for a globular protein (Equation 1). From the slope of the

linear fit one can determine the R_g and hence the overall size of the protein. In addition, deviations from linearity in the Guinier plots indicate aggregation. The insets in Figure 3-2 and 25 show the Guinier plots for oxyHbI and oxyMb in the absence and presence of H_2S. The linearity of the Guinier plots of both proteins with and without H_2S indicates no detectable aggregation. As shown in Table 3-1, the R_g of oxyHbI was determined to be ~18.0 Å and no change in this value was detected after exposure of H_2S. Similarly, the R_g of oxyMb and SMb were determined to be 16.8 and 16.7 Å, respectively, indicating similar overall sizes.

$$I(q) = I(0)\exp(-\tfrac{1}{3}R_g^2 q^2) \qquad (1)$$

3.1.2 Pair Distribution Function, P(r)

The shapes and maximum dimensions (D_{max}) of proteins can also be determined directly from their SAXS/WAXS scattering data. Indirect Fourier transformation of the scattering data $I(q)$ yields a pair distribution function *P(r)*, which is a histogram of distances between pairs of elements within the entire volume of the scattering protein (Equation 2) [58, 66]. In general, the *P(r)* function is a real space representation of the scattering data and provides an approximation of the shape and dimension of a protein in solution, see Figure 3-4. For example, globular proteins have a symmetric bell-shaped *P(r)*, whereas unfolded particles have an extended tail. In addition, multi-domain proteins often yield *P(r)* with multiple shoulders and oscillations corresponding to intra an inter-subunit distances [58, 66].

$$P(r) = \frac{r^2}{2\pi^2}\int_0^\infty q^2 I(q)\frac{\sin qr}{qr}\,dq \qquad (2)$$

Figure 3-5 shows the *P(r)* plots of oxyHbI in the absence (black line) and presence of H_2S (red line). The contours of the *P(r)* plots are characteristic of a globular protein with somewhat

Protein	R_g (Guinier) (Å)	R_g (Gnom) (Å)	D_{max} (Å)
oxyHbI	17.90 (± 0.06)	18.16 (± 0.04)	60
oxyHbI + H_2S	18.10 (± 0.66)	17.81 (± 0.05)	60
oxyMb	16.80 (± 0.13)	16.32 (± 0.04)	50
SMb (oxyMb + H_2S)	16.70 (± 0.38)	15.98 (± 0.02)	50

Table 3-1. Structural parameters determined by Guinier approximation and indirect Fourier transformation of SAXS/WAXS data. (Table taken, and reprinted from publication: Sulfmyoglobin Conformational Change: A Role in the Decrease of Oxy-myoglobin Functionality; Elddie Román-Morales, Erika López-Alfonzo, Ruth Pietri, and Juan López-Garriga; *Biochemistry and Biophysics Reports* (2016) 7: 386-393 DOI: 10.1016/j.bbrep.2016.07.002 with permission from publisher Elsevier)

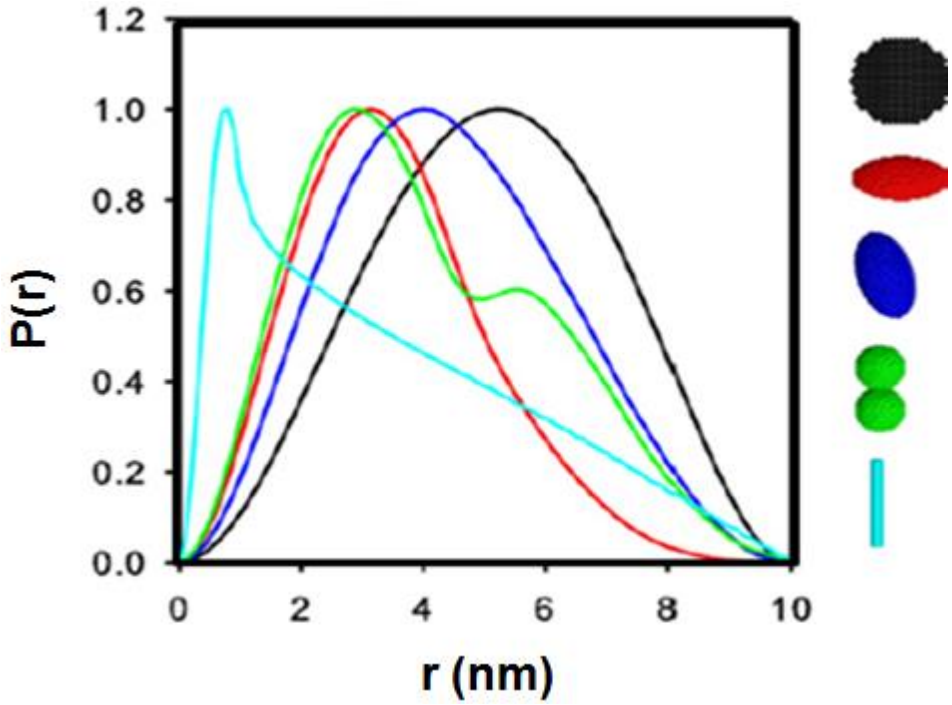

Figure 3-4. P(r) function grants a real space representations of the scattering data, providing an approximation of the shape and dimension of a protein in solution. (Image taken, modified, and reprinted from publication: Structural Characterization of Proteins and Complexes using Small-angle X-ray Solution Scattering; Haydyn D.T. Mertens and Dimitri I. Svergun; *Journal of Structural Biology* (2010) 172: 128-141 DOI: 10.1016/j.jsb.2010.06.012 with permission 4004730300781 from publisher Elsevier)

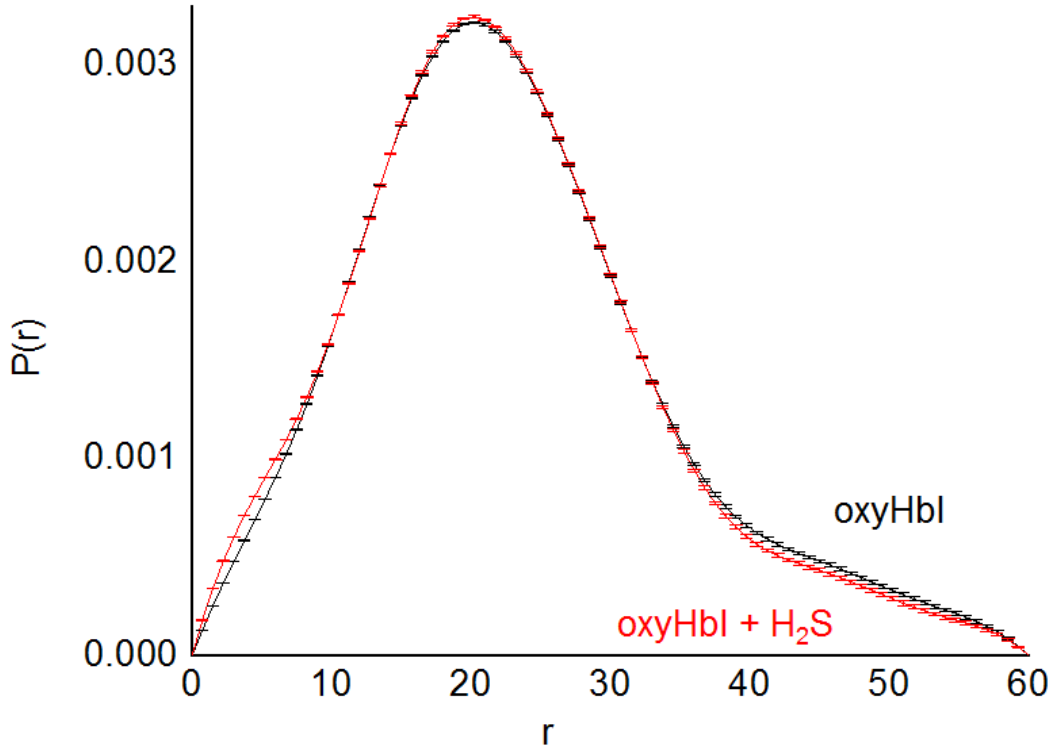

Figure 3-5. *P(r)* plots normalized to *I(0)* (*q* range = 0.024-0.442 $Å^{-1}$ for oxyHbI, 0.039-0.44 $Å^{-1}$ for oxyHbI in the presence of H_2S. (Image taken, modified, and reprinted from publication: Sulfmyoglobin Conformational Change: A Role in the Decrease of Oxy-myoglobin Functionality; Elddie Román-Morales, Erika López-Alfonzo, Ruth Pietri, and Juan López-Garriga; *Biochemistry and Biophysics Reports* (2016) 7: 386-393 DOI: 10.1016/j.bbrep.2016.07.002 with permission from publisher Elsevier)

elongated sphere envelope [66]. There is no significant change in the *P(r)* plot of oxyHbI after the protein has interacted with H_2S, indicating that the presence of H_2S does not alter significantly the envelope or structural conformation of HbI. Figure 3-6 shows the *P(r)* plots of oxyMb (black line) and SMb, formed after interaction of oxyMb with H_2S (red line). Interestingly, the Mb conformation upon SMb complex formation shows a new *P(r)* contour with two distinct peaks. This is characteristic of two predominant regions within the overall globular conformation, as observed for calmodulin and thrombin-like enzymes [72, 73]. Thus, the data suggest that SMb induces internal structural fluctuations, generating two distinctive regions within the overall dimension of the protein [72-75], without inducing a significant change in the overall protein dimension (D_{max}) [74, 76]. Similar *P(r)* profiles have been reported for *Rhinodrilus alatus* and *Glossoscolex paulistus* hemoglobins at basic pH and in the presences of urea respectively. The authors associated the two peaks to unfold and flexible forms of the proteins [77, 78]. In addition, *P(r)* plots displaying two peaks in their contours have been suggested for proteins with U-shape or two-domain envelopes [66, 72, 73]. In this case, it is more likely that the Mb envelope acquires a very small degree of a U-shape or cleft in its global shape upon SMb complex formation. The suggested increase in fluctuation or flexibility observed in the *P(r)* plot can be profoundly evaluated using Kratky and Porod plots.

3.1.3 Kratky and Porod Plots

SAXS/WAXS data is also commonly used to identify protein flexibility. Proteins that vary in flexibility and conformation can be recognized from the scattering data using the Kratky and Porod plots defined by the following equation [59]:

$$V_p = 2\pi^2 I(0)/Q \qquad Q = \int_0^{\infty} q^2 I(q)\,dq \qquad (3)$$

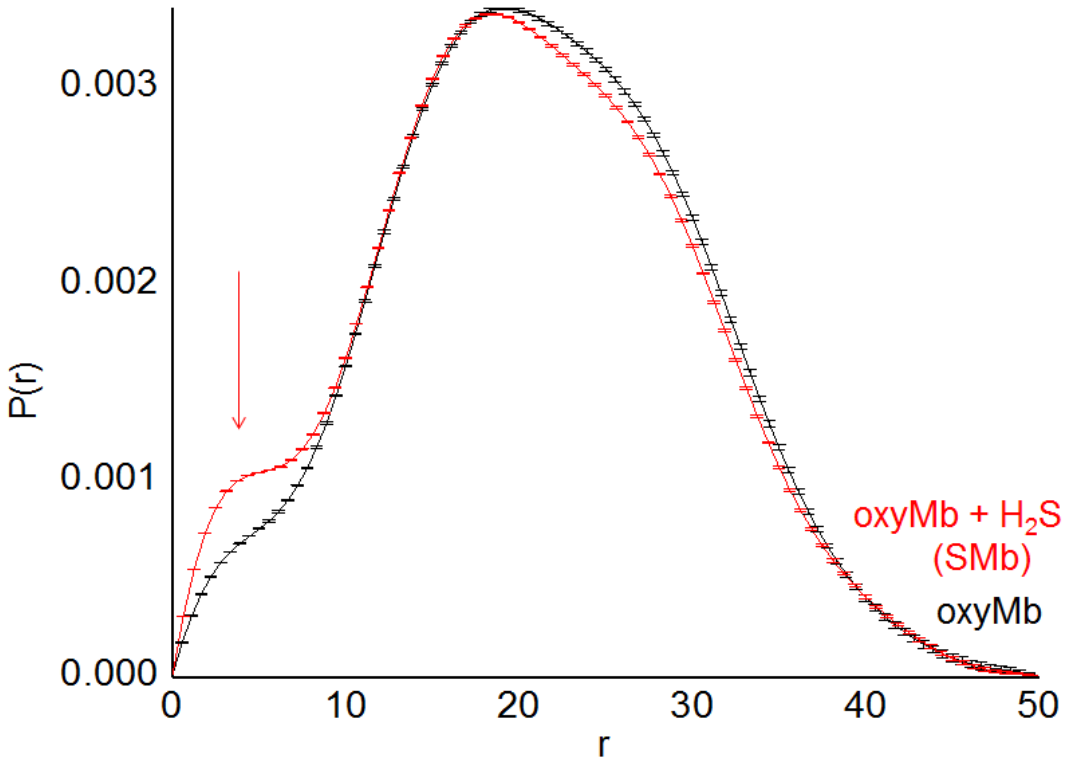

Figure 3-6. *P(r)* plots normalized to *I(0)* (*q* range = 0.025-0.5 $Å^{-1}$ for oxyMb and 0.036-0.05 $Å^{-1}$ for SMb). (Image taken, modified, and reprinted from publication: Sulfmyoglobin Conformational Change: A Role in the Decrease of Oxy-myoglobin Functionality; Elddie Román-Morales, Erika López-Alfonzo, Ruth Pietri, and Juan López-Garriga; *Biochemistry and Biophysics Reports* (2016) 7: 386-393 DOI: 10.1016/j.bbrep.2016.07.002 with permission from publisher Elsevier)

V_p is the hydrated particle volume (e.g. protein) and Q is the Porod invariant, a direct measurement of the density contrast. According to the Kratky analysis, a plot of $q^2I(q)$ vs q should display a bell-shape with a clear maximum for compact globular proteins. Proteins with dual structure (compact and flexible regions) will show at low q a maximum that resembles the order region within the ensemble and at higher q a "tail" that represents the disordered or flexible region [59, 66, 76, 79, 80]. With increasing protein flexibility, the "tail" segment of the Kratky plot will raise, indicating an increase in disordered/flexible structure within the protein conformation. For example, a completely unfolded protein will exhibit a plateau "tail" [76, 79, 81]. On the other hand, the Porod approximation states that a plot of $q^4I(q)$ vs q^4 should display crescent-hyperbolic tendency arriving to a plateau as q increases for compact globular proteins. The loss of plateau suggests an increase in protein flexibility [59, 76]. Overall, Kratky and Porod plots are employed to qualitatively assess the relationship between flexibility and protein volume. Proteins that posses a dual structure with compact and flexible regions within their structural domain can be identified using both approximations [59, 76].

Figure 3-7 shows the Kratky plots of oxyHbI in the absence (black line) and presence of H_2S (red line). A bell-like shape was observed, demonstrating a compact globular protein with some flexibility represented by a "tail" at higher q. The tail rises a little when HbI is in the presence of H_2S, implying an increase in protein flexibility produced by H_2S. Figure 3-8 shows the Kratky plots of oxyMb (black line) and SMb formed by the interaction of oxyMb with H_2S (red line). It also shows a bell-shape with a "tail", indicating a compact globular protein with some flexibility. However, SMb formation clearly produces a "tail" that rises even more. This suggests that the SMb complex induces a greater change in the protein structural conformation

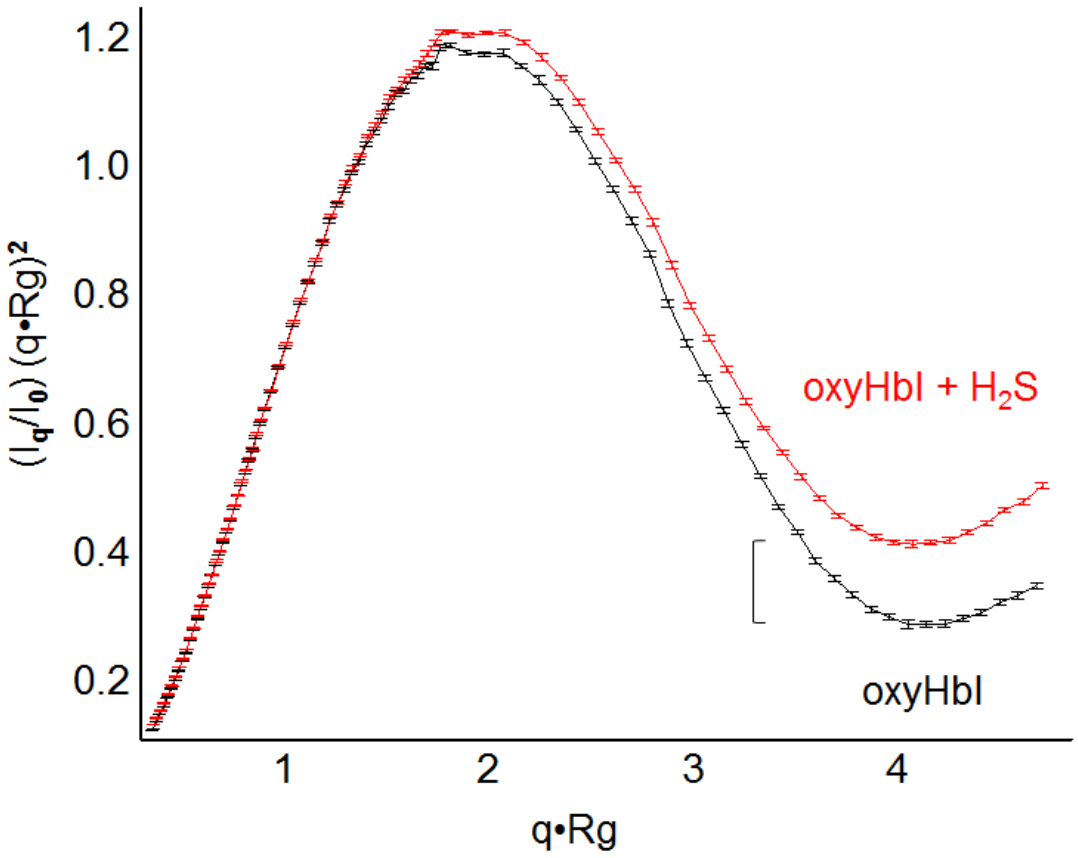

Figure 3-7. Dimensionless *Kratky* plots (*q* range = 0.02-0.26 $Å^{-1}$) of oxyHbI in the absence (black line) and presence of H_2S (red line). (Image taken, modified, and reprinted from publication: Sulfmyoglobin Conformational Change: A Role in the Decrease of Oxy-myoglobin Functionality; Elddie Román-Morales, Erika López-Alfonzo, Ruth Pietri, and Juan López-Garriga; *Biochemistry and Biophysics Reports* (2016) 7: 386-393 DOI: 10.1016/j.bbrep.2016.07.002 with permission from publisher Elsevier)

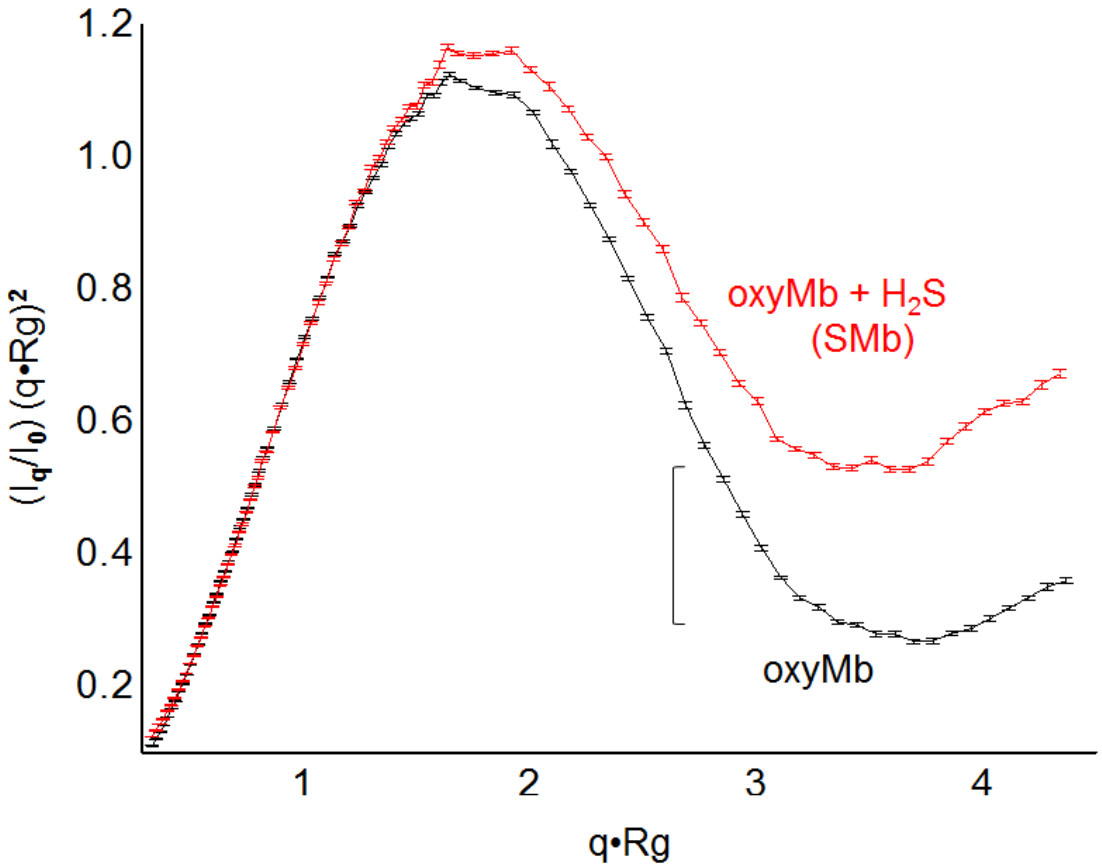

Figure 3-8. Dimensionless *Kratky* plots (*q* range = 0.02-0.26 $Å^{-1}$) of oxyMb (black line) and SMb (red line, product of oxyMb and H_2S interaction). (Image taken, modified, and reprinted from publication: Sulfmyoglobin Conformational Change: A Role in the Decrease of Oxy-myoglobin Functionality; Elddie Román-Morales, Erika López-Alfonzo, Ruth Pietri, and Juan López-Garriga; *Biochemistry and Biophysics Reports* (2016) 7: 386-393 DOI: 10.1016/j.bbrep.2016.07.002 with permission from publisher Elsevier)

where a significant increase in packing flexibility in acquired. Figure 3-9 shows the Porod plots of oxyHbI in the absence (black line) and presence of H_2S (red line). The plots demonstrate the classical hyperbolic shape curve arriving to a plateau as *q* increases, before and after H_2S exposure, indicating no significant change in protein flexibility. Figure 3-10 shows the Porod plots of oxyMb (black line) and SMb formed by the interaction of oxyMb with H_2S (red line). OxyMb demonstrates a classical hyperbolic shape curve arriving to a plateau as *q* increases, characteristic of a globular, compact, and rigid conformation. Interestingly, once the SMb complex is formed, a loss in the plateau is observed representative of a gain in conformational flexibility that is not observed in HbI upon H_2S exposure. This change in protein structural conformation, specifically induced by the SMb formation, is different from the structural change induced by ligand migration towards the protein active site, given that: (1) before H_2S exposure, the protein was in a O_2 saturated environment where structural changes associated to ligand migration through the protein had already occurred and (2) both proteins had the same H_2S exposure. Regarding this, the distinction in the Kratky and Porod plots of both proteins, when expose to H_2S, is due to the SMb formation since HbI does not form the sulfheme complex [21, 22].

Overall, the scattering curves of SMb showed that the peaks at $q>0.2$ are practically unresolved, indicating an increase in protein fluctuations and mobility as a consequence of SMb complex formation. The two peaks in the SMb *P(r)* plot demonstrated changes in internal structural conformation, suggesting formation of a small cleft on the protein envelope with a two distinctive flexible regions. The Kratky and Porod plots supports increase in flexibility, and the decrease in rigidity and compactness.

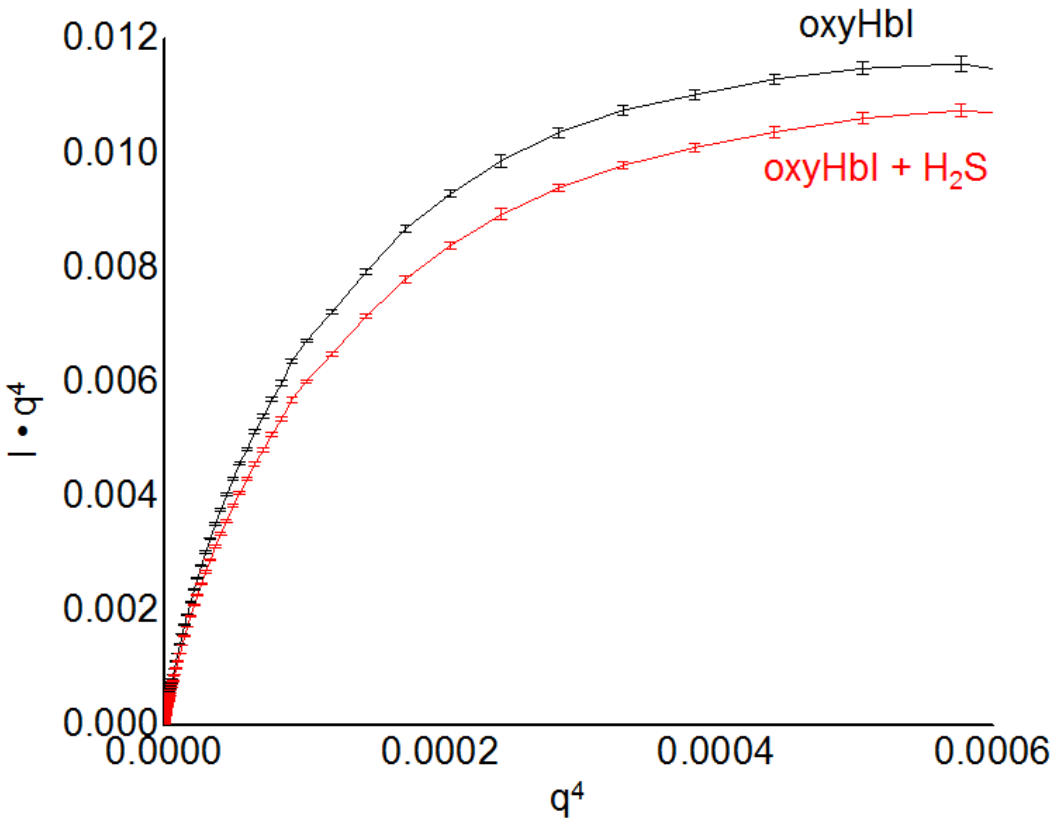

Figure 3-9. *Porod* plots (*q* range = 0.02-0.16 $Å^{-1}$) of oxyHbI in the absence (black line) and presence of H_2S (red line). (Image taken, modified, and reprinted from publication: Sulfmyoglobin Conformational Change: A Role in the Decrease of Oxy-myoglobin Functionality; Elddie Román-Morales, Erika López-Alfonzo, Ruth Pietri, and Juan López-Garriga; *Biochemistry and Biophysics Reports* (2016) 7: 386-393 DOI: 10.1016/j.bbrep.2016.07.002 with permission from publisher Elsevier)

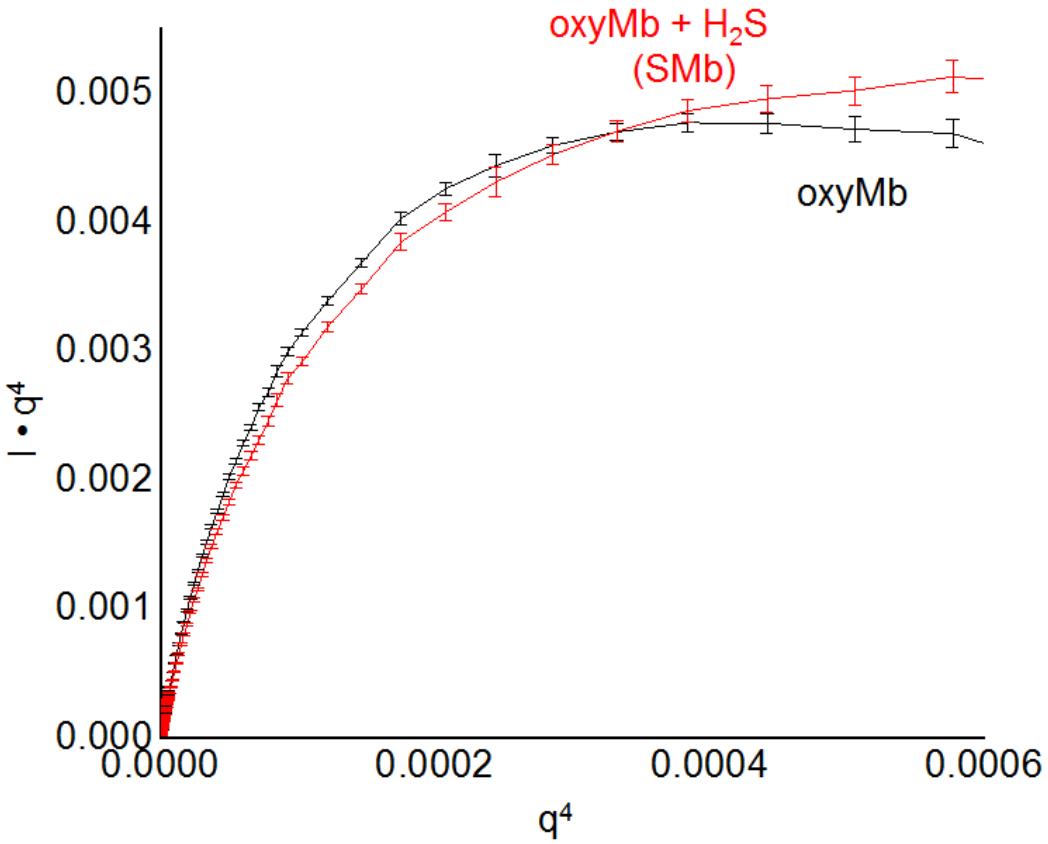

Figure 3-10. *Porod* plots (*q* range = 0.02-0.16 $Å^{-1}$) of oxyMb (black line) and SMb (red line, product of oxyMb and H_2S interaction). (Image taken, modified, and reprinted from publication: Sulfmyoglobin Conformational Change: A Role in the Decrease of Oxy-myoglobin Functionality; Elddie Román-Morales, Erika López-Alfonzo, Ruth Pietri, and Juan López-Garriga; *Biochemistry and Biophysics Reports* (2016) 7: 386-393 DOI: 10.1016/j.bbrep.2016.07.002 with permission from publisher Elsevier)

3.1.4 Three Dimensional Models and Scattering from High Resolution Models

To acquire a visual perspective of the global surface features of SMb conformational effect, three-dimensional surfaces from SAXS/WAXS scattering data were produced for oxyMb and SMb. The three-dimensional scattering surfaces of the proteins were generated using the Dummy Atom Model Minimization method. The algorithm represents a protein as a collection of dummy atoms in a constrained volume with a maximum diameter defined experimentally by D_{max}. It employs simulated annealing to generate the three-dimensional surface, and it calculates the scattering curve of the surface to evaluate its discrepancy (χ^2) with the experimental data (Equation 4) [66].

$$\chi^2 = \frac{1}{N-1}\sum_{i=1}^{N}\left(\frac{I_{\exp}(q_i) - cI_{calc}(q_i)}{\sigma(q_i)}\right)^2 \qquad (4)$$

Here $I_{exp}(q)$ and $I_{calc}(q)$ are the experimental and computed profiles, respectively, $\sigma(q)$ is the experimental error of the measured profile, N is the number of points in the profile, and c is the scaling factor.

Figure 3-11 shows the surfaces of oxyMb and SMb, formed by the interaction of oxyMb with H_2S. The surfaces demonstrated general globular structures and reveal differences in their shapes, where the SMb envelope has a small cleft with two distinct regions. As shown in Figure 3-12, the scattering curves of the three-dimensional surfaces fit the experimental data well, yielding χ^2 values of 0.8 and 2.1 for oxyMb and SMb, respectively. This was also confirmed by the residual analysis of the experimental and calculated scattering curves (Figure 3-13), yielding R^2 values of 0.9998 and 0.9997 for oxyMb and SMb, respectively.

This local change was not observed in the SMb crystallographic structure probably due to the protein constriction that can occur during the process of crystal formation, which does not

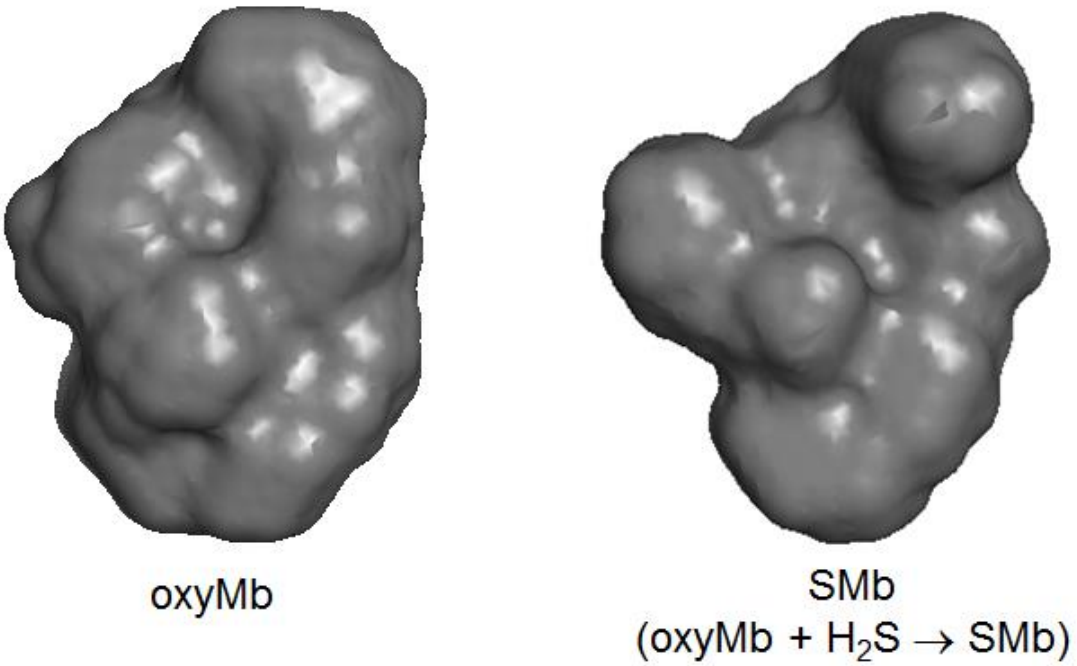

Figure 3-11. SAXS/WAXS three-dimensional surfaces of oxyMb (left) and SMb (right). (Image taken, modified, and reprinted from publication: Sulfmyoglobin Conformational Change: A Role in the Decrease of Oxy-myoglobin Functionality; Elddie Román-Morales, Erika López-Alfonzo, Ruth Pietri, and Juan López-Garriga; *Biochemistry and Biophysics Reports* (2016) 7: 386-393 DOI: 10.1016/j.bbrep.2016.07.002 with permission from publisher Elsevier)

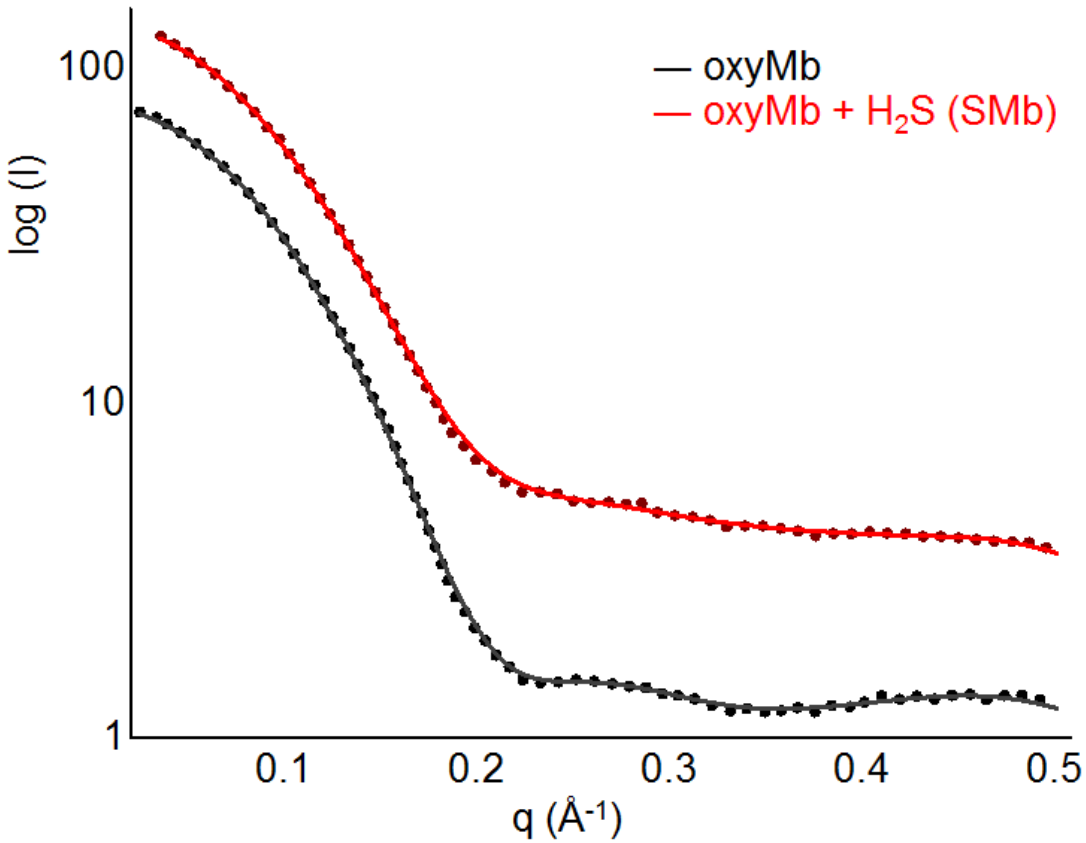

Figure 3-12. Comparison of the experimental SAXS/WAXS data of oxyMb (black-dotted lines) and SMb (red-dotted lines) with the corresponding calculated scattering curves of their theoretical models (solid lines). The *q* range used for the theoretical models was the same as those used in the *P(r)* function. The curves were offset for better appraisal (oxyMb has $x^2 = 0.8$ and $R^2 = 0.99984$; SMb has $x^2 = 2.2$ and $R^2 = 0.99975$). (Image taken, modified, and reprinted from publication: Sulfmyoglobin Conformational Change: A Role in the Decrease of Oxy-myoglobin Functionality; Elddie Román-Morales, Erika López-Alfonzo, Ruth Pietri, and Juan López-Garriga; *Biochemistry and Biophysics Reports* (2016) 7: 386-393 DOI: 10.1016/j.bbrep.2016.07.002 with permission from publisher Elsevier)

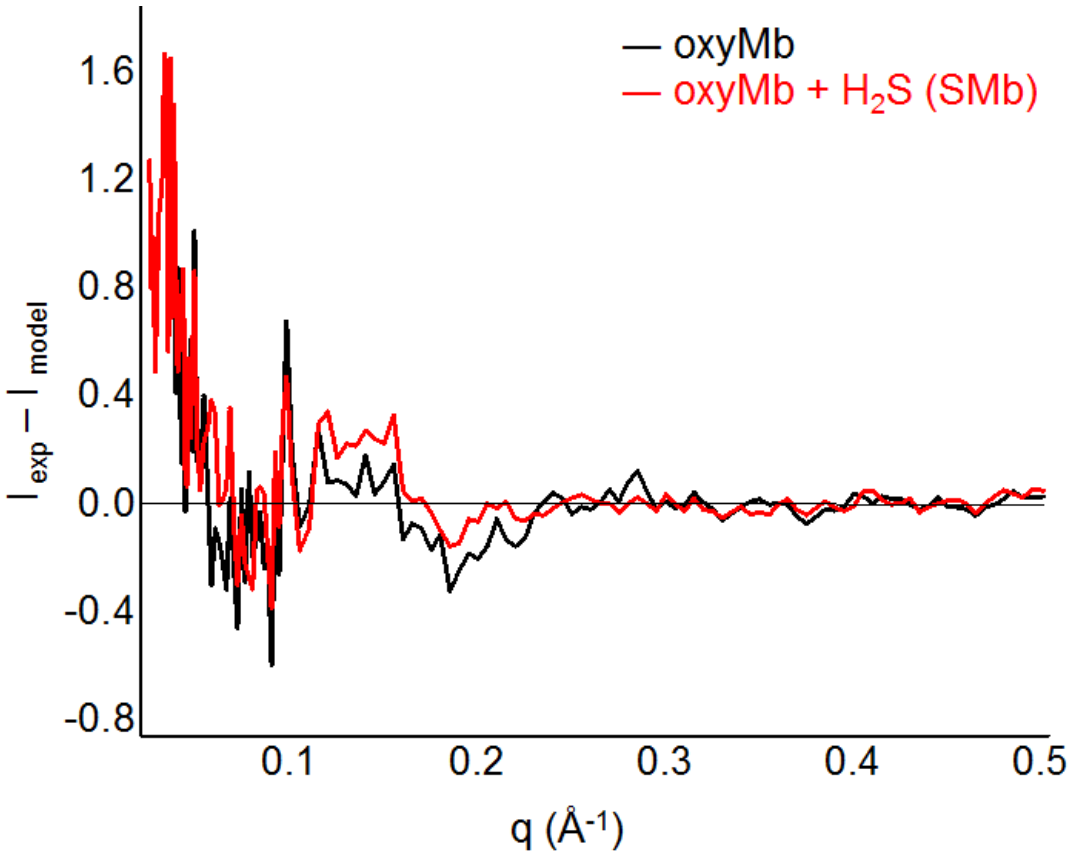

Figure 3-13. Residual plots of the experimental minus the calculated scattering curves of oxyMb (black line) and SMb (red line) theoretical models. (Image taken, modified, and reprinted from publication: Sulfmyoglobin Conformational Change: A Role in the Decrease of Oxy-myoglobin Functionality; Elddie Román-Morales, Erika López-Alfonzo, Ruth Pietri, and Juan López-Garriga; *Biochemistry and Biophysics Reports* (2016) 7: 386-393 DOI: 10.1016/j.bbrep.2016.07.002 with permission from publisher Elsevier)

take place in SAX/WAXS since it is in solution. To corroborate this interpretation, the theoretical scattering curves of oxyMb and SMb atomic models (PDB ID:1MBO and 1YMC, respectively) were obtained using CRYSOL software [65]. The program uses multipole expansion for fast calculation of spherically averaged scattering profile and takes into account the hydration shell. It also compares the theoretical scattering curve with the SAXS/WAXS experimental data by fitting the curves and minimizing the discrepancy. The theoretical scattering curves obtained from the PDB structures were further analyzed to calculate the corresponding theoretical *P(r)* functions. In general, an atomic model that provides a good fit to the data is considered a valid description of the structure in solution.

As Figure 3-14 shows, the theoretical scattering curve of oxyMb atomic model fits the SAXS/WAXS experimental data well, implying similarities of both crystal and solution structures. The corresponding *P(r)* functions support the above suggestion (Figure 3-15). However, Figure 3-16 demonstrates that the theoretical scattering curve of SMb crystal structure poorly correlates with the scattering data of SMb in solution, indicating that the atomic model does not describe well the protein in solution. In fact, the peak at ~4 Å is not so well defined in the theoretical *P(r)* function of SMb atomic model, as shown in Figure 3-17, suggesting that the internal structural fluctuations are hampered by crystal packing forces, which limit the range of conformational motion accessible to the protein.

3.1.5 Further Outlooks and SAX/WAX Summary

Taken together, the data suggest that SMb complex induces a conformational change increasing protein flexibility and fluctuations with decreasing rigidity. This change is specific of SMb and different from conformational change produce by ligand migration or heme Fe-ligand binding. Regarding this, the Mb's Xe cavities have been demonstrated to play a crucial role in

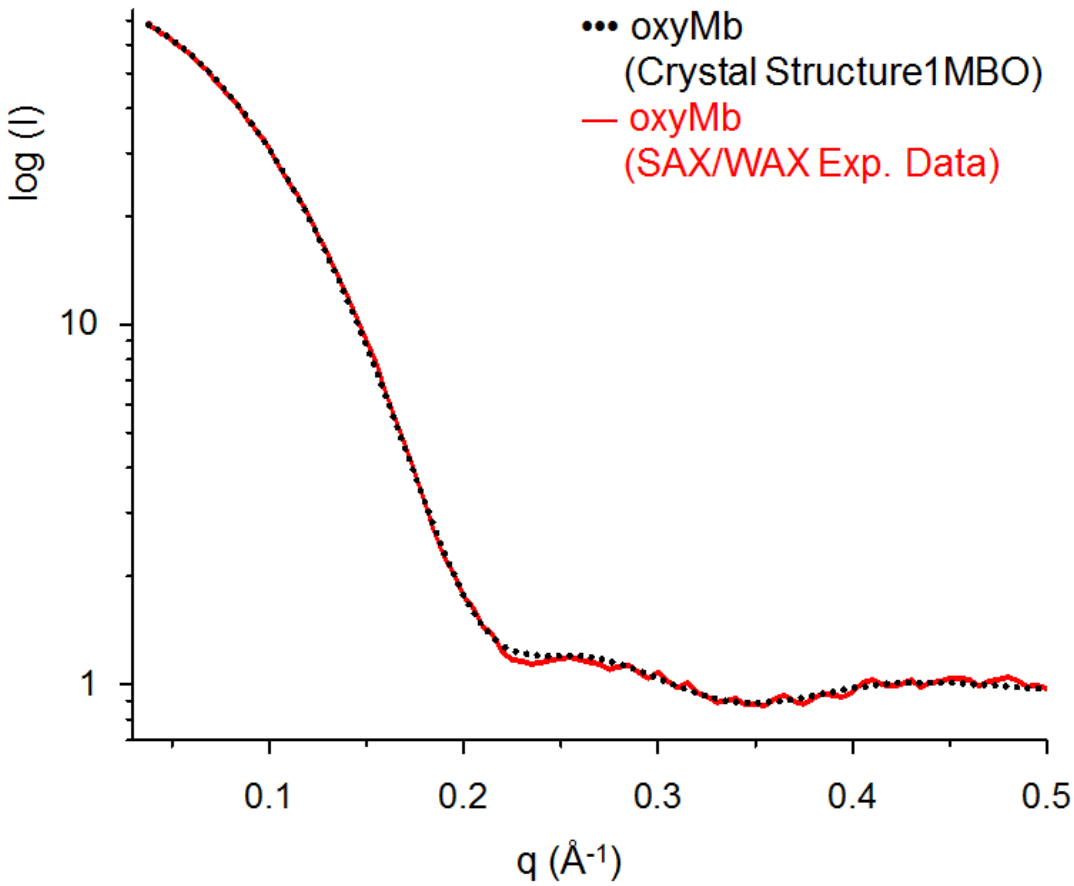

Figure 3-14. Comparison of the SAXS/WAXS scattering curves of the oxyMb from the SAXS/WAXS experimental data (red-line) and crystal structure (black-dotted line), PDB file 1MBO. (Image taken, modified, and reprinted from publication: Sulfmyoglobin Conformational Change: A Role in the Decrease of Oxy-myoglobin Functionality; Elddie Román-Morales, Erika López-Alfonzo, Ruth Pietri, and Juan López-Garriga; *Biochemistry and Biophysics Reports* (2016) 7: 386-393 DOI: 10.1016/j.bbrep.2016.07.002 with permission from publisher Elsevier)

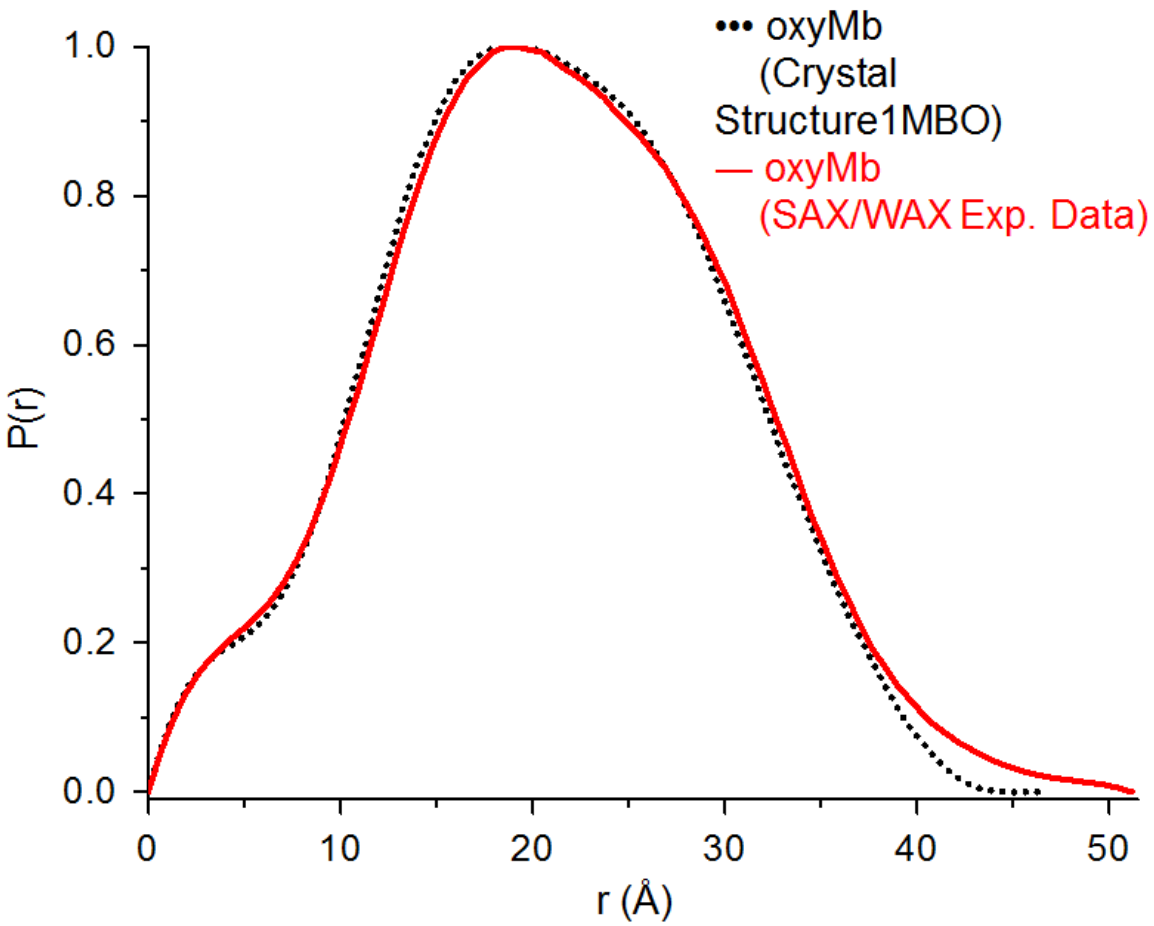

Figure 3-15. Comparison of the SAXS/WAXS corresponding P(r) plots of the oxyMb from the SAXS/WAXS experimental data (red-line) and crystal structure (black-dotted line), PDB file 1MBO. (Image taken, modified, and reprinted from publication: Sulfmyoglobin Conformational Change: A Role in the Decrease of Oxy-myoglobin Functionality; Elddie Román-Morales, Erika López-Alfonzo, Ruth Pietri, and Juan López-Garriga; *Biochemistry and Biophysics Reports* (2016) 7: 386-393 DOI: 10.1016/j.bbrep.2016.07.002 with permission from publisher Elsevier)

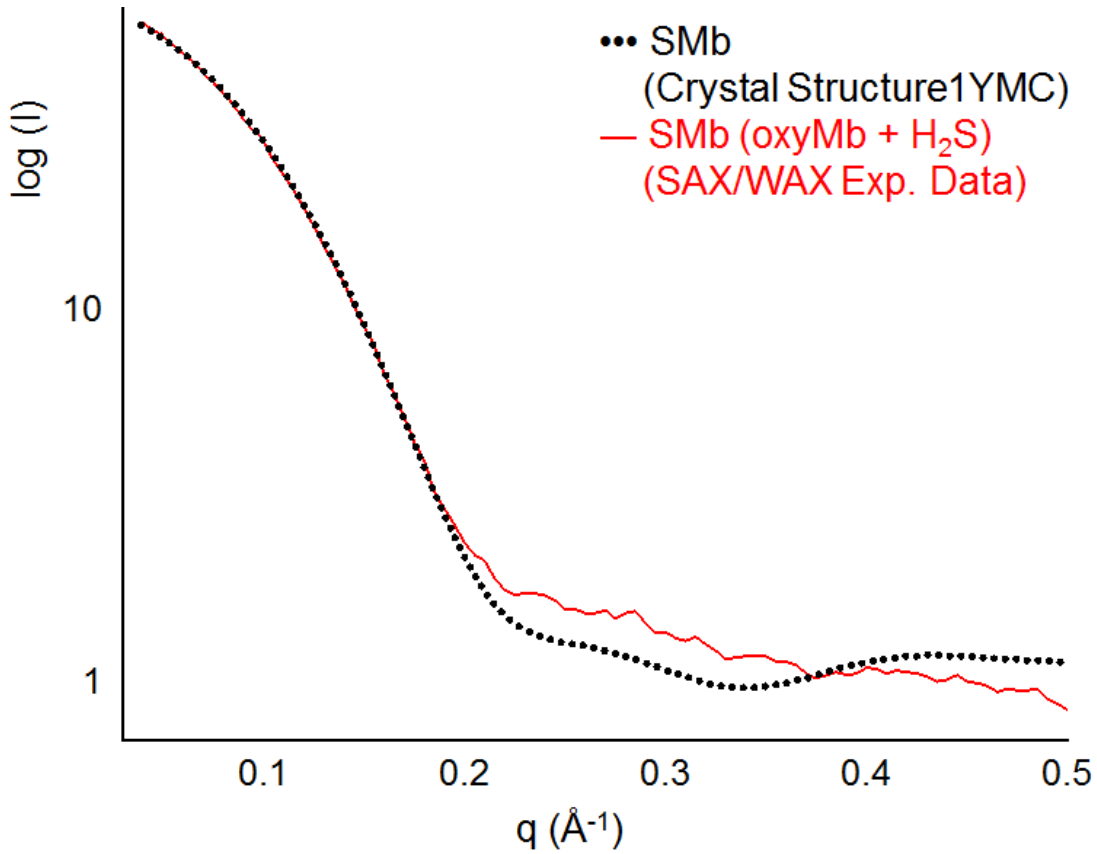

Figure 3-16. Comparison of the SAXS/WAXS scattering curves of the SMb from the SAXS/WAXS experimental data (red-line) and crystal structure (black-dotted line), PDB file 1YMC. (Image taken, modified, and reprinted from publication: Sulfmyoglobin Conformational Change: A Role in the Decrease of Oxy-myoglobin Functionality; Elddie Román-Morales, Erika López-Alfonzo, Ruth Pietri, and Juan López-Garriga; *Biochemistry and Biophysics Reports* (2016) 7: 386-393 DOI: 10.1016/j.bbrep.2016.07.002 with permission from publisher Elsevier)

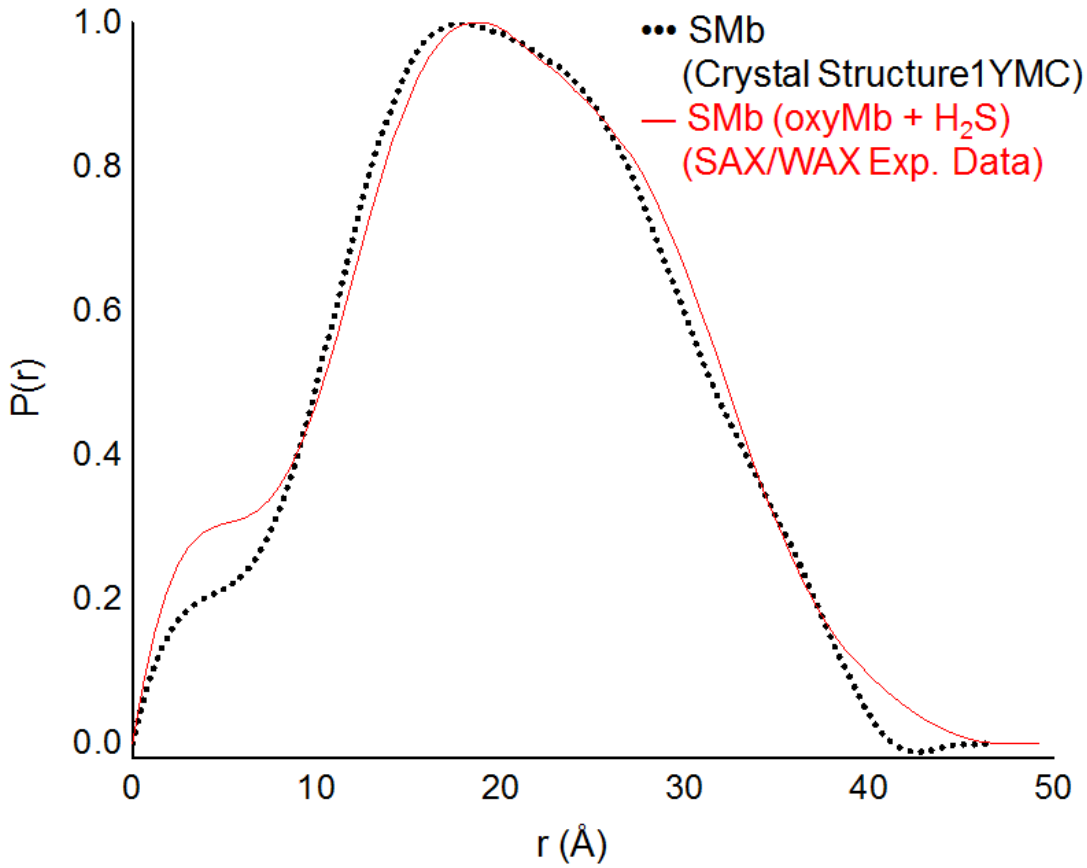

Figure 3-17. Comparison of the SAXS/WAXS corresponding P(r) plots of the SMb from the SAXS/WAXS experimental data (red-line) and crystal structure (black-dotted line), PDB file 1YMC. (Image taken, modified, and reprinted from publication: Sulfmyoglobin Conformational Change: A Role in the Decrease of Oxy-myoglobin Functionality; Elddie Román-Morales, Erika López-Alfonzo, Ruth Pietri, and Juan López-Garriga; *Biochemistry and Biophysics Reports* (2016) 7: 386-393 DOI: 10.1016/j.bbrep.2016.07.002 with permission from publisher Elsevier)

the protein functionality by regulating ligand entry and release from the active site [15-17]. The ligand migration in the cavity produces a structural expansion of the cavity itself follow-on by gating motions of the surrounding residues that leads to a self-opening of the migrating channel [17]. The cavity comes back to its original volume once the ligand has left the cavity, mimicking a breathing motion [17, 82]. The final channel is created by the rotating motion of the distal His opening the gate toward the active heme site [17]. Any change in the size and shape of these pockets directly affects the Mb function, which results in significant physiological effects [15-17]. Olson *et al*. [16] demonstrated that a decrease in the size of the cavity produced a more rigid and compact packing. As a result, it lowers the rate of ligand capture by making it difficult for the ligand to arrive to the active site. However, if the ligand is able to arrive to the active site, dissociation is even more difficult since the ligand is "trapped" in the active site, leading to an overall increase in O_2 affinity [16]. Upon SMb formation, the opposite is observed, a decrease in O_2 affinity. On this basis, we propose that the observed changes in conformation and increase in protein flexibility play a role in the decrease in O_2 affinity by SMb, in addition to the reported local structural change on the heme. These structural changes would facilitate ligand entry but destabilize even more ligand bonding, leading to an overall decrease in O_2 affinity.

Furthermore, in addition to the heme-Fe ligand transport, it has been suggested that the conformational cavities are capable of carrying additional ligands, such as NO, giving Mb higher carrying capacity than (1:1) stoichiometry and further physiological roles (e.g. scavenger) [14-17, 82]. In this study we demonstrated that the inner structure of Mb is altered by the formation of SMb by increasing protein flexibility, movement, and fluctuation. On this basis, considering the constant ligand competition and the increase in protein flexibility of SMb, enhancement of

H_2S entry and O_2 displacement may be possible. This could lead to a plausible H_2S transports flux, in addition to the known rapid diffusive flux of free H_2S.

The nature of the proteins should be further studied, given that, it is intriguing that a protein whose functionality is H_2S transport does not suffer a significant conformational change while a protein whose "main functionality" is O_2 storage and transport suffers significant conformational change, when exposed to H_2S. Furthermore, it opens the door to explore the conformation change associated with the reaction of oxy-Hemoglobin with H_2S, which only shows a decrease in O_2 affinity of 135 folds [46], suggesting that cooperativity may play an important role in protecting oxy-Hemoglobin functionality

3.2. Local Structure Evaluation

The local SMb complex characterization was focused on evaluating the heme-Fe environment to identify the possible ligands that are naturally bound to the heme-Fe once the SMb complex is formed, which provides an additional obstacle and competition for the O_2-heme Fe interaction and protein functionality. Electron paramagnetic resonance (EPR) is one of the techniques used to characterize metalloproteins since it measures the discrete energy difference between the lower and higher energy states, therefore, gaining information about the protein structure and chemical environment as observed with any absorption spectroscopy technique. However, it is sensitive to only paramagnetic (unpaired electron) samples given that the evaluated energy difference is due to the interaction of unpaired electron with an applied magnetic field (B_0). The sample is irradiated with a set microwave frequency while changing the magnetic field [83].

The applied magnetic field induces the separation of the two degenerated energy states producing two states with different energies. The magnetic moment (μ) of the electron is aligned with the applied magnetic field (B_0) in the lower energy state ($m_s = -1/2$) and against the applied magnetic field in the higher energy state ($m_s = +1/2$) ($\mu = m_s g\beta$, where β is the conversion constant of Bohr magneton and g is the g-factor of an electron). An electron in a molecule also possesses an orbital angular momentum (L) that affects the energy between the electron states. This means that the electron also feels a second magnetic field produced by an orbiting positive charge (nucleus) and/or second orbiting negative charge (second unpaired electron) leading to what is known as the spin-orbit coupling that depends on their relative orbital orientations and distances. The above mention conditions determine the degree of separation between the energy levels when an external magnetic field is applied, and is defined by Equation 5:

$$\Delta E = h\upsilon = g\beta B_0 \qquad (5)$$

where h is Planck constant, υ is the applied constant frequency, and B_0 is the applied magnetic field (that can be measured). Given that, the g-factor peak arises when the magnetic field energy is equal to the energy difference of the two spin states, so that their corresponding energy matches the energy of the microwave radiation as illustrated in Figure 3-18. Therefore, the chemical information of the nature of the bond between the electron and the molecule is obtained through the g-factor value [83]. Thus, a change in the g value indicates a change in the chemical environment surrounding the electron, hence, the heme-Fe atom. A low spin specie is define as a strong metal-ligand interaction. It has fewer unpaired electron since the crystal field splitting energy is greater than the electron pairing energy. Hence, electrons will fill up all the lower energy orbitals first and pair with electrons in these orbitals before moving to the higher energy orbitals [83]. Therefore, a change in electron spin will require higher magnetic field energy. On the other hand, high spin specie is defined as a weak metal-ligand interaction. It has more unpaired electron since the pairing energy is greater than the crystal field energy, the electrons will occupy all the orbitals first and then pair up [83]. Consequently, a change in electron spin will require less magnetic field energy.

Different SMb-Ligand (SMb-L) complexes were characterized by Berzofsky et al. using EPR spectroscopy [26]. They manipulated the SMb samples to bind different types of ligands to the sulfheme-Fe. At room temperature, the EPR spectra of all SMb samples were essentially high spin species with g values around 6. However, the EPR spectra of frozen SMb samples showed a general axial symmetric (D_{4h}; $g_x = g_y > g_z$) EPR spectra of a high spin species at g = 6 with

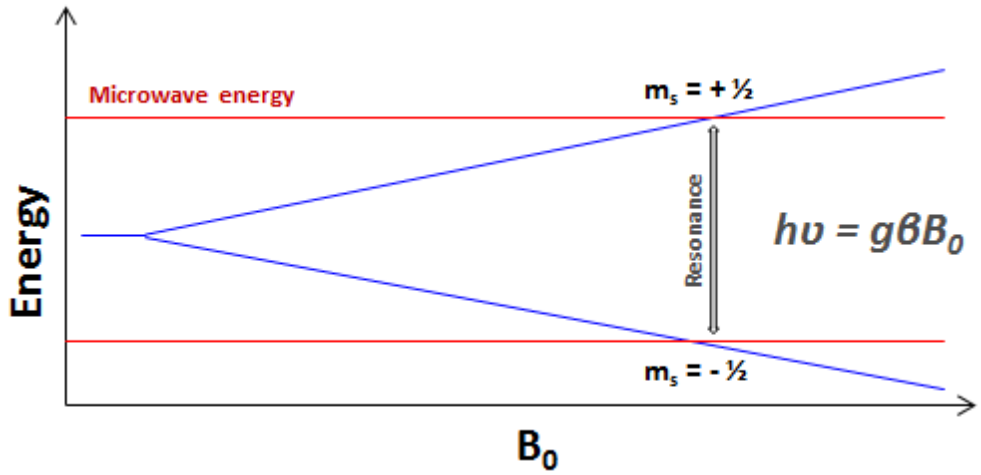

Figure 3-18. Electron resonance. The magnetic field energy equals the energy difference of the two spin states, and their corresponding energy matches the energy of the microwave radiation.

rhombic symmetric (C_{2v}; $g_x \neq g_y \neq g_z$) low spin components around g = 2. Each Mb-L and SMb-L complex had characteristic low field EPR resonances producing different g values [26, 84]. Table 3-2 and Figure 3-19 show the corresponding low field g values of the Mb-L and SMb-L complexes characterized by Berzofsky et al. that were observed in our study. Figure 3-20 illustrate a scheme of the potential routes for all possible protein-ligand complexes that may be observed in the interaction of met-Mb with H_2O_2 and H_2S.

3.2.1 Control samples evaluation

EPR spectra of met-Mb, met-Mb in the presence of H_2O_2, and met-Mb in the presence of only H_2S were obtain and considered as controls of the reaction for the SMb complex formation. The concentration ratio of [Mb:H_2O_2:H_2S] was [1:1:1] to have a closer recreation of what would be observe physiologically, but with enough reactants to produce sufficient SMb-ligand concentration to enable their clear detection and analysis. Figure 3-21 illustrates the EPR high and low field regions of met-Mb in the absence of H_2O_2 and H_2S. The characteristic axial symmetry ($g_x = g_y < g_z$) EPR spectra of the met-Mb complex was observed with its corresponding high and low field g values around 6.0 and 2.0, respectively [85]. Figure 3-22 demonstrates the EPR high and low field regions of met-Mb in the presence of H_2O_2 with a [1:1] concentration ratio of [Mb:H_2O_2]. It is known that the interaction of met-Mb with H_2O_2 has a reaction rate of 6 x 10^2 $M^{-1}s^{-1}$ [86-88] and generates the cation-radical intermediate Comp I, which subsequently grabs an electron from the protein to produce the "stable" Comp II. As a consequence, radicals in the protein are produced. This is evidenced by the presence of the characteristic "protein radical" peak at g = 2 that has been suggested to be produced by a tyrosyl radical resonance [85, 88, 89]. Also, a decrease in intensity of the met-Mb high field peak at g = 6 is observed since the met-complex is been consumed in the reaction with H_2O_2 to form the ferryl species Comp I and II.

Ligand	Ferric-Mb			Ferric-SMb			
	g_1	g_2	g_3	g_1	g_2	g_3	g_4
H_2O				2.50	2.26	1.83	2.0
H_2S	2.56	2.25	1.83	2.38	2.26	1.91	

Table 3-2. EPR low spin g values of Mb and SMb [26, 84, 90].

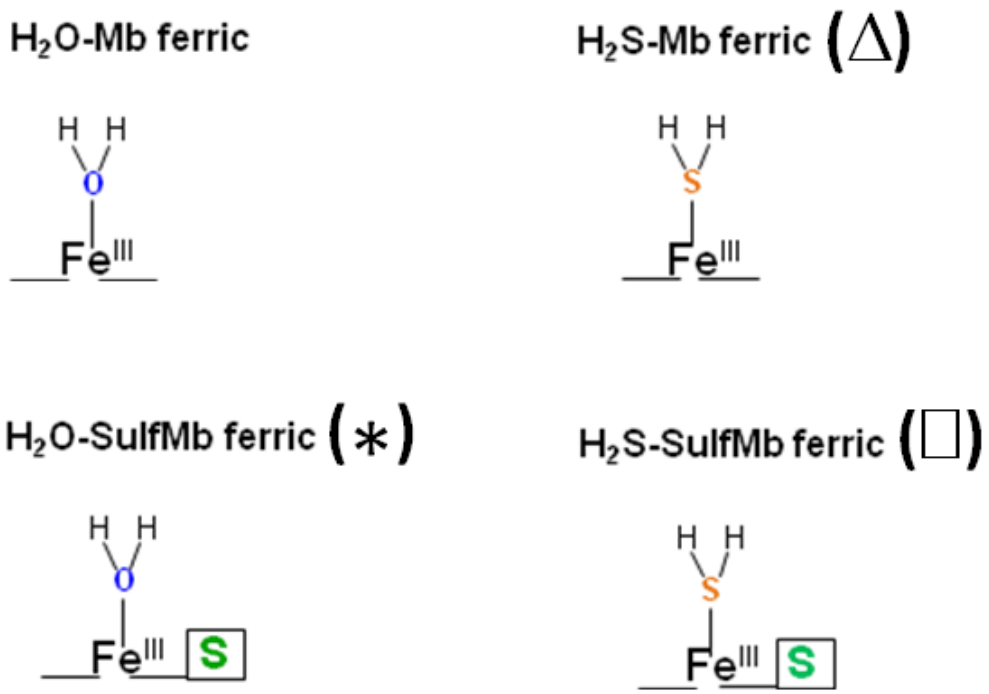

Figure 3-19. Observed Mb and SMb species in EPR [26, 84, 90]. (The S symbol represents the sulfur ring. The H_2O-SMb complex is represented by an (∗), the H_2S-SMb complex is represented by an (□), and the H_2S-Mb complex is represented by an (∆) in the EPR spectra shown ahead).

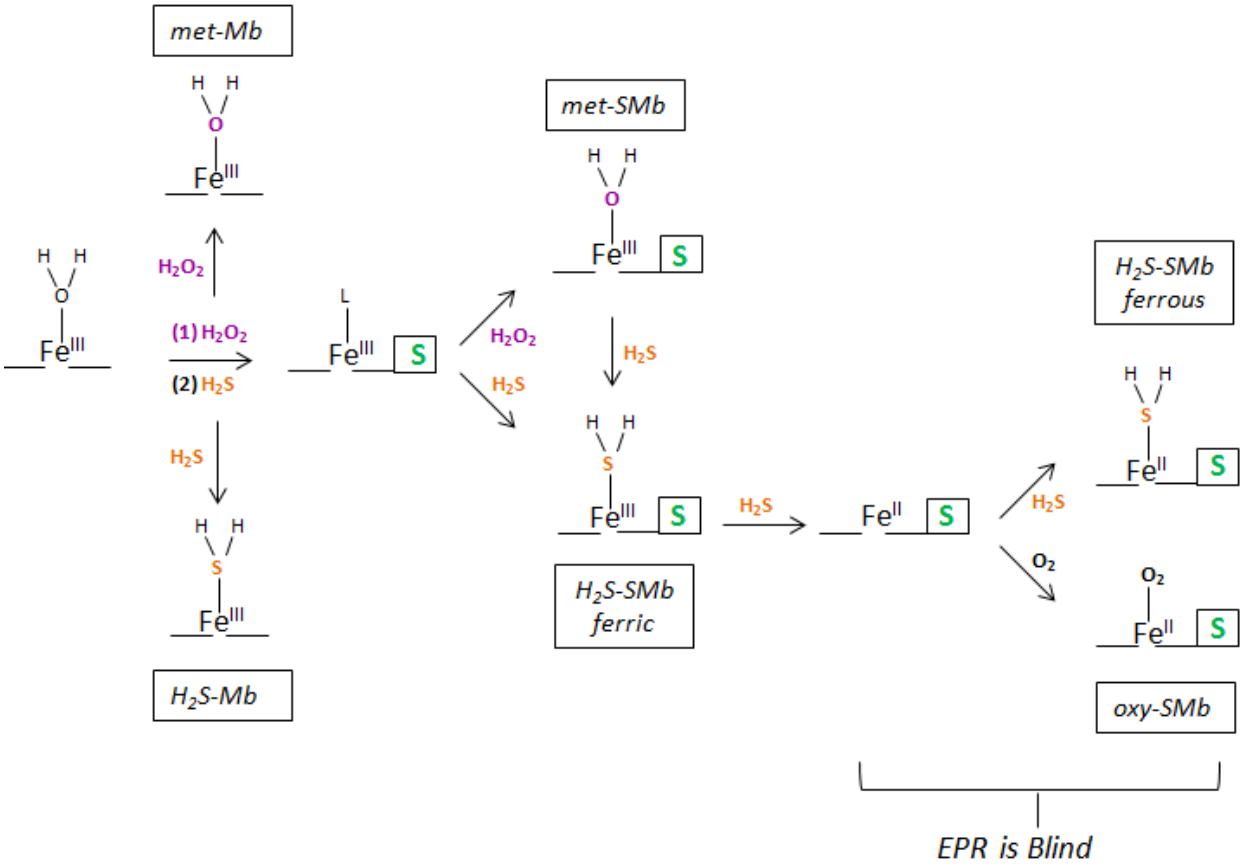

Figure 3-20. Scheme of the all possible protein-ligand complexes and their corresponding routes that may be observed in the interaction of met-Mb with H_2O_2 and H_2S.

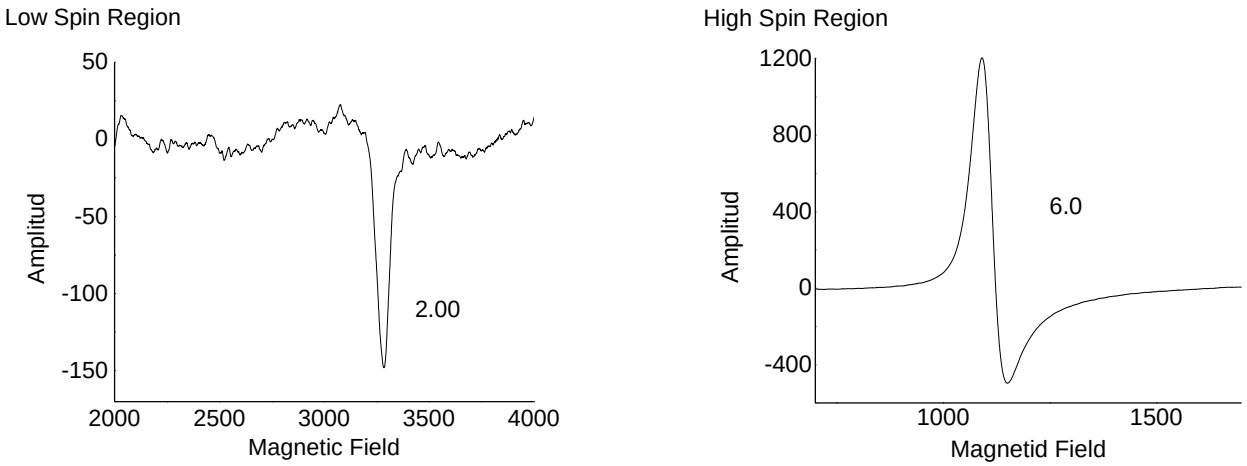

Figure 3-21. EPR high and low fields spectra of met-Mb [85].

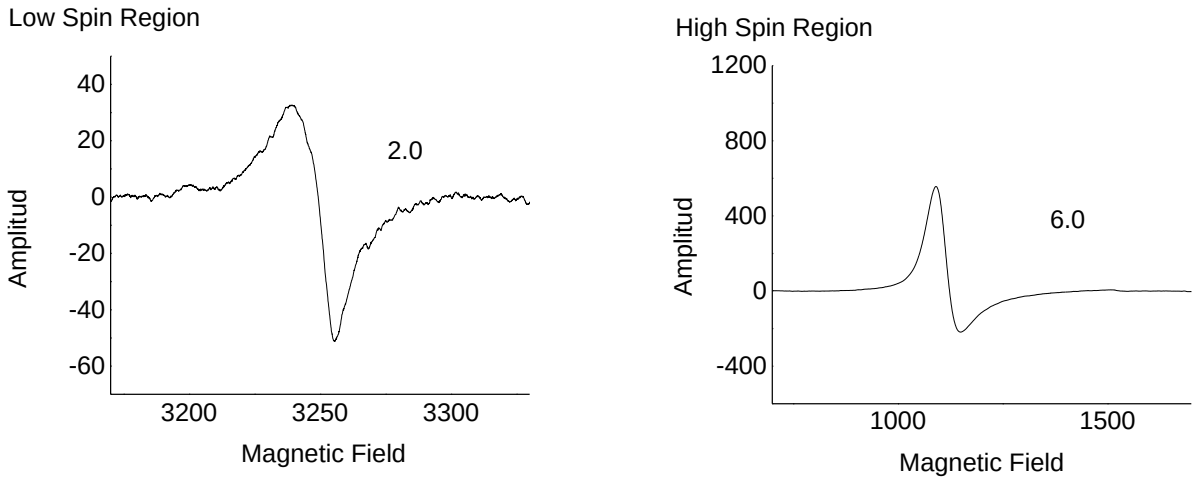

Figure 3-22. EPR high and low field spectra of met-Mb in the presence of H_2O_2 with a [1:1] concentration ration of [Mb:H_2O_2] [85, 88, 89].

Given that the reaction has a concentration ratio of [1:1], not all of the H_2O_2 migrate to the active site of all the Mb proteins to ensure the complete transformation of met-Mb to the ferryl species. That is why the signal at g = 6 of the met-Mb complex is still clearly observed. The met-Mb g resonance at 2.0 is probably also present; however, it overlaps the radical signal that is much larger and would overwhelm it. Figure 3.23 shows the EPR spectra of met-Mb in the presence of H_2S with an [1:1] concentration ratio of [Mb:H_2S]. The characteristic rhombic symmetric EPR spectra of the H_2S-Mb complex with g values at 2.56, 2.26, and 1.91 [26, 90] were observed, in addition to the residual of un-reactive met-Mb at g = 2. The interaction of Mb with H_2S has a reaction rate of approximately 1.5×10^3 $M^{-1}s^{-1}$ [90].

Given that H_2S is a dissolved gas, in solution it maintains equilibrium between the air/atmosphere (undissolved gas) and water (dissolved gas). At the same time, it maintains equilibrium between the H_2S and SH^- species ($H_2S \Leftrightarrow HS^-$), where the abundance of each sulfur specie depends on the pH of the solution. At pH = 6.5, approximately 80-70% of the sulfur specie present in solution is H_2S and 30-20% is HS^- [1, 19, 20, 25, 91-99]. To evaluate the effect that this would have on the H_2S-Mb complex formation, more H_2S was added to the met-Mb sample compensating for the loss of H_2S as consequence of pH and head space; resulting in a "real" [1:1] concentration ratio of [Mb:H_2S]. Figure 3-24 shows the EPR high and low field regions of the product from the reaction of met-Mb and H_2S at a "real" [1:1] concentration ratio. Additional decrease in the intensity of the high field band indicates that more met-Mb has reacted with H_2S to form the H_2S-Mb complex. This is of no surprise since there is more H_2S in solution available for reaction, which increases the probability of H_2S molecules reaching more Mb's active sites. However, a decrease in the intensity of the characteristic g values of the H_2S-Mb complex suggests that the increase in H_2S concentration activates the reduction capacity of

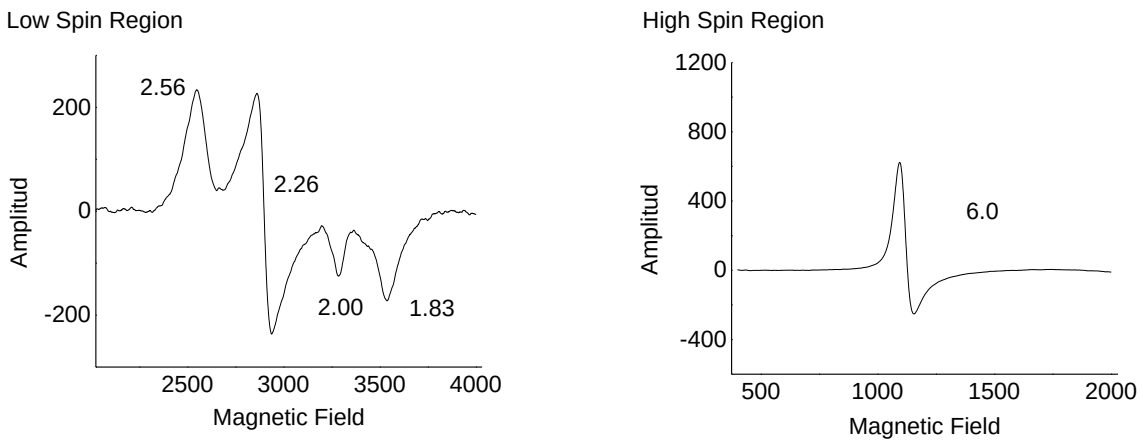

Figure 3-23. EPR spectra of met-Mb in the presence of H_2S with an [1:1] concentration ratio of [Mb:H_2S] [26, 84, 90].

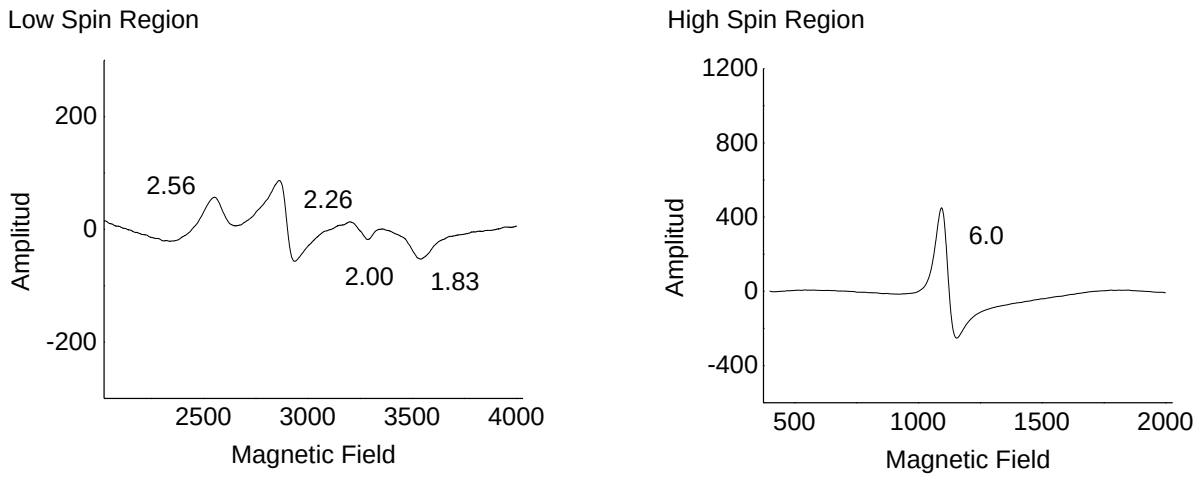

Figure 3-24. EPR spectra of the reaction between met-Mb with H_2S at a "real" [1:1] concentration ratio [26, 84, 90].

H_2S, leading to the reduction of the ferric heme-Fe to ferrous heme-Fe and loss in signal intensity [19, 20]. Apart from the expected heme-Fe reduction induce by the increase H_2S concentration in solution, no significant change in the Mb-L product formation can be observed.

3.2.2 Effect of pH on the SMb-ligand complexes formation

The effect of the pH in a protein may have a significantly impact not only on the protein reaction and products formation, but also on the protein structure given that it involves a change in protonation and/or deprotonation of the molecules within the protein and the reactants. Therefore, the generated species during the reaction of the SMb formation and their abundance may vary with change in pH. EPR data of the SMb products would provide insights of this inquiry.

It has been suggested that the SMb formation rate increases with decreasing pH, thus, its concentration also increases with decreasing pH [37]. Its reaction rate at pH = 6 is approximately 2.5 x $10^6 M^{-1}s^{-1}$ [37]. All previous analysis were performed at pH = 6.5 in order to obtain higher SMb complex concentration, to facilitate the detection and analysis of the complex without inducing significant perturbation of the protein stability and structure. At pH = 6.5, approximately 80-70% of the dissolved sulfur specie is H_2S and the distal histidine involved in the formation of the SMb complex is protonated [49, 50]. Figure 3-25 shows UV-Vis spectra of ferric SMb derivate formation after the interaction of met-Mb with H_2O_2 and H_2S in a [1:1:1] concentration ratio at pH of 6.5, as indicated by the presence of the band around 720 nm. Only the evaluation of the high field signals yielded discrimination between the SMb species since all SMb products showed a similar low field EPR resonance peak around g = 6 [26], which also coincided with the unreacted met-Mb complex signal. Figure 3-26 shows the EPR high field region of the interaction of met-Mb with H_2O_2 and H_2S in a [1:1:1] concentration ratio at pH of

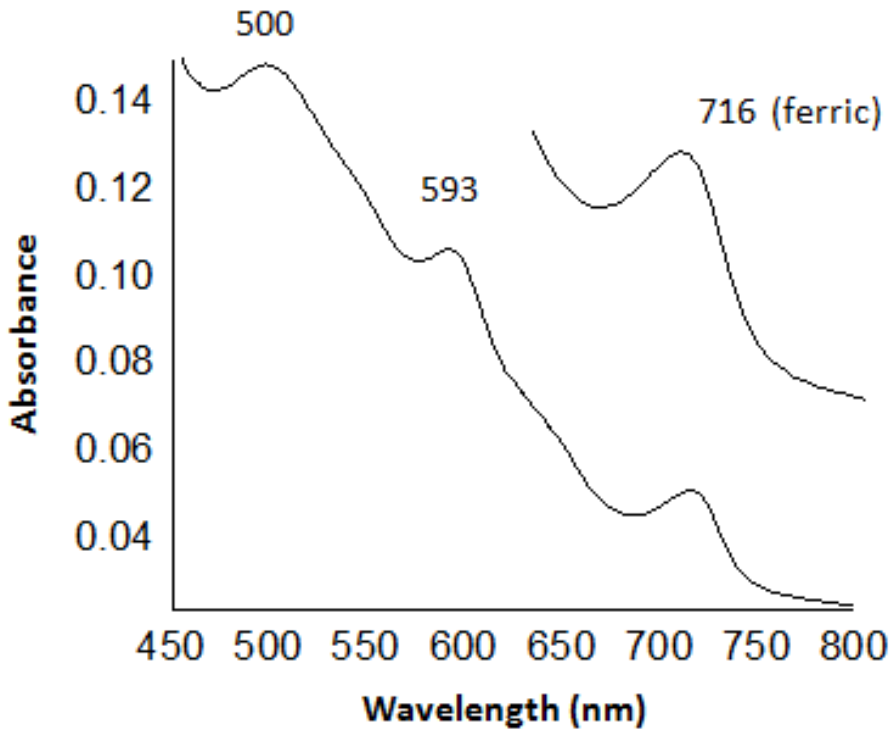

Figure 3-25. Formation of the ferric SMb species obtained from the interaction of met-Mb with H_2O_2 and H_2S in a [1:1:1] concentration ratio at pH of 6.5.

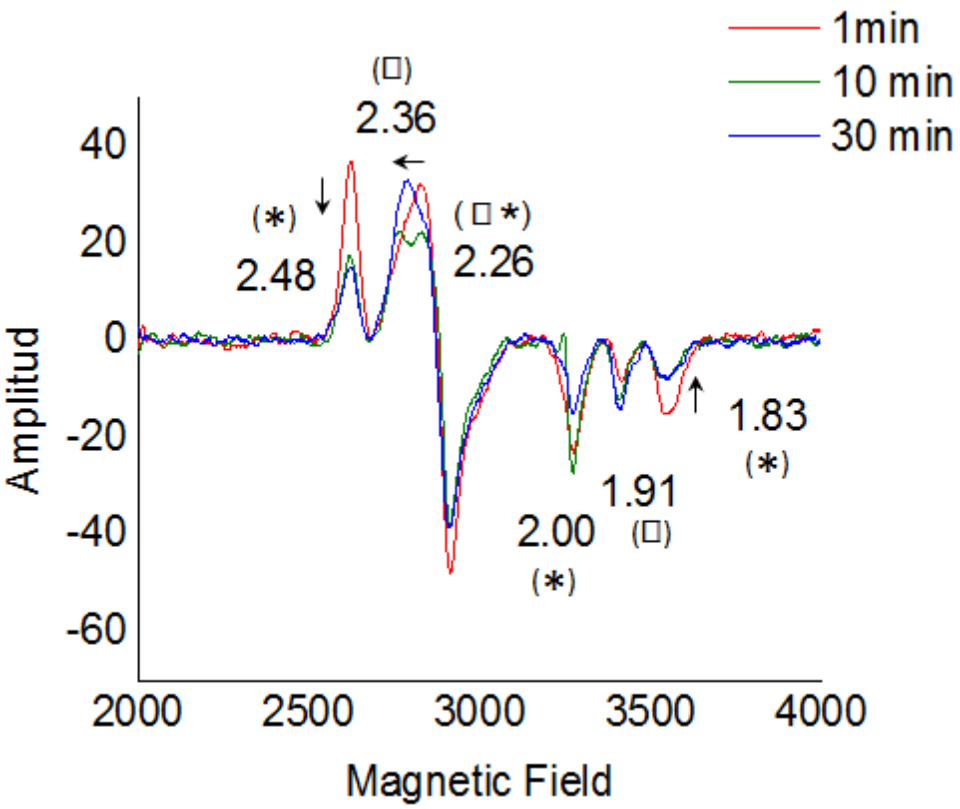

Figure 3-26. High field region of the species formed through time when met-Mb reacts with H_2O_2 and H_2S in a [1:1:1] concentration ratio at a pH of 6.5. (H_2O-SMb complex is represented by an (∗) and the H_2S-SMb complex is represented by an (□)**).**

6.5 at 1, 10, and 30 minutes of reaction. The H_2O-SMb complex signals were observed with g values at 2.48, 2.26, and 1.83. The g value at 2.0 may be a mixture of the residual unreacted met-Mb and the H_2O-SMb complex signals. A peak at g = 1.91 corresponding to H_2S-SMb complex was also present at that time. The other g values (2.26 and 2.36) characteristic of the H_2S-SMb complex are probably also present but are most likely coinciding or overwhelmed (respectively) by the H_2O-SMb complex signal at g = 2.26. After 10 min of interaction, a new band characteristic of the H_2S-SMb complex with g = 2.36 resonance was observed, which later defined and increase in intensity after 30 min of interaction. The decrease in intensity through time of the 2.48 and 1.83 bands, in addition to the presence and definition of the bands at 1.91 and 2.36, respectively, suggests the conversion of the H_2O-SMb complex to the H_2S-SMb derivate. It is important to remember that the incorporated sulfur atom across the β-β double bond has electron withdrawing density capacity, reducing the electron density of the heme-Fe. Therefore, the heme-Fe will have a stronger interaction with an electron donating atom. Sulfur is less electronegative than oxygen, and as a result, it is a better electron donating atom. Thus, it is no surprise that H_2S molecule displaced the bonded H_2O molecule, leading to the conversion of H_2O-SMb complex to H_2S-SMb complex. Figure 3-27 illustrates the routes dominated by the formation of the H_2S-SMb and H_2O-SMb, emphasized by the red arrows. It is no surprise that the SMb formation route (2.5×10^6 $M^{-1}s^{-1}$) [37] dominants over the Mb + H_2O_2 (6×10^2 $M^{-1}s^{-1}$) [86-88] and Mb + H_2S (1.6×10^4 $M^{-1}s^{-1}$) [90] reaction routes given the significant difference in their corresponding reactions rates. Evaluation of the effect of increasing H_2S concentration to acquire a "real" [1:1] concentration ratio of [Mb:H_2S], only accelerated the reaction and provided the H_2S molecule the opportunity to react with unreacted met-Mb resulting in the H_2S-Mb complex formation in addition to the H_2S-SMb and H_2O-SMb derivates, as seen in Figure 3-28. The

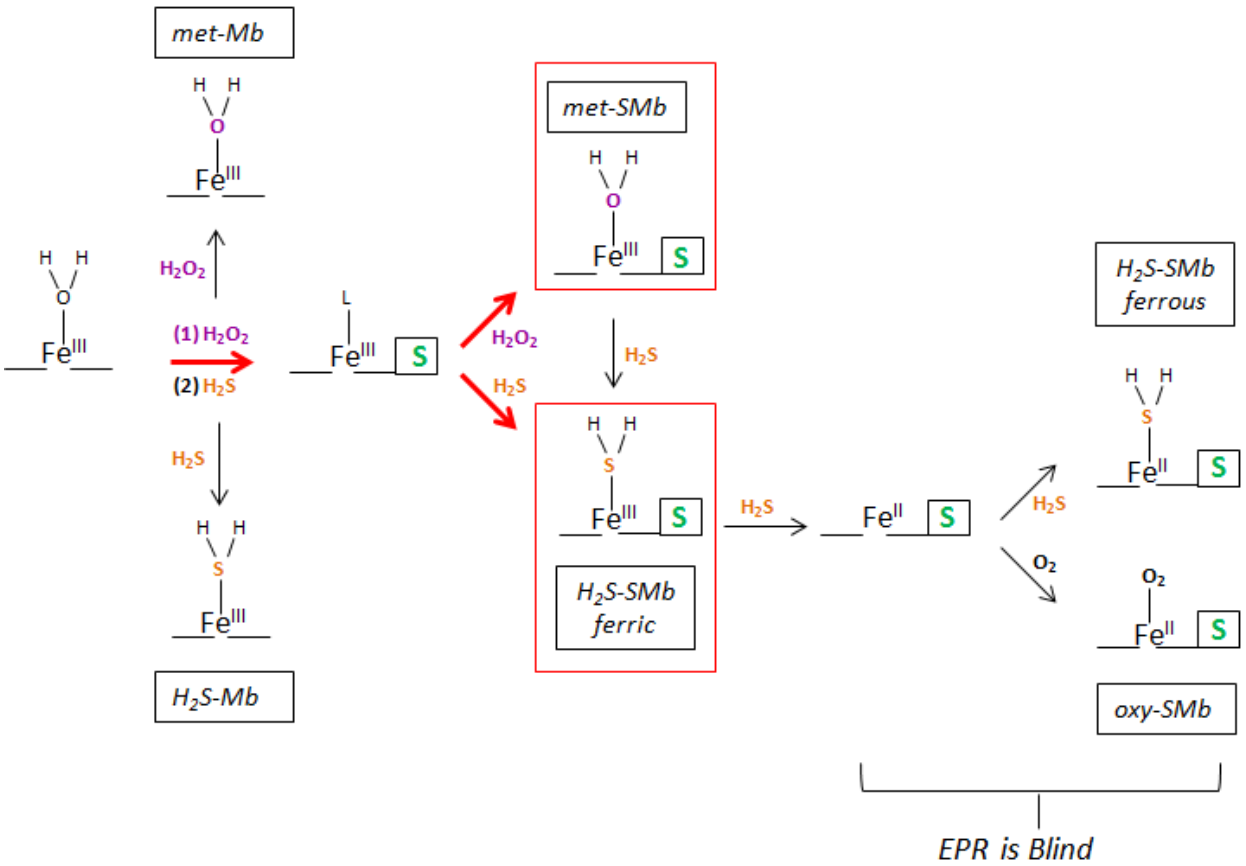

Figure 3-27. Routes dominated by the formation of the H_2S-SMb and H_2O-SMb (emphasize by the red arrows) when met-Mb reacts with H_2O_2 and H_2S in a [1:1:1] concentration ratio at a pH of 6.5.

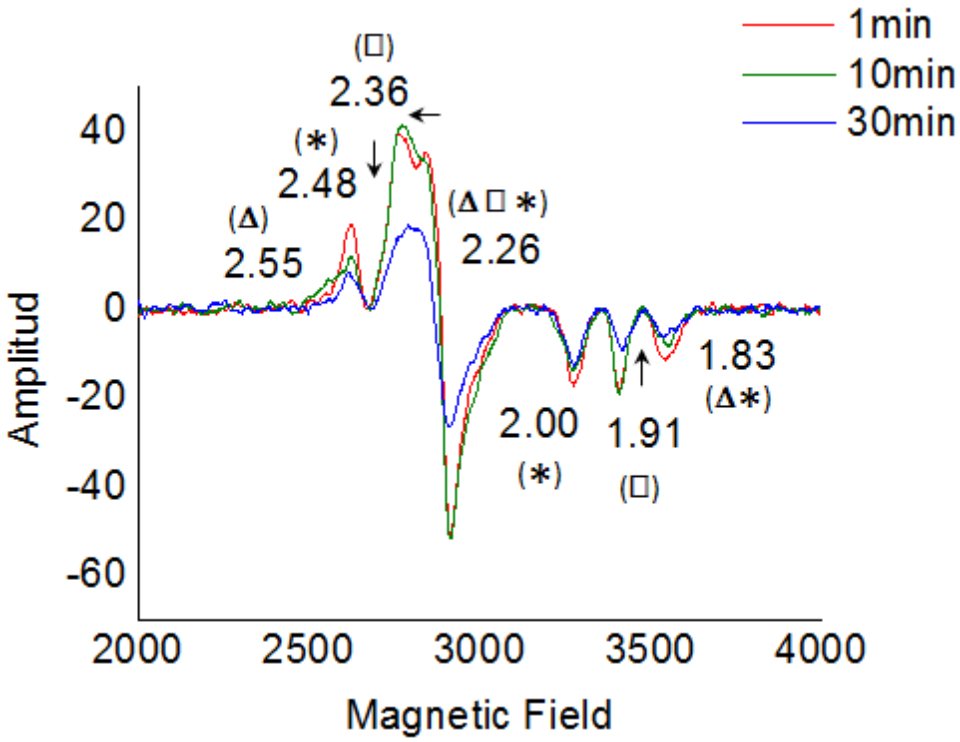

Figure 3-28. EPR shows the low field region of the species formed through time when met-Mb reacts with H_2O_2 and H_2S in a "real" [1:1:1] concentration ratio at a pH of 6.5. (H_2O-SMb complex is represented by an (∗), the H_2S-SMb complex is represented by an (□), and the H_2S-Mb complex is represented by an (△)).

dominated reaction routes that lead to the H_2S-Mb, H_2S-SMb and H_2O-SMb complexes formation is shown in Figure 3-29.

However, our objective was to identify the SMb-L complexes that naturally take place as products during the SMb complex formation, and hence, serve as physiological competitors for the binding of O_2 to the heme-Fe. Therefore, identification of the protein-ligand complexes generated during the SMb formation at 7.4 pH (physiological pH) and their comparison with those observed at 6.5 pH, determines all possible SMb-L derivates that can be generated in the SMb reaction, in addition to distinguishing between the SMb-L complexes that will always be present independently of the pH from those that are limited by pH. It is important to remember that at pH of 7.4 only ~30% of H_2S is present in solution and the distal histidine involved in the SMb formation is deprotonated [49, 50]. Figure 3-30 shows the formation of the ferrous and ferric SMb species obtained from the interaction of met-Mb with H_2O_2 and H_2S in a [1:1:1] concentration ratio at pH of 7.4, as indicated by the presence of the bands at around 618 and 720 nm, respectively. Figure 3-31 shows the low field EPR region of the species formed through time when met-Mb reacts with H_2O_2 and H_2S in a [1:1:1] concentration ratio at a pH of 7.4. Initially, at 1 min of interaction, the presence of both H_2S-Mb (g = 2.56, 2.25, and 1.83) and H_2S-SMb (g = 2.36, 2.26, and 1.91) complexes were observed. Subsequently, after 30 min of interaction, the H_2S-Mb complex was consumed in the reaction and/or the bound-H_2S molecule was displaced during the reaction, as indicated by the decrease in the band intensity until vanishing. Nonetheless, a small band (g = 2.50) corresponding to the H_2O-SMb was observed after approximately 30 minutes of interaction. Interestingly, the intensity of the band related to the H_2S-SMb remains relatively constant through time, indicating a stable H_2S-SMb complex or the continuous formation of this derivate. It is not surprising to see at the beginning of the reaction a

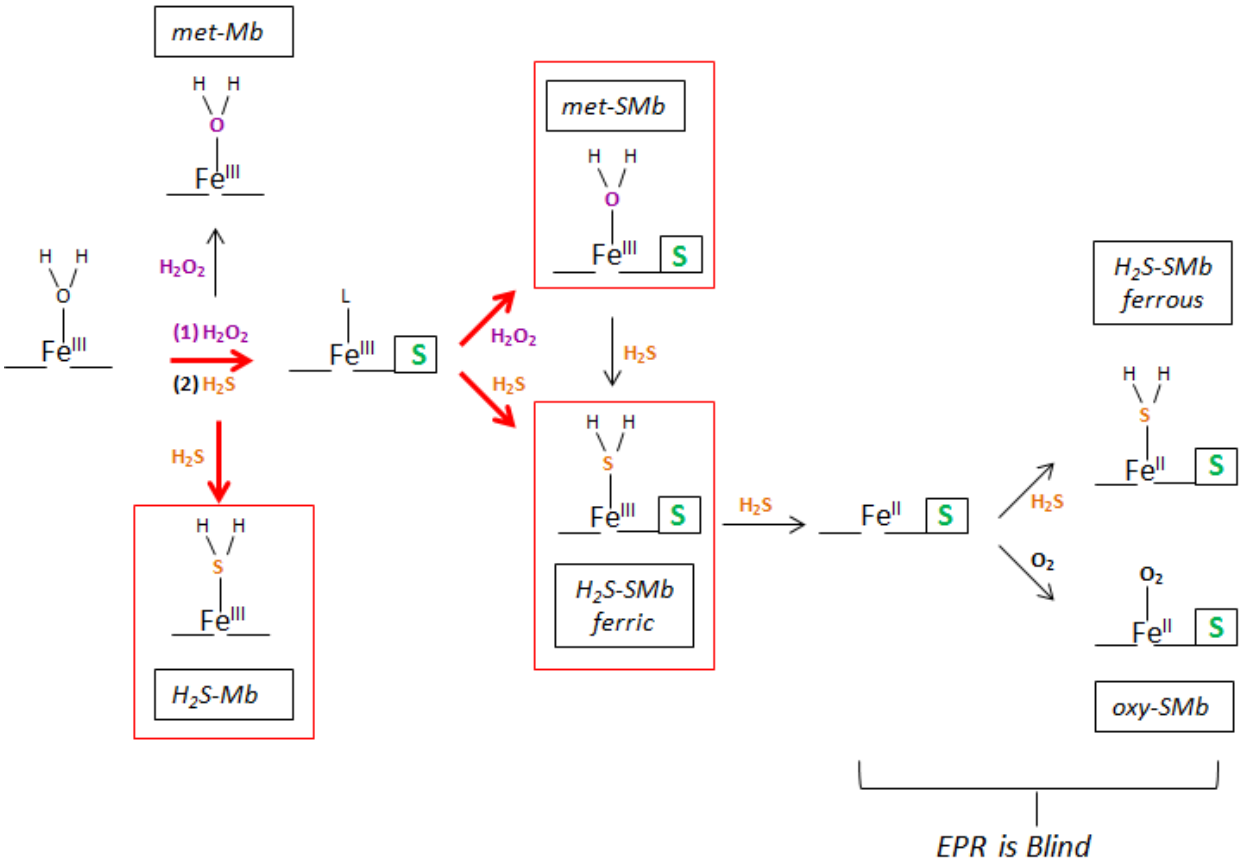

Figure 3-29. Routes dominated by the formation of the H_2S-SMb and H_2O-SMb (emphasize by the red arrows) when met-Mb reacts with H_2O_2 and H_2S in a "real" [1:1:1] concentration ratio at a pH of 6.5.

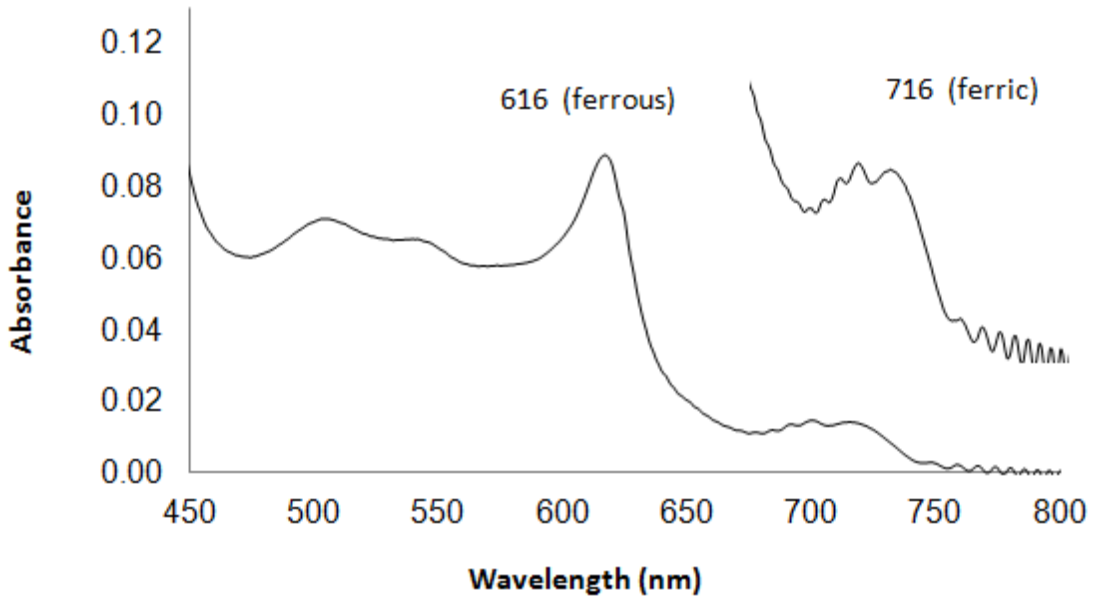

Figure 3-30. Formation of the ferrous and ferric SMb species obtained from the interaction of met-Mb with H_2O_2 and H_2S in a [1:1:1] concentration ratio at pH of 7.4. (The wiggles in the spectra line around 675-700 nm and 750-800 nm regions are due to instrumental noise)

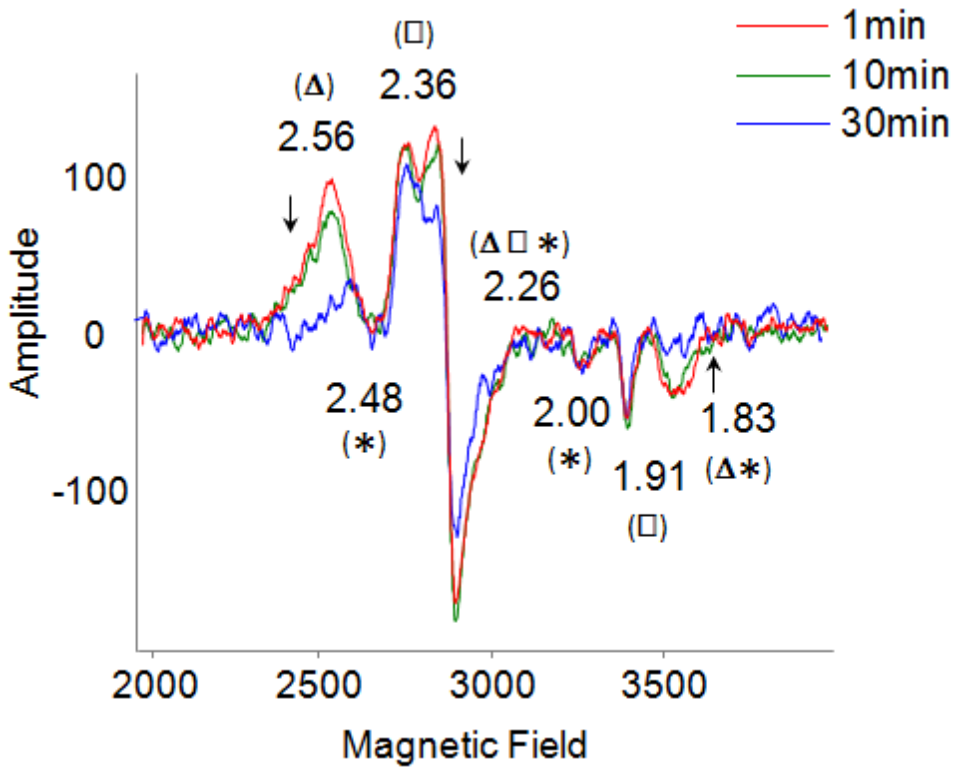

Figure 3-31. Low field EPR region of the species formed through time when met-Mb reacts with H_2O_2 and H_2S in a [1:1:1] concentration ratio at a pH of 7.4. (H_2O-SMb complex is represented by an (∗), the H_2S-SMb complex is represented by an (□), and the H_2S-Mb complex is represented by an (Δ)).

high intensity signal characteristic of the H_2S-Mb complex since at pH=7.4 the deprotonated distal histidine stabilizes the bound H_2S ligand through a hydrogen bond. Figure 3-32 illustrates the scheme of the dominated routes leading to the formation of the H_2S-Mb, H_2S-SMb, and H_2O-SMb. Thus, change in pH does not affect the types of SMb-L final products that are generated during the SMb complex formation, which can be generalized as H_2S-SMb and H_2O-SMb. The principal difference was their stability and relative abundance.

3.2.3 Extreme physiological H_2S and H_2O_2 conditions

To determine how the physiological dominant routes and major SMb species are affected with significant increase in H_2S and H_2O_2 concentration, evaluation of the [Mb:H_2O_2:H_2S] concentration ratio of extreme H_2O_2 condition at [1:5:3] and H_2S condition at [1:5:90] on the predominant SMb-L complexes was performed. Figure 3-33 shows the UV-Vis spectra of extreme H_2O_2 condition at [1:5:3] with a pH of 7.4. The formation of only the ferric SMb specie around 720 nm was observed. It is no surprise that the reaction route is probably dominated by the higher concentration reactant, H_2O_2, inducing the oxidation of the heme-Fe with subsequently turn over to ferric heme-Fe instead of the heme-Fe reduction route induce by the increase in H_2S concentration. Figure 3-34 shows the EPR low field region of the species formed through time when met-Mb reacts with H_2O_2 and H_2S in a [1:5:3] concentration ratio at a pH of 7.4. Both H_2O-SMb and H_2S-SMb complexes are observed initially, been H_2S-SMb the dominant SMb specie. Also, two bands with different intensity at 2.26 resonances were also observed, been probably the one with higher intensity corresponding to the higher intensity H_2S-SMb complex signals and the lower intensity 2.26 resonance to the lower intensity H_2O-SMb complex signals. However, the H_2S-SMb Complex band intensity decreases significantly through time, probably due to the displacement of H_2S by the higher concentration reactant

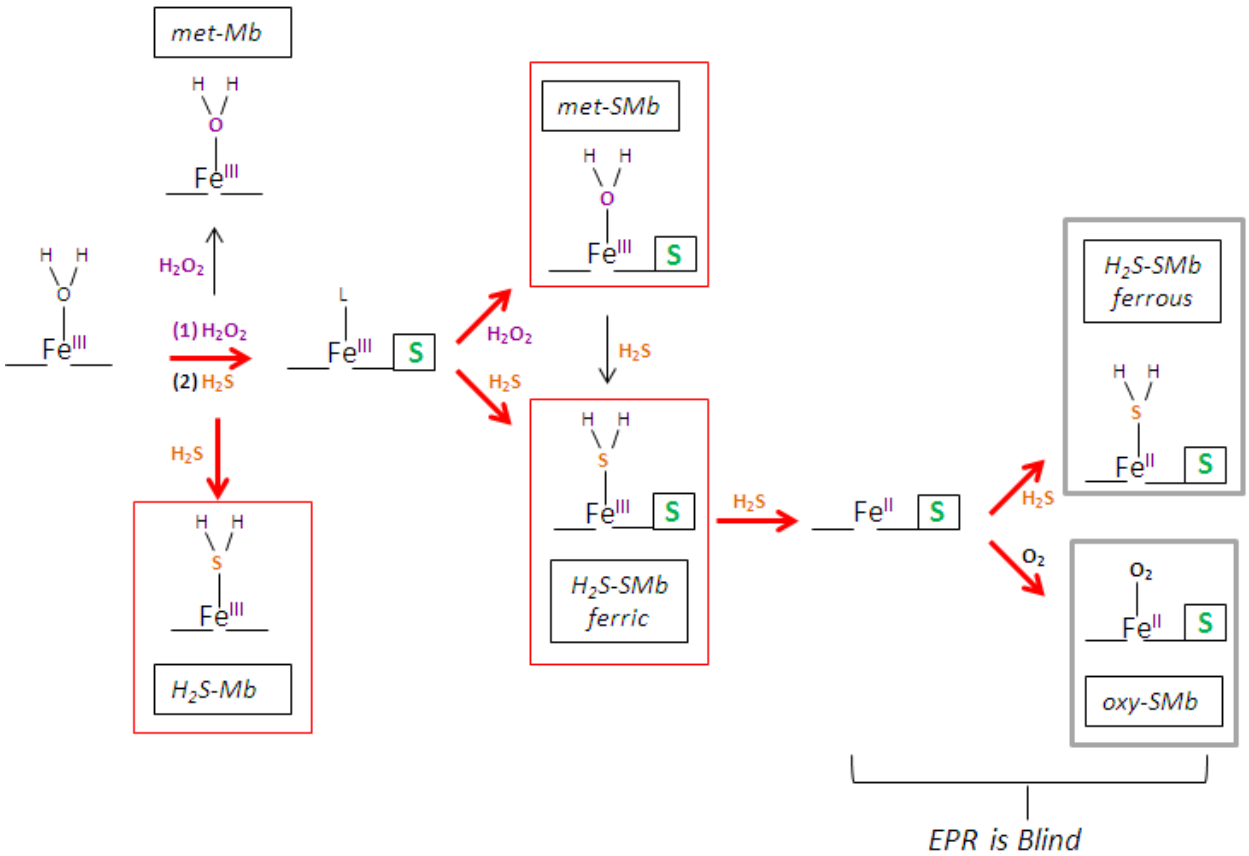

Figure 3-32. Routes dominated by the formation of the H_2S-Mb, H_2S-SMb and H_2O-SMb (emphasize by the red arrows) when met-Mb reacts with H_2O_2 and H_2S in a [1:1:1] concentration ratio at a pH of 7.4.

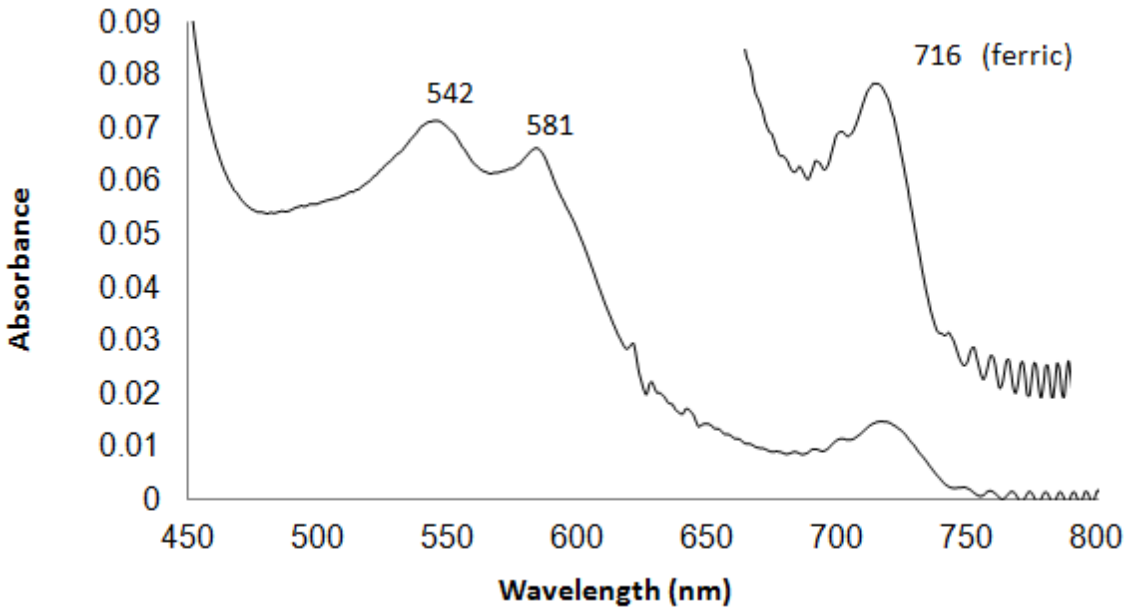

Figure 3-33. UV-Vis spectra of the SMb complex formation in an extreme H_2O_2 condition with [1:5:3] concentration ration at pH=7.4. (The wiggles in the spectra line around 675-700 nm and 750-800 nm regions are due to instrumental noise)

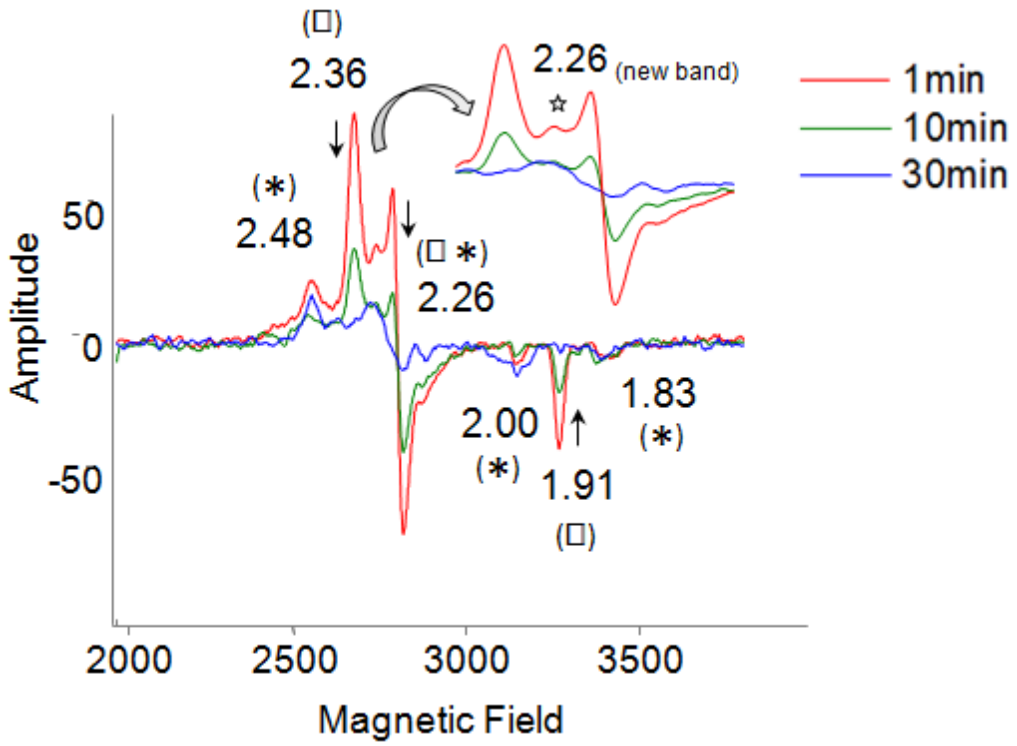

Figure 3-34. EPR low field region of the species formed through time when met-Mb reacts with H_2O_2 and H_2S in a [1:5:3] concentration ratio at a pH of 7.4. (H_2O-SMb complex is represented by an (∗), and the H_2S-SMb complex is represented by an (□)). The new band at 2.26 is represented by a star.

H_2O_2. Since both reactants have higher concentration than the protein, the reaction will lead towards the SMb formation by the increase in probability of both reactants reaching the same heme pocket. Hence, reducing the concentration of residual unreactive met-Mb and its interaction with H_2S leading to the H_2S-Mb formation. Figure 3-35 illustrates the scheme of the dominated routes that lead to the formation of the H_2S-SMb and H_2O-SMb complexes.

The UV-Vis spectra of extreme H_2S condition at pH=7.4 with [1:5:90] concentration ratio is shown in Figure 3-36; where formation of only the ferrous SMb specie around 620 nm was observed. It is no surprise that in this case the reaction route is probably dominated by the higher concentration reactant, H_2S. It suggests that the significant increase in H_2S concentration activates the reduction capacity of H_2S, leading to the reduction of the ferric heme-Fe to ferrous heme-Fe. Figure 3-37 shows the low field region of the species formed through time when met-Mb interacts with H_2O_2 and H_2S in a [1:5:90] concentration ratio at a pH of 7.4. The lack of signal in all the EPR spectra serves as evidence of the reducing capacity of H_2S, were all the heme-Fe was transformed to its ferrous state. Figure 3-38 illustrates the scheme of the dominated routes that lead to the formation of the possible theorized ferrous SMb-ligand products (H_2S-SMb and, in the presence of O_2, O_2-SMb). The decrease in electron density of the heme-Fe induced by the incorporated sulfur atom withdrawing electron capacity and heme distortion produces a heme-Fe^{II} with a character of heme-Fe^{III}. The oxygen molecule has better interaction with heme-Fe^{II} than with heme-Fe^{III}. The acquired heme-Fe^{II} with a heme-Fe^{III} character weakens the Fe-O_2 interaction; however, it strengthens the Fe-H_2S interaction. Also, the heme-Fe will have a stronger interaction with an electron donating atom; S has more electron donating capacity than O. Therefore, this two concepts combine suggests that the formation of the ferrous H_2S-SMb complex would be preferred over the ferrous O_2-SMb complex, in the presence of O_2.

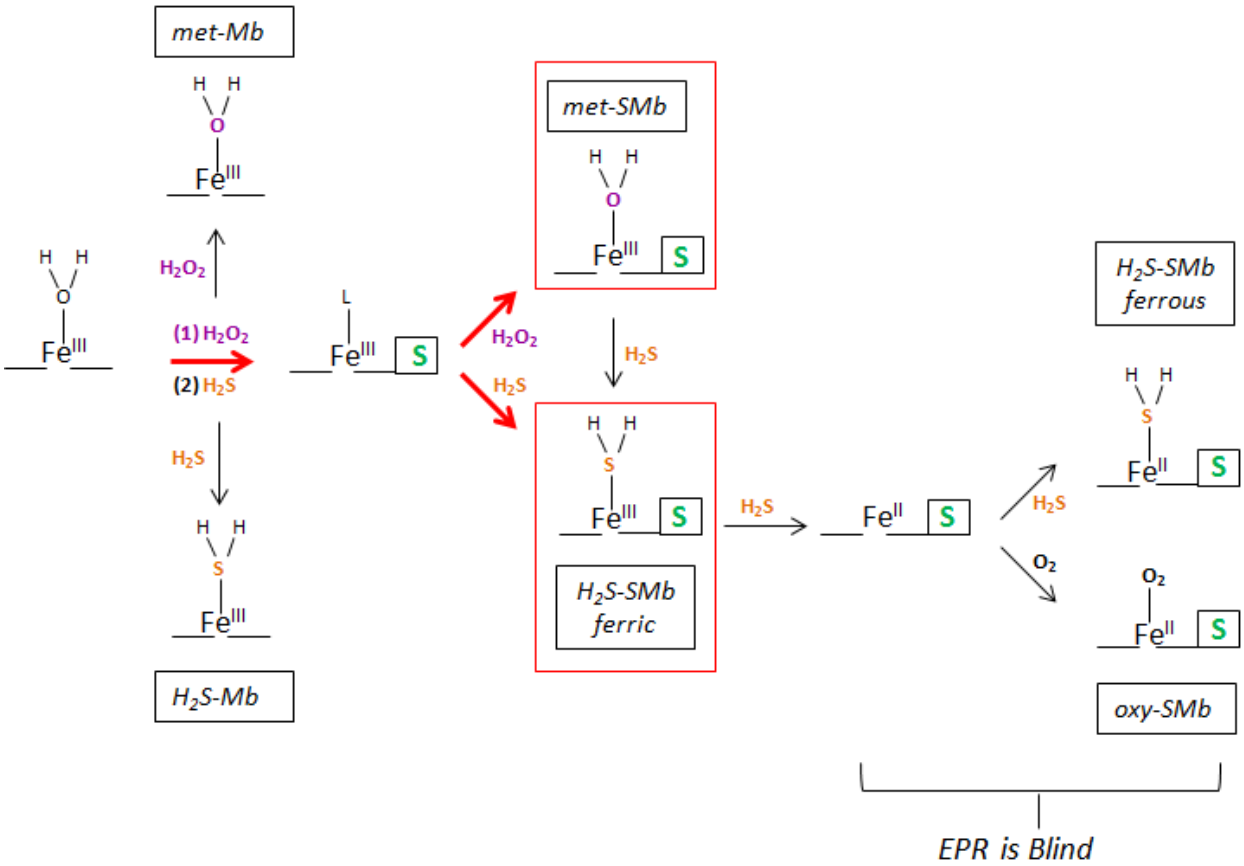

Figure 3-35. Routes dominated by the formation of the H_2S-SMb and H_2O-SMb (emphasize by the red arrows) when met-Mb reacts with H_2O_2 and H_2S in a [1:5:3] concentration ratio at a pH of 7.4.

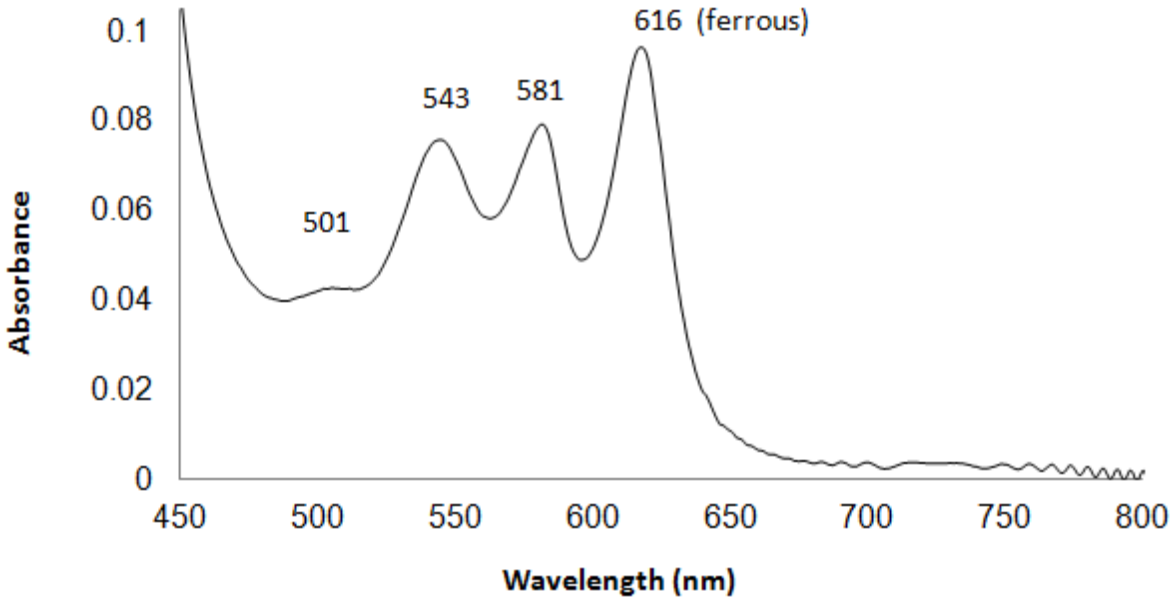

Figure 3-36. UV-Vis spectra of the SMb complex formation in an extreme H_2S condition with [1:5:90] concentration ration at pH=7.4. (The wiggles in the spectra line around 675-700 nm and 750-800 nm regions are due to instrumental noise)

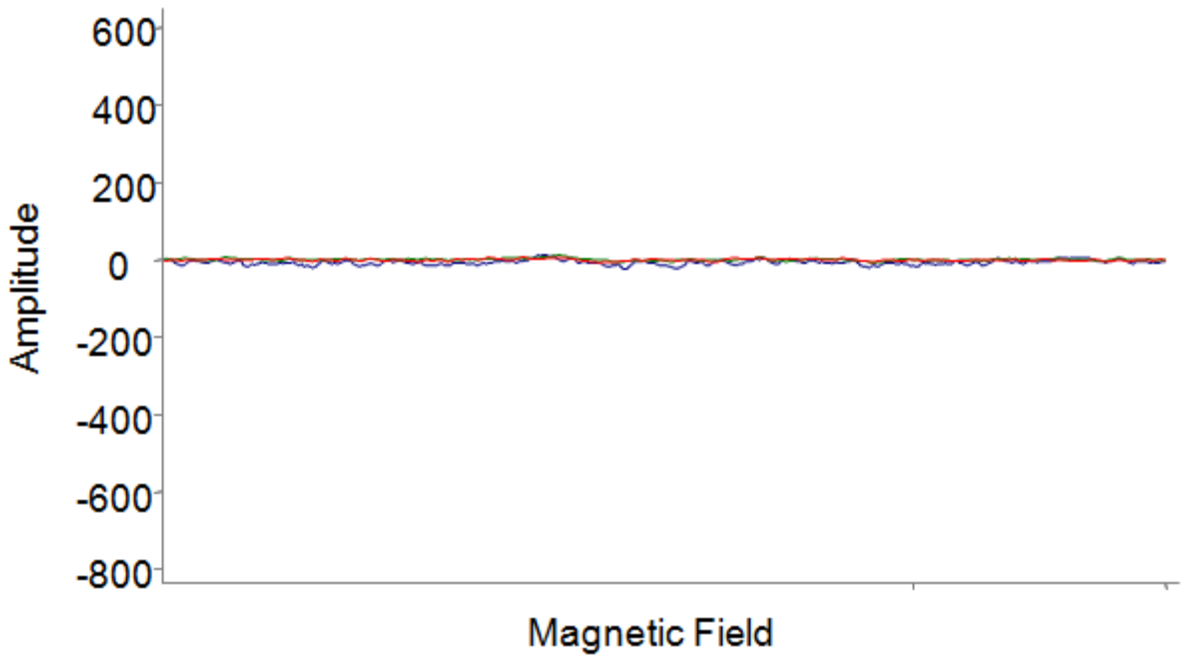

Figure 3-37. EPR high and low field regions through time when met-Mb reacts with H_2O_2 and H_2S in a [1:5:90] concentration ratio at a pH of 7.4.

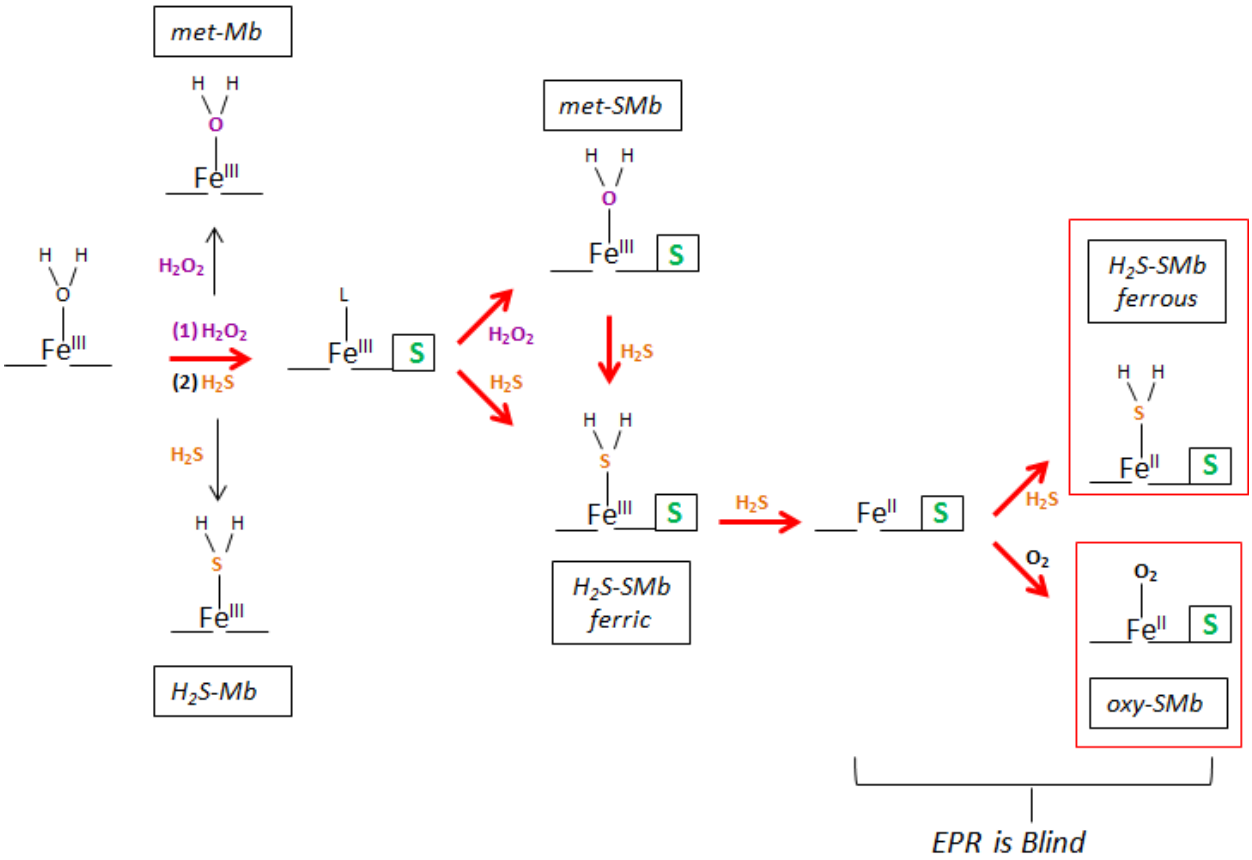

Figure 3-38. Routes dominated by the formation of the ferrous H_2S-SMb and O_2-SMb (emphasize by the red arrows) when met-Mb reacts with H_2O_2 and H_2S in a [1:5:90] concentration ratio at a pH of 7.4.

3.2.4 Further Outlooks and EPR Summary

Taken together, the possible final products of the SMb complex formation are H_2O-SMb, O_2-SMb, ferric and ferrous H_2S-SMb. In order for O_2 to bind to the sulfheme-Fe, it will have to compete with H_2O and H_2S ligands, in addition to the ferric heme-Fe oxidation state. Interestingly, although absorption bands at around 720, 620, and 618 nm have been assigned to metaquo, oxy, and deoxy sulfheme complexes, Figure 3-39 shows an example of the deconvolution of one of the many absorption spectra of the SMb complex formation where under the characteristic sulfheme bands was present another set of bands. This new bands may correspond to other SMb-ligand complexes like ferric and ferrous H_2S-SMb that are not yet reported, in addition to different SMb isomers bound to various ligands. However, identifying and discerning between them will require further analysis and other techniques, for example resonance Raman.

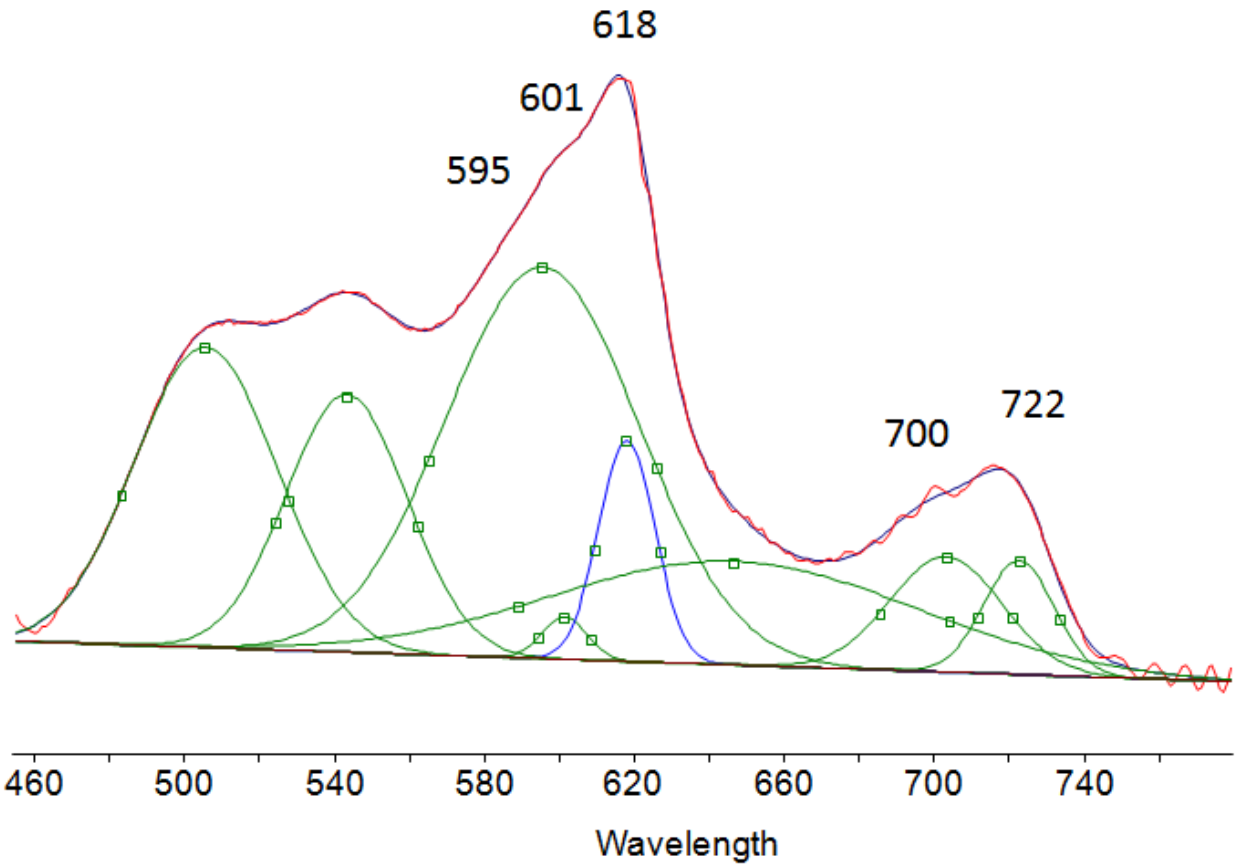

Figure 3-39. Deconvolution of one of the many absorption spectra of the SMb complex formation. (The wiggles in the spectra line around 630-722 nm and 740-800 nm regions are due to instrumental noise)

Chapter 4. Conclusion

CHAPTER 4: CONCLUSION

The focus of this study was to: (1) evaluate the local heme-Fe environment by using EPR technique to determine the possible final suflheme-ligand products that serve as O_2 adversaries; and (2) identify additional chemical changes that contributes to the decrease in O_2 affinity by evaluating the global conformational environment using SAX/WAX technique.

The local structure analysis demonstrated that the possible final products of the SMb complex formation were H_2O-SMb, O_2-SMb, ferric and ferrous H_2S-SMb. In order for O_2 to bind to the sulfheme-Fe, it will have to compete with H_2O and H_2S as ligands, in addition to the low O_2 interaction with the ferric heme-Fe oxidation state. The presence of this SMb-ligand species hinders the O_2-protein interaction, resulting in an impairment of the protein functionality.

Also, the global structural analysis suggests that the SMb complex formation induces a conformational change that increases the protein flexibility, movement and fluctuations while decreasing the protein rigidity and forming a cleft. This conformational change is specific of SMb and different from the conformational change produce by ligand migration or heme Fe-ligand binding. Furthermore, the theoretical scattering curve of SMb crystal structure poorly correlates with the scattering data of SMb in solution, suggesting that the internal structural fluctuations are hampered by crystal packing forces, which limit the range of conformational motion accessible to the protein.

Given that any change in the size and shape of the protein global structure directly affects the protein function, we proposed that the observed changes in conformation and increase in protein flexibility play a role in the decrease in O_2 affinity. These structural changes would facilitate ligand entry but destabilize even more ligand bonding, leading to an overall decrease in O_2 affinity. Moreover, the constant ligand competition and the increase in protein flexibility

provides enhancement of H_2S entry and O_2 displacement. This could lead to a plausible H_2S transports flux, in addition to the known rapid diffusive flux of free H_2S.

Overall, in addition to the decrease in oxygen affinity induce by the S atom electron withdrawing capacity and heme distortion produced by the sulfur-ring incorporation; there are two additional aspects that play a role in the reduced protein functionality: ligand competition and conformational change.

REFERENCES

1. **di Masi A, Ascenzi P: H2S: a "double face" molecule in health and disease. *BioFactors* 2013, 39(2):186-196.**
2. **Olson KR, Straub KD: The Role of Hydrogen Sulfide in Evolution and the Evolution of Hydrogen Sulfide in Metabolism and Signaling. *Physiology* 2016, 31(1):60-72.**
3. **Reiffenstein RJ, Hulbert WC, Roth SH: Toxicology of hydrogen sulfide. *Annu Rev Pharmacol Toxicol* 1992, 32:109-134.**
4. **Li L, Moore PK: Putative biological roles of hydrogen sulfide in health and disease: a breath of not so fresh air? *Trends in pharmacological sciences* 2008, 29(2):84-90.**
5. **Zheng Y, Ji X, Ji K, Wang B: Hydrogen sulfide prodrugs-a review. *Acta pharmaceutica Sinica B* 2015, 5(5):367-377.**
6. **Kajimura M, Fukuda R, Bateman RM, Yamamoto T, Suematsu M: Interactions of multiple gas-transducing systems: hallmarks and uncertainties of CO, NO, and H2S gas biology. *Antioxid Redox Signal* 2010, 13(2):157-192.**
7. **Wu D, Hu Q, Zhu Y: Therapeutic application of hydrogen sulfide donors: the potential and challenges. *Frontiers of medicine* 2015.**
8. **Rose P, Moore PK, Zhun YZ: H2S Biosynthesis and Catabolism: New Insights from Molecular Studies. *Cell Mol Life Sci* 2016.**
9. **Beata O: Medical Functions of Hydrogen Sulfide. *Adv Clin Chem* 2016, 74:195-210.**
10. **Cacanyiova S, Berenyiova A, Kristek F: The Role of Hydrogen Sulfide in Blood Pressure Regulation. *Physiol Res* 2016, 65:S273-S289.**
11. **Cao X, Bian JS: The Role of Hydrogen Sulfide in Renal System. *Front Pharmacol* 2016, 7:385-397.**
12. **Dou Y, Wang Z, Chen G: The Role of Hydrogen Sulfide in Stroke. *Med Gas Res* 2016, 6(2):79-84.**

13. **Tomasova L, Konopelski P, Ufnal M: Gut Bacteria and Hydrogen Sulfide: The New Old Players in Circulatory System Homeostasis.** ***Molecules*** **2016, 21:1558-1576.**

14. **Brunori M: Myoglobin strikes back.** ***Protein science : a publication of the Protein Society*** **2010, 19(2):195-201.**

15. **Brunori M, Bourgeois D, Vallone B: The structural dynamics of myoglobin.** ***Journal of structural biology*** **2004, 147(3):223-234.**

16. **Olson JS, Soman J, Phillips GN, Jr.: Ligand pathways in myoglobin: a review of Trp cavity mutations.** ***IUBMB life*** **2007, 59(8-9):552-562.**

17. **Tomita A, Kreutzer U, Adachi S, Koshihara SY, Jue T: 'It's hollow': the function of pores within myoglobin.** ***The Journal of experimental biology*** **2010, 213(Pt 16):2748-2754.**

18. **Lapelosa M, Abrams CF: A computational study of water and CO migration sites and channels inside myoglobin.** ***Journal of chemical theory and computation*** **2013, 9(2):1265-1271.**

19. **Pietri R, Lewis A, Leon RG, Casabona G, Kiger L, Yeh SR, Fernandez-Alberti S, Marden MC, Cadilla CL, Lopez-Garriga J: Factors controlling the reactivity of hydrogen sulfide with hemeproteins.** ***Biochemistry*** **2009, 48(22):4881-4894.**

20. **Pietri R, Roman-Morales E, Lopez-Garriga J: Hydrogen sulfide and hemeproteins: knowledge and mysteries.** ***Antioxid Redox Signal*** **2011, 15(2):393-404.**

21. **Rios-Gonzalez BB, Roman-Morales EM, Pietri R, Lopez-Garriga J: Hydrogen sulfide activation in hemeproteins: the sulfheme scenario.** ***J Inorg Biochem*** **2014, 133:78-86.**

22. **Roman-Morales E, Pietri R, Ramos-Santana B, Vinogradov SN, Lewis-Ballester A, Lopez-Garriga J: Structural determinants for the formation of sulfhemeprotein complexes.** ***Biochem Biophys Res Commun*** **2010, 400(4):489-492.**

23. **Noor M, Beutler E: Acquired sulfhemoglobinemia. An underreported diagnosis?** ***West J Med*** **1998, 169(6):386-389.**

24. Harangi M, Matyus J, Nagy E, Nagy E, Paragh G, Balla J, Olah AV: Identification of sulfhemoglobinemia after surgical polypectomy. *Clin Toxicol (Phila)* 2007, 45(2):189-192.

25. Olson KR: Hydrogen sulfide: both feet on the gas and none on the brake? *Front Physiol* 2013, 4:2.

26. Berzofsky JA, Peisach J, Blumberg WE: Sulfheme proteins. I. Optical and magnetic properties of sulfmyoglobin and its derivatives. *The Journal of biological chemistry* 1971, 246(10):3367-3377.

27. Berzofsky JA, Peisach J, Alben JO: Sulfheme proteins. 3. Carboxysulfmyoglobin: the relation between electron withdrawal from iron and ligand binding. *J Biol Chem* 1972, 247(12):3774-3782.

28. Berzofsky JA, Peisach J, Blumberg WE: Sulfheme proteins. II. The reversible oxygenation of ferrous sulfmyoglobin. *J Biol Chem* 1971, 246(23):7366-7372.

29. Chatfield MJ, La Mar GN: 1H nuclear magnetic resonance study of the prosthetic group in sulfhemoglobin. *Arch Biochem Biophys* 1992, 295(2):289-296.

30. Chatfield MJ, La Mar GN, Balch AL, Lecomte JT: Multiple forms of sulfmyoglobin as detected by 1H nuclear magnetic resonance spectroscopy. *Biochem Biophys Res Commun* 1986, 135(1):309-315.

31. Chatfield MJ, La Mar GN, Balch AL, Smith KM, Parish DW, LePage TJ: Proton NMR study of the influence of heme vinyl groups on the formation of the isomeric forms of sulfmyoglobin. *FEBS Lett* 1986, 206(2):343-346.

32. Chatfield MJ, La Mar GN, Kauten RJ: Proton NMR characterization of isomeric sulfmyoglobins: preparation, interconversion, reactivity patterns, and structural features. *Biochemistry* 1987, 26(22):6939-6950.

33. Chatfield MJ, La Mar GN, Lecomte JTJ, Balch AL, Smith KM, Langry KC: Identification of the Altered Pyrrole in Sulfmyoglobin and an Extractable "Sulfhemin": Participation of

the 4-vinyl Group in the Saturation of the Pyrrole in One Form of Sulfmyoglobin. ***J Am Chem Soc*** **1986, 108:7108-7110.**

34. Chatfield MJ, La Mar GN, Parker WO, Jr., Smith KM, Leung H-K, Morris IK: Nuclear Magnetic Resonance Study of the Molecular and Electronic Structure of the Stable Green Sulfhemin Prosthetic Group Extracted from Sulfmyoglobin. ***Juornal of the American Chemical Society*** **1988, 110:6352-6358.**

35. Chatfield MJ, La Mar GN, Smith KM, Leung HK, Pandey RK: Identification of the altered pyrrole in the isomeric sulfmyoglobins: hyperfine shift patterns as indicators of ring saturation in ferric chlorins. ***Biochemistry*** **1988, 27(5):1500-1507.**

36. Berzofsky JA, Peisach J, Horecker BL: Sulfheme proteins. IV. The stoichiometry of sulfur incorporation and the isolation of sulfhemin, the prosthetic group of sulfmyoglobin. ***J Biol Chem*** **1972, 247(12):3783-3791.**

37. Libardi SH, Pindstrup H, Cardoso DR, Skibsted LH: Reduction of Ferrylmyoglobin by Hydrogen Sulfide. Kinetics in Relation to Meat Greening. ***J Agric Food Chem*** **2013.**

38. Nicholls P: The formation and properties of sulphmyoglobin and sulphcatalase. ***Biochem J*** **1961, 81:374-383.**

39. Romero FJ, Ordonez I, Arduini A, Cadenas E: The reactivity of thiols and disulfides with different redox states of myoglobin. Redox and addition reactions and formation of thiyl radical intermediates. ***J Biol Chem*** **1992, 267(3):1680-1688.**

40. Michel HO: A Study of Sulfhemoglobin. ***The Journal of Biological Chemistry*** **1938, 126:323-348.**

41. Morell DB, Chang Y, Clezy PS: ***Biochim Biophys Acta*** **1967, 136:121-130.**

42. Timkovich R, Vavra MR: Proton NMR spectroscopy of sulfmyoglobin. ***Biochemistry*** **1985, 24(19):5189-5196.**

43. Andersson LA, Loehr TM, Lim AR, Mauk AG: Sulfmyoglobin. Resonance Raman spectroscopic evidence for an iron-chlorin prosthetic group. *J Biol Chem* 1984, 259(24):15340-15349.

44. Park CM, Nagel RL, Blumberg WE, Peisach J, Magliozzo RS: Sulfhemoglobin. Properties of partially sulfurated tetramers. *J Biol Chem* 1986, 261(19):8805-8810.

45. Parker WO, Jr., Chatfield MJ, La Mar GN: Determination of the chirality of the saturated pyrrole in sulfmyoglobin using the nuclear Overhauser effect. *Biochemistry* 1989, 28(4):1517-1525.

46. Carrico RJ, Blumberg WE, Peisach J: The reversible binding of oxygen to sulfhemoglobin. *J Biol Chem* 1978, 253(20):7212-7215.

47. Jennings ML: Transport of H2S and HS- Across the Human Red Blood Cell Membrane: Rapid H2S Diffusion and AE1-Mediated Cl-/HS- Exchange. *American Journal of Physiology Cell Physiology* 2013, 305(9):C941-C950.

48. Kraus DW, Wittenberg JB: Hemoglobins of the Lucina pectinata/bacteria symbiosis. I. Molecular properties, kinetics and equilibria of reactions with ligands. *J Biol Chem* 1990, 265(27):16043-16053.

49. Li S, Hong M: Protonation, tautomerization, and rotameric structure of histidine: a comprehensive study by magic-angle-spinning solid-state NMR. *J Am Chem Soc* 2011, 133(5):1534-1544.

50. Shimahara H, Yoshida T, Shibata Y, Shimizu M, Kyogoku Y, Sakiyama F, Nakazawa T, Tate S, Ohki SY, Kato T *et al*: Tautomerism of histidine 64 associated with proton transfer in catalysis of carbonic anhydrase. *J Biol Chem* 2007, 282(13):9646-9656.

51. Arbelo-Lopez HD, Simakov NA, Smith JC, Lopez-Garriga J, Wymore T: Homolytic Cleavage of Both Heme-Bound Hydrogen Peroxide and Hydrogen Sulfide Leads to the Formation of Sulfheme. *J Phys Chem B* 2016, 120(30):7319-7331.

52. Read KR: Transamination in certain tissue homogenates of the bivalved molluscs Mytilus edulis L. and Modiolus Modiolus L. *Comp Biochem Physiol* 1962, 7:15-22.

53. Leon RG, Munier-Lehmann H, Barzu O, Baudin-Creuza V, Pietri R, Lopez-Garriga J, Cadilla CL: High-level production of recombinant sulfide-reactive hemoglobin I from Lucina pectinata in Escherichia coli. High yields of fully functional holoprotein synthesis in the BLi5 E. coli strain. *Protein Expr Purif* 2004, 38(2):184-195.

54. Ramos C, Pietri R, Lorenzo W, Roman E, Granell LB, Cadilla CL, Lopez-Garriga J: Recombinant Hemoglobin II From Lucina Pectinata: A Large-Scale Method for Hemeprotein Expression in E. coli. *Protein J* 2010, 29(2):143-151.

55. Silfa E, Almeida M, Cerda J, Wu S, Lopez-Garriga J: Orientation of the heme vinyl groups in the hydrogen sulfide-binding hemoglobin I from Lucina pectinata. *Biospectroscopy* 1998, 4(5):311-326.

56. Allaire M, Yang L: Biomolecular solution x-ray scattering at the National Synchrotron Light Source. *Journal of Synchrotron Radiation* 2011, 18:41-44.

57. Petoukhov M, Franke D, Shkumatov A, Tria G, Kikhney A, Gajda M, Gorba C, Mertens HDT, Konarev PV, Svergun DI: New developments in the ATSAS program package for small-angle scattering data analysis. *Journal of Applied Crystallography* 2012, 45:342-350.

58. Pietri R, Zerbs S, Corgliano DM, Allaire M, Collart FR, Miller LM: Biophysical and structural characterization of a sequence-diverse set of solute-binding proteins for aromatic compounds. *The Journal of biological chemistry* 2012, 287(28):23748-23756.

59. Rambo RP, Tainer JA: Characterizing flexible and intrinsically unstructured biological macromolecules by SAS using the Porod-Debye law. *Biopolymers* 2011, 95(8):559-571.

60. Konarev PV, Sokolova VV, Koch MHJ, Svergun DI: PRIMUS. A Windows PC-based system for angle scattering drug analysis. *Journal of Applied Crystallography* 2003, 36:1277-1282.

61. Svergun DI: Determination of the regularization parameter in indirect-transform methods using perceptual criteria. *Journal of Applied Crystallography* 1992, 25:495-503.

62. Svergun DI: Restoring low resolution structure of biological macromolecules from solution scattering using simulated annealing. *Biophysical Journal* 1999, 76(2879-2886).

63. Volkov VV, Svergun DI: Uniqueness of ab initio shape determination in small angle x-ray scattering. *Journal of Applied Crystallography* 2003, 36:860-864.

64. Kozin MB, Svergun DI: Automated matching of high and low resolution structural models. *Journal of Applied Crystallography* 2001, 34:33-41.

65. Svergun DI, Barberato C, Koch MHJ: CRYSOL-A program to evaluate x-ray solution scattering of biological macromolecules from atomic coordinates. *Journal of Applied Crystallography* 1995, 28:768-773.

66. Mertens HD, Svergun DI: Structural characterization of proteins and complexes using small-angle X-ray solution scattering. *Journal of structural biology* 2010, 172(1):128-141.

67. Fischetti RF, Rodi DJ, Gore DB, Makowski L: Wide-angle X-ray solution scattering as a probe of ligand-induced conformational changes in proteins. *Chemistry & biology* 2004, 11(10):1431-1443.

68. Makowski L, Bardhan J, Gore D, Lal J, Mandava S, Park S, Rodi DJ, Ho NT, Ho C, Fischetti RF: WAXS studies of the structural diversity of hemoglobin in solution. *Journal of molecular biology* 2011, 408(5):909-921.

69. Makowski L, Gore D, Mandava S, Minh D, Park S, Rodi DJ, Fischetti RF: X-ray solution scattering studies of the structural diversity intrinsic to protein ensembles. *Biopolymers* 2011, 95(8):531-542.

70. Makowski L, Rodi DJ, Mandava S, Minh DD, Gore DB, Fischetti RF: Molecular crowding inhibits intramolecular breathing motions in proteins. *Journal of molecular biology* 2008, 375(2):529-546.

71. Cho HS, Dashdorj N, Schotte F, Graber T, Henning R, Anfinrud P: Protein structural dynamics in solution unveiled via 100-ps time-resolved x-ray scattering. *Proceedings of the National Academy of Sciences of the United States of America* 2010, 107(16):7281-7286.

72. Guedes HL, Silva FP, Jr., Netto CC, de Salles CM, Alexandre G, Oliveira CL, Torriani I, De Simone SG: Structural characterization and low-resolution model of BJ-48, a thrombin-like enzyme from Bothrops jararacussu venom. *Biophysical chemistry* 2008, 132(2-3):159-164.

73. Krueger JK, Olah GA, Rokop SE, Zhi G, Stull JT, Trewhella J: Structures of calmodulin and a functional myosin light chain kinase in the activated complex: a neutron scattering study. *Biochemistry* 1997, 36(20):6017-6023.

74. Kitahara R, Hata K, Maeno A, Akasaka K, Chimenti MS, Garcia-Moreno EB, Schroer MA, Jeworrek C, Tolan M, Winter R *et al*: Structural plasticity of staphylococcal nuclease probed by perturbation with pressure and pH. *Proteins* 2011, 79(4):1293-1305.

75. Neves D, Estrozi LF, Job V, Gabel F, Schoehn G, Dessen A: Conformational states of a bacterial alpha2-macroglobulin resemble those of human complement C3. *PloS one* 2012, 7(4):e35384.

76. Hammel M: Validation of macromolecular flexibility in solution by small-angle X-ray scattering (SAXS). *European biophysics journal : EBJ* 2012, 41(10):789-799.

77. Carvalho FA, Carvalho JW, Santiago PS, Tabak M: Urea-induced unfolding of Glossoscolex paulistus hemoglobin, in oxy- and cyanomet-forms: a dissociation model. *International journal of biological macromolecules* 2013, 52:340-348.

78. Carvalho JW, Carvalho FA, Santiago PS, Tabak M: Thermal stability of extracellular hemoglobin of Rhinodrilus alatus (HbRa): DLS and SAXS studies. *European biophysics journal : EBJ* 2016.

79. Kozlowska M, Tarczewska A, Jakob M, Szpotkowski K, Wojtas M, Rymarczyk G, Ozyhar A: Calponin-like Chd64 is partly disordered. ***PloS one*** **2014, 9(5):e96809.**

80. Yokouchi T, Izumi Y, Matsufuji T, Jinbo Y, Yoshino H: Unfolding intermediate of a multidomain protein, calmodulin, in urea as revealed by small-angle X-ray scattering. ***FEBS letters*** **2003, 551(1-3):119-122.**

81. Uzawa T, Akiyama S, Kimura T, Takahashi S, Ishimori K, Morishima I, Fujisawa T: Collapse and search dynamics of apomyoglobin folding revealed by submillisecond observations of alpha-helical content and compactness. ***Proceedings of the National Academy of Sciences of the United States of America*** **2004, 101(5):1171-1176.**

82. Tomita A, Sato T, Ichiyanagi K, Nozawa S, Ichikawa H, Chollet M, Kawai F, Park SY, Tsuduki T, Yamato T ***et al*****: Visualizing breathing motion of internal cavities in concert with ligand migration in myoglobin.** ***Proceedings of the National Academy of Sciences of the United States of America*** **2009, 106(8):2612-2616.**

83. Hagen WR: EPR spectroscopy as a probe of metal centres in biological systems. ***Dalton transactions*** **2006(37):4415-4434.**

84. Kraus DW, Wittenberg JB, Lu JF, Peisach J: Hemoglobins of the Lucina pectinata/bacteria symbiosis. II. An electron paramagnetic resonance and optical spectral study of the ferric proteins. ***J Biol Chem*** **1990, 265(27):16054-16059.**

85. Svistunenko DA: Reaction of haem containing proteins and enzymes with hydroperoxides: the radical view. ***Biochim Biophys Acta*** **2005, 1707(1):127-155.**

86. Alayash AI, Ryan BA, Eich RF, Olson JS, Cashon RE: Reactions of sperm whale myoglobin with hydrogen peroxide. Effects of distal pocket mutations on the formation and stability of the ferryl intermediate. ***J Biol Chem*** **1999, 274(4):2029-2037.**

87. Wazawa T, Matsuoka A, Tajima G, Sugawara Y, Nakamura K, Shikama K: Hydrogen peroxide plays a key role in the oxidation reaction of myoglobin by molecular oxygen. A computer simulation. ***Biophys J*** **1992, 63(2):544-550.**

88. Witting PK, Douglas DJ, Mauk AG: Reaction of human myoglobin and H2O2. Involvement of a thiyl radical produced at cysteine 110. ***J Biol Chem*** **2000, 275(27):20391-20398.**

89. Witting PK, Mauk AG: Reaction of human myoglobin and H2O2. Electron transfer between tyrosine 103 phenoxyl radical and cysteine 110 yields a protein-thiyl radical. ***J Biol Chem*** **2001, 276(19):16540-16547.**

90. Bostelaar T, Vitvitsky V, Kumutima J, Lewis BE, Yadav PK, Brunold TC, Filipovic M, Lehnert N, Stemmler TL, Banerjee R: Hydrogen Sulfide Oxidation by Myoglobin. ***J Am Chem Soc*** **2016, 138(27):8476-8488.**

91. Calvert JW, Coetzee WA, Lefer DJ: Novel insights into hydrogen sulfide--mediated cytoprotection. ***Antioxid Redox Signal*** **2010, 12(10):1203-1217.**

92. Carballal S, Trujillo M, Cuevasanta E, Bartesaghi S, Moller MN, Folkes LK, Garcia-Bereguiain MA, Gutierrez-Merino C, Wardman P, Denicola A ***et al*****: Reactivity of hydrogen sulfide with peroxynitrite and other oxidants of biological interest.** ***Free Radic Biol Med*** **2011, 50(1):196-205.**

93. Jennings MJ: Transport of Hydrogen Sulfide and Hydrosulfide Anion Across the Human Red Blood Cell Membrane. ***The American Journal of Physiology - Cell Physiology*** **2013.**

94. Kimura H, Shibuya N, Kimura Y: Hydrogen sulfide is a signaling molecule and a cytoprotectant. ***Antioxid Redox Signal*** **2012, 17(1):45-57.**

95. Klingerman CM, Trushin N, Prokopczyk B, Haouzi P: H2s Concentrations in the Arterial Blood during H2s Administration in Relation to Its Toxicity and Effects on Breathing. ***Am J Physiol Regul Integr Comp Physiol*** **2013.**

96. Predmore BL, Lefer DJ, Gojon G: Hydrogen sulfide in biochemistry and medicine. *Antioxid Redox Signal* 2012, 17(1):119-140.

97. Shatalin K, Shatalina E, Mironov A, Nudler E: H2S: a universal defense against antibiotics in bacteria. *Science* 2011, 334(6058):986-990.

98. Whiteman M, Cheung NS, Zhu YZ, Chu SH, Siau JL, Wong BS, Armstrong JS, Moore PK: Hydrogen sulphide: a novel inhibitor of hypochlorous acid-mediated oxidative damage in the brain? *Biochem Biophys Res Commun* 2005, 326(4):794-798.

99. Whiteman M, Le Trionnaire S, Chopra M, Fox B, Whatmore J: Emerging role of hydrogen sulfide in health and disease: critical appraisal of biomarkers and pharmacological tools. *Clin Sci (Lond)* 2011, 121(11):459-488.

Appendix

(Scientific Publications)

A.1 Hydrogen Sulfide and Hemeproteins: Knowledge and Mysteries

A.2 Hydrogen Sulfide Activation in Hemeproteins: The Sulfheme Scenario

A.3 Sulfmyoglobin Conformational Change: A Role in the Decrease of Oxy-Mb Functionality

A.1

Hydrogen Sulfide and Hemeproteins: Knowledge and Mysteries

ANTIOXIDANTS & REDOX SIGNALING
Volume 15, Number 2, 2011
© Mary Ann Liebert, Inc.
DOI: 10.1089/ars.2010.3698

FORUM REVIEW ARTICLE

Hydrogen Sulfide and Hemeproteins: Knowledge and Mysteries

Ruth Pietri, Elddie Román-Morales, and Juan López-Garriga

Abstract

Historically, hydrogen sulfide (H_2S) has been regarded as a poisonous gas, with a wide spectrum of toxic effects. However, like ·NO and CO, H_2S is now referred to as a signaling gas involved in numerous physiological processes. The list of reports highlighting the physiological effects of H_2S is rapidly expanding and several drug candidates are now being developed. As with ·NO and CO, not a single H_2S target responsible for all the biological effects has been found till now. Nevertheless, it has been suggested that H_2S can bind to hemeproteins, inducing different responses that can mediate its effects. For instance, the interaction of H_2S with cytochrome *c* oxidase has been associated with the activation of the ATP-sensitive potassium channels, regulating muscle relaxation. Inhibition of cytochrome *c* oxidase by H_2S has also been related to inducing a hibernation-like state. Although H_2S might induce these effects by interacting with hemeproteins, the mechanisms underlying these interactions are obscure. Therefore, in this review we discuss the current state of knowledge about the interaction of H_2S with vertebrate and invertebrate hemeproteins and postulate a generalized mechanism. Our goal is to stimulate further research aimed at evaluating plausible mechanisms that explain H_2S reactivity with hemeproteins. *Antioxid. Redox Signal.* 15, 393–404.

Introduction

Hydrogen sulfide (H_2S) is a well-known poisonous gas whose cytotoxic effects have been studied for >300 years (65). Under physiological conditions, ~30% of H_2S is undissociated and ~70% is dissociated to hydrosulfide ion (pKa of 6.8). H_2S is also soluble in water and plasma (1 g in 242 ml at 20°C) and it can penetrate cells of all types by simple diffusion (34). It is this property that makes H_2S a broad-spectrum toxicant. Interestingly, the discovery that the human body naturally produces H_2S has dramatically changed the reputation of this gas from a toxic pollutant to a biologically relevant molecule. H_2S is now considered to be an important physiological mediator with a wide variety of roles, including regulation of neuronal activity and muscle relaxation, which are associated with the activation of N-methyl-D-aspartate receptors and ATP-sensitive potassium (K_{ATP}) channels, respectively (5, 33, 34, 38, 45, 77). Activation of the K_{ATP} channels has been related to the interaction of H_2S with several cysteine residues within the complex (27). It has also been suggested that K_{ATP} activation might be mediated by the interaction of H_2S with hemeproteins such as cytochrome *c* oxidase (CcO), myoglobin (Mb), and hemoglobin (Hb), which decreases cellular ATP and activates K_{ATP} channels (19, 30, 75, 77).

CcO is one of the key enzymes responsible for cellular respiration, whereas Mb and Hb are involved in oxygen (O_2) transport. The reaction between CcO and H_2S induces modification of the heme a_3 and Cu_B centers in the enzyme, reversibly inhibiting its activity and reducing ATP production (18, 19, 29, 53–55). The reduction in cellular ATP can then activate the K_{ATP} channels, which are otherwise blocked by ATP. In Mb and Hb, H_2S can also bind and modify the heme. The resulting derivatives, named sulfmyoglobin, sulfhemoglobin, or sulfheme species (6–9, 16), have lower O_2 affinity, thereby reducing O_2 transport and ATP production in the mitochondria, which can in principle, also activate the K_{ATP} channels.

The interaction of H_2S with CcO has also been implicated in the stimulation of a hibernation-like state in animals that do not normally hibernate (18, 44, 48). In this regard, it has been shown that H_2S reduces O_2 consumption and metabolic activity in mice, allowing the rodent to survive low O_2 concentrations that are otherwise lethal to them. In particular, the reduction in metabolic activity has been related to the decrease of cellular ATP induced by the interaction of H_2S with CcO and Hb/Mb. Based on these findings researchers are now investigating the possibility of injecting H_2S into patients with conditions related to insufficient blood supply to temporarily reduce metabolic activity and O_2 demand until they receive

Department of Chemistry, University of Puerto Rico, Mayagüez, Puerto Rico.

the appropriate treatment (48). Moreover, a number of drug candidates that mimic H_2S effects are now in development (46, 47, 50, 75). Therefore, understanding the mechanisms underlying the interaction of H_2S with its targets is crucial for the successful development of H_2S-based drugs. In fact, in the presence of sulfide, hemeproteins show different chemical reactivities. H_2S coordinates preferentially to the open sixth position of ferric iron (Fe^{III}) (34, 40, 61). Upon coordination, the gas can form a stable low spin Fe^{III}-SH_2 complex or it can reduce the ferric iron producing an unstable, Fe^{II}-SH_2 intermediate, which is rapidly converted to the unligated ferrous iron (Fe^{II}) (40, 61). H_2S can also react with oxy-hexacoordinated hemes (Fe^{II}-O_2) to form Fe^{III}-SH_2, most probably by nucleophilic displacement of the bound superoxide (40). Reaction of H_2S with Fe^{II}-O_2 can also modify the heme active center producing sulfheme complexes.

In CcO, H_2S modifies enzyme activity by binding and reducing the metal centers, whereas in Mb and Hb, H_2S reacts with the oxy form of the proteins (Fe^{II}-O_2) generating the sulfheme derivative. Why does H_2S react differently with these hemeproteins? What is the role of the heme iron oxidation state? Further, how does H_2S interact with hemeproteins to generate different intermediates and products? Remarkably, interactions of H_2S with hemeproteins have been recognized and studied for many years in invertebrate organisms (2, 26, 40, 41, 78, 80), making these systems excellent models to understand the reactivity of H_2S with other hemeproteins. In this review, we will evaluate the interaction of H_2S with vertebrate hemeproteins and correlate these interactions using the invertebrate hemeproteins as models. The metabolism of H_2S is briefly described, followed by an overview of sulfide reactivity with hemeproteins. Importantly, the attacking and coordinated sulfide species (*i.e.*, whether it is H_2S or the hydrosulfide ion) is unknown. Since at physiological pH, the predominant form is the hydrosulfide ion (HS^-), it has been suggested that it might be the attacking and the bound species. However, in Mb and other hemeproteins, sulfide binding decreases at alkaline pH, suggesting that the undissociated H_2S might be the attacking species in some hemeproteins (12, 40). In fact, the slow association rate observed at neutral pH has been ascribed to the rate-limiting protonation of HS^- to H_2S (40). Like H_2O, once H_2S binds to the heme, an equilibrium between Fe^{III}-SH^- and Fe^{III}-SH_2 can occur. Although it has not been possible to determine which form of sulfide is coordinated in hemeproteins, the term "H_2S" is generally used. Hence, in the remainder of this review, H_2S refers to the combination of the undissociated species and the hydrosulfide anion.

Overview of H_2S Metabolism in Humans

Endogenous H_2S in humans is produced directly by two pyridoxal phosphate (PLP)-dependent enzymes, cystathionine β-synthase (CBS, EC 4.2.1.22) and cystathionine γ-lyase (CSE, EC 4.4.1.1), and indirectly by 3-mercaptopyruvate sulfur transferase (3MST, EC 2.8.1.2) (33, 34, 38, 71). The catalytic core of CBS is constituted by two main domains, a PLP-containing domain and a heme-containing domain (Fig. 1A). CBS produces H_2S at the PLP active site through multiple reactions but preferably *via* condensation of cysteine and homocysteine (Fig. 1B) (33). The heme in CBS is a six-coordinate, low spin protoporphyrin IX with cysteine and histidine residues serving as endogenous axial ligands. This

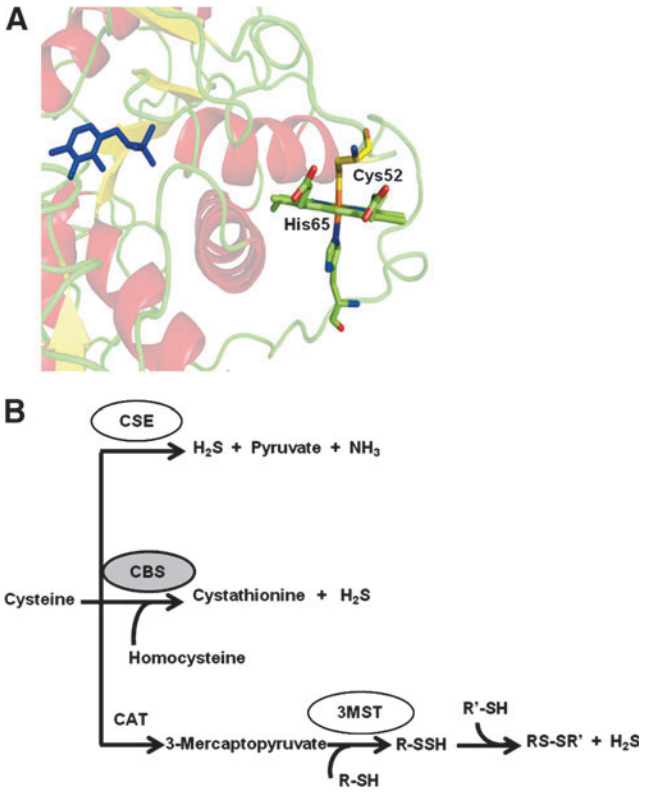

FIG. 1. Structure of CBS and H_2S generation. (A) Structure of the pyridoxal phosphate and heme domains of CBS generated from PDB file 1M54. **(B)** Enzymatic pathways of H_2S production in humans. The gas is produced by CBS, CSE, and MST from cysteine. H_2S, hydrogen sulfide; CBS, cystathionine β-synthase; CSE, cystathionine γ-lyase; MST, mercaptopyruvate sulfur transferase. (To see this illustration in color the reader is referred to the web version of this article at www.liebertonline.com/ars).

heme is believed to have a regulatory function and inhibits CBS activity upon binding CO in the ferrous state or by undergoing a redox-dependent ligand switch (3, 4, 13, 35, 62, 69, 70, 79). Binding of CO in ferrous CBS perturbs the heme environment and this is communicated to the PLP active site, resulting in a shift in the tautomeric equilibrium of PLP from the active ketoenamine to the inactive enolimine state (35, 79). CSE is mainly present in the peripheral tissues and under normal conditions, it catalyzes the α,β-elimination of cysteine, producing H_2S, pyruvate, and NH_3 (Fig. 1B) (17, 33, 34, 38). On the other hand, 3MST catalyzes the desulfuration of 3-mercaptopyruvate, which is produced from cysteine by cysteine aminotransferase. Unlike CBS and CSE, the final product of the 3MST enzymatic reaction is persulfide, not H_2S (33). H_2S is expected to be generated from the persulfide product only under reducing conditions (33, 34, 38).

Once generated by either enzymatic pathway, H_2S acts on target cells to either regulate neural or muscle activities (Fig. 2) (31, 33, 34, 38). In the brain, H_2S has been suggested to act as a neuromodulator and a neuroprotector by facilitating the induction of hippocampal long-term potentiation and protecting the neurons from oxidative stress. These effects have been related to the activation of N-methyl-D-aspartate receptors and to an increase in glutathione levels (34, 38). As a muscle relaxant, H_2S dilates blood vessels as well as gastrointestinal,

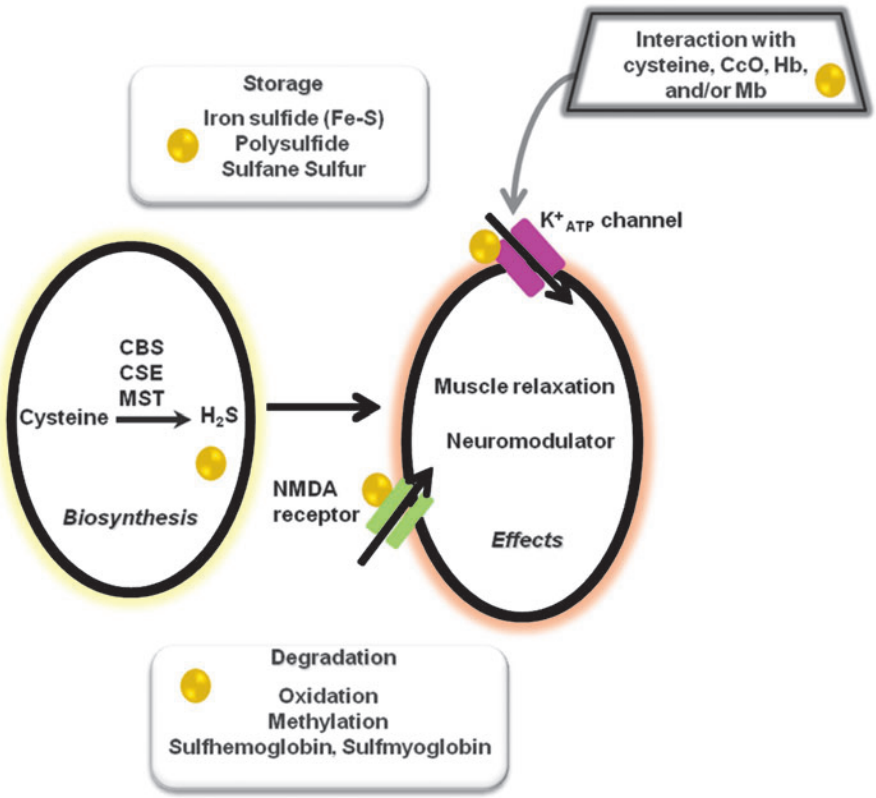

FIG. 2. Schematic representation of H_2S biosynthesis, biological effects, and degradation. One of the H_2S generating enzymes, CBS, is a hemeprotein. H_2S can act on the target cell or on the same cell by activating the K_{ATP} channels, a process that might involve sulfide interaction with hemeproteins. H_2S can also activate of N-methyl-D-aspartate receptors, regulating in turn neural activity. H_2S can be degraded to other, less toxic compounds through its reactivity with hemoglobin (Hb) or myoglobin (Mb). For instance, degradation of sulfhemoglobin and sulfmyoglobin by the physiologic turnover of red blood cells is considered to be one of the pathways for H_2S removal. The figure only highlights the heme-dependent pathways that might play a role in H_2S degradation. K_{ATP}, ATP-sensitive potassium. (To see this illustration in color the reader is referred to the web version of this article at www.liebertonline.com/ars).

pulmonary, and nasal tissues and is also involved in smooth muscle relaxation of the human penile corpus cavernosum tissue (33, 34, 38, 45, 77). The muscle relaxation effect has been attributed to opening of the K_{ATP} channels. It has also been shown that at low O_2 levels, inhibition of CcO by H_2S stimulates muscle relaxation directly without activating the K_{ATP} channels (39).

H_2S is mainly degraded in the mitochondria through a series of oxidation reactions (33, 34, 38), which convert the gas to sulfite (SO_3^{-2}), thiosulfate ($S_2O_3^{-2}$), and sulfate (SO_4^{-2}). In addition, H_2S can be catabolized by cytosolic methylation to dimethylsulfide (34). Interaction of H_2S with Mb and Hb to form the sulfheme complex has also been suggested to be one of pathways for H_2S removal (34, 46, 75).

Interaction of H_2S with Vertebrate Hemeproteins

Cytochrome c oxidase

CcO is involved in the final step of aerobic respiration and reduces O_2 to water. It contains two hemes, heme *a* and heme a_3, and two copper centers, Cu_A and Cu_B (Fig. 3). The catalytic center comprises the heme a_3, the Cu_B, and a tyrosine residue, which is coordinated to Cu_B. Physiologically, the complex receives electrons from cytochrome *c* and transfers them through Cu_A, heme *a*, and the heme a_3-Cu_B center. The reduced ferrous (Fe^{II}) heme a_3 binds O_2 and transfers electrons to the ligand, reducing O_2 to water. During this process, protons are translocated across the mitochondrial membrane, establishing an electrochemical potential that is used by another enzyme to synthesize ATP.

The effects of sulfide on the activity of CcO were known since the 18th century; however, the inhibition of enzyme by H_2S was first described by Keilin in 1929, who observed a substantial reduction of CcO activity after exposure of different tissues to the gas (36). Using various spectroscopic approaches, Nicholls and others later demonstrated that H_2S binds directly to the ferric (Fe^{III}) heme a_3 center and completely inhibits CcO activity (Fig. 3A) (28, 29, 53–55). However, they observed that at low (nearly stoichiometric) H_2S concentrations, the gas stimulates O_2 consumption without having an inhibitory effect and that >1 mol of H_2S was required for complete inhibition of the enzyme. Based on these findings, a generalized mechanism was proposed, which explained the interaction of H_2S with the resting enzyme as depicted in Figure 3B. At low sulfide levels (1:1 stoichiometry) H_2S binds and reduces the ferric heme a_3 center in a reaction that results in the formation of a ferrous heme a_3-SH_2 intermediate, release of sulfide (as an SH radical or as elemental sulfur), and O_2 uptake. They suggested that under these circumstances, H_2S could act as a substrate instead of an inhibitor (54, 55). At moderate concentrations (1:2 stoichiometry), H_2S also coordinates and reduces the Cu_B center with the concomitant formation of a stable Cu_B-SH_2 moiety. It was presumed that the heme a_3-Cu_B-SH_2 center adopts a new conformational state, which is unable to form a stable complex with O_2. It was therefore suggested that at higher H_2S concentrations (1:3 stoichiometry), full inhibition of CcO results because H_2S binds tightly to ferric heme a_3, either because heme a_3 is in a different conformational state or because the Cu_B-SH_2 complex restrains the electron transfer process to the ferric heme. Recently, Collman and coworkers confirmed that at low concentrations, the gas indeed reduces heme a_3 without inducing inhibition (18). They also observed that at moderate H_2S concentrations, the gas binds to the ferrous heme a_3 of CcO

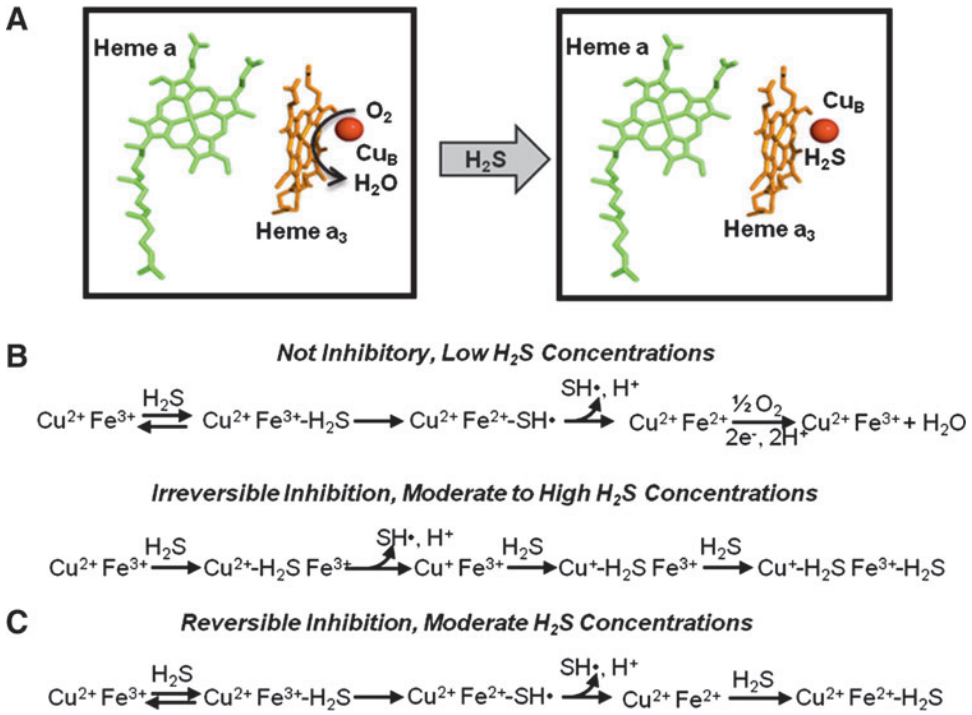

FIG. 3. Structure of the CcO catalytic center and its reactivity with H_2S. (A) The heme a_3 and Cu_B catalytic centers of CcO under normal conditions and upon inhibition by H_2S. Schemes for H_2S interaction with CcO as suggested by Nicholls (29, 52, 53, 55) **(B)** and by Collman **(C)** (17). At low to moderate concentrations, H_2S interacts with the heme a_3/Cu_B binuclear center, modifying CcO activity and at higher concentrations, H_2S binds directly to the ferric heme a_3 group inhibiting CcO. CcO, Cytochrome *c* oxidase. (To see this illustration in color the reader is referred to the web version of this article at www.liebertonline.com/ars).

with the immediate formation of a ferrous heme a_3-SH_2 derivative that reversibly inhibits CcO activity (Fig. 3C) (18). In the presence of O_2, H_2S is rapidly displaced restoring CcO activity.

These models beg the question as to how at low H_2S concentrations, the gas reduces the metal centers of CcO without inhibiting its activity, whereas at higher concentrations complete inhibition is observed. We have demonstrated recently that heme reduction is greatly enhanced at high H_2S concentrations and in proteins having proton acceptor groups in the vicinity of the ligand (61). Hence, to propose a plausible mechanism to explain the binding and inhibition kinetics of H_2S with CcO, H_2S concentration and the polarity of the ligand binding site should be considered. We propose that at low sulfide concentration, the polar environment near heme a_3, which includes the Cu_B center and a tyrosine residue, may stimulate heme a_3 reduction by H_2S. At higher concentrations (1:3 stoichiometry), H_2S also binds and reduces the Cu_B and heme a_3 centers, forming a stable Cu_B-SH_2 moiety and the unstable heme Fe^{II}-SH_2 inhibitory complex, as suggested by Collman *et al.* (18). At this stage, reduction of Cu_B and heme a_3 may be facilitated by the presence of slight H_2S excess. However, since an excess of H_2S enhances heme reduction, exhaustion of the gas might limit heme a_3 reduction, stabilizing in turn the final heme a_3 Fe^{III}-SH_2 inhibitory species. Based on this model one can hypothesize that at moderate concentrations, H_2S can exert protective effects in mammals. Under these conditions the affinity of heme a_3 for O_2 decreases, diminishing in turn cellular ATP, which can in principle stimulate muscle relaxation.

Hb and Mb

Vertebrate Hb and Mb are globular hemeproteins whose physiological functions are related to their ability to bind molecular O_2. In mammals, Hb consists of four globular chains, each containing a heme group. In contrast, Mb is a monomeric globular protein with a single heme group. In both hemeproteins, O_2 binds directly to the ferrous iron. O_2 binding is stabilized in part by a neighboring histidine residue (Fig. 4) and is later released for utilization in mitochondrial ATP production. Both Hb and Mb bind H_2S in the ferric state as a heme ligand. However, the affinity is very low and heme reduction by H_2S is rapidly observed with the concomitant formation of the deoxy Fe^{II} and/or oxy Fe^{II}-O_2 derivatives.

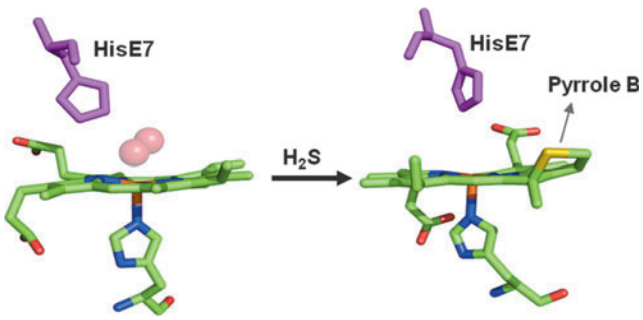

FIG. 4. The active site of Mb with bound oxygen (left) and after exposure to H_2S (right). The final sulfheme product is a modified chlorin-type heme with a sulfur atom incorporated into one of the pyrrole rings. The structures were generated using PDB files 1MBO (left) and 1YMC (right), respectively. In Hbs, the amino acids are arranged in six to eight helical segments that are labeled A to H with the first residue of segment A being A1. In the figure, HisE7 refers to the histidine residue at position 7 of helix E, which in human Hb and Mb stabilizes O_2 through hydrogen bonding interactions.

The reaction of H_2S with Hb and Mb was first recognized in 1863 by Hoppe-Seyler, who observed the formation of a green compound when the proteins were exposed to the gas in the presence of O_2 (37, 52). He described these new compounds as sulfhemoglobin and sulfmyoglobin with a characteristic absorption band at $\sim$618 nm. In 1933, Keillin showed that O_2 was essential for the formation of these compounds and that they were only obtained from the oxy (Fe^{II}-O_2) and met (Fe^{III}-OH_2) forms of the proteins (37). However, in the met complex, prior reduction of the heme by H_2S was required to produce the sulfheme derivatives. It was later shown that these sulfhemoglobin and sulfmyoglobin complexes consisted of a chlorin type heme in which one of the pyrrole rings was modified by the incorporation of the sulfur atom across the β-β double bond of the pyrrole "B" (Fig. 4) (6–9, 16). Incorporation of the sulfur atom was suggested to remove electron density from the ferrous iron toward the periphery of the chlorin ring. The delocalization of π electron density away from the iron was supported in part by vibrational analysis of the sulfheme-CO complexes, in which an increase in the stretching frequency of bound CO was observed (6, 14). A decrease in electron density of the "d" iron orbitals decreases the backbonding density form the iron to the antibonding π*orbital of carbon monoxide, increasing in turn the energy of the CO vibrational normal mode. Since O_2 forms a stable complex only with ferrous heme, the electron delocalization away from the iron in the sulfheme chlorin ring was therefore expected to decrease O_2 affinity (14). Subsequent studies demonstrated that, in fact, the sulfheme compounds were able to bind O_2 reversibly but with a much lower affinity than the unmodified proteins and that O_2 binding was dictated by the specific aspect of the overall hemeprotein structure (6, 8, 14). O_2 binding in sulfmyoglobin was shown to be $\sim$2500-fold lower, whereas binding in sulfhemoglobin was reduced by a factor of $\sim$135 (14). In Mb and Hb, the final sulfheme product cannot be reconverted to the normal hemeproteins by natural mechanisms in the red cells (8).

Like methemoglobin, which results from the autoxidation of the ferrous iron to the nonfunctional ferric state of the protein, high levels of sulfhemoglobin can be potentially toxic. The inability of both sulfmyoglobin and sulfhemoglobin to bind O_2 effectively can lead to sulfhemoglobinemia, a rare cause of cyanosis induced by drugs such as phenacetin, dapsone, sulphonamides, and metoclopramide, and by exposure to other sulfur-containing compounds (57, 68, 76). However, moderate concentrations of sulfhemoglobin are well tolerated despite the low O_2 binding (1, 25). This has been explained by the observed right shift in the Hb-O_2 dissociation curve, which indicates that although it is more difficult for sulfhemoglobin to bind O_2, it facilitates O_2 delivery to tissues. Also, in most patients, sulfhemoglobinemia has few adverse clinical consequences and are usually resolved spontaneously by normal erythrocyte destruction (1). Therefore, formation of these sulfheme complexes at moderate levels and their destruction by the physiologic turnover of red blood cells can be considered to be one of the pathways for H_2S degradation. It is also reasonable to suggest that the reduced O_2 binding in the sulfheme derivatives decreases ATP synthesis, which in turn could activate the K_{ATP} channels. Further, the presence of the sulfheme complexes could represent a control mechanism for O_2 uptake by CcO during periods of hibernation.

Importantly, the mechanism by which the sulfheme derivative is formed is unknown. It has been suggested that oxo-ferryl intermediates may be involved in sulfheme formation since sulfhemoglobin and sulfmyoglobin can also be generated with hydrogen peroxide (H_2O_2). It is well known that the reaction of O_2 or H_2O_2 with hemeproteins produces ferryl Compound I, ($Fe^{IV}=O$ $Por^{\bullet+}$) and Compound II ($Fe^{IV}=O$ Por) (20–23, 64). Curiously, the reaction of CcO with either O_2 or H_2O_2 also produces oxo-ferryl intermediates, but sulfheme formation has not been detected on this protein. Why do Hb and Mb form sulfheme while CcO does not? As discussed in the next section, we have observed that the histidine residue near the heme in Hb and Mb is essential for sulfheme formation. In CcO, the histidine residues near the heme a_3 center are not adequately orientated to form the sulfheme complex.

Interaction of H_2S with Invertebrate Hemeproteins

From bacteria to plants and animals, hemeproteins are found in virtually all organisms (78). In many invertebrate systems, the reactivity of hemeproteins, and in particular Hbs, toward H_2S has been associated with relevant physiological processes. Marine invertebrates living in sulfide-rich environments represent such an example (2, 40, 41). One of the best studied of these organisms is the clam, *Lucina pectinata*, and we therefore begin with a description of H_2S interaction with clam Hb.

Hemoglobin I from L. pectinata

The clam *L. pectinata* lives in sulfide-rich mangroves and it is specifically abundant in the southwest coasts of Puerto Rico. The nutritional needs of this clam, which lacks a mouth and gut, are met by a symbiotic relationship with sulfide-oxidizing bacteria. Bacteria living inside the gill oxidize H_2S in the presence of O_2 and this energy is utilized to synthesize organic nutrients for the invertebrate. Wittenberg and coworkers demonstrated that the protein responsible for delivering H_2S to the bacteria is a hemeprotein called hemoglobin I or HbI (40, 41). HbI is a monomeric protein (Fig. 5A) and it is one of the few known H_2S carriers. Binding of H_2S by HbI not only maintains the symbiotic relationship with the bacteria, but also protects the clam from H_2S toxicity. The affinity of ferric HbI for H_2S is very high and results from fast association ($k_{on} = 2.3\times10^5$ $M^{-1}s^{-1}$) and very slow dissociation (k_{off} 0.22×10^{-3} s^{-1}) rate constants. Structural studies of the HbI active site have shown that this protein has a glutamine residue at the distal ligand binding site, instead of the equivalent histidine typically found in many invertebrate and vertebrate organisms (66). In addition to glutamine, HbI has phenylalanine residues near the heme, generating what is known as the "Phe-cage."

A close-up of the unusual amino acid composition of the HbI distal ligand binding site is shown in Figure 5B and is believed to be responsible for the high H_2S affinity. Indeed, early spectroscopic studies of HbI with other well-known ligands (such as CO, cyanide, H_2O, and O_2) suggested that glutamine is flexible and controls ligand access to the HbI heme pocket and that hydrogen bonding and other interactions with the Phe-cage contribute to ligand stability (15, 51, 60). Using site-directed mutagenesis, and spectroscopic and theoretical

approaches, we have shown that protein fluctuations are required to allow H_2S access to the HbI distal heme site.

Once in the distal heme site, the flexibility of glutamine allows the ligand to bind rapidly to the ferric iron (24, 43, 59–61, 63). The gaseous ligand is stabilized in part by a hydrogen bonding interaction with glutamine (61, 66). H_2S release is dictated by two competing processes involving slow dissociation of H_2S from the ferric adduct and heme iron reduction followed by H_2S liberation (Fig. 5C). The former process dominates at low H_2S concentrations, and the latter at high concentrations (61). Heme reduction is facilitated by the hydrogen bond between glutamine and bound H_2S and replacement of this residue by valine, which disrupts the hydrogen bond, precludes reduction. In addition, the reduction process is greatly enhanced in HbI mutants having proton acceptor groups near the bound H_2S. For instance, replacement of glutamine by histidine results in rapid heme reduction. Further, the HbI glutamine → histidine mutant was the only one in which sulfheme formation was observed after heme reduction. It is plausible that histidine plays an essential role in sulfheme formation and in other hemeproteins lacking a corresponding histidine residue, sulfheme formation is not seen (Table 1). Collectively, these data suggest that the distal-site environment in hemeproteins controls not only H_2S binding and stabilization, but heme reduction and sulfheme formation as well.

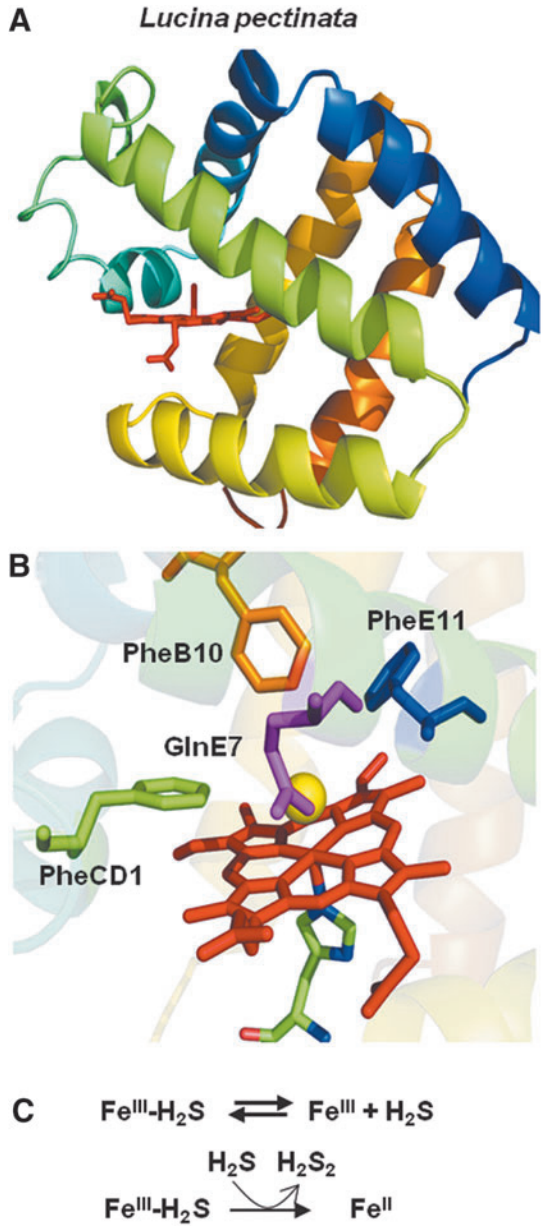

FIG. 5. Structure of *Lucina pectinata* HbI (PDB:1MOH) and its reactivity with H_2S. (A–C) HbI tertiary structure, heme active site, and its reaction with H_2S, respectively. The nomenclature in **(B)** refers to the positions of the amino acids near the heme. In *L. pectinata* HbI, the first reaction in **(C)** dominates at low H_2S concentrations and the second one at higher ligand concentrations.

Several factors control H_2S reactivity with hemeproteins: (i) accessibility of H_2S to the heme cavity, (ii) H_2S concentration, which influences heme reduction, (iii) polarity of the distal environment surrounding the bound H_2S, and (iv) orientation of the distal side residues. We have proposed a general scheme to describe the interaction of H_2S with hemeproteins (Fig. 6). At low H_2S concentrations (3 to 10 molar excess), hemeproteins with a relatively open distal pocket will react with H_2S readily forming the heme-SH_2 complex (Fe^{III}-SH_2). Sulfide release is then dictated by two competing processes involving simple H_2S dissociation and heme iron reduction. Hemeproteins with low polarity environments in the vicinity of the iron, form a stable heme-SH_2 species and sulfide release is dictated by slow H_2S dissociation without inducing significant heme reduction. Hemeproteins in which active-site residues are not oriented to form strong hydrogen bonding interactions with H_2S also show the same reactivity. In contrast, hemeproteins with hydrogen bond acceptor groups, oriented to favor strong interactions with the bound ligand, can stimulate heme reduction. As in HbI, strong hydrogen bond interactions between the hemeproteins and the bound H_2S can facilitate rapid deprotonation of H_2S, stimulating formation of an Fe^{II}-SH· intermediate by one electron transfer from the Fe^{III}-SH^- species. Reduction of the heme by the Fe^{III}-SH^- species is supported by the fact that in model porphyrinate systems, coordination of HS^- to ferric iron produces Fe^{II} high spin derivatives (58). In the presence of a slight excess of H_2S, the latter can react with the Fe^{II}-SH· radical intermediate producing deoxy heme Fe^{II} and a

Table 1. Representation of the Different Hemeproteins Evaluated for Sulfheme Formation and Their Corresponding E7 Residues

Protein	*E7 Residue*	*Sulheme*[a]
Horse heart Mb	His	Yes (618 nm)
Human Hb	His	Yes (620 nm)
Lucina Pectinata HbII and HbIII	Gln	No
L. Pectinata Hbl	Gln	No
HbI PheE11Val	Gln	No
HbI PheB10Leu	Gln	No
HbI GlnE7His	His	Yes (622 nm)
Macrobdella decora Hb	His	Yes (620 nm)
Lumbricus terrestris Hb	His	Yes (620 nm)

[a]Data from ref. (67).

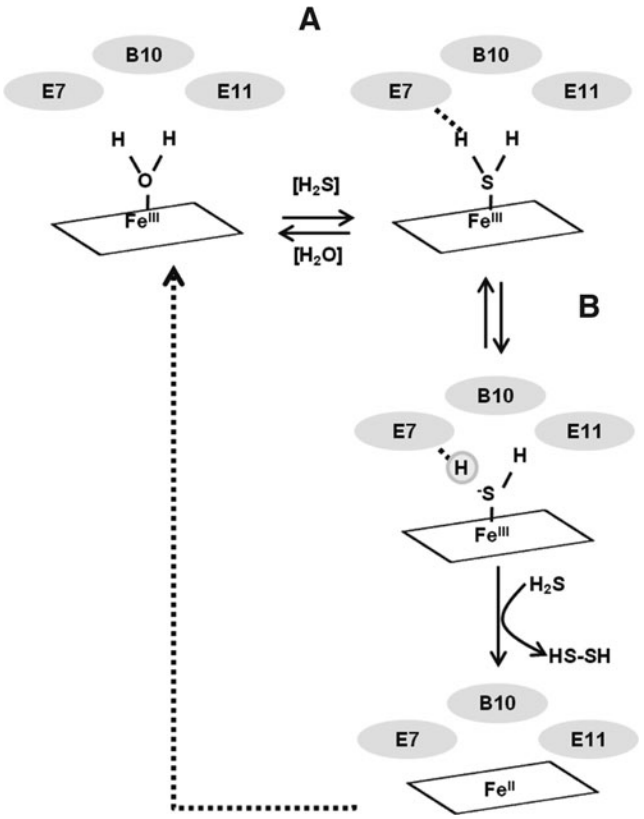

FIG. 6. Generalized reactions for H_2S reactivity with hemeproteins. Reaction **(A)** involves H_2S interaction with hemeproteins having nonpolar or hydrogen bond donor residues in their heme active site, while **(B)** engages the interaction of the bound gaseous ligand with hydrogen bond acceptor groups near the heme. Residues in E7, E11, and B10 positions are very important in regulating the binding and discrimination of ligands in hemeproteins.

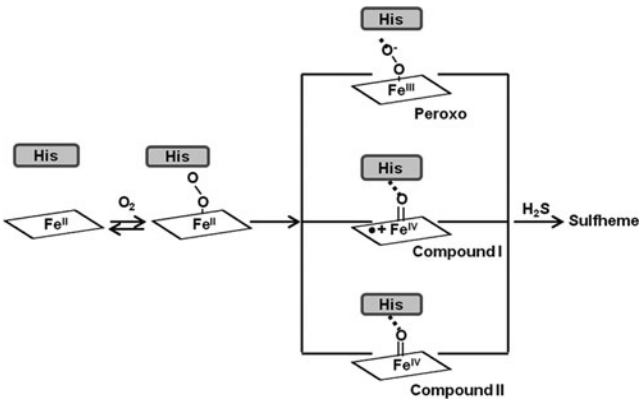

FIG. 7. Proposed mechanism for sulfheme formation. Suggested intermediates upon reaction of H_2O_2, in the presence of H_2S, with His distal Si proteins that produces the suflheme derivates.

polysulfide species (61). This is also supported by the observation that the interaction of ·SH radicals with H_2S, in the presence of slight sulfide excess, produces polysulfide and H_2S compounds, and that at higher concentrations, these polysulfides can produce elemental sulfur (73). We also suggest that following heme reduction and in the presence of O_2, proteins having a histidine residue in their heme environment can promote sulfheme formation. In fact, we have recently evaluated the role of histidine in sulfheme formation by introducing point mutations in the *L. pectinata* HbI heme pocket to mimic the distal site of Mb and to identify the residues involved in sulfheme formation (67). Formation of the sulfheme product was monitored by the characteristic 620 nm band and by resonance Raman spectroscopy. Sulfheme production was only observed in the HbI glutamine → histidine mutant and in proteins having histidine in their heme active site, including human Hb and Mb and the giant Hbs from *Macrobdella decora* and *Lumbricus terrestris* (67). The 620 nm band is only observed after addition of H_2S to the proteins and is assigned to the sulfheme derivative. We hypothesize that after heme reduction, the ferrous iron coordinates O_2 and the histidine residue stabilizes the peroxo or the oxo-ferryl intermediates, which in the presence of H_2S stimulates sulfheme formation (Fig. 7).

In the context of the physiological function of HbI, we hypothesize that at low sulfide concentrations (1:1 stoichiometry), simple dissociation and heme reduction are involved in the delivery of H_2S to the symbiotic bacteria. However, under these conditions, the slow release of H_2S dominates over the heme reduction reaction. On the other hand, at high H_2S concentrations, its delivery is facilitated by the heme reduction reaction, which simultaneously promotes the formation of polysufides, and elemental sulfur. These elemental sulfur compounds are then stored within clam tissues and used by the bacterial endosymbionts during sulfide starvation or at low H_2S concentrations. Indeed, Lechaire and coworkers showed that the gill tissues of *L. pectinata* contain elemental sulfur produced by the clam (42). They suggested that this compound may act as an energy source for the bacteria during sporadic depletion of environmental H_2S.

In humans, H_2S might also be stored in the body as polysulfides and released in response to physiologic stimuli (Fig. 2) (34, 38). Therefore, heme reduction and polysulfide and elemental sulfur formation may be relevant products resulting from the interaction of H_2S with hemeproteins in our body. In fact, these products have been suggested to form in CcO and flavocytochrome *c* sulfide dehydrogenase (53–55, 73).

Hbs from the worm Riftia pachyptila

The giant tubeworm *R. pachyptila* is another interesting invertebrate that lives in the sulfide-rich deep-sea hydrothermal vents and is also characterized by the presence of symbiotic sulfide-oxidizing bacteria that need to be supplied with both H_2S and O_2 (2). *Riftia* supplies H_2S and O_2 to the endosymbionts by binding both ligands simultaneously at two different sites in its extracellular Hbs. Two of these Hbs are dissolved in the vascular blood of *Riftia*, and have been designated V1 and V2, and a third one, named C1, is found in the coelomic fluid of the worm (2, 26, 80). These Hbs are giant and complex proteins with molecular weights ranging from ~ 3500 kDa for V1 to ~400 kDa for V2 and C1. They appear to bind O_2 in their heme groups and H_2S in other sites remote from the hemes. It was initially thought that the binding of H_2S occurred at "free cysteine" or cysteine residues not

involved in disulfide bonds (2, 80). However, the role of cysteines in H_2S binding was questioned by Flores and coworkers, who solved the crystal structure of the worm C1 Hb (26). They showed that this Hb (Fig. 8A) consists of 24 heme-containing globin chains tightly associated to form a hollow sphere with 12 zinc ions bound near the sphere. The authors showed that the Zn^{2+} ions bind H_2S readily and that the cysteine residues previously proposed as sulfide-binding sites were located in hydrophobic environments that might restrict access to H_2S.

Whether H_2S binds to the Zn^{2+} ions or the cysteine residues is still unclear; however, what is clear is that the heme groups in the Hbs from *R. pachyptila* do not interact directly with the gas. Instead, these sites are limited to O_2 binding only. The exclusion of H_2S from the heme cavity might be due to restricted accessibility. As Figure 8A shows, the protein is gigantic in comparison to the other Hbs (Figs. 5A and 9A), which likely plays a role in restraining rapid access of H_2S to the hemes as discussed below. In fact, it has been shown that H_2S binding to HbI from *L. pectinata* is nearly 1000 times slower than binding of O_2, suggesting that protein fluctuations are required to allow sulfide access to the heme distal site probably due to the bulkier character of H_2S (40, 61). Thus, direct binding of H_2S to the hemes in *Riftia* Hb may require large protein fluctuations, delaying in turn the entrance of the ligand to the distal active site. In addition, as shown in Figure 8A, the hemes (in red) are buried in the protein matrix, consistent with the model that H_2S binding to the zincs, which are located in the exposed hollow sphere, is more facile (26). The binding of H_2S to the zinc ion sites would have the benefit of avoiding sulfheme formation. Although the C1 Hb in *Riftia* has a histidine residue near the heme (Fig. 8B), formation of a sulfheme complex has not been detected. In contrast, sulf-

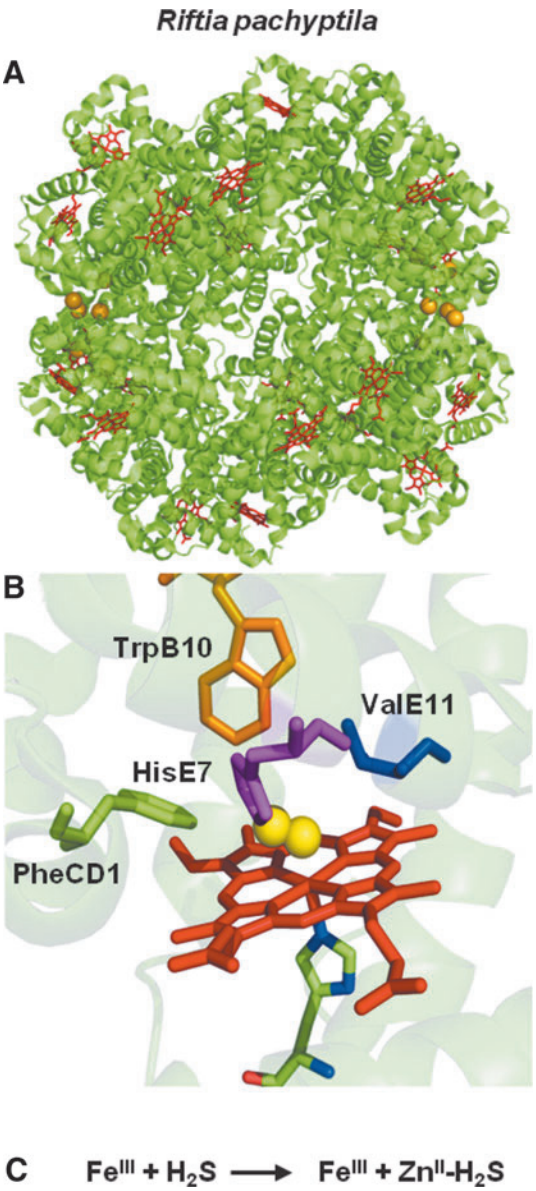

FIG. 8. Structure of *Riftia pachyptila* C1 Hb (PDB: 1YHU) and its reactivity with H_2S. (A–C) C1 Hb quaternary structure, heme active site, and its reaction with H_2S, respectively. The nomenclature in **(B)** refers to the positions of the amino acids near the heme.

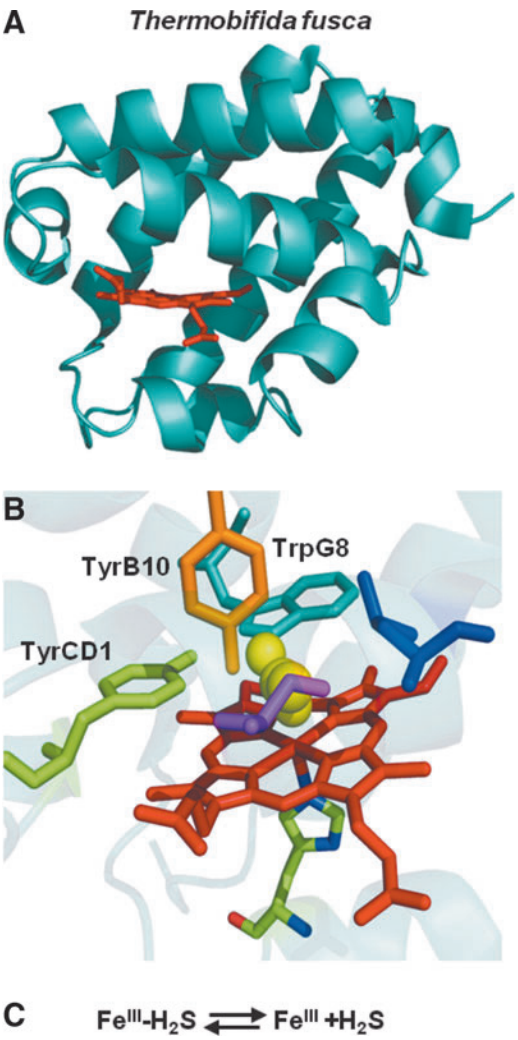

FIG. 9. Structure of *Thermobifida fusca* truncated Hb (PDB: 2BMM) and its reactivity with H_2S. (A–C) *T. fusca* trHb tertiary structure, heme active site, and its reaction with H_2S, respectively. The nomenclature in **(B)** refers to the positions of the amino acids near the heme.

heme formation has been observed in Hbs from *M. decora* and *L. terrestris*, which live in sulfide-free environments and also contain histidine at the ligand binding site (67, 74, 78). Similar to *Riftia*, these Hbs are large, consisting of 144 heme-containing globin chains with an analogous quaternary structure. Structural studies have demonstrated that "free cysteine residues" are absent in these Hbs and that if zinc is present, the content is low (*e.g.*, one zinc atom in *Lumbricus* hemoglobin) (2, 72). This implies that in the presence of O_2, H_2S diffuses through these proteins without encountering alternative binding sites and once at the heme site, can interact directly with heme forming the sulfheme derivatives. These observations also support the notion that histidine is required for the formation of the sulfheme derivatives. On this basis, we suggest that in *R. pachyptila*, the zinc ions (or the cysteine residues) transport H_2S to the symbiotic bacteria and protect the worm from H_2S toxicity by impeding access to the hemes, thus avoiding sulfheme formation, which can limit O_2 transportation.

Hbs from Bacillus subtilis *and* Thermobifida fusca

B. subtilis and *T. fusca* are rod-shaped bacteria that are usually found in soils and can tolerate extreme environmental conditions. These organisms have specialized truncated Hbs (Bs-trHb for *B. subtilis* and Tf-trHb for *T. fusca*) that have high affinity for H_2S and are believed to play a possible physiological role in the bacteria (56). In particular, these Hbs have been suggested to be involved in sulfur metabolism in these microorganisms, including cysteine biosynthesis and thiol-based redox homeostasis. While direct experimental evidence for the role of Hb in sulfur metabolism is lacking, the high affinity of both Bs-trHb (5.0×10^6 M^{-1}) and Tf-trHb (2.8×10^6 M^{-1}) for H_2S provides relevant paradigms for studying the interaction of H_2S with hemeproteins.

It has been recently shown that, like HbI from *L. pectinata*, the affinity of the trHbs for H_2S results from the very rapid association and extremely slow dissociation kinetics (Table 2) (56). Like HbI, these trHbs are monomeric proteins (Fig. 9A) and their H_2S binding constants suggest that the gas has rapid access to the bound heme. The crystal structure of Tf-trHb (Fig. 9B) reveals that its distal site is characterized by the presence of aromatic amino acids surrounding the heme group, including tyrosine residues and a tryptophan residue. As shown recently, replacement of tryptophan, which has a larger volume (227.8 $Å^3$) with phenylalanine, which has smaller volume (189.9 $Å^3$) (81), increases the association constant by a factor of 50, consistent with the suggestion that in the trHbs, H_2S association is controlled in part by the space in the vicinity of the heme (56). Moreover, since the rate of sulfide association is $\sim$2000 slower than of O_2 in Tf-trHb, protein fluctuations that allow access of the larger H_2S ligand to the distal site may also be required in this Hb (11, 27).

To explain the slow H_2S dissociation observed in these trHbs, it was suggested that tryptophan acts as a hydrogen bond donor in both Bs-trHb and Tf-trHb, stabilizing the bound sulfide, and retarding its release. Unlike HbI, this electrostatic interaction does not promote heme reduction and H_2S release. This does not however contradict the reaction scheme proposed in Figure 6. As stated above, heme reduction is only invoked for proteins having residues with hydrogen bond acceptor groups near the heme. From an electrostatic point of view, one can infer that when hydrogen bond donating residues interact with the bound H_2S, a significant charge transfer occurs from the lone pair electrons of the acceptor sulfur ligand to the orbital of the donor, thereby increasing the ionization potential of the gaseous ligand and consequently, its ability to donate an electron to the heme iron decreases (10).

Overall, the available structures of Hb C1 from *R. pachyptila* and the Hbs from *B. subtilis*, *T. fusca*, and *L. pectinata*, supports the model that binding of sulfide to hemeproteins is dictated by ligand accessibility to the heme group and the dielectric of the heme environment.

Role of H_2S Reactivity with Hemeproteins: Concluding Comments and Future Perspective

Based on the discussion of H_2S interactions with vertebrate and invertebrate hemeproteins, we can summarize that at least four reactions influence H_2S reactivity with hemeproteins: (i) binding of H_2S to alternate sites such as cysteine, copper, and zinc ions, (ii) coordination of H_2S to the ferric heme iron without inducing reduction or sulfheme production, (iii) binding of H_2S to the ferric iron with subsequent reduction of the heme, and (iv) incorporation of H_2S into one of the pyrrole rings of the heme, generating the sulfheme derivative. In hemeproteins having nonpolar or hydrogen bond donating residues in their heme binding site, H_2S is slowly liberated from the ferric heme without involvement of redox chemistry. In contrast, proteins with hydrogen bond acceptor groups near the heme, promote reduction of the

Table 2. Oxygen and H_2S Association and Dissociation Constants of *Lucina pectinata* HbI, *Bacillus subtilis*, and *Thermobifida fusca* Truncated Hemoglobins and a Tf-TrpG8Phe Mutant

Protein	Fe^{III}-H_2S k_{on} ($M^{-1}S^{-1}$)	Fe^{III}-H_2S k_{off} (S^{-1})	Fe^{II}-O_2 k_{on} ($M^{-1}S^{-1}$)	Fe^{II}-O_2 k_{off} (S^{-1})
L. Pectinata Hbl[a]	2.3×10^5	0.00022	$100–200\times10^6$	61
Bs-trHb	$1.3\times10^{4,b}$	0.0026[b]	$30\times10^{6,c}$	0.0048[c]
Tf-trHb	$5\times10^{3,b}$	0.0018[b]	$0.9\times10^{6,d}$	0.07[d]
Tf-TrpG8Phe	$4.1\times10^{4,b}$	0.36[b]		

[a]Data from ref. (40).
[b]Data from ref. (56).
[c]Data from ref. (28).
[d]Data from ref. (11).
TrHb, truncated hemoglobins.

heme iron by a second H_2S molecule with the concomitant formation of polysulfides and/or S°. Subsequent to heme reduction, hemeproteins having histidine residues in their active site can also form the sulfheme complex in the presence of O_2 and a slight H_2S excess (Fig. 7).

In human Hb and Mb as well as in catalase (52) and lactoperoxidase (49), the histidine residue near the heme might plays an essential role in sulfheme formation. In CcO, the histidine residues within the catalytic center do not have the proper orientation to interact directly with the heme a_3-O_2 moiety, preventing interaction with the heme-peroxo or oxoferryl intermediates, thus avoiding in turn sulfheme production. This might explain in part why H_2S induces reduction of the Cu_B and the heme a_3 center, in CcO without stimulating sulfheme formation. H_2S also reduces the heme iron of cytochrome *c* (18, 55). In cytochrome *c*, the heme is coordinated by a methionine and a histidine residue at the distal and proximal sites, respectively. Although the mechanism by which H_2S reduces the heme center in cytochrome *c* is unclear, it has been suggested that sulfide can bind and reduce the heme iron thus affecting the redox state of the protein (28, 55). Interestingly, the heme in CBS, the hemeprotein that catalyzes H_2S biosynthesis, also has a cysteine ligand at the distal site and a histidine at the proximal site (69, 70). Thus, the interaction of H_2S with CBS and cytochrome *c* warrants further investigations. Moreover, it has been suggested recently that human neuroglobin, a member the globin super-family, which is found in the central nervous system, might influence H_2S levels, thus protecting cells from sulfide toxicity (12). However, H_2S binding to neuroglobin appears to be complex and a thorough investigation of the mechanism of its interaction with sulfide is needed.

Based on the published literature, the reactivity of H_2S with hemeproteins can be summarized by the generalized reactions shown in Figures 6 and 7. Key issues that remain to be investigated include (a) the role of the distal heme a_3 environment in CcO reduction at low H_2S concentrations and the reduction of the Cu_B and the heme a_3 center at moderate concentrations, (b) the direct role of histidine in sulfheme formation, (c) the intermediates associated with sulfheme formation, (d) the reactivity of the H_2S/HS^- pair with other hemeproteins like cytochrome *c*, CBS, and human neuroglobin, and (e) identifying additional hemeprotein targets of H_2S. Insights into these issues will allow unraveling of the mysteries associated with H_2S reactivity in hemeproteins, and allow assessment of the physiological implications of these interactions.

Acknowledgments

This work was supported in part by funds from the National Science Foundation (Grant 0843608) and NIH-NIGMS/MBRS-SCORE 5 S06GM008103-36. We thank the graduate student Laura B. Granell for her assistance during the work.

References

1. Aravindhan N and Chisholm DG. Sulfhemoglobinemia presenting as pulse oximetry desaturation. *Anesthesiology* 93: 883–884, 2000.
2. Bailly X and Vinogradov S. The sulfide binding function of annelid hemoglobins: relic of an old biosystem? *J Inorg Biochem* 1: 142–150, 2005.
3. Banerjee R, Evande R, Kabil O, Ojha S, and Taoka S. Reaction mechanism and regulation of cystathionine beta-synthase. *Biochim Biophys Acta* 1647: 30–35, 2003.
4. Banerjee R and Zou CG. Redox regulation and reaction mechanism of human cystathionine-beta-synthase: a PLP-dependent hemesensor protein. *Arch Biochem Biophys* 433: 144–156, 2005.
5. Benavides GA, Squadrito GL, Mills RW, Patel HD, Isbell TS, Patel RP, Darley-Usmar VM, Doeller JE, and Kraus DW. Hydrogen sulfide mediates the vasoactivity of garlic. *Proc Natl Acad Sci USA* 104: 17977–17982, 2007.
6. Berzofsky JA, Peisach J, and Alben JO. Sulfheme proteins. III. Carboxysulfmyoglobin: the relation between electron withdrawal from iron and ligand binding. *J Biol Chem* 247: 3774–3782, 1972.
7. Berzofsky JA, Peisach J, and Blumberg WE. Sulfheme proteins. I. Optical and magnetic properties of sulfmyoglobin and its derivatives. *J Biol Chem* 246: 3367–3377, 1971.
8. Berzofsky JA, Peisach J, and Blumberg WE. Sulfheme proteins. II. The reversible oxygenation of ferrous sulfmyoglobin. *J Biol Chem* 246: 7366–7372, 1971.
9. Berzofsky JA, Peisach J, and Horecker BL. Sulfheme proteins. IV. The stoichiometry of sulfur incorporation and the isolation of sulfhemin, the prosthetic group of sulfmyoglobin. *J Biol Chem* 247: 3783–3791, 1972.
10. Biswal HS, Shirhatti PR, and Wategaonkar S. O-H...O versus O-H...S hydrogen bonding I: Experimental and computational studies on the p-cresol x H_2O and p-cresol x H_2S complexes. *J Phys Chem A* 113: 5633–5643, 2009.
11. Bonamore A, Ilari A, Giangiacomo L, Bellelli A, Morea V, and Boffi A. A novel thermostable hemoglobin from the actinobacterium *Thermobifida fusca*. *FEBS J* 272: 4189–4201, 2005.
12. Brittain T, Yosaatmadja Y, and Henty K. The interaction of human neuroglobin with hydrogen sulphide. *IUBMB Life* 60: 135–138, 2008.
13. Carballal S, Madzelan P, Zinola CF, Graña M, Radi R, Banerjee R, and Alvarez B. Dioxygen reactivity and heme redox potential of truncated human cystathionine beta-synthase. *Biochemistry* 47: 3194–3201, 2008.
14. Carrico RJ, Blumberg WE, and Peisach J. The reversible binding of oxygen to sulfhemoglobin. *J Biol Chem* 253: 7212–7215, 1978.
15. Cerda J, Echevarria Y, Morales E, and López-Garriga J. Resonance Raman studies of the heme-ligand active site of hemoglobin I from *Lucina pectinata*. *Biospectroscopy* 5: 289–301, 1999.
16. Chatfield MJ and La Mar GN. ^{1}H nuclear magnetic resonance study of the prosthetic group in sulfhemoglobin. *Arch Biochem Biophys* 295: 289–296, 1992.
17. Chiku T, Padovani D, Zhu W, Singh S, Vitvitsky V, and Banerjee R. H_2S biogenesis by human cystathionine γ-lyase leads to the novel sulfur metabolites lanthionine and homolanthionine and is responsible to the grade of hyperhomocysteinemia. *J Biol Chem* 284: 11601–11612, 2009.
18. Collman JP, Ghosh S, Dey A, and Decréau RA. Using a functional enzyme model to understand the chemistry behind hydrogen sulfide induced hibernation. *Proc Natl Acad Sci USA* 106: 22090–22095, 2009.
19. Cooper CE and Brown GC. The inhibition of mitochondrial cytochrome oxidase by the gases carbon monoxide, nitric oxide, hydrogen cyanide and hydrogen sulfide: chemical

mechanism and physiological significance. *J Bioenerg Biomembr* 40: 533–539, 2008.
20. Cooper CE, Jurd M, Nicholls P, Wankasi MM, Svistunenko DA, Reeder BJ, and Wilson MT. On the formation, nature, stability and biological relevance of the primary reaction intermediates of myoglobins with hydrogen peroxide. *Dalton Trans* 7: 3483–3488, 2005.
21. De Jesús-Bonilla W, Cortés-Figueroa JE, Souto-Bachiller FA, Rodríguez L, and López-Garriga J. Formation of compound I and compound II ferryl species in the reaction of hemoglobin I from *Lucina pectinata* with hydrogen peroxide. *Arch Biochem Biophys* 390: 304–308, 2001.
22. De Jesús-Bonilla W, Cruz A, Lewis A, Cerda J, Bacelo DE, Cadilla CL, and López-Garriga J. Hydrogen-bonding conformations of tyrosine B10 tailor the hemeprotein reactivity of ferryl species. *J Biol Inorg Chem* 11: 334–342, 2006.
23. De Jesús-Bonilla W, Ramírez-Meléndez E, Cerda J, and López-Garriga J. Evidence for nonhydrogen bonded compound II in cyclic reaction of hemoglobin I from *Lucina pectinata* with hydrogen peroxide. *Biopolymers* 67: 178–185, 2002.
24. Fernandez-Alberti S, Bacelo DE, Binning RC Jr., Echave J, Chergui M, and Lopez-Garriga J. Sulfide-binding hemoglobins: Effects of mutations on active-site flexibility. *Biophys J* 91: 1698–1709, 2006.
25. Finch CA. Methemoglobinemia and sulfhemoglobinemia. *New Engl J Med* 239: 470–478, 1948.
26. Flores JF, Fisher CR, Carney SL, Green BN, Freytag JK, Schaeffer SW, and Royer WE Jr. Sulfide binding is mediated by zinc ions discovered in the crystal structure of a hydrothermal vent tubeworm hemoglobin. *Proc Natl Acad Sci USA* 102: 2713–2718, 2005.
27. Giangiacomo L, Ilari A, Boffi A, Morea V, and Chiancone E. The truncated oxygen-avid hemoglobin from *Bacillus subtilis*: X-ray structure and ligand binding properties. *J Biol Chem* 280: 9192–9202, 2005.
28. Hill BC and Nicholls P. Cytochrome c reduction by cysteine plus copper: a pseudosubstrate system for cytochrome c oxidase. *Can J Biochem* 58: 499–503, 1980.
29. Hill BC, Woon TC, Nicholls P, Peterson J, Greenwood C, and Thomson AJ. Interactions of sulphide and other ligands with cytochrome c oxidase. An electron-paramagnetic-resonance study. *Biochem J* 224: 591–600, 1984.
30. Hughes MN, Centelles MN, and Moore KP. Making and working with hydrogen sulfide: the chemistry and generation of hydrogen sulfide *in vitro* and its measurement *in vivo*: a review. *Free Radic Biol Med* 47: 1346–1353, 2009.
31. Ishigami M, Hiraki K, Umemura K, Ogasawara Y, Ishii K, and Kimura H. A source of hydrogen sulfide and a mechanism of its release in the brain. *Antioxid Redox Signal* 11: 205–214, 2009.
32. Jiang B, Tang G, Cao K, Wu L, and Wang R. Molecular mechanism for H_2S-induced activation of K_{ATP} channels. *Antioxid Redox Signal* 12: 1167–1178, 2010.
33. Kabil O and Banerjee R. The redox biochemistry of hydrogen sulfide. *J Biol Chem* 285: 21903–21907, 2010.
34. Kajimura M, Fukuda R, Bateman RM, Yamamoto T, and Suematsu M. Interactions of multiple gas-transducing systems: hallmarks and uncertainties of CO, NO, and H_2S gas biology. *Antioxid Redox Signal* 13: 157–192, 2010.
35. Karunakaran V, Benabbas A, Sun Y, Zhang Z, Singh S, Banerjee R, and Champion PM. Investigations of low-frequency vibrational dynamics and ligand binding kinetics of cystathionine beta-synthase. *J Phys Chem B* 114: 3294–3306, 2010.
36. Keilin D. Cytochrome and respiratory enzymes. *Proc R Soc London B* 104: 206–252, 1929.
37. Keilin D. On the Combination of methaemoglobin with H_2S. *Proc R Soc London B* 113: 393–404, 1933.
38. Kimura H. Hydrogen sulfide: from brain to gut. *Antioxid Redox Signal* 12: 1111–1123, 2010.
39. Kiss L, Deitch EA, and Szabó C. Hydrogen sulfide decreases adenosine triphosphate levels in aortic rings and leads to vasorelaxation via metabolic inhibition. *Life Sci* 83: 589–594, 2008.
40. Kraus DW and Wittenberg JB. Hemoglobins of the *Lucina pectinata*/bacteria symbiosis. I. Molecular properties, kinetics and equilibria of reactions with ligands. *J Biol Chem* 265: 16043–16053, 1990.
41. Kraus DW, Wittenberg JB, Lu JF, and Peisach J. Hemoglobins of the *Lucina pectinata*/bacteria symbiosis. II. An electron paramagnetic resonance and optical spectral study of the ferric proteins. *J Biol Chem* 265: 16054–16059, 1990.
42. Lechaire JP, Frébourg G, Gaill F, and Gros O. *In situ* localization of sulphur in the thioautotrophic symbiotic model *Lucina pectinata* (Gmelin, 1791) by cryo-EFTEM microanalysis. *Biol Cell* 98: 163–170, 2006.
43. León RG, Munier-Lehmann H, Barzu O, Baudin-Creuza V, Pietri R, López-Garriga J, and Cadilla CL. High-level production of recombinant sulfide-reactive hemoglobin I from *Lucina pectinata* in *Escherichia coli*. High yields of fully functional holoprotein synthesis in the BLi5 *E. coli* strain. *Protein Expr Purif* 38: 184–195, 2004.
44. Leslie M. Nothing rotten about hydrogen sulfide's medical promise. *Science* 320: 1155–1157, 2008.
45. Li L and Moore PK. An overview of the biological significance of endogenous gases: new roles for old molecules. *Biochem Soc Trans* 35: 1138–1141, 2007.
46. Li L and Moore PK. Putative biological roles of hydrogen sulfide in health and disease: a breath of not so fresh air? *Trends Pharmacol Sci* 29: 84–90, 2008.
47. Mancardi D, Penna C, Merlino A, Del Soldato P, Wink DA, and Pagliaro P. Physiological and pharmacological features of the novel gasotransmitter: hydrogen sulfide. *Biochim Biophys Acta* 1787: 864–872, 2009.
48. Morrison ML, Blackwood JE, Lockett SL, Iwata A, Winn RK, and Roth MB. Surviving blood loss using hydrogen sulfide. *J Trauma* 65: 183–188, 2008.
49. Nakamura S, Nakamura M, Yamazaki I, and Morrison M. Reactions of ferryl lactoperoxidase (compound II) with sulfide and sulfhydryl compounds. *J Biol Chem* 259: 7080–7085, 1984.
50. Nakao A, Sugimoto R, Billiar TR, and McCurry KR. Therapeutic antioxidant medical gas. *J Clin Biochem Nutr* 44: 1–13, 2009.
51. Nguyen BD, Zhao X, Vyas K, La Mar GN, Lile RA, Brucker EA, Phillips GN Jr., Olson JS, and Wittenberg JB. Solution and crystal structures of a sperm whale myoglobin triple mutant that mimics the sulfide-binding hemoglobin from *Lucina pectinata*. *J Biol Chem* 273: 9517–9526, 1998.
52. Nicholls P. The formation and properties of sulphmyoglobin and sulphcatalase. *Biochem J* 81: 374–383, 1961.
53. Nicholls P. Inhibition of cytochrome c oxidase by sulphide. *Biochem Soc Trans* 3: 316–319, 1975.
54. Nicholls P and Kim JK. Oxidation of sulphide by cytochrome aa3. *Biochim Biophys Acta* 637: 312–320, 1981.
55. Nicholls P and Kim JK. Sulphide as an inhibitor and electron donor for the cytochrome c oxidase system. *Can J Biochem* 60: 613–623, 1982.

56. Nicoletti FP, Comandini A, Bonamore A, Boechi L, Boubeta FM, Feis A, Smulevich G, and Boffi A. Sulfide binding properties of truncated hemoglobins. *Biochemistry* 49: 2269–2278, 2010.
57. Park CM and Nagel RL. Sulfhemoglobinemia. *New Engl J Med* 310: 1579–1584, 1984.
58. Pavlik JW, Noll BC, Oliver AG, Schulz CE, and Scheidt WR. Hydrosulfide (SH^-) coordination in iron porphyrinates. *Inorg Chem* 49: 1017–1026, 2010.
59. Pietri R, Granell L, Cruz A, De Jesús W, Lewis A, Leon R, Cadilla CL, and López-Garriga J. Tyrosine B10 and heme-ligand interactions of *Lucina pectinata* hemoglobin II: control of heme reactivity. *Biochim Biophys Acta* 1747: 195–203, 2005.
60. Pietri R, León RG, Kiger L, Marden MC, Granell LB, Cadilla CL, and López-Garriga J. Hemoglobin I from *Lucina pectinata*: a model for distal heme-ligand control. *Biochim Biophys Acta* 1764: 758–765, 2006.
61. Pietri R, Lewis A, León RG, Casabona G, Kiger L, Yeh SR, Fernandez-Alberti S, Marden MC, Cadilla CL, and López-Garriga J. Factors controlling the reactivity of hydrogen sulfide with hemeproteins. *Biochemistry* 48: 4881–4894, 2009.
62. Puranik M, Weeks CL, Lahaye D, Kabil O, Taoka S, Nielsen SB, Groves JT, Banerjee R, and Spiro TG. Dynamics of carbon monoxide binding to cystathionine beta-synthase. *J Biol Chem* 281: 13433–13438, 2006.
63. Ramirez E, Cruz A, Rodriguez D, Uchima L, Pietri R, Santana A, López-Garriga J, and López GE. Effects of active site mutations in haemoglobin I from *Lucina pectinata*: a molecular dynamic study. *Mol Simul* 34: 715–725, 2008.
64. Reeder BJ. The redox activity of hemoglobins: from physiologic functions to pathologic mechanisms. *Antioxid Redox Signal* 13: 1087–1123, 2010.
65. Reiffenstein RJ, Hulbert WC, and Roth SH. Toxicology of hydrogen sulfide. *Annu Rev Pharmacol Toxicol* 32: 109–134, 1992.
66. Rizzi M, Wittenberg JB, Coda A, Ascenzi P, and Bolognesi M. Structural bases for sulfide recognition in *Lucina pectinata* hemoglobin I. *J Mol Biol* 258: 1–5, 1996.
67. Román-Morales E, Pietri R, Ramos-Santana B, Vinogradov SN, Lewis-Ballester A, and López-Garriga J. Structural determinants for the formation of sulfhemeprotein complexes. *Biochem Biophys Res Commun* 400: 489–492, 2010.
68. Schmitter CR. Sulfhemoglobinemia and methemoglobinemia: uncommon causes of cyanosis. *Anesthesiology* 43: 586–587, 1975.
69. Singh S, Madzelan P, and Banerjee R. Properties of an unusual heme cofactor in PLP-dependent cystathionine beta-synthase. *Nat Prod Rep* 24: 631–639, 2007.
70. Singh S, Madzelan P, Stasser J, Weeks CL, Becker D, Spiro TG, Penner-Hahn J, and Banerjee R. Modulation of the heme electronic structure and cystathionine beta-synthase activity by second coordination sphere ligands: the role of heme ligand switching in redox regulation. *J Inorg Biochem* 103: 689–697, 2009.
71. Singh S, Padovani D, Leslie RA, Chiku T, and Banerjee R. Relative contributions of cystathionine beta-synthase and gamma-cystathionase to H_2S biogenesis via alternative trans-sulfuration reactions. *J Biol Chem* 284: 22457–22466, 2009.
72. Standley PR, Mainwaring MG, Gotoh T, and Vinogradov SN. The calcium, copper and zinc content of some annelid extracellular haemoglobins. *Biochem J* 249: 915–916, 1988.
73. Steudel R. Mechanism for the formation of elemental sulfur from aqueous sulfide in chemical and microbiological desulfurization processes. *Ind Eng Chem Res* 35: 1417–1423, 1996.
74. Suzuki T and Vinogradov SN. Globin and linker sequences of the giant extracellular hemoglobin from the leech *Macrobdella decora*. *J Protein Chem* 22: 231–242, 2003.
75. Szabó C. Hydrogen sulphide and its therapeutic potential. *Nat Rev Drug Discov* 6: 917–935, 2007.
76. Van Veldhuizen PJ and Wyatt A. Metoclopramide induced sulfhemoglobinemia. *Am J Gastroenterol* 90: 1010–1011, 1995.
77. Wagner F, Asfar P, Calzia E, Radermacher P, and Szabó C. Bench-to-bedside review: hydrogen sulfide—the third gaseous transmitter: applications for critical care. *Crit Care* 13: 213–221, 2009.
78. Weber RE and Vinogradov SN. Nonvertebrate hemoglobins: functions and molecular adaptations. *Physiol Rev* 81: 569–628, 2001.
79. Weeks CL, Singh S, Madzelan P, Banerjee R, and Spiro TG. Heme regulation of human cystathionine beta-synthase activity: insights from fluorescence and Raman spectroscopy. *J Am Chem Soc* 131: 12809–12816, 2009.
80. Zal F, Leize E, Lallier FH, Toulmond A, Van Dorsselaer A, and Childress JJ. S-Sulfohemoglobin and disulfide exchange: the mechanisms of sulfide binding by *Riftia pachyptila* hemoglobins. *Proc Natl Acad Sci USA* 95: 8997–9002, 1998.
81. Zamyatnin AA. Protein volume in solution. *Prog Biophys Mol Biol* 24: 107–123, 1972.

Address correspondence to:
Dr. Juan López-Garriga
Department of Chemistry
University of Puerto Rico
Mayagüez Campus
P.O. Box 9019
Mayagüez 00681-9019
Puerto Rico

E-mail: sonw@caribe.net

Date of first submission to ARS Central, October 7, 2010; date of acceptance, November 4, 2010.

Abbreviations Used

3MST = 3 mercaptopyruvate sulfur transferase
CBS = cystathionine β-synthase
CcO = cytochrome *c* oxidase
CSE = cystathionine γ-lyase
Fe^{II} = deoxy heme
Fe^{II}-O_2 = oxy heme
Fe^{III}-O_2^- = peroxo
Fe^{III}-OH_2 = met heme
Fe^{IV} = O $Por^{\bullet+}$=ferryl Compound I
Fe^{IV} = O=ferryl Compound II
Hb = hemoglobin
H_2S = hydrogen sulfide
K_{ATP} = ATP-sensitive potassium
Mb = myoglobin
PLP = pyridoxal phosphate
Sulfheme = sulfhemoglobin or sulfmyoglobin
trHb = truncated hemoglobins

A.2

Hydrogen Sulfide Activation in Hemeproteins: The Sulfheme Scenario

NIH Public Access
Author Manuscript
J Inorg Biochem. Author manuscript; available in PMC 2015 April 01.

Published in final edited form as:
J Inorg Biochem. 2014 April ; 133: 78–86. doi:10.1016/j.jinorgbio.2014.01.013.

Hydrogen Sulfide Activation in Hemeproteins: The Sulfheme Scenario

Bessie B. Ríos-González[a], **Elddie M. Román-Morales**[a], **Ruth Pietri**[a], and **Juan López-Garriga**[a,*]

[a]Department of Chemistry, University of Puerto Rico, Mayagüez Campus, PO Box 9019, Mayagüez, Puerto Rico 00681-9019

Abstract

Traditionally known as a toxic gas, hydrogen sulfide (H_2S) is now recognized as an important biological molecule involved in numerous physiological functions. Like nitric oxide (•NO) and carbon monoxide (CO), H_2S is produced endogenously in tissues and cells and can modulate biological processes by acting on target proteins. For example, interaction of H_2S with the oxygenated form of human hemoglobin and myoglobin produces a sulfheme protein complex that has been implicated in H_2S degradation. The presence of this sulfheme derivative has also been used as a marker for endogenous H_2S synthesis and metabolism. Remarkably, human catalases and peroxidases also generate this sulfheme product. In this review, we describe the structural and functional aspects of the sulfheme derivative in these proteins and postulate a generalized mechanism for sulfheme protein formation. We also evaluate the possible physiological function of this complex and highlight the issues that remain to be assessed to determine the role of sulheme proteins in H_2S metabolism, detection and physiology.

Keywords

Sulfhemoglobin; Hydrogen sulfide; Sulfheme protein; Sulfperoxidase; Histidine; Ferryl intermediate

1. Introduction

Hydrogen sulfide (H_2S), historically viewed as a toxic gas, has emerged as a biologically relevant molecule with significant therapeutic potential [1–3]. Endogenous H_2S in humans is produced by cystathionine β-synthase (CBS), cystathionine γ-lyase (CSE), and 3-mercaptopyruvate sulfur transferase (3MST) [4]. Once generated, H_2S penetrates cell membranes by simple diffusion and acts on target biomolecules to modulate numerous biological responses. Several molecular targets have been identified, including proteins, enzymes, transcription factors, and membrane ion channels [1]. As with nitric oxide and carbon monoxide, the other two bioactive gases, H_2S can also interact with heme-containing proteins to regulate biological activities [5–7]. Remarkably, the reactivity of hemeproteins toward H_2S has been associated with relevant physiological processes in many invertebrate systems living in sulfide-rich environments.

© 2014 Elsevier Inc. All rights reserved.

*Corresponding author: Juan López Garriga, juan.lopez16@upr.edu, Tel: +1-787-265-5453, Fax: +1-787-265-5476.

Publisher's Disclaimer: This is a PDF file of an unedited manuscript that has been accepted for publication. As a service to our customers we are providing this early version of the manuscript. The manuscript will undergo copyediting, typesetting, and review of the resulting proof before it is published in its final citable form. Please note that during the production process errors may be discovered which could affect the content, and all legal disclaimers that apply to the journal pertain.

NIH-PA Author Manuscript
NIH-PA Author Manuscript
NIH-PA Author Manuscript

NIH-PA Author Manuscript

NIH-PA Author Manuscript

NIH-PA Author Manuscript

The clam *Lucina pectinata*, which lacks a mouth and gut, lives in sulfide-rich mangroves and its nutritional needs are met by a symbiotic relationship with sulfide oxidizing bacteria. Bacteria living inside the gill oxidize H_2S in the presence of oxygen (O_2) and this energy is utilized to synthesize organic nutrients for the invertebrate. The protein responsible for delivering H_2S to the bacteria is a hemeprotein called hemoglobin I (HbI) [8], which binds H_2S in the ferric heme iron with very high affinity (Figure 1a). The orientation of the vinyl and the flexibility of the propionate peripheral groups of the heme, together with its dynamic behavior facilitate H_2S binding in this hemeprotein [9–11]. Interaction of H_2S with nearby residues also contributes to the affinity of HbI for H_2S [8, 12]. This protein has a glutamine (Gln) residue at the distal ligand-binding site, instead of the equivalent histidine (His) typically found in many invertebrate and vertebrate organisms. We have shown that H_2S is stabilized in part by a hydrogen bonding interaction with Gln. H_2S release is dictated by two competing processes involving slow dissociation of H_2S from the ferric adduct and heme iron reduction followed by H_2S liberation [13, 14]. Heme reduction by H_2S has also been observed in porphyrinates [15] and in phosphodiesterase (Ec DOS-PAS) [16]. We have also shown that replacing Gln with His in HbI, H_2S not only induces heme reduction [17] but it also generates a sulfheme derivative where another sulfur atom is incorporated in one of the pyrrole rings of the heme [18]. It is plausible that His plays an essential role in sulfheme formation.

The giant tubeworm *Riftia pachyptila* is another invertebrate that lives in the sulfide-rich hydrothermal vents and is also characterized by the presence of symbiotic sulfide-oxidizing bacteria that need to be supplied with both H_2S and O_2 [19]. *Riftia* supplies H_2S and O_2 to the endosymbionts by binding both ligands simultaneously at two different sites in its extracellular hemoglobins (Hbs). The worm binds O_2 in the iron heme groups and H_2S in other sites of the proteins. It has been suggested that binding of H_2S occurs at “free cysteine” or cysteine residues (Cys) not involved in disulfide bonds [19]. Likewise, the marine worm *Oligobrachia mashikoi*, which harbors endosymbiotic bacteria and lives in a sulfide rich environment, have Hbs that bind O_2 and H_2S and similar to *Riftia* it can transport both ligands simultaneously [20]. Structural analyses of *Oligobrachia* and *Riftia* Hbs showed that their sulfide-binding Cys residues are well conserved and that these residues play a principal role in sulfide binding (Figures 1b and 1c). These conserved Cys residues are found in other animals living in sulfide-rich habitats. These facts support the notion that Cys residues are involved in sulfide binding and that this interactions would have the benefit of avoiding sulfheme formation. Although the hemoglobins in *Riftia* and *Oligobrachia* have a His residue near the heme (Fig 1b and 1c), formation of a sulfheme complex has not been detected [19, 21]. In contrast, sulfheme formation has been observed in the hemoglobins from *Lumbricus terrestris*, which inhabits sulfide-free environments and contains His at the ligand-binding site. Structural studies demonstrated that “free Cys residues” are absent in these Hbs (Figure 1d), implying that in the presence of O_2, H_2S diffuses through these proteins without encountering alternative binding sites and once at the heme site, it can interact directly with the heme forming the sulfheme derivatives. These observations strongly suggest that His is required for the formation of the sulfheme derivatives. In *R. pachyptila* and *O. mashikoi*, the Cys residues transport H_2S to the symbiotic bacteria and protect the worms from sulfheme formation, which can limit O_2 transportation.

Human hemoglobin and myoglobin have His at the heme distal site and also form sulfheme in the presence of H_2S and O_2 or hydrogen peroxide (H_2O_2). Indeed, formation of these sulfheme complexes at moderate levels and their destruction by the physiologic turnover of red blood cells have been considered to be one of the pathways for H_2S degradation in humans [22]. The presence of these sulfheme derivatives has also been used as a marker of endogenous H_2S synthesis [23, 24]. Remarkably, human catalases and peroxidases have His

NIH-PA Author Manuscript

NIH-PA Author Manuscript

NIH-PA Author Manuscript

at their active site and also generate these sulfheme derivatives [25]. Thus, it is plausible that sulfheme derivatives might play a physiological role *in vivo*. This review focuses on the structural and functional characteristics of human sulfhemoglobin, sulfmyoglobin and other sulfheme proteins. We discuss the role of the distal His as a unique amino acid that triggers the formation of the sulfheme species and propose a mechanism that involves interaction of H_2S with ferric hydroperoxide and compound II intermediates.

2. Interaction of H_2S with myoglobin and hemoglobin

2.1. General Aspects of sulfhemoglobin and sulfmyoglobin

Hemoglobin and myoglobin are globular hemeproteins whose functions involve the binding of O_2 to the ferrous iron (Fe^{II}) of the heme group (protoporphyrin IX). Hemoglobin (Hb) is a tretrameric protein that transports O_2 with cooperative structure fluctuations from lungs to muscles, while myoglobin (Mb) is monomeric and stores O_2 in the muscle cells. In the presence of sulfide, both Mb and Hb undergo two different chemical reactions. Both proteins are capable of binding H_2S in the open sixth position of the ferric heme iron (Fe^{III}) but with very low affinity [8, 10]. H_2S can also react rapidly with the oxy and ferryl forms of Mb and Hb producing the so-called sulfheme derivatives.

In 1866, Hoppe-Seyler observed the formation of a green product after reacting Hb-O_2 with H_2S and called this green derivatives sulfhemoglobin (sulfHb). Michel et al. showed the formation of an analogous compound upon interaction of Mb-O_2 with H_2S and termed the complex sulfmyoglobin (sulfMb) [25–27]. These derivatives have a sulfur atom incorporated in the heme pyrrole B with a characteristic optical band around 620 nm [26, 28–31]. The displacement of the band depends on heme-Fe oxidation and ligation states, as well as the type of the sulfheme isomer [26, 32–34]. These sulfheme derivatives exhibit lower affinity towards O_2 compared to the native proteins [33, 35, 36] and cannot be reverted to the normal functional proteins by natural mechanism in the red cells. High levels of sulfHb and sulfMb can be poisonous since they alter the protein O_2 transport or storage functionalities, causing a cyanosis known as sulfhemoglobinemia [14]. Possible symptoms are chocolate brown arterial blood, fatigue, chest pain and tightness, dizziness, pallor, livid discoloration of the skin and lips, bluish stain on finger tips, foul urine and breath, and tremor of the upper and lower extremities [37–39]. It is very common for sulfhemoglobinemia to be initially misdiagnosed as methemoglobinemia [37, 38, 40]. A helpful note for its diagnostic is the lack of respiratory distress for the degree of cyanosis, [37] and near normal O_2 tension [41]. It can lead to end-organ damage and death when high sulfHb levels are reached (approximately 60%) [40]. In order to be clinically detectable the sulfHb concentration should be more than 5 g/L (approximately 80 μM) [37, 38] while normal concentrations are below 0.37 g/L (approximately 5.8 μM) [38]. Its identification is usually performed by spectrophotometry, co-oximetry, gas chromatography or HPLC [37, 40]. Treatment involves suspected chemical agent suspension, external O_2 supply [37] and in severe cases, blood transfusion [40].

2.2. Sulfhemoglobin and sulfmyoglobin formation

The mechanism for sulfHb and sulfMb formation is still unclear, however, it can be generated from the reaction of the Hb-O_2 and Mb-O_2 derivatives with H_2S, as well as in the presence of H_2O_2 and other thiol compounds [42]. In the case of H_2O_2, the heme ferryl species have been implicated in the formation of the sulfheme derivatives [18]. Figure 2 shows that interaction of H_2O_2 with Hb and Mb leads to the formation of ferric hydroperoxide and the ferryl species compound I (Fe^{IV}=O Por $^{\bullet+}$) and compound II (Fe^{IV}=O), which generate reactive O_2 species that can damage cellular processes.

NIH-PA Author Manuscript

NIH-PA Author Manuscript

NIH-PA Author Manuscript

OxyHb and oxyMb can also generate these ferryl species. It has been suggested that the reaction of H_2S with ferryl compound II is crucial for sulfMb and sulfHb formation and two major overall reactions have been proposed [25, 27]. In 1961, Nicholls proposed that sulfMb can be formed stoichiometrically by the reaction of heme ferryl compound II with H_2S and that a mixture of ferric sulfMb and small quantities of ferrous sulfMb were generated as final products (Reaction 1) [25, 43]. He also observed that ferric sulfMb could then be reduced to ferrous sulfMb by H_2S excess. On the other hand, Berzofsky et al. observed that ferrous sulfMb (77%) was the major product of the reaction between 1 mol of H_2S and 1 mol of Mb ferryl compound II [44]. As shown in Reaction 2, Berzofsky also suggested that the hydrosulfide ion (HS^-) may be the initial reactant species since at physiological pH, 30% of H_2S is undissociated and ~70% dissociates to HS^- (pKa of 7.04) [44].

$$\mathrm{Mb-Compound\,II+H_2S} \rightarrow \begin{pmatrix} \mathrm{sulfMbFe^{II}+H_2O} \\ \mathrm{sulfMbFe^{III}+H_2O+e^-} \end{pmatrix} \quad (1)$$

$$\mathrm{Mb-Compound\,II+HS^-} \rightarrow \mathrm{sulfMbFe^{II}+HO^-} \quad (2)$$

Nonetheless, in 1938, Michel demonstrated that at pH 6 about 20% of Hb was converted to sulfHb, while at pH 8 only 9% of the sulfHb product was obtained. In addition, it has been shown recently that the rate of sulfMb formation decreases 250-fold at basic pH values where the predominant species is HS^-[45]. Thus, in both Hb and Mb the effect of increasing the pH is to decrease the rate and amount of sulfheme formation. This inverse correlation between pH and sulfheme formation, suggests that at basic conditions (pH>7) formation of the sulfheme product is slow and restricted, which reduces the possibility of HS^- as the reactive sulfur species. Accordingly, it is plausible that the initial reactants involved in sulfheme formation are ferryl compound II and undissociated H_2S.

In addition, we have proposed that His plays an essential role in sulfheme formation and that the interaction of H_2S with the His-ferryl-heme ternary complex triggers the formation of the sulfheme derivative [18]. As discussed in detail latter, we have observed that hemoglobins lacking a corresponding distal His are able to form the ferryl compound I and compound II species in the presence of H_2S but sulfheme formation is not seen. Thus, formation of sulfheme requires a concerted interaction between the reactants and the distal His. On these bases, sulfheme formation can be rationalized by the reaction scheme shown in Figure 3a, which takes into account the role of His in sulfheme formation. Incorporating the His interaction, the first step is the formation of a ternary complex intermediate involving His, ferryl compound II and the heme-protein moiety. His donates a proton to the ferryl species, generating a highly reactive protonated ferryl compound II, which interacts with H_2S yielding in turn a sulfide radical (HS•) and ferric heme Mb or Hb. The HS• then attacks the porphyrin ring, producing the final sulfheme derivative. Romero and coworkers showed that Mb compound II also reacts with some thiols, yielding thiyl radical species and ferric Mb with the subsequent formation of sulfMb. It is important to mention that Nicholls, Berzofsky and others used catalase in their experiments to remove excess of H_2O_2 and to prevent the cyclic process shown in Figure 2 [26, 43, 44]. In the absence of catalase, the cyclic reaction in Figure 2 is operative and depending on the H_2O_2 concentration, ferric hydroperoxide can represent an additional initial reactant center for sulfheme complex formation. In this scenario, sulfheme formation can be described by the reaction scheme shown in Figure 3b. Here, the ternary complex intermediate involves His, ferric hydroperoxide and the heme-protein moiety. The His-ferric hydroperoxide ternary complex in the presence of H_2S forms the {Fe(III)OOHH_2S} intermediate, which can trigger heterolytic or homolytic cleavage of the O-O bond. Heterolysis yields heme ferryl

NIH-PA Author Manuscript

NIH-PA Author Manuscript

NIH-PA Author Manuscript

compound I and SH^-, while homolysis generates ferryl compound II and the HS• species. Since the rate of sulfMb formation decreases with the hydrosulfide HS^- ion, we suggest that the ferryl compound II and the HS• species are the predominant intermediates in the reaction of sulfheme formation. The HS• then attacks the ferryl compound II, producing the final sulfheme derivative. Curiously, Romero et al. also observed that in the absence of catalase the reaction of Mb compound II with thiols generated higher concentration of thiyl radicals [42], which accumulates during the cyclic reaction in Figure 2 and can react with either the ferric hydroperoxide or the ferryl centers.

2.3. Structural aspects of sulfHb and sulfMb

In sulfHb and sulfMb the sulfur atom is incorporated in one of the pyrrole rings of the heme, which lowers their affinity for O_2. The chemical nature of the modified heme in both sulfHb and sulfMb was a matter of debate for many years and the precise physiological structure of these derivatives remains elusive. It is now well accepted that sulfHb and sulfMb consist of a modified heme in which a sulfur atom adds to the pyrrole B of the porphyrin system. Using labeled sulfur (^{35}S) experiments it was first determined that only one atom of sulfur was incorporated into the heme group of sulfMb [26–28, 44, 46]. Later, proton NMR studies of sulfMb identified the sulfur atom on pyrrole B by analyzing the chemical shifts of the heme 1,3,5,8-methyls and the 2,4-vinyl substitutions [31, 34, 47]. Based on NMR and resonance Raman data it was then proved that the sulfur atom is incorporated across the double β-β bond of pyrrole B either as episulfide or thiochlorin, with a heme-chlorin type structure [26, 28, 30, 31, 34, 44, 47, 48]. The band at 620 nm observed in the optical spectra of sulfHb and sulfMb reflects the nature of the chlorin structure. Heme-chlorin structure and other metallo-chlorin derivatives are characterized by a saturated C_β-C_β bond in one of the pyrrole ring of the porphyrin, which reduces the symmetry of heme porphyrin from $D_{4h,}$ typical of native Hb and Mb, to a C_{2v} system (Figure 4a). This reduction induces a distortion of the macrocycle planarity and changes in the heme electronic properties, resulting in the activation of other electronic transitions at higher wavelengths. When a sulfur atom adds to the pyrrole B, the C_β-C_β bond becomes saturated, adopting a chlorin like structure with a visible band at 620 nm. Therefore, it is clear that the incorporation of the sulfur atom involves disruption of the ring conjugation to that of chlorin, which reduces O_2 affinity in both sulfHb and sulfMb [18, 33, 35, 36, 48]. NMR and crystallographic studies demonstrated that in fact, conversion of Mb to sulfMb did not affect the heme cavity or the overall protein structure and that the observed changes in O_2 binding arise entirely from the local electronic changes of heme-chlorin structure [34, 47, 49].

Proton NMR studies of several sulfMbCN complexes revealed that there are at least three isomeric forms of the chlorin structure that may affects O_2 affinity [29, 30]. As shown in Figure 4b, each sulfheme isomer, named sulfMbA, sulfMbB and sulfMbC, have different chemical properties and hence, different reactivity and stability [29, 34]. These differences reside in the porphyrin periphery alterations where the incorporated sulfur lays since all three isomers where observed at different pH, temperature and protein concentration [29]. In general, the NMR spectra of all isomers showed symmetry reduction of the prosthetic group and alteration of the π conjugation of pyrrole B [34]. The sulfMbA structure is an episulfide across the β-β bond, which is rapidly reconverted to the protoheme when the heme is extracted from the protein [28, 34, 50, 51]. SulfMbB is characterized by a “ring opened episulfide” [34], while sulfMbC is described as a thiochlorin structure. SulfMbA is converted to both sulfMbB and sulfMbC, but conversion from sulfMbB to sulfMbC has not been observed, indicating that sulfMbA is the precursor of the other two sulfhemes species [28, 34]. SulfMbC is the most stable isomeric form and is only observed when the 4-vinyl is on heme [30, 52]. Replacing this vinyl group with hydrogen only yields sulfMbA and sulfMbB and two other red sulfMb isomers (D and E), which apparently forms from the

NIH-PA Author Manuscript

NIH-PA Author Manuscript

NIH-PA Author Manuscript

former two isomers [52]. It is worthwhile to mention that the predominant isomeric species depends on experimental conditions such as pH and the nature of the oxidation and coordination states of the heme iron [28, 34]. Nonetheless, the sulfMbC isomer is the terminal sulfMb product and it appears to predominate at physiological conditions, implying that the stability and reactivity of this compound may account for the reduced O_2 affinity in sulfMb.

SulfHb on the other hand, shows mainly the sulfHbA isomer with only a 10% of the sulfMbB counterpart [34]. In addition, sulfHbA does not go through isomeric interconversion probably due to internal flexibility limitation [28]. SulfMb and sulfHb isomers have different chemical reactivity, which can in principle influence O_2 affinity in both proteins.

2.4. Structural and functional Implications of sulfHb and sulfMb

Similar to the native proteins, sulfMb and sulfHb bind numerous ligands at distal site of the heme iron [25, 26, 29, 31–33, 35]. Spontaneous autoxidation as well as oxidation state interconversion with different reducing and oxidation reagents are also maintained in these sulfheme derivatives without disturbing the sulfur ring. However, O_2 affinity is substantially reduced in both sulfMb and sulfHb. In this section we evaluate O_2 binding in sulfMb and sulfHb and the factors that may influence O_2 affinity in these proteins. Reconversion of the native proteins from the sulfheme derivatives and the possible physiological implications of sulfMb and sulfHb are also discussed.

The reversible reaction of O_2 with sulfMb was first recognized by Berzofsky et al., who observed that the 616 nm band, characteristic of ferrous sulfMb, shifted to 624 nm when deoxy sulfMb was exposed to O_2. Also, a shift of the Soret band from 424 nm (deoxy sulfMb) to 408 nm was detected. The authors observed that the shifts were completely reversed when the same sample was exposed to an argon atmosphere, and attributed the spectral displacements to the reversible binding of O_2 [33]. They also showed that the oxygen-binding curve of sulfMb was characterized by a rectangular hyperbolic shape, similar to native Mb, which led them to conclude that sulfMb was in fact able to bind O_2 reversibly in a concentration dependent manner. However, the concentration of O_2 required to saturate half of the sulfMb molecules, known as $p^{1/2}$ in the binding curve, was ~ 2,500 higher than that of the native protein (530 mmHg for sulfMb and 0.21 mmHg for Mb), indicating much lower O_2 affinity for the former [33].

Following Berzofsky approach, Carrico and coworker [35] studied the reversible binding of O_2 in sulfHb and observed that when the ferrous sulfHb complex was exposed to O_2, the band at 619 nm was displaced to 623 nm. They assigned these optical changes to formation of the oxy sulfHb derivative (sulfHb-O_2). As with native Hb, the O_2 binding curve was found to be sigmoidal, which supported the fact that sulfHb was able to reversibly bind O_2. The sigmoidal shape, a characteristic of cooperative behavior, also indicated that sulfHb retained some cooperative character of the native protein. Nonetheless, the $p^{1/2}$ of sulfHb was 63mmHg, while that of native Hb under similar conditions was 0.46mmHg. On this bases, it was concluded that the affinity of sulfHb for O_2 was 135 lower that the native protein [35].

The substantial decrease in O_2 affinity, in both sulfMb and sulfHb, has been attributed to the electron withdrawing character of the heme-chlorin structure. Incorporation of the sulfur atom to the β-β double bond of the pyrrole B removes electron density from the iron towards the periphery of the chlorine ring, reducing the ability of the iron to donate electron density back to the bound ligand and as a consequence, the iron affinity for O_2 decreases. It is well known that when O_2 binds to the ferrous heme in Mb and Hb, it donates two electrons to the

NIH-PA Author Manuscript

NIH-PA Author Manuscript

NIH-PA Author Manuscript

heme iron, increasing complex, the iron donates electron density to the in turn the electron density on the iron. To stabilize the π orbital of the O_2, producing ferric superoxide (Fe^{III}-$OO^{\bullet -}$) [33]. Hence, the inability of sulfMb and sulfHb to effectively transfer electron density to O_2, destabilizes the complex and lowers their affinity for O_2. Although this interpretation sheds light on the reduced affinity of sulfMb and sulfHb for O_2, it does not explain the differences of O_2 affinity between sulfMb and sulfHb. As described above, sulfMb was shown to be ~2500-fold lower, whereas O_2 binding in sulfHb was reduced by a factor of ~135. The higher affinity of sulfHb for O_2 can be rationalized by the fact that not all four hemes are modified by H_2S and the protein is a partially sulfurated tetramer, leaving hemes available for normal O_2 binding [36]. The chemical nature of the sulfHb isomeric structure can also explain the observed higher O_2 affinity. The episulfide structure of the sulfHb isoform (sulfHbA) is more nucleophilic and less electronegative than the thiochlorin of sulfMb (sulfMbC), which can in principle decrease the electron withdrawing character of the chlorin structure in the former, resulting in higher O_2 affinity. This is consistent with the reduced intensity of the 620 nm band in the optical absorption spectra of sulfHb as opposed to sulfMb. This band arises from the forbidden electronic transition in the visible or Q region of the spectra that becomes partially allowed due to configuration interactions between the heme-chlorin orbitals. Distortion of the heme planarity increases the energy of heme orbitals and as a consequence the intensity of the band associated with the forbidden transition also increases. In sulfHb, the small intensity of the 620 nm band reflects less distortion of the heme macrocycle, which decreases the electron withdrawing characteristic of the typical chlorin derivative [18].

The reconversion of the sulheme products to the native functional proteins has been studied for many years. In 1961, Nicholls [25] was the first to observe the reconversion of sulfMb to native Mb, when he exposed the sulfMb sample to H_2O_2. Similar results were obtained when he exposed sulfMb to dithionite in the presence of O_2 or cyanide (CN^-), which also produces H_2O_2. Therefore, the reversion of sulfMb to Mb appears to be mediated by H_2O_2 in a reaction that may involve products associated with the spontaneous oxidation of H_2O_2. Photo-excitation of the sulfMb-CO complex also induced reconversion of the sulfheme derivative to the normal Mb-CO species. Berzofsky et al. [32] observed that when a sulfMb-CO sample was exposed to successive periods of irradiation, the Soret band shifted from 413 nm, typical of the sulfMb-CO complex, to 422 nm with a progressive disappearance of the 612 nm band. The results were explained in terms of the differences in activation energy, both in the ground and excite state of the chlorin structure. In the ground state, large activation energy is required to release the bound sulfur and to unsaturated the pyrrole ring. During photo-excitation, the structure reaches an electronic excited state that reduces the activation energy, resulting in a thermodynamically favored reconversion of the native Mb-CO complex [32].

The sulfMb reversion process was further studied by extracting the sulfheme prosthetic group of under various conditions [44]. The sulfhemin complex was unstable at all conditions and was rapidly converted to the protohemin and a mixture of sulfur containing molecules in which 50% was found to be SO_4^{2-}. The presence of peroxides increases the decomposition rate of sulfhemin, supporting the notion that H_2O_2 or products associated with its oxidation are probably required to initiate the reversibility process [25, 44]. In addition to the peroxides, $HgCl_2$ and $Hg(OAc)_2$ were shown to decompose the sulfhemin derivative as well as. It appears that Hg^{2+} removes the sulfur atom from the sulfhemin molecule, generating the intact porphyrin system and a stable HgS compound [44]. Although reversion of the sulfheme products to the native derivatives has been observed under several experimental conditions, the analogous process has not been detected *in vivo*. This suggests that the only mechanism of sulfHb and sulfMb removal in our body is through the natural decomposition of these molecules in tissues and cells. Curiously, it was

NIH-PA Author Manuscript

NIH-PA Author Manuscript

NIH-PA Author Manuscript

demonstrated recently that H_2S diffuses rapidly across the red blood cell and that erythrocytes and plasma consume endogenous H_2S [53]. Klingerman et al. also showed that once in the blood, H_2S interacts primarily with Hb and not with proteins in the plasma [54]. Thus, it is plausible that oxyHb interacts with H_2S to form sulfHb, which is then eliminated by the natural destruction of red blood cells. Furthermore, the long normal life span of erythrocytes indicates that sulfHb can be detected and that indeed, it can be used as a biomarker for H_2S generation in cells.

3. Interaction of H_2S with enzymes

Enzymes are found in bacteria, fungi, plants and animals and their function is to serve as biological catalysts. They accelerate reactions that are necessary to sustain life but some inhibitors decrease the reaction rate and turnover of enzymes. Similar to human Hb and Mb, there is a set of some enzymes like lactoperoxidase and catalase that react with H_2S, forming analogous sulfheme derivatives. Nonetheless, published information about the interaction of H_2S with these enzymes is limited [25, 43]. In this section we discuss the current knowledge about the interaction of H_2S with some heme peroxidases and catalase and correlate these interactions with human Hb and Mb.

3.1 Heme peroxidase (Lactoperoxidase and Myeloperoxidase)

Heme peroxidases are enzymes that catalyze the oxidation of a number of inorganic and organic compounds using H_2O_2 as the primary substrate. These enzymes turn reactive O_2 species like H_2O_2, which damage cell structure, to harmless product by adding hydrogen from a donor molecule. Lactoperoxidase (LPO) and myeloperoxidase (MPO) are two important heme-containing peroxidases involved in the immune defense system [55–58]. Both defend the system from invading microorganism by the bactericidal activities of the oxidized substrates [56, 59]. For example, MPO catalyzes the formation of hypochlorous acid (HOCl) from chloride species and H_2O_2, which has antimicrobial activity and kills other pathogens in humans [59]. In the resting form, the heme groups of LPO and MPO are penta-coordinated with the iron in the high spin ferric state. As shown in Figure 5, the distal sites of both enzymes have His and arginine (Arg), [57, 60, 61] which are important in their catalytic activities, specifically in the formation and stabilization of ferryl intermediates [62]. The generalized mechanism is similar to that shown in Figure 2. Interaction of the enzymes with H_2O_2 generates the ferryl compound I and compound II intermediates. As opposed to Hb and Mb, compound I is quite stable in these enzymes. Compound II is generated by the donation of an electron from a reducing substrate to the porphyrin cation radical ($Por^{\bullet +}$) or compound I. The enzymes then return to their resting state by another electron transfer reaction from a second substrate, which reduces compound II with the concomitant formation of the ferric enzyme, a second radical substrate and a water molecule. The electron donor molecules vary from inorganic compounds such, as halides (X^-), to organic (AH_2) substrates, which are oxidized to hypohalous acids (HOX) and organic radicals ($\bullet AH$), respectively [63].

The catalytic activity of LPO is inhibited by sulfhydryl compounds such as methylmercaptoimidazole (MMI) and thiouracil [64, 65]. Ohtaki and coworkers suggested that the irreversible inactivation of the enzyme was induced by the reaction of compound II with the antithyroid drug MMI [66]. In 1984, Nakamura and coworkers also evaluated the interactions of LPO with H_2S, MMI, cysteine and dithiothreitol in the presence of H_2O_2 [43]. They found that as Hb and Mb, the reaction of H_2S with the enzyme in the presence of H_2O_2, yielded a sulfheme derivative, which they named sulflactoperoxidase. The ferrous sulflactoperoxidase complex has a characteristic band at approximately 638 nm whereas the ferric derivative has bands at 605 nm and 727 nm [43]. Reaction of MMI with resting LPO yielded a spectrum with visible band at 592 nm and 635 nm and based on the similarity with

NIH-PA Author Manuscript

NIH-PA Author Manuscript

NIH-PA Author Manuscript

the one obtained with H_2S, the authors suggested that sulflactoperoxidase was also formed with MMI.

Although the molecular mechanism of sulflactoperoxidase formation from H_2S and the subsequent inactivation of the enzyme have not been described, the analogous processes have been well evaluated with the sulfur-containing compound MMI [43, 64–68]. Ohtaki in 1982 and Nakamura in 1984, suggested that LPO compound II was reduced to the ferric state by one electron transfer from MMI with the concomitant formation of a MMI radical [43, 66]. The presence of the MMI radical was later confirmed by EPR studies and it was also shown that the radical did not interact directly with the heme iron. The authors suggested that the MMI radical must bind to a specific site of heme porphyrin ring and that the unpaired electron of the radical was then transferred to the heme ferryl group [67]. It was also proposed in that study that the distal His might influence MMI oxidation and subsequent binding to the heme porphyrin. Remarkably, this supports the unique role of the distal His in sulfheme formation as suggested previously [18]. Overall, it is now believed that MMI interacts with LPO ferryl compound II, inducing the formation of a thiyl radical that inhibits LPO irreversibly by reacting directly with the heme porphyrin system. Based on the optical spectra reported by Nakamura it is plausible that the MMI radical interacts with the heme and generates sulflactoperoxidase, which inhibit the enzyme activity[43]. A similar mechanism can be invoked for the inactivation of LPO by H_2S. Moreover, the fact that the optical spectra of LPO in the presence of H_2S and H_2O_2 shows bands similar to sulfHb and sulfMb, strongly suggest that the heme group of the sulflactoperoxidase derivative is a chlorin type structure in which the sulfur atom is incorporated across the β-β double bond of the pyrrole B [44, 47, 69].

Like LPO, MPO activity is inhibited in the presence of H_2S and H_2O_2 [70, 71]. The mechanism of inhibition has not been described and warrants further investigation. It has been speculated that the inhibition may be mediated by the formation of the sulheme derivative, which lowers the affinity of the enzyme for the substrates [25, 70, 71]. Although formation of the sulfheme derivative has not yet been demonstrated experimentally in MPO, the enzyme has a His residue in the heme distal site that in the presence of H_2S and the natural H_2O_2 substrate can contribute to sulfheme formation (Figure 5b).

It has been suggested recently that H_2S interacts with HOCl, the enzymatic product of MPO, and prevents oxidative damage *in vivo*. As mentioned before HOCl possesses antimicrobial activity in cells. Nevertheless, excessive production of HOCl can cause oxidative stress to proteins, lipids, DNA and RNA. HOCl seems to contribute to the oxidative damage of these biomolecules in patients with Alzheimer's disease (AD) since high levels of MPO are found in the prefrontal cortex, hippocampal microglia and neurons. Whiteman et al. showed that H_2S prevents oxidative damage in neuronal cells exposed to HOCl and suggested that the direct interaction of both reactants could be an important mechanism for HOCl removal *in vivo* in AD patients [72]. Likewise, it has been suggested that HOCl can also modify low-density lipoproteins (LDL) associated with the formation of arteriosclerotic plaques. In 2007 Laggner and coworkers demonstrated the ability of H_2S to prevent modification of LDL by HOCl either via direct interaction with HOCl or inhibition of MPO [71]. Nonetheless, it has been suggested recently that the reaction of H_2S with HOCl is not favorable *in vivo*, unless it could accumulate at high local concentrations [73]. Thus, it is highly possible that H_2S stops HOCl oxidative damage by limiting MPO activity via sulfheme formation.

It is evident that LPO forms sulflactoperoxidase and that MPO must probably generate the analogous compound, however, the physiological implication of these derivatives remains unknown and warrants additional examination. Moreover, interaction of H_2S and the possible physiological role of these interactions should be further evaluated in other

NIH-PA Author Manuscript

NIH-PA Author Manuscript

NIH-PA Author Manuscript

peroxidases, in particular those having His at the active site and are involved in H_2O_2 and O_2 chemistry. For example, thyroid peroxidase (TPO), an enzyme that participates in hormone biosynthesis and uses H_2O_2 as a substrate, is inactivated by MMI possibly through the formation of a sulfheme like derivative [43]. The sulfheme TPO complex may also be produced in the presence of H_2S. In fact, amino acid sequence alignment shows that TPO has His in the active distal site, which is involved in the enzyme catalytic activity and probably may play a crucial role in sulfheme formation [57, 74]. Although we focus in human peroxidases, the dehaloperoxidase-hemoglobin from the invertebrate *Amphitrite ornate* forms the sulfheme product and has His near the heme [75]. Indeed, as we describe next, catalase has a His in the distal active site and generates the sulfheme derivative upon reaction with H_2S.

3.2 Catalase

Catalase is a heme-containing enzyme found in many bacteria and almost all plants and animals. The protein is a tetramer and each monomer contains a heme group [76–78]. As Reaction 3 shows, the enzyme protects the cells by converting H_2O_2 into water and O_2 [79]. The proposed mechanism occurs in two steps and involves the ferryl intermediates [80]. In the first step the enzyme reacts with H_2O_2 to form compound I. In the second step, compound I reacts with another molecule of H_2O_2 and the enzyme returns to the resting state. Two electrons are transferred to one molecule of H_2O_2 and then two electrons are accepted from a second H_2O_2. Catalase does not form compound II as part of the normal catalytic cycle but at low concentration of H_2O_2 and in the presence of one electron donor generation of compound II has been observed. The efficiency of the catalytic reactions is improved by the interaction of the active site His and Asn residues (His and Asn in the positions 74 and 147, respectively) with the ferryl intermediates.

$$\begin{gathered} 2H_2O_2 \rightarrow 2H_2O + O_2 \\ \text{Step 1.} \quad [Fe^{III}Por] + H_2O_2 \rightarrow [Fe^{IV}{=}O\ Por\bullet^+] + H_2O \\ \text{Step 2.} \quad [Fe^{IV}{=}O\ Por\bullet^+] + H_2O_2 \rightarrow [Fe^{III}Por] + H_2O + O_2 \end{gathered} \tag{3}$$

Step 1. $[Fe^{III}Por] + H_2O_2 \rightarrow [Fe^{IV}{=}O\ Por\bullet^+] + H_2O$

Step 2. $[Fe^{IV}{=}O\ Por\bullet^+] + H_2O_2 \rightarrow [Fe^{III}Por] + H_2O + O_2$

Catalase is inhibited by ligands like cyanide, azide, 3-amino-1,2,4-triazol and nitric oxide [81–84]. Also, as Beers and Sizer proposed, H_2S could inhibit catalase in two ways: it may form an inactive compound with the primary catalase peroxide complex and that it may react directly with either the protein moiety or with the heme group [85]. Nicholls then proposed that the interaction of H_2S with catalase was similar to that of Mb in which H_2S reacts with the ferryl compound II intermediate and modifies the heme porphyrin system to produce the analogous sulfheme derivatives [25]. The product of the reaction of catalase with H_2S and H_2O_2 yielded an optical spectrum with a characteristic band at 635 nm and was therefore ascribed to ferrous sulfcatalase. Ferric sulfcatalase was also observed with absorption bands at 585 nm and 710 nm. Based on this, Bersofsky suggested that the structure of sulfcatalase should be similar to sulfMb and sulfHb [26, 44, 47, 69]. Therefore, these observations support the notion that the sulfheme product is generated in presence of O_2 and/or H_2O_2 and that the distal His residue near the iron regulates sulfheme formation. Interestingly, catalase can be regenerated from sulfcatalase by oxidizing agents like O_2 and ethyl hydroperoxide and by small molecules like cyanide and azide, and sodium dithionite [25].

NIH-PA Author Manuscript

NIH-PA Author Manuscript

NIH-PA Author Manuscript

4. Role of His in sulfheme protein formation

Several mechanistic aspects of sulfheme protein formation remain unknown. However, there are enough experimental evidences that can provide an insight into the characteristics of sulfheme protein generation. For example, as mentioned in this review, we have suggested that His is directly involved in sulfheme protein formation. In this respect, we have shown that the cytoplasmic HbI, HbII and HbIII from *L. pectinata*, which have Gln instead of His, do not form the sulfheme derivatives [18]. In addition to Gln, HbI has a cluster of Phe residues near the heme, while in HbII and HbIII one of the Phe is replaced with Tyr. Thus, it appears that neither Gln, Phe nor Tyr are involved in sulfheme protein formation. Moreover, as Table 1 shows, sulfheme was not detected in the HbI Gln/Val, Gln/Asn and Gln/Arg mutants, while the product was only observed in the Gln/His variant [14, 18]. Similarly, it was shown recently that the native Ec DOS-PAS heme sensor, which has Met and Arg in its distal site, does not form the sulfheme complex, supporting the role His in sulfheme formation [86]. Mutations of these residues by Ala, Ile, Leu and Glu did not induce formation of sulfheme, instead a verdoheme product was observed in the Arg/Ala and Arg/Ile mutants. Verdoheme is a modified heme that has oxygen incorporated in the α-meso heme position. It is known for being one of the heme degradation steps in heme oxygenase [86]. Thus, it is evident that amino acids with: *(i)* non-polar aliphatic groups like glycine, alanine, valine and isoleucine, *(ii)* polar uncharged groups like glutamine and asparagine, *(iii)* aromatic group like phenylalanine and tyrosine, and *(iv)* positively charged groups like lysine and arginine, are not involved in the synthesis of the sulfheme species.

As shown in Table 1, His is a common feature in those proteins that generate sulfheme, reiterating the role of His in the reaction of sulfheme. Thus, with the exception of cytochrome c oxidase, horseradish peroxidase, and the phosphodiesterase His mutant (Ec DOS-PAS Met95His), distal His seems to be essential for sulfheme formation. In cytochrome c oxidase, the catalytic center includes a heme porphyrin (a_3), a copper (Cu_B) center and three His residues, which are coordinated to Cu_B. The fact that heme a_3-Cu_B binuclear centers are directly involved in the catalytic activity of the enzyme precludes sulfheme formation. Interestingly, both LPO and horseradish peroxidase (HRP) have a His and Arg in their active site, which are important for their enzymatic activity, but only the former generates sulfheme, while the latter does not [25, 43]. This exclusive behavior can be attributed to the distance between the His and the heme iron, which is shorter in LPO (4.94 Å), as opposed to HRP (6.00 Å) (Figure 5a and 5d). On the other hand, the His residue in the Ec DOS-PAS Met95His mutant is coordinated to the heme iron, which blocks H_2O_2 binding and sulfheme formation [86]. Clearly, this shows that the orientation and position of the His residue at the heme active site are crucial for the synthesis of the sulfheme product. The fact that only proteins that have His at the distal site generate sulfheme, the reactivity of this residue should be taken into account when considering the mechanism of sulfheme protein formation.

5. Summary and Future Perspectives

In view of the current data we suggest that: *(a)* the formation of the sulfheme derivate requires a His residue in the heme distal site with an adequate orientation to form an active ternary complex; *(b)* the ternary complex intermediate involves His, ferric hydroperoxide or compound II and the heme-protein moiety; *(c)* interaction of this heme cluster with H_2S triggers formation of the SH•, yielding the final ferrous or ferric sulheme product. These observations and the tautomeric nature [87, 88] and orientation of distal His, which can behave as an acid-base catalyst, allows suggesting the general mechanisms shown in Figure 3. Due to the cyclic nature of the reaction between hemeproteins and H_2O_2 (Figure 2), it is difficult to assign the initial peroxide adduct (ferric hydroperoxide or compound II)

NIH-PA Author Manuscript

NIH-PA Author Manuscript

NIH-PA Author Manuscript

responsible for sulfheme formation. Assuming that in the presence of an H_2O_2 scavenger the end product of the reaction is compound II, then the predominant reaction can be summarized as shown in Figure 3a. On the other hand if the cyclic reaction is operative, the reaction can be described as demonstrated in Figure 3b. In both scenarios the SH• appears to be the reactive species that attack the double β-β bond of pyrrole B.

It is clear that much remains to be investigated before implicating sulfheme proteins in any physiological function. Nonetheless, the fact that this complex is also produced during the catalytic reaction of heme-peroxidases and catalases, strongly suggests that this derivative can also be generated in other heme-containing enzymes involved in O_2 chemistry. Also, albeit the concentration of endogenous H_2S may be too low to generate sulfheme *in vivo*, exposure of H_2S by donors can induce formation of the complex, which can be used in turn to assess the presence of exogenous H_2S in tissues and cells. Key issues that requires further investigation to address the above hypotheses include: *(a)* the precise peroxide adduct involved in sulfheme formation, *(b)* the subsequent reaction of the thiyl radical with the heme ferric or ferryl compound II intermediate, *(c)* the final sulfheme product (ferric versus ferrous) and *(d)* the stability, decay and reversibility of the sulfheme complex *in vitro and in vivo*. Insights into these issues will determine the role of sulheme proteins in H_2S metabolism, detection and physiology.

Acknowledgments

We thank NIH-RISE 2 Best (Grant R25SGM088023) and the National Science Foundation (Grant 0843608) for their financial support.

Abbreviations

HbI	hemoglobin I
Hbs	hemoglobins
sulfHb	sulfhemoglobin
sulfMb	sulfmyoglobin
MMI	methylmercaptoimidazole
HRP	horseradish peroxidase
HS•	sulfide radical
(Fe ^{IV}=O)	compound II
Fe^{III}-OO•	ferric superoxide
LPO	lactoperoxidase
MPO	myeloperoxidase
Por•$^+$	porphyrin cation radical

References

1. Kashfi K, Olson KR. Biochem Pharmacol. 2013; 85:689–703. [PubMed: 23103569]
2. Kimura H, Shibuya N, Kimura Y. Antioxid Redox Signal. 2012; 17:45–57. [PubMed: 22229673]
3. Olson KR. Am J Physiol Regul Integr Comp Physiol. 2011; 301:R297–312. [PubMed: 21543637]
4. Singh S, Banerjee R. Biochim Biophys Acta. 2011; 1814:1518–1527. [PubMed: 21315854]
5. Kabil O, Banerjee R. J Biol Chem. 2010; 285:21903–21907. [PubMed: 20448039]

NIH-PA Author Manuscript

NIH-PA Author Manuscript

NIH-PA Author Manuscript

6. Kajimura M, Fukuda R, Bateman RM, Yamamoto T, Suematsu M. Antioxid Redox Signal. 2010; 13:157–192. [PubMed: 19939208]
7. Li Q, Lancaster JR Jr. Nitric Oxide. 2013; 35C:21–34. [PubMed: 23850631]
8. Kraus DW, Wittenberg JB. J Biol Chem. 1990; 265:16043–16053. [PubMed: 2398044]
9. Colón JFC, Silfa E, Garriga JL. J Am Chem Soc. 1998; 120:9312–9317.
10. Fernandez-Alberti S, Bacelo DE, Binning RC Jr, Echave J, Chergui M, Lopez-Garriga J. Biophys J. 2006; 91:1698–1709. [PubMed: 16782787]
11. Silfa E, Almeida M, Cerda J, Wu S, Lopez-Garriga J. Biospectroscopy. 1998; 4:311–326. [PubMed: 9787907]
12. Rizzi M, Wittenberg JB, Coda A, Ascenzi P, Bolognesi M. J Mol Biol. 1996; 258:1–5. [PubMed: 8613980]
13. Pietri R, Leon RG, Kiger L, Marden MC, Granell LB, Cadilla CL, Lopez-Garriga J. Biochim Biophys Acta. 2006; 1764:758–765. [PubMed: 16380302]
14. Pietri R, Roman-Morales E, Lopez-Garriga J. Antioxid Redox Signal. 2011; 15:393–404. [PubMed: 21050142]
15. Pavlik JW, Noll BC, Oliver AG, Schulz CE, Scheidt WR. Inorg Chem. 2010; 49:1017–1026. [PubMed: 20038134]
16. Takahashi H, Sekimoto M, Tanaka M, Tanaka A, Igarashi J, Shimizu T. J Inorg Biochem. 2012; 109:66–71. [PubMed: 22387619]
17. Pietri R, Lewis A, Leon RG, Casabona G, Kiger L, Yeh SR, Fernandez-Alberti S, Marden MC, Cadilla CL, Lopez-Garriga J. Biochemistry. 2009; 48:4881–4894. [PubMed: 19368335]
18. Roman-Morales E, Pietri R, Ramos-Santana B, Vinogradov SN, Lewis-Ballester A, Lopez-Garriga J. Biochem Biophys Res Commun. 2010; 400:489–492. [PubMed: 20732304]
19. Bailly X, Vinogradov S. J Inorg Biochem. 2005; 99:142–150. [PubMed: 15598498]
20. Numoto N, Nakagawa T, Kita A, Sasayama Y, Fukumori Y, Miki K. Proc Natl Acad Sci U S A. 2005; 102:14521–14526. [PubMed: 16204001]
21. Arp AJ, Childress JJ, Vetter RD. J Exp Biol. 1987; 128:139–158.
22. Predmore BL, Lefer DJ, Gojon G. Antioxid Redox Signal. 2012; 17:119–140. [PubMed: 22432697]
23. Perna AF, Luciano MG, Ingrosso D, Pulzella P, Sepe I, Lanza D, Violetti E, Capasso R, Lombardi C, De Santo NG. Nephrol Dial Transplant. 2009; 24:3756–3763. [PubMed: 19654230]
24. Whiteman M, Le Trionnaire S, Chopra M, Fox B, Whatmore J. Clin Sci (Lond). 2011; 121:459–488. [PubMed: 21843150]
25. Nicholls P. Biochem J. 1961; 81:374–383. [PubMed: 14479446]
26. Berzofsky JA, Peisach J, Blumberg WE. J Biol Chem. 1971; 246:3367–3377. [PubMed: 4324899]
27. Michel HO. J Biol Chem. 1938; 126:323–348.
28. Bondoc LL, Chau MH, Price MA, Timkovich R. Biochemistry. 1986; 25:8458–8466. [PubMed: 3828290]
29. Chatfield MJ, La Mar GN, Balch AL, Lecomte JT. Biochem Biophys Res Commun. 1986; 135:309–315. [PubMed: 3954774]
30. Chatfield MJ, La Mar GN, Lecomte JTJ, Balch AL, Smith KM, Langry KC. J Am Chem Soc. 1986; 108:7108–7110.
31. Timkovich R, Vavra MR. Biochemistry. 1985; 24:5189–5196. [PubMed: 4074688]
32. Berzofsky JA, Peisach J, Alben JO. J Biol Chem. 1972; 247:3774–3782. [PubMed: 5033389]
33. Berzofsky JA, Peisach J, Blumberg WE. J Biol Chem. 1971; 246:7366–7372. [PubMed: 4331435]
34. Chatfield MJ, La Mar GN, Kauten RJ. Biochemistry. 1987; 26:6939–6950. [PubMed: 3427054]
35. Carrico RJ, Blumberg WE, Peisach J. J Biol Chem. 1978; 253:7212–7215. [PubMed: 29895]
36. Park CM, Nagel RL, Blumberg WE, Peisach J, Magliozzo RS. J Biol Chem. 1986; 261:8805–8810. [PubMed: 3722175]
37. Harangi M, Matyus J, Nagy E, Nagy E, Paragh G, Balla J, Olah AV. Clin Toxicol (Phila). 2007; 45:189–192. [PubMed: 17364641]
38. Noor M, Beutler E. West J Med. 1998; 169:386–389. [PubMed: 9866446]

NIH-PA Author Manuscript

NIH-PA Author Manuscript

NIH-PA Author Manuscript

39. Tangerman A, Bongaerts G, Agbeko R, Semmekrot B, Severijnen R. J Clin Pathol. 2002; 55:631–633. [PubMed: 12147663]
40. Baranoski GV, Chen TF, Kimmel BW, Miranda E, Yim D. J Biomed Opt. 2012; 17:97005. [PubMed: 22975680]
41. Gopalachar AS, Bowie VL, Bharadwaj P. Ann Pharmacother. 2005; 39:1128–1130. [PubMed: 15886294]
42. Romero FJ, Ordonez I, Arduini A, Cadenas E. J Biol Chem. 1992; 267:1680–1688. [PubMed: 1309791]
43. Nakamura S, Nakamura M, Yamazaki I, Morrison M. J Biol Chem. 1984; 259:7080–7085. [PubMed: 6725282]
44. Berzofsky JA, Peisach J, Horecker BL. J Biol Chem. 1972; 247:3783–3791. [PubMed: 5033390]
45. Libardi SH, Pindstrup H, Cardoso DR, Skibsted LH. J Agric Food Chem. 2013
46. Morell DB, Chang Y, Clezy PS. Biochim Biophys Acta. 1967; 136:121–130. [PubMed: 6032032]
47. Chatfield MJ, La Mar GN, Smith KM, Leung HK, Pandey RK. Biochemistry. 1988; 27:1500–1507. [PubMed: 3365403]
48. Andersson LA, Loehr TM, Lim AR, Mauk AG. J Biol Chem. 1984; 259:15340–15349. [PubMed: 6511796]
49. Evans SV, Sishta BP, Mauk AG, Brayer GD. Proc Natl Acad Sci U S A. 1994; 91:4723–4726. [PubMed: 8197124]
50. Scharberg MA, La Mar GN. J Am Chem Soc. 1993; 115:6513–6521.
51. Scharberg MA, La Mar GN. J Am Chem Soc. 1993; 115:6522–6528.
52. Chatfield MJ, La Mar GN, Balch AL, Smith KM, Parish DW, LePage TJ. FEBS Lett. 1986; 206:343–346. [PubMed: 3758356]
53. Jennings MJ. Am J Physiol - Cell Ph. 2013
54. Klingerman CM, Trushin N, Prokopczyk B, Haouzi P. Am J Physiol Regul Integr Comp Physiol. 2013
55. Arnhold J, Flemmig J. Arch Biochem Biophys. 2010; 500:92–106. [PubMed: 20399194]
56. Kussendrager KD, van Hooijdonk AC. Br J Nutr. 2000; 84(Suppl 1):S19–25. [PubMed: 11242442]
57. Furtmuller PG, Zederbauer M, Jantschko W, Helm J, Bogner M, Jakopitsch C, Obinger C. Arch Biochem Biophys. 2006; 445:199–213. [PubMed: 16288970]
58. Zamocky M, Jakopitsch C, Furtmuller PG, Dunand C, Obinger C. Proteins. 2008; 72:589–605. [PubMed: 18247411]
59. Stanković S, Majkić-Singh N. J Med Biochem. 2011; 30:230–236.
60. Fiedler TJ, Davey CA, Fenna RE. J Biol Chem. 2000; 275:11964–11971. [PubMed: 10766826]
61. Singh AK, Singh N, Sharma S, Singh SB, Kaur P, Bhushan A, Srinivasan A, Singh TP. J Mol Biol. 2008; 376:1060–1075. [PubMed: 18191143]
62. Battistuzzi G, Bellei M, Bortolotti CA, Sola M. Arch Biochem Biophys. 2010; 500:21–36. [PubMed: 20211593]
63. Bertini, I.; Gray, HB.; Stiefel, EI.; Valentine, JS. Biological Inorganic Chemistry. Structure and Reactivity. 1. University Science Books; United States of America: 2007.
64. Edelhoch H, Irace G, Johnson ML, Michot JL, Nunez J. J Biol Chem. 1979; 254:11822–11830. [PubMed: 91609]
65. Michot JL, Nunez J, Johnson ML, Irace G, Edelhoch H. J Biol Chem. 1979; 254:2205–2209. [PubMed: 429280]
66. Ohtaki S, Nakagawa H, Nakamura M, Yamazaki I. J Biol Chem. 1982; 257:761–766. [PubMed: 6172424]
67. Bandyopadhyay U, Bhattacharyya DK, Chatterjee R, Banerjee RK. Biochem J. 1995; 306(Pt 3): 751–757. [PubMed: 7702570]
68. Doerge DR. Arch Biochem Biophys. 1986; 244:678–685. [PubMed: 3947087]
69. Chatfield MJ, La Mar GN. Arch Biochem Biophys. 1992; 295:289–296. [PubMed: 1316736]
70. Claesson R, Granlund-Edstedt M, Persson S, Carlsson J. Infect Immun. 1989; 57:2776–2781. [PubMed: 2547720]

NIH-PA Author Manuscript

NIH-PA Author Manuscript

NIH-PA Author Manuscript

71. Laggner H, Muellner MK, Schreier S, Sturm B, Hermann M, Exner M, Gmeiner BM, Kapiotis S. Free Radic Res. 2007; 41:741–747. [PubMed: 17577734]
72. Whiteman M, Cheung NS, Zhu YZ, Chu SH, Siau JL, Wong BS, Armstrong JS, Moore PK. Biochem Biophys Res Commun. 2005; 326:794–798. [PubMed: 15607739]
73. Carballal S, Trujillo M, Cuevasanta E, Bartesaghi S, Moller MN, Folkes LK, Garcia-Bereguiain MA, Gutierrez-Merino C, Wardman P, Denicola A, Radi R, Alvarez B. Free Radic Biol Med. 2011; 50:196–205. [PubMed: 21034811]
74. Loughran NB, O'Connor B, O'Fagain C, O'Connell MJ. BMC Evol Biol. 2008; 8:101. [PubMed: 18371223]
75. Nicoletti FP, Thompson MK, Franzen S, Smulevich G. J Biol Inorg Chem. 2011; 16:611–619. [PubMed: 21298302]
76. Schroeder WA, Shelton JR, Shelton JB, Robberson B, Apell G, Fang RS, Bonaventura J. Arch Biochem Biophys. 1982; 214:397–421. [PubMed: 7082009]
77. Sumner JB, Dounce AL. Science. 1937; 85:366–367. [PubMed: 17776781]
78. Sumner JB, Gralen N. Science. 1938; 87:284. [PubMed: 17831682]
79. Michiels C, Raes M, Toussaint O, Remacle J. Free Radic Biol Med. 1994; 17:235–248. [PubMed: 7982629]
80. Purwar N, McGarry JM, Kostera J, Pacheco AA, Schmidt M. Biochemistry. 2011; 50:4491–4503. [PubMed: 21524057]
81. Brown GC. Eur J Biochem. 1995; 232:188–191. [PubMed: 7556149]
82. Chance B. J Biol Chem. 1949; 179:1299–1309. [PubMed: 18134592]
83. Keilin D, Hartree EF. Biochem J. 1945; 39:148–157. [PubMed: 16747875]
84. Margoliash E, Novogrodsky A. Biochem J. 1958; 68:468–475. [PubMed: 13522646]
85. Beers RF Jr, Sizer IW. Science. 1954; 120:32–33. [PubMed: 13168390]
86. Du Y, Liu G, Yan Y, Huang D, Luo W, Martinkova M, Man P, Shimizu T. BioMetals. 2013; 26:839–852.10.1007/s10534-013-9640-4 [PubMed: 23736976]
87. Shimahara H, Yoshida T, Shibata Y, Shimizu M, Kyogoku Y, Sakiyama F, Nakazawa T, Tate S, Ohki SY, Kato T, Moriyama H, Kishida K, Tano Y, Ohkubo T, Kobayashi Y. J Biol Chem. 2007; 282:9646–9656. [PubMed: 17202139]
88. Li S, Hong M. J Am Chem Soc. 2011; 133:1534–1544. [PubMed: 21207964]

NIH-PA Author Manuscript

NIH-PA Author Manuscript

NIH-PA Author Manuscript

Highlights

- Sulfhemoglobin has been implicated in H_2S detection and metabolism.
- The mechanistic, structural and functional aspects of sulfheme are presented.
- Formation of sulfheme requires His, hydroperoxide or compound II and H_2S.
- This cluster triggers formation of the SH•, yielding the final sulfheme product.
- This can also be applied to other heme enzymes involved in O_2 and H_2O_2 chemistry.

NIH-PA Author Manuscript
NIH-PA Author Manuscript
NIH-PA Author Manuscript

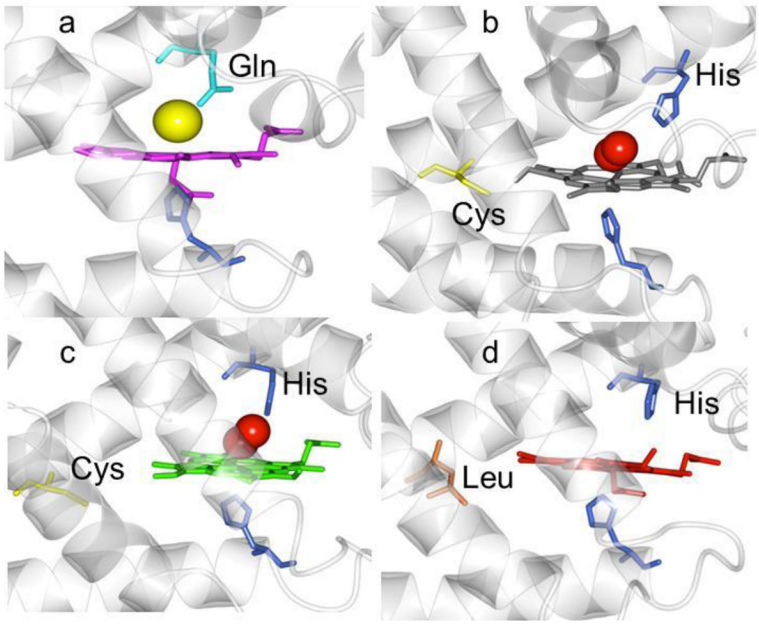

Figure 1.

Distal active site of: (a) *L. pectinata* (PDB:1MOH), (b) *R. pachyptila* (PDB: 1YHU), (c) *O. mashikoi* (PBD:2ZS0), and (d)*L. terrestris* (PDB:1X9F). In *L. pectinata*, H_2S (shown as the sphere) binds to the ferric heme iron. *R. pachyptila* and *O. mashikoi* bind H_2S in the free Cys residue and O_2 in the heme iron center shown as spheres. In *L. terrestris*, the Cys residue is replaced by Leu, and in the presence of O_2, H_2S diffuses through the protein without encountering alternative binding sites and once at the heme site, it can interact directly with heme forming the sulfheme derivative.

NIH-PA Author Manuscript

NIH-PA Author Manuscript

NIH-PA Author Manuscript

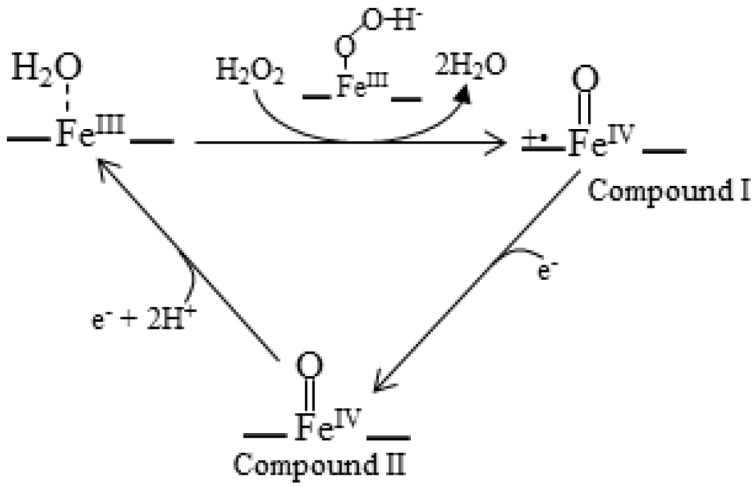

Figure 2.
Cyclic reaction of myoglobin with hydrogen peroxide.

NIH-PA Author Manuscript

NIH-PA Author Manuscript

NIH-PA Author Manuscript

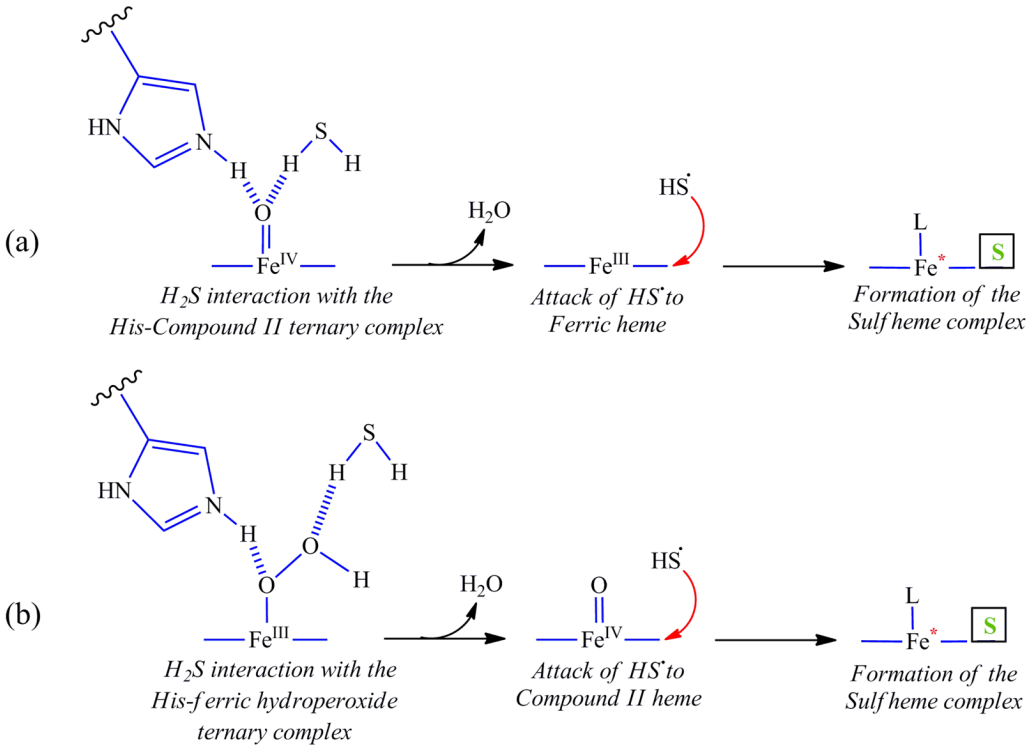

Figure 3.
Proposed mechanism for sulfheme protein formation.

NIH-PA Author Manuscript

NIH-PA Author Manuscript

NIH-PA Author Manuscript

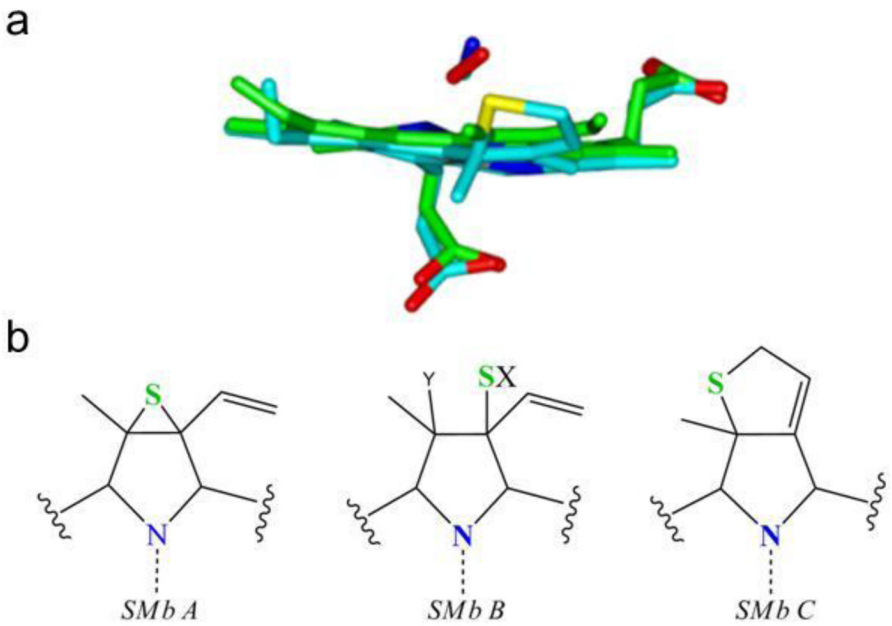

Figure 4.

Structure of: (a) Mb with bound oxygen (green, PDB: 1MBO) and after exposure of H_2S (blue, PDB: 1YMC), and (b) SulfMb isoforms. The final sulfheme product is a modified chlorin-type heme with a sulfur atom incorporated into one of the pyrrole rings. Several isoform were identified in which sulfMbA is an episulfide, while sulfMbB and sulfMbC are characterized by a ring opened episulfide and a thiochlorin, respectively.

NIH-PA Author Manuscript
NIH-PA Author Manuscript
NIH-PA Author Manuscript

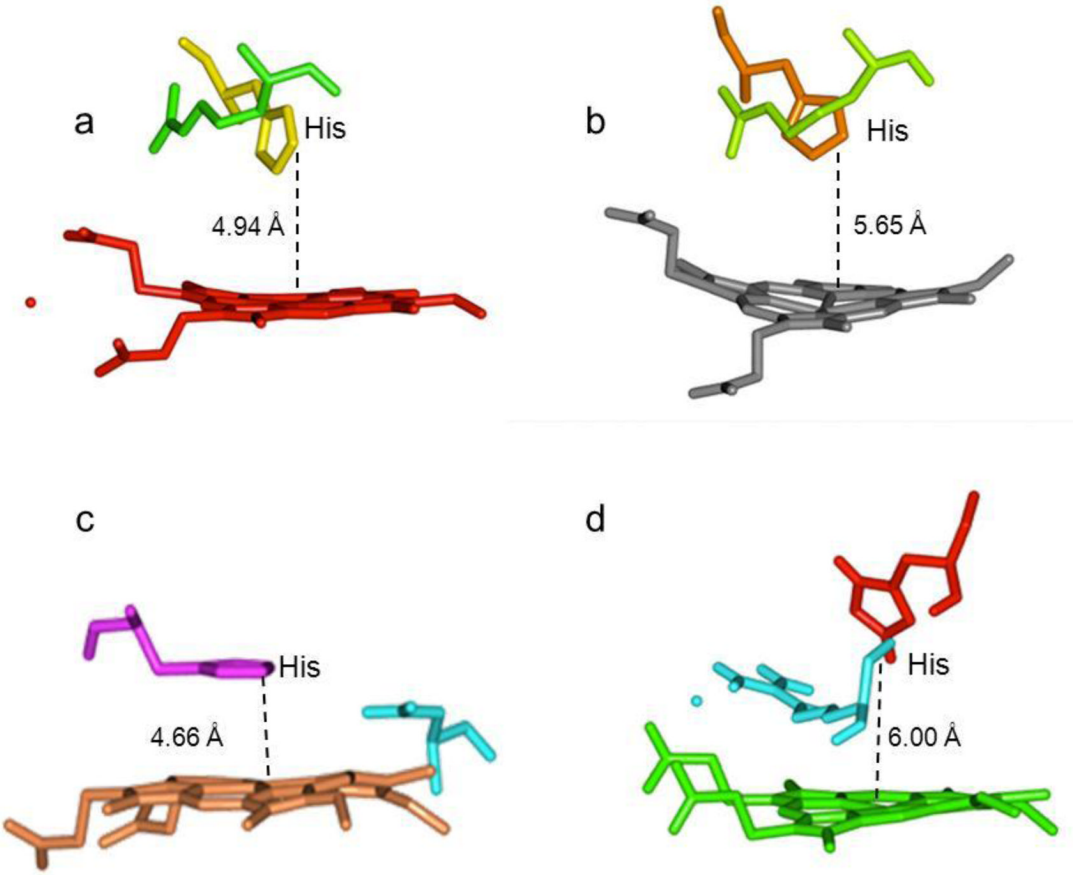

Figure 5.
Distal active site of: (a) LPO (PDB: 2NQX), (b) MPO (PDB:1CXP), (c) catalase (PDB: 3RGP) and (d) HRP (PDB:1ATJ). The structures show the distances from the iron to the NE2 of the distal His.

NIH-PA Author Manuscript
NIH-PA Author Manuscript
NIH-PA Author Manuscript

Table 1

Sulfheme formation in different hemeproteins

Protein	Key distal site residues	Sulfheme
Horse heart Mb	His	Yes (618 nm)
Human Hb	His	Yes (620 nm)
L. pectinata HbII and HbIII[a]	Gln	No
L. pectinata HbI	Gln	No
HbI Gln64Asn[b]	Asn	No
HbI Gln64His[b]	His	Yes (624 nm)
HbI Phe29His[b]	Gln	No
HbI Phe68His[b]	Gln	No
HbI Phe29Leu[b]	Gln	No
HbI Gln64Arg[b]	Arg	No
HbI Phe68Val[b]	Gln	No
Macrobdella decora Hbs[c]	His	Yes (620 nm)
Lumbricus terrestris Hbs[c]	His	Yes (620 nm)
Catalase	His	Yes (635 nm)
Lactoperoxidase	His	Yes (638 nm)
Dehaloperoxidase[d]	His	Yes (620 nm)
Horseradish peroxidase	Arg	No
Cytochrome c oxidase	His (cyt a_3)	No
Heme-O_2 sensor Ec Dos Pas	Met, Arg	No
Ec Dos Pas Met95Ala[e]	Ala	No
Ec Dos Pas Met95His[e]	His	No
Ec Dos Pas Met95Leu[e]	Leu	No
Ec Dos Pas Arg97Ala[e]	Ala	No
Ec Dos Pas Arg97Glu[e]	Glu	No
Ec Dos Pas Arg97Ile[e]	Ile	No

[a] HbII and HbIII are O_2 transport proteins found in *L. pectinata* [8].

[b] Point mutants of HbI from *L. pectinata*. The numbers represent the position of the amino acid in the polypeptide chain [17, 18].

[c] *Macrobdella decora* and *Lumbricus terrestris* are invertebrates that live is sulfide-free environments and have large Hbs that transport O_2 [18].

[d] This enzyme is found in the marine worm *Amphitrite ornate* and is believed to be involved in H_2S catabolism [75].

[e] Point mutants of the heme sensor phosphodiesterase from *Escherichia coli* (Ec DOS PAS) [86].

A.3

Sulfmyoglobin Conformational Change: A Role in the Decrease of Oxy-Mb Functionality

Biochemistry and Biophysics Reports 7 (2016) 386–393

Contents lists available at ScienceDirect

Biochemistry and Biophysics Reports

journal homepage: www.elsevier.com/locate/bbrep

Sulfmyoglobin conformational change: A role in the decrease of oxy-myoglobin functionality

Elddie Román-Morales, Erika López-Alfonzo, Ruth Pietri, Juan López-Garriga *

Department of Chemistry, University of Puerto Rico, Mayagüez Campus, PO BOX 9019, Mayagüez, Puerto Rico 00681-9019

ARTICLE INFO

Article history:
Received 25 January 2016
Received in revised form
28 June 2016
Accepted 1 July 2016
Available online 7 July 2016

Keywords:
Sulfmyoglobin (SMb)
Myoglobin (Mb)
Hemoglobin I (HbI)
Hydrogen sulfide (H_2S)
SAXS
WAXS

ABSTRACT

This work is focused at understanding the interaction of H_2S with Myoglobin (Mb), in particular the Sulfmyoglobin (SMb) product, whose physiological role is controversial and not well understood. The scattering curves, Guinier, Kratky, Porod and *P(r)* plots were analyzed for oxy-Mb and oxy-Hemoglobin I (oxyHbI) in the absence and presence of H_2S, using Small and Wide Angle X-ray Scattering (SAXS/WAXS) technique. Three dimensional models were also generated from the SAXS/WAXS data. The results show that SMb formation, produced by oxyMb and H_2S interaction, induces a change in the protein conformation where its envelope has a very small cleft and the protein is more flexible, less rigid and compact. Based on the direct relationship between Mb's structural conformation and its functionality, we suggest that the conformational change observed upon SMb formation plays a contribution to the protein decrease in O_2 affinity and, therefore, on its functionality.

© 2016 The Authors. Published by Elsevier B.V. This is an open access article under the CC BY-NC-ND license (http://creativecommons.org/licenses/by-nc-nd/4.0/).

1. Introduction

Hydrogen Sulfide (H_2S) is a gas with a "rotten egg" like smell produced in different systems in nature and industrial processes [1,2]. Through the years, H_2S was known as a toxic gas that disrupts the respiratory process by inhibition of the cytochrome c oxidase (CcO) [1–5]. It also forms sulfhemoglobinemia, a rare blood condition with anemic/cyanotic symptoms, induced by the increase concentration of Sulfmyoglobin (SMb) and Sulfhemoglobin (SHb) complexes [5–9]. However, another side of the H_2S molecule arose when it was discovered that there were three proteins [cysthathionine β-synthase (CBS), cysthathionine γ-lyase (CSE), and 3-mercaptopyruvate sulfur transferase (MST)] that produced H_2S physiologically and were present in different parts of the human body [1–5]. Different cytoprotective roles have been associated to H_2S in the respiratory, vascular, nervous, endocrine and gastrointestinal systems [1–5]. For this reason, H_2S has been evaluated as a potential therapeutic tool for the treatment of multiple diseases [10,11]. Nevertheless, the concept of H_2S therapy should be treated with caution since there is a thin line between its cytoprotective and cytotoxic aspects defined by concentration. The H_2S physiological concentration has been suggested to be low, ranging from nM to μM [1–3]. When a person is exposed to high H_2S concentration, there is an increase in physiological H_2S concentration that leads to the cytotoxic effects dominating over cytoprotective [2]. This is important when developing an efficient therapeutic tool, where the beneficial effects are maximized and the harmful effects minimized. The process for developing a resourceful H_2S therapy requires a better understanding of the chemistry of H_2S with different systems, in particular, protein interaction with this molecule.

Our research is focused at understanding one of the products of the interaction of H_2S with hemeproteins, in particular the sulfheme proteins (SMb and SHb), whose physiological role is controversial and not well understood. When myoglobin (Mb) and hemoglobin (Hb) are exposed to H_2S in the presence of oxygen (O_2) or hydrogen peroxide (H_2O_2), a sulfur atom incorporates across the β-β double bond of the pyrrole B, as shown in Fig. 1 [7,8]. This sulfur ring formation can be identified by its characteristic absorption bands around 620 or 715 nm, depending on the bound-ligand and oxidation state of the heme-iron [7]. Resonance Raman is another tool for the recognition of the sulfheme complex formation by evaluation of the vinyl modes bands (1620 and 1026 cm^{-1}) and the satellites bands around υ_4 [7,8]. Moreover, the presence of a properly oriented distal His residue is crucial for the sulfheme complex formation. This was determined by analyzing the H_2S reactive Hemoglobin I (HbI) from the clam *Lucina pectinata* that interestingly does not form the sulfheme complex, given that it lacks of a distal His residue [7,8]. When the sulfheme complex forms, Mb decreases its O_2 affinity by approximately 2500 folds. This significant decrease in O_2 affinity was

* Corresponding author.
E-mail address: juan.lopez16@upr.edu (J. López-Garriga).

http://dx.doi.org/10.1016/j.bbrep.2016.07.002
2405-5808/© 2016 The Authors. Published by Elsevier B.V. This is an open access article under the CC BY-NC-ND license (http://creativecommons.org/licenses/by-nc-nd/4.0/).

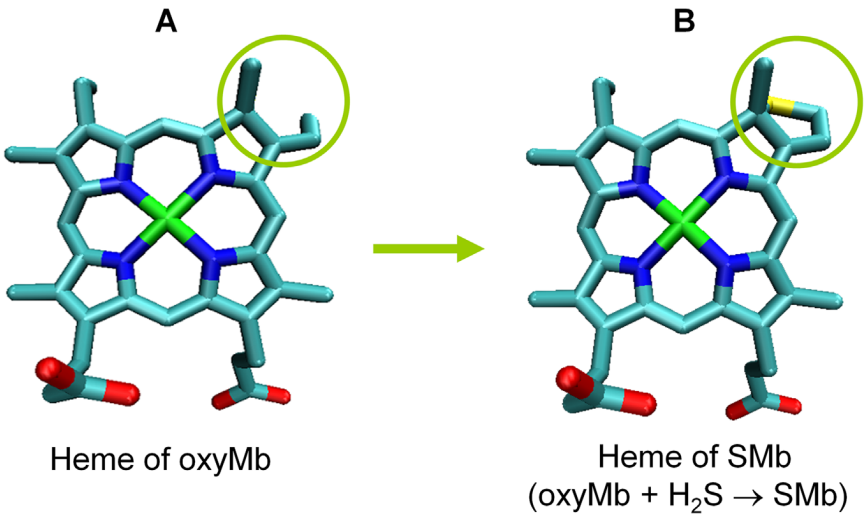

Fig. 1. Sulfmyoglobin (SMb) Structure. Myoglobin (A, left) and SMb isomer C (B, right); PDB files 1MBO (Mb) and 1YMC (SMb).

determined by comparing the 50% oxygenation values in the oxygen binding curve of Mb and SMb (0.79 and 0.00028 atm, respectively) [12]. Berzofsky et al. determined the local chemical change that plays a part in the decrease of the protein functionality. They evaluated the bond strength of the heme Fe-ligand of Mb and SMb by IR studies. A 10 cm^{-1} red-shift was observed in the IR spectra of the SMb complex, representative of a decrease in electron density, bond order and strength of the heme-ligand interaction. They attributed this to the electron withdrawing effect of the sulfur atom in the heme macrocycle, resulting in a decrease in electron density of the Fe. As a consequence, the heme-Fe^{II} acquired a character of heme-Fe^{III}; thus, weakening the Fe-ligand bond since the metal-ligand π contribution is compromised. This is also favored by the rupture of the heme group conjugation produced by the heme distortion, as result of the sulfur ring incorporation [12,13]. Moreover, Berzofsky et al. suggested that a 0.5 cm^{-1} shift corresponds to a decrease in O_2 affinity by a factor of 10, which indicates that this local chemical structural change contributes to only a 200 fold decrease in O_2 affinity [12], representing only 8% of the total decrease in affinity (2500 folds) determined by the oxygen binding curve. Therefore, there are other significant changes occurring in the protein as a consequence of the sulfheme complex formation that also contribute to the decrease in protein functionality.

2. Material and methods

2.1. Sample preparation

Myoglobin (Mb) from equine heart was purchased from Sigma-Aldrich. Recombinant HbI (rHbI) was prepared and purified as previously reported [23] and used as control. Both proteins were dissolved in a 100 mM Succinic Acid, 100 mM Potassium dihydrogen phosphate, and 1 mM EDTA buffer, 6.5 pH (all purchased in Sigma-Aldrich). The oxy-derivatives were prepared by adding [1:15] concentration ratio of [protein: sodium dithionite] under anaerobic conditions followed by O_2 purging [4]. The H_2S solution was prepared by dissolving sodium sulfide (purchased in Alfa-Aesar) in the previously mention anaerobic buffer. The sulfheme complex formation was monitored through its characteristic 620 nm band by UV–vis spectroscopy using an Agilent 8453 spectrophotometer [8]. The sulfheme complex was acquired by adding H_2S to the oxyMb complex in a [1:70] concentration ratio of [oxyMb: H_2S] that provides the highest intensity and stability of the 620 nm characteristic band.

2.2. SAXS/WAXS data acquisition and processing

SAXS/WAXS data were recorded on oxyMb and oxyHbI in the absence and presence of H_2S. The 620 nm band was monitored before and after data acquisition for both proteins. The band was only detected in oxyMb after addition of H_2S since oxyHbI does not form the sulfheme derivative. The 100 mM succinic acid, 100 mM potassium dihydrogen phosphate, and 1 mM EDTA buffer was used as a background. In the absence of H_2S, the scattering data of oxyMb were first collected at 5, 6, 10, and 11 mg/mL. The optimal protein concentration was found to be 11 mg/mL and the scattering data in the presence of H_2S were therefore collected at this concentration. For HbI the final protein concentration was 6.7 mg/mL. The SAXS/WAXS data was collected simultaneously at the X-9 Beamline of the National Synchrotron Light Source at Brookhaven National Laboratory using a PILATUS 300k SAXS detector and a Photonic Science CCD WAXS detector [24]. For triplicated data acquisition, 20 μL of sample was continuously flowed through a 1-mm diameter capillary where it was exposed to the x-ray beam for 30 s. Initial data processing was performed using the pyXS-v2 software package developed at X9. The program converted the two-dimensional scattering patterns recorded on the SAXS/WAXS detectors into one-dimensional scattering profiles. Three scattering patterns of each sample were obtained, averaged, and buffer (background) subtracted. Further SAXS/WAXS data processing and analysis were performed using 2.5.2 ATSAS Package [25,26]. Guinier, Kratky and Porod [20] analyses were conducted using Primus [27] The pair distribution functions were evaluated using GNOM [28]. 3-D surfaces were generated using DAMMIN [29], averaged using DAMAVER [30], and superimposed using SUPCOMB [31]. The theoretical scattering profiles of oxyMb and SMb atomic models were evaluated using CRYSOL [32]. Pymol was used for graphical visualization and figure generation.

3. Results and discussion

Characterization of oxyMb and oxyHbI with and without H_2S was conducted using their overall dimensions and shapes, as well as their internal structural features derived from SAXS and WAXS scattering data, respectively.

3.1. Scattering curve and Guinier plot

In SAXS/WAXS, the intensity of the scattered X-ray beam is

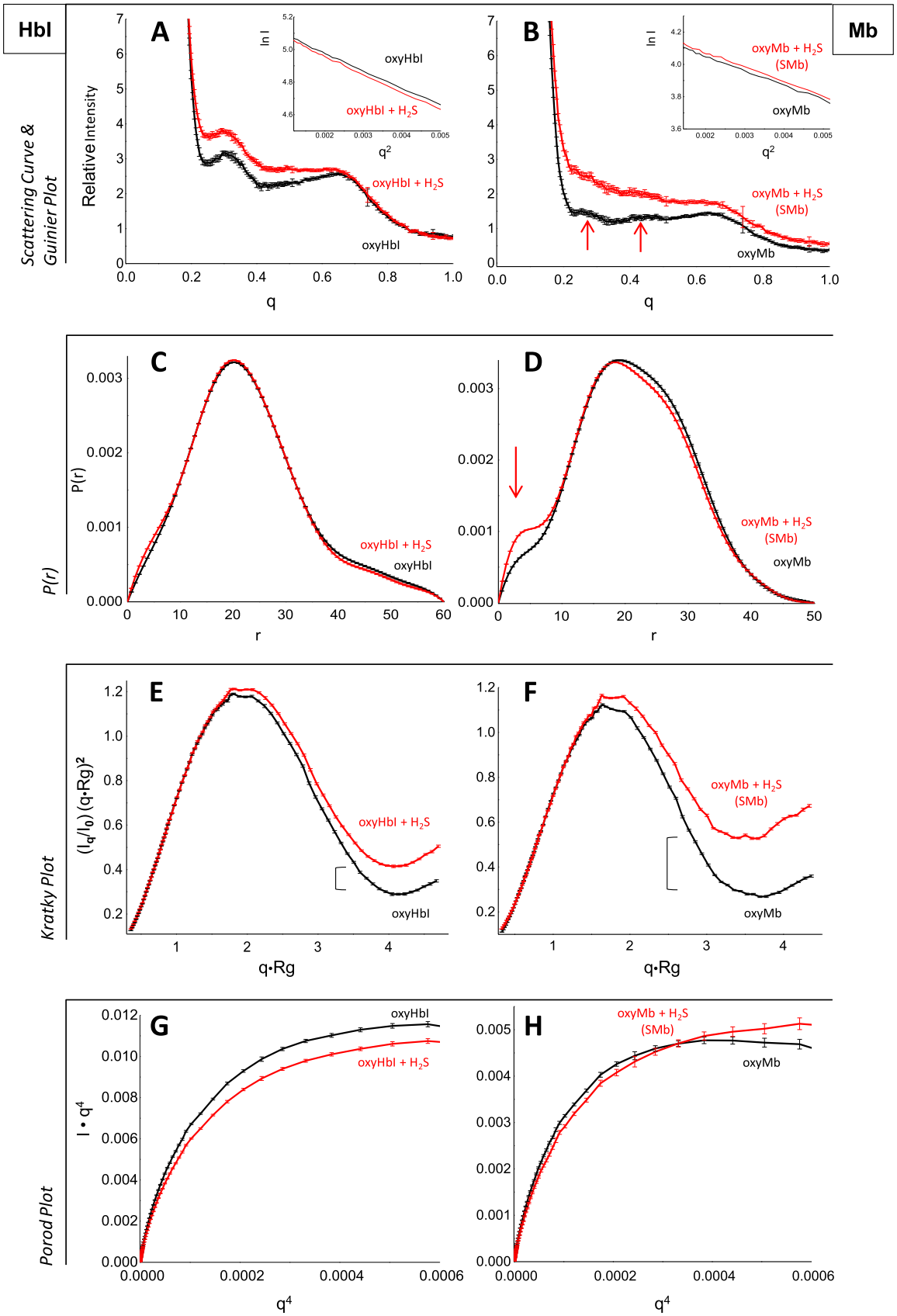

Fig. 2. SAXS and WAXS analysis. Left panel is oxyHbI in the absence (black line) and presence of H_2S (red line). Right panel is oxyMb (black line) and SMb (red line, product of oxyMb and H_2S interaction). A and B; SAXS/WAXS scattering curves (showing q range of 0.19–1.0 $Å^{-1}$), with their corresponding Guinier Plot (inset; q range =0.030–0.072 $Å^{-1}$ for HbI and 0.038–0.072 $Å^{-1}$ for Mb). C and D; *P(r)* plots normalized to *I(0)* (q range =0.024–0.442 $Å^{-1}$ for oxyHbI, 0.039–0.44 $Å^{-1}$ for oxyHbI in the presence of H_2S, 0.025–0.5 $Å^{-1}$ for oxyMb and 0.036–0.05 $Å^{-1}$ for SMb). E and F; Dimensionless *Kratky* plots (q range =0.02–0.26 $Å^{-1}$). G and H; *Porod* plots (q range =0.02–0.16 $Å^{-1}$). (For interpretation of the references to color in this figure legend, the reader is referred to the web version of this article.)

measured as a function of the momentum transfer vector q, ($q=4\pi sin\theta)/\lambda$), where θ is the scattering angle and λ is the beam wavelength [19,26]. The transfer vector q is inversely related to the real space distance between scattering centers d within the particle ($q = 2\pi/d$) [19,26]. Thus, the low q region in the scattering pattern ($\sim$0.01–0.05 Å^{-1}) represents vectors of length $\sim$600–100 Å and differences in the intensity within this region would reflect changes in the overall shape of the molecule. Conversely, at higher q, the length space distance d between centers become smaller and changes in this region suggest fluctuations in internal structural features [18,22]. Overall, it can be generalized that an increase in protein fluctuations or mobility is illustrated by a decrease in the definition or sharpness of peaks, in the high q region of the scattering curve of the protein [18,22,33,34].

Fig. 2A shows the scattering curves ($I(q)$ vs q) of the oxyHbI complex in the absence (black line) and presence of H_2S (red line). The HbI scattering curves maintain the same scattering central maxima in the presence or absence of H_2S. This indicates that the overall shape and internal structure of the protein remain unchanged in the presence of H_2S. Fig. 2B illustrates the scattering curves of oxyMb (black line) in the presence of H_2S, which leads to the formation of the SMb complex (red line). In addition to an evident increase in protein mobility and fluctuations characterized by a decrease in peak definition and sharpness, a noticeable fading of the scattering peaks at $\sim$0.27 and 0.43 Å^{-1} was observed upon SMb complex formation. When comparing the scattering curves of Mb and HbI after addition of H_2S, the scattering pattern with the greatest degree of change is that observed for Mb (e.g. q region at 0.27–0.43 Å^{-1}) as a result of SMb complex formation. It is important to mention that oxyHbI reacts with H_2S to form ferric hemoglobin sulfide in which H_2S coordinates to the ferric heme iron (Fe^{III}-H_2S) most probably by nucleophilic displacement of the bound superoxide [35]. In contrast, reaction of oxyMb with H_2S modifies the heme active center (Fig. 1) producing SMb [7,8]. Thus, the data indicate that H_2S binding to the ferric heme in oxyHbI does not induces significant global and internal structural changes, while modification of the heme macrocycle in oxyMb produces internal structural fluctuations. Overall, SMb shows greater variation of structural conformational changes upon interaction with H_2S, as evidence by the loss of scattering peaks. The structural distances that were present in oxyMb (represented by the scattering peaks at 0.27 and 0.43 Å^{-1}or d space of $\sim$23–15 Å) are no longer the most abundant as a consequence of the structural conformational change associated to the SMb complex. Interestingly, time resolved X-ray scattering data on MbCO showed that the disappearance of the peaks in these regions was due to tertiary structural relaxation, specifically to displacement of the E and F helices [36]. It is therefore plausible that SMb induce changes in these helices as well.

One parameter that can be determined directly from the SAXS data in the low q region ($\sim$0.01–0.05 Å^{-1}) is the radius of gyration or R_g, using the Guinier approximation [19,26]. The R_g is the root mean square distance of an object from its center of mass and provides a measure of the overall size of the protein. According to the Guinier approximation, at very small q ($q < 1.3/R_g$) a plot of ln $I(q)$ versus q^2 should be linear for a globular protein (Eq. (1)). From the slope of the linear fit one can determine the R_g and hence the overall size of the protein. In addition, deviations from linearity in the Guinier plots indicate aggregation [19,26]. The insets in Fig. 2A and B show the Guinier plots for oxyHbI and oxyMb in the absence and presence of H_2S. The linearity of the Guinier plots of both proteins with and without H_2S indicates no detectable aggregation. As shown in Table 1, the R_g of oxyHbI was determined to be $\sim$18.0 Å and no change in this value was detected after exposure of H_2S. Similarly, the R_g of oxyMb and SMb were determined to be 16.8 and 16.7 Å, respectively, indicating similar overall sizes [19].

Table 1
Structural parameters determined by Guinier approximation and indirect Fourier transformation of SAXS/WAXS data.

Protein	R_g (Guinier) (Å)	R_g (Gnom) (Å)	D_{max} (Å)
oxyHbI	17.90 ($\pm$0.06)	18.16 ($\pm$0.04)	60
oxyHbI + H_2S	18.10 ($\pm$0.66)	17.81 ($\pm$0.05)	60
oxyMb	16.80 ($\pm$0.13)	16.32 ($\pm$0.04)	50
SMb (oxyMb + H_2S)	16.70 ($\pm$0.38)	15.98 ($\pm$0.02)	50

$$I(q) = I(0)exp(-1/3R_g^2q^2) \quad (1)$$

3.2. Pair distribution function, P(r)

The shapes and maximum dimensions (D_{max}) of proteins can also be determined directly from their SAXS/WAXS scattering data. Indirect Fourier transformation of the scattering data $I(q)$ yields a pair distribution function $P(r)$, which is a histogram of distances between pairs of elements within the entire volume of the scattering protein (Eq. (2)) [19,26]. In general, the $P(r)$ function is a real space representation of the scattering data and provides an approximation of the shape and dimension of a protein in solution. For example, globular proteins have a symmetric bell-shaped $P(r)$, whereas unfolded particles have an extended tail. In addition, multi-domain proteins often yield $P(r)$ with multiple shoulders and oscillations corresponding to intra an inter-subunit distances [19,26].

$$P(r) = \frac{r^2}{2\pi^2}\int_0^\infty q^2 I(q)\frac{sinqr}{qr}dq \quad (2)$$

Fig. 2C shows the $P(r)$ plots of oxyHbI in the absence (black line) and presence of H_2S (red line). The contours of the $P(r)$ plots are characteristic of a globular protein with somewhat elongated sphere envelope [19]. There is no significant change in the $P(r)$ plot of oxyHbI after the protein has interacted with H_2S, indicating that the presence of H_2S does not alter significantly the envelope or structural conformation of HbI. Fig. 2D shows the $P(r)$ plots of oxyMb (black line) and SMb, formed after interaction of oxyMb with H_2S (red line). Interestingly, the Mb conformation upon SMb complex formation shows a new $P(r)$ contour with two distinct peaks. This is characteristic of two predominant regions within the overall globular conformation, as observed for calmodulin and thrombin-like enzymes [21,37]. Thus, the data suggest that SMb induces internal structural fluctuations, generating two distinctive regions within the overall dimension of the protein [21,37–39] without inducing a significant change in the overall protein dimension (D_{max}) [38,40]. Similar $P(r)$ profiles have been reported for *Rhinodrilus alatus* and *Glossoscolex paulistus* hemoglobins at basic pH and in the presences of urea respectively. The authors associated the two peaks to unfold and flexible forms of the proteins [41,42]. In addition, $P(r)$ plots displaying two peaks in their contours have been suggested for proteins with U-shape or two-domain envelopes [19,21,37]. In this case, it is more likely that the Mb envelope acquires a very small degree of a U-shape or cleft in its global shape upon SMb complex formation. The suggested increase in fluctuation or flexibility observed in the $P(r)$ plot can be profoundly evaluated using Kratky and Porod plots.

3.3. Kratky and Porod plots

SAXS/WAXS data is also commonly used to identify protein flexibility. Proteins that vary in flexibility and conformation can be recognized from the scattering data using the Kratky and Porod plots defined by the following equation [20]:

$$V_p = 2\pi^2 I(0)/Q \quad Q = \int_0^\infty q^2 I(q) dq \tag{3}$$

V_p is the hydrated particle volume (e.g. protein) and Q is the Porod invariant, a direct measurement of the density contrast [20]. According to the Kratky analysis, a plot of $q^2I(q)$ vs q should display a bell-shape with a clear maximum for compact globular proteins. Proteins with dual structure (compact and flexible regions) will show at low q a maximum that resembles the order region within the ensemble and at higher q a "tail" that represents the disordered or flexible region [19,20,40,43,44]. With increasing protein flexibility, the "tail" segment of the Kratky plot will raise, indicating an increase in disordered/flexible structure within the protein conformation. For example, a completely unfolded protein will exhibit a plateau "tail" [40,43,45]. On the other hand, the Porod approximation states that a plot of $q^4I(q)$ vs q^4 should display crescent-hyperbolic tendency arriving to a plateau as q increases for compact globular proteins. The loss of plateau suggests an increase in protein flexibility [20,40]. Overall, Kratky and Porod plots are employed to qualitatively assess the relationship between flexibility and protein volume. Proteins that posses a dual structure with compact and flexible regions within their structural domain can be identified using both approximations [20,40].

Fig. 2E shows the Kratky plots of oxyHbI in the absence (black line) and presence of H_2S (red line). A bell-like shape was observed, demonstrating a compact globular protein with some flexibility represented by a "tail" at higher q. The tail rises a little when HbI is in the presence of H_2S, implying an increase in protein flexibility produced by H_2S. Fig. 2F shows the Kratky plots of oxyMb (black line) and SMb formed by the interaction of oxyMb with H_2S (red line). It also shows a bell-shape with a "tail", indicating a compact globular protein with some flexibility. However, SMb formation clearly produces a "tail" that rises even more. This suggests that the SMb complex induces a greater change in the protein structural conformation where a significant increase in packing flexibility in acquired.

Fig. 2G shows the Porod plots of oxyHbI in the absence (black line) and presence of H_2S (red line). The plots demonstrate the classical hyperbolic shape curve arriving to a plateau as q increases, before and after H_2S exposure, indicating no significant change in protein flexibility. Fig. 2H shows the Porod plots of oxyMb (black line) and SMb formed by the interaction of oxyMb with H_2S (red line). OxyMb demonstrates a classical hyperbolic shape curve arriving to a plateau as q increases, characteristic of a globular, compact, and rigid conformation. Interestingly, once the SMb complex is formed, a loss in the plateau is observed representative of a gain in conformational flexibility that is not observed in HbI upon H_2S exposure. This change in protein structural conformation, specifically induced by the SMb formation, is different from the structural change induced by ligand migration towards the protein active site, given that: (1) before H_2S exposure, the protein was in a O_2 saturated environment where structural changes associated to ligand migration through the protein had already occurred and (2) both proteins had the same H_2S exposure. Regarding this, the distinction in the Kratky and Porod plot's of both proteins, when expose to H_2S, is due to the SMb formation since HbI does not form the sulfheme complex [7,8].

Overall, the scattering curves of SMb showed that the peaks at $q > 0.2$ are practically unresolved, indicating an increase in protein fluctuations and mobility as a consequence of SMb complex formation. The two peaks in the SMb $P(r)$ plot demonstrated changes in internal structural conformation, suggesting formation of a small cleft on the protein envelope with a two distinctive flexible

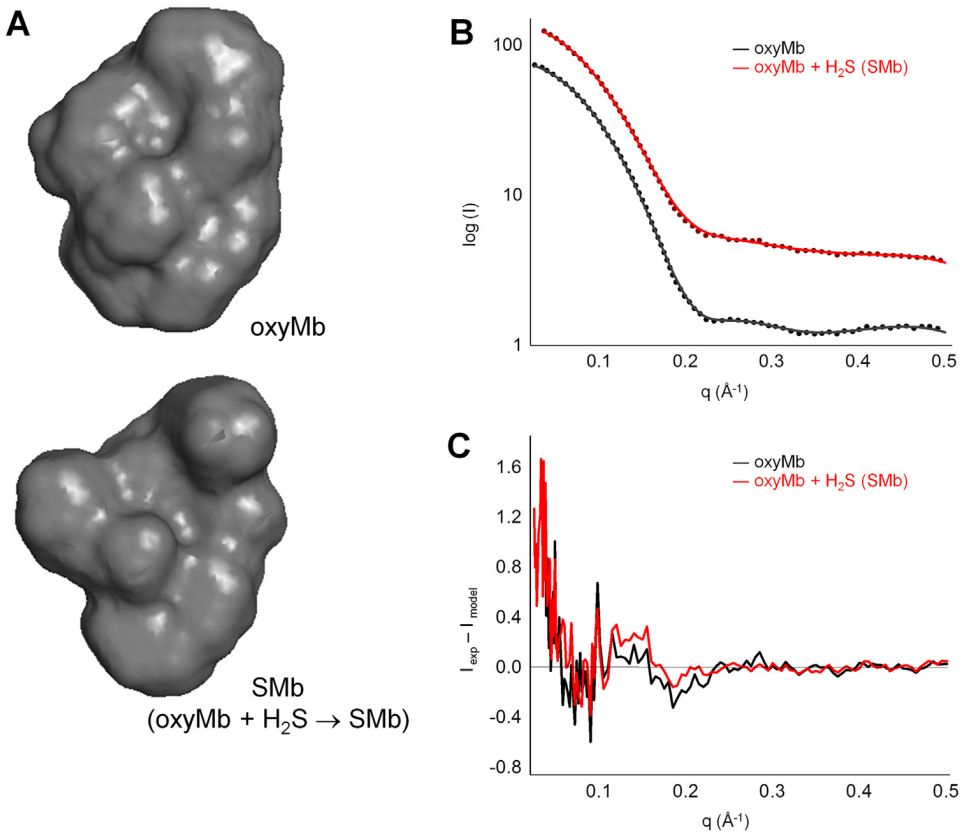

Fig. 3. SAXS/WAXS three dimensional models. A; SAXS/WAXS three-dimensional surfaces of oxyMb (top-left) and SMb (bottom-left). B; Comparison of the experimental SAXS/WAXS data of oxyMb (black-dotted lines) and SMb (red-dotted lines) with the corresponding calculated scattering curves of their theoretical models (solid lines). The q range used for the theoretical models was the same as those used in the $P(r)$ function. The curves were offset for better appraisal (oxyMb has $x^2 = 0.8$ and $R^2 = 0.99984$; SMb has $x^2 = 2.2$ and $R^2 = 0.99975$). C; Residual plots of the experimental minus the calculated scattering curves of oxyMb (black line) and SMb (red line) theoretical models.

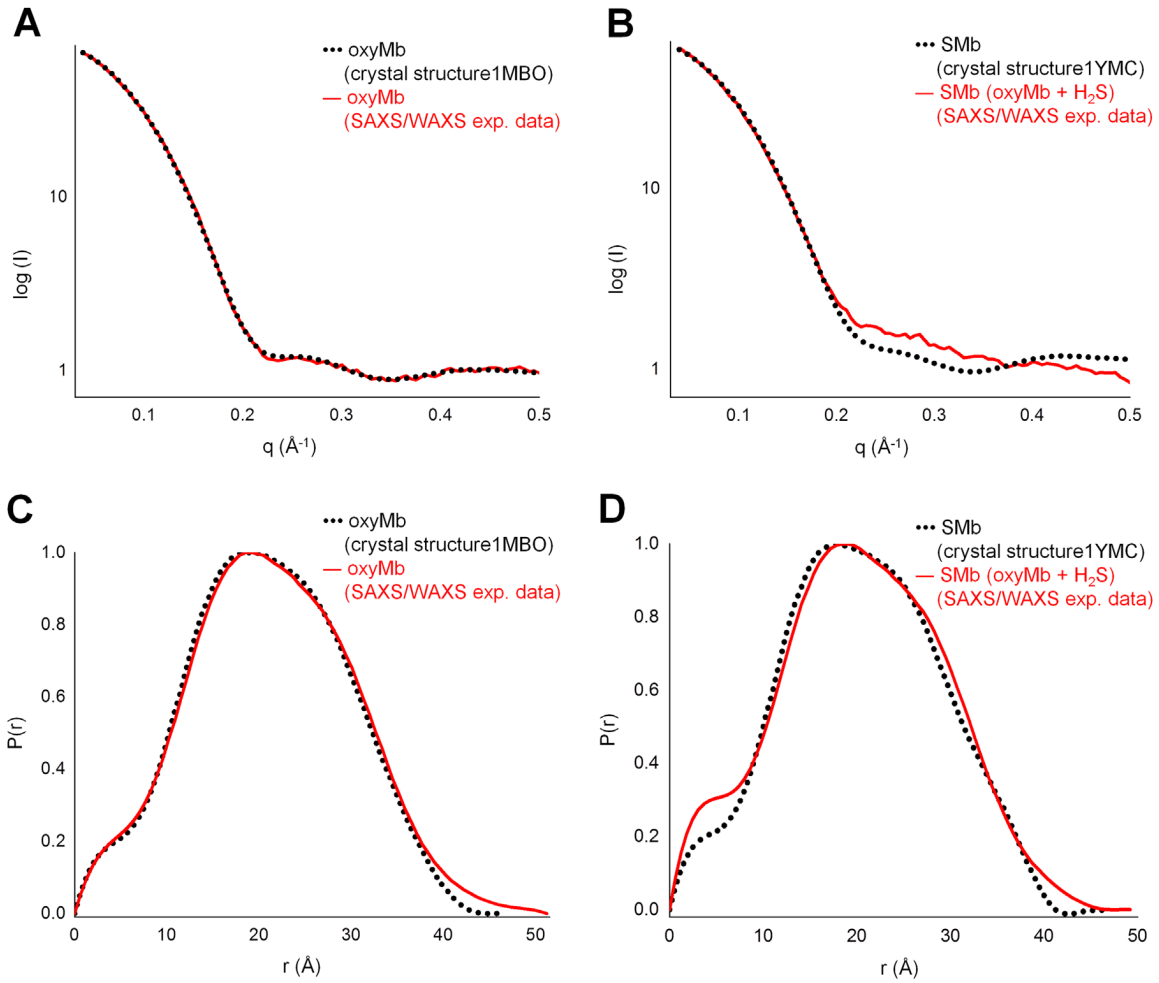

Fig. 4. Comparison of the SAXS/WAXS and crystallographic data. Left panel is oxyMb from the SAXS/WAXS experimental data (red-line) and crystal structure (black-dotted line), PDB file 1MBO. Right panel is SMb from the SAXS/WAXS experimental data (red-line) and crystal structure (black-dotted line), PDB file 1 YMC. A and B; Scattering curves. C and D; The corresponding P(r) plots.

regions. The Kratky and Porod plots supports increase in flexibility, decrease in rigidity and compactness.

3.4. Three dimensional models and scattering from high resolution models

To acquire a visual perspective of the global surface features of SMb conformational effect, three-dimensional surfaces from SAXS/WAXS scattering data were produced for oxyMb and SMb. The three-dimensional scattering surfaces of the proteins were generated using the Dummy Atom Model Minimization method [29]. The algorithm represents a protein as a collection of dummy atoms in a constrained volume with a maximum diameter defined experimentally by D_{max}. It employs simulated annealing to generate the three-dimensional surface, and it calculates the scattering curve of the surface to evaluate its discrepancy (χ^2) with the experimental data (Eq. (4)) [19].

$$\chi^2 = \frac{1}{N-1}\sum_{i=1}^{N}\left(\frac{I_{exp}(q_i) - cI_{calc}(q_i)}{\sigma(q_i)}\right)^2 \quad (4)$$

Here $I_{exp}(q)$ and $I_{calc}(q)$ are the experimental and computed profiles, respectively, $\sigma(q)$ is the experimental error of the measured profile, N is the number of points in the profile, and c is the scaling factor.

Fig. 3A shows the surfaces of oxyMb and SMb, formed by the interaction of oxyMb with H_2S. The surfaces demonstrated general globular structures and reveal differences in their shapes, where the SMb envelope has a small cleft with two distinct regions. As shown in Fig. 3B, the scattering curves of the three-dimensional surfaces fit the experimental data well, yielding χ^2 values of 0.8 and 2.1 for oxyMb and SMb, respectively. This was also confirmed by the residual analysis of the experimental and calculated scattering curves (Fig. 3C), yielding R^2 values of 0.9998 and 0.9997 for oxyMb and SMb, respectively.

This local change was not observed in the SMb crystallographic structure probably due to the protein constriction that can occur during the process of crystal formation, which does not take place in SAX/WAXS since it is in solution. To corroborate this interpretation, the theoretical scattering curves of oxyMb and SMb atomic models (PDB ID:1MBO and 1YMC, respectively) were obtained using CRYSOL software [32]. The program uses multipole expansion for fast calculation of spherically averaged scattering profile and takes into account the hydration shell. It also compares the theoretical scattering curve with the SAXS/WAXS experimental data by fitting the curves and minimizing the discrepancy. The theoretical scattering curves obtained from the PDB structures were further analyzed to calculate the corresponding theoretical *P (r)* functions. In general, an atomic model that provides a good fit to the data is considered a valid description of the structure in solution.

As Fig. 4A shows, the theoretical scattering curve of oxyMb

atomic model fits the SAXS/WAXS experimental data well, implying similarities of both crystal and solution structures. The corresponding *P(r)* functions support the above suggestion (Fig. 4C). However Fig. 4B demonstrates that the theoretical scattering curve of SMb crystal structure poorly correlates with the scattering data of SMb in solution, indicating that the atomic model does not describe well the protein in solution. In fact, the peak at ~4 Å is not so well defined in the theoretical *P(r)* function of SMb atomic model, as shown in Fig. 4D, suggesting that the internal structural fluctuations are hampered by crystal packing forces, which limit the range of conformational motion accessible to the protein.

3.5. Conclusion and further outlooks

Taken together, the data suggest that SMb complex induces a conformational change increasing protein flexibility and fluctuations with decreasing rigidity. This change is specific of SMb and different from conformational change produce by ligand migration or heme Fe-ligand binding. Regarding this, the Mb's Xe cavities have been demonstrated to play a crucial role in the protein functionality by regulating ligand entry and release from the active site [14–16]. The ligand migration in the cavity produces a structural expansion of the cavity itself follow-on by gating motions of the surrounding residues that leads to a self opening of the migrating channel [16]. The cavity comes back to its original volume once the ligand has left the cavity, mimicking a breathing motion [16,17]. The final channel is created by the rotating motion of the distal His opening the gate toward the active heme site [16]. Any change in the size and shape of these pockets directly affects the Mb function, which results in significant physiological effects [14–16]. Olson et al. [15] demonstrated that a decrease in the size of the cavity produced a more rigid and compact packing. As a result, it lowers the rate of ligand capture by making it difficult for the ligand to arrive to the active site. However, if the ligand is able to arrive to the active site, dissociation is even more difficult since the ligand is "trapped" in the active site, leading to an overall increase in O_2 affinity [15]. Upon SMb formation, the opposite is observed, a decrease in O_2 affinity. On this basis, we propose that the observed changes in conformation and increase in protein flexibility play a role in the decrease in O_2 affinity by SMb, in addition to the reported local structural change on the heme. These structural changes would facilitate ligand entry but destabilize even more ligand bonding, leading to an overall decrease in O_2 affinity.

Furthermore, in addition to the heme-Fe ligand transport, it has been suggested that the conformational cavities are capable of carrying additional ligands, such as NO, giving Mb higher carrying capacity than (1:1) stoichiometry and further physiological roles (e.g. scavenger) [14–17,46]. In this study we demonstrated that the inner structure of Mb is altered by the formation of SMb by increasing protein flexibility, movement, and fluctuation. On this basis, considering the constant ligand competition and the increase in protein flexibility of SMb, enhancement of H_2S entry and O_2 displacement may be possible. This could lead to a plausible H_2S transports flux, in addition to the known rapid diffusive flux of free H_2S.

The nature of the proteins should be further studied, given that, it is intriguing that a protein whose functionality is H_2S transport does not suffer a significant conformational change while a protein whose "main functionality" is O_2 storage and transport suffers significant conformational change, when exposed to H_2S. Furthermore, it opens the door to explore the conformation change associated with the reaction of oxy-Hemoglobin with H_2S, which only shows a decrease in O_2 affinity of 135 folds [47], suggesting that cooperativity may play an important role in protecting oxy-Hemoglobin functionality.

Acknowledgment

This work was supported in part by funds from the NSF (Grant 0843608), and fellowships from NIH-RISE2Best (Grant R25GM088023), and Alfred P. Sloan (NACME Grant 2010-3-02). We thank Dr. Lisa Miller, Mr. Vito Graziano, and Dr. Mark Allaire for the X9-SAXS/WAXS facilities at NSLS.

This research used resources of beamline X9 of the National Synchrotron Light Source, a U.S. Department of Energy (DOE) Office of Science User Facility operated for the DOE Office of Science by Brookhaven National Laboratory under Contract No. DE-AC02-98CH10886.

Appendix A. Transparency document

Supplementary data associated with this article can be found in the online version at http://dx.doi.org/10.1016/j.bbrep.2016.07.002.

References

[1] A. di Masi, P. Ascenzi, H2S: a "double face" molecule in health and disease, BioFactors 39 (2) (2013) 186–196.
[2] K.R. Olson, K.D. Straub, The role of hydrogen sulfide in evolution and the evolution of hydrogen sulfide in metabolism and signaling, Physiology 31 (1) (2016) 60–72.
[3] L. Li, P.K. Moore, Putative biological roles of hydrogen sulfide in health and disease: a breath of not so fresh air? Trends Pharmacol. Sci. 29 (2) (2008) 84–90.
[4] R. Pietri, A. Lewis, R.G. Leon, G. Casabona, L. Kiger, S.R. Yeh, S. Fernandez-Alberti, M.C. Marden, C.L. Cadilla, J. Lopez-Garriga, Factors controlling the reactivity of hydrogen sulfide with hemeproteins, Biochemistry 48 (22) (2009) 4881–4894.
[5] R. Pietri, E. Roman-Morales, J. Lopez-Garriga, Hydrogen sulfide and hemeproteins: knowledge and mysteries, Antioxid. Redox Signal. 15 (2) (2011) 393–404.
[6] K. Murphy, C. Ryan, E.M. Dempsey, P.W. O'Toole, R.P. Ross, C. Stanton, C. A. Ryan, Neonatal sulfhemoglobinemia and hemolytic anemia associated with intestinal *Morganella morganii*, Pediatrics 136 (6) (2015) e1641–e1645.
[7] B.B. Rios-Gonzalez, E.M. Roman-Morales, R. Pietri, J. Lopez-Garriga, Hydrogen sulfide activation in hemeproteins: the sulfheme scenario, J. Inorg. Biochem. 133 (2014) 78–86.
[8] E. Roman-Morales, R. Pietri, B. Ramos-Santana, S.N. Vinogradov, A. Lewis-Ballester, J. Lopez-Garriga, Structural determinants for the formation of sulfhemeprotein complexes, Biochem. Biophys. Res. Commun. 400 (4) (2010) 489–492.
[9] M. Noor, E. Beutler, Acquired sulfhemoglobinemia. An underreported diagnosis? West. J. Med. 169 (6) (1998) 386–389.
[10] D. Wu, Q. Hu, Y. Zhu, Therapeutic application of hydrogen sulfide donors: the potential and challenges, Frontiers of Medicine, 2015.
[11] Y. Zheng, X. Ji, K. Ji, B. Wang, Hydrogen sulfide prodrugs-a review, Acta Pharm. Sin. B 5 (5) (2015) 367–377.
[12] J.A. Berzofsky, J. Peisach, W.E. Blumberg, Sulfheme proteins. II. The reversible oxygenation of ferrous sulfmyoglobin, J. Biol. Chem. 246 (23) (1971) 7366–7372.
[13] J.A. Berzofsky, J. Peisach, J.O. Alben, Sulfheme proteins. 3. Carboxysulfmyoglobin: the relation between electron withdrawal from iron and ligand binding, J. Biol. Chem. 247 (12) (1972) 3774–3782.
[14] M. Brunori, D. Bourgeois, B. Vallone, The structural dynamics of myoglobin, J. Struct. Biol. 147 (3) (2004) 223–234.
[15] J.S. Olson, J. Soman, G.N. Phillips Jr, Ligand pathways in myoglobin: a review of Trp cavity mutations, IUBMB Life 59 (8–9) (2007) 552–562.
[16] A. Tomita, U. Kreutzer, S. Adachi, S.Y. Koshihara, T. Jue, 'It's hollow': the function of pores within myoglobin, J. Exp. Biol. 213 (Pt 16) (2010) 2748–2754.
[17] A. Tomita, T. Sato, K. Ichiyanagi, S. Nozawa, H. Ichikawa, M. Chollet, F. Kawai, S. Y. Park, T. Tsuduki, T. Yamato, et al., Visualizing breathing motion of internal cavities in concert with ligand migration in myoglobin, Proc. Natl. Acad. Sci. USA 106 (8) (2009) 2612–2616.
[18] R.F. Fischetti, D.J. Rodi, D.B. Gore, L. Makowski, Wide-angle X-ray solution scattering as a probe of ligand-induced conformational changes in proteins, Chem. Biol. 11 (10) (2004) 1431–1443.
[19] H.D. Mertens, D.I. Svergun, Structural characterization of proteins and complexes using small-angle X-ray solution scattering, J. Struct. Biol. 172 (1) (2010) 128–141.
[20] R.P. Rambo, J.A. Tainer, Characterizing flexible and intrinsically unstructured biological macromolecules by SAS using the Porod-Debye law, Biopolymers 95 (8) (2011) 559–571.
[21] H.L. Guedes, F.P. Silva Jr., C.C. Netto, C.M. de Salles, G. Alexandre, C.L. Oliveira,

I. Torriani, S.G. De Simone, Structural characterization and low-resolution model of BJ-48, a thrombin-like enzyme from *Bothrops jararacussu* venom, Biophys. Chem. 132 (2–3) (2008) 159–164.
[22] L. Makowski, J. Bardhan, D. Gore, J. Lal, S. Mandava, S. Park, D.J. Rodi, N.T. Ho, C. Ho, R.F. Fischetti, WAXS studies of the structural diversity of hemoglobin in solution, J. Mol. Biol. 408 (5) (2011) 909–921.
[23] R.G. Leon, H. Munier-Lehmann, O. Barzu, V. Baudin-Creuza, R. Pietri, J. Lopez-Garriga, C.L. Cadilla, High-level production of recombinant sulfide-reactive hemoglobin I from Lucina pectinata in Escherichia coli. High yields of fully functional holoprotein synthesis in the BLi5 *E. coli* strain, Protein Expr. Purif. 38 (2) (2004) 184–195.
[24] M. Allaire, L. Yang, Biomolecular solution x-ray scattering at the National Synchrotron Light Source, J. Synchrotron Radiat. 18 (2011) 41–44.
[25] M. Petoukhov, D. Franke, A. Shkumatov, G. Tria, A. Kikhney, M. Gajda, C. Gorba, H.D.T. Mertens, P.V. Konarev, D.I. Svergun, New developments in the ATSAS program package for small-angle scattering data analysis, J. Appl. Crystallogr. 45 (2012) 342–350.
[26] R. Pietri, S. Zerbs, D.M. Corgliano, M. Allaire, F.R. Collart, L.M. Miller, Biophysical and structural characterization of a sequence-diverse set of solute-binding proteins for aromatic compounds, J. Biol. Chem. 287 (28) (2012) 23748–23756.
[27] P.V. Konarev, V.V. Sokolova, M.H.J. Koch, D.I. Svergun, A. PRIMUS, Windows PC-based system for angle scattering drug analysis, J. Appl. Crystallogr. 36 (2003) 1277–1282.
[28] D.I. Svergun, Determination of the regularization parameter in indirect-transform methods using perceptual criteria, J. Appl. Crystallogr. 25 (1992) 495–503.
[29] D.I. Svergun, Restoring low resolution structure of biological macromolecules from solution scattering using simulated annealing, Biophys. J. 76 (1999) 2879–2886.
[30] V.V. Volkov, D.I. Svergun, Uniqueness of ab initio shape determination in small angle x-ray scattering, J. Appl. Crystallogr. 36 (2003) 860–864.
[31] M.B. Kozin, D.I. Svergun, Automated matching of high and low resolution structural models, J. Appl. Crystallogr. 34 (2001) 33–41.
[32] D.I. Svergun, C. Barberato, M.H.J. Koch, CRYSOL-A program to evaluate x-ray solution scattering of biological macromolecules from atomic coordinates, J. Appl. Crystallogr. 28 (1995) 768–773.
[33] L. Makowski, D. Gore, S. Mandava, D. Minh, S. Park, D.J. Rodi, R.F. Fischetti, X-ray solution scattering studies of the structural diversity intrinsic to protein ensembles, Biopolymers 95 (8) (2011) 531–542.
[34] L. Makowski, D.J. Rodi, S. Mandava, D.D. Minh, D.B. Gore, R.F. Fischetti, Molecular crowding inhibits intramolecular breathing motions in proteins, J. Mol. Biol. 375 (2) (2008) 529–546.
[35] D.W. Kraus, J.B. Wittenberg, Hemoglobins of the Lucina pectinata/bacteria symbiosis. I. Molecular properties, kinetics and equilibria of reactions with ligands, J. Biol. Chem. 265 (27) (1990) 16043–16053.
[36] H.S. Cho, N. Dashdorj, F. Schotte, T. Graber, R. Henning, P. Anfinrud, Protein structural dynamics in solution unveiled via 100-ps time-resolved x-ray scattering, Proc. Natl. Acad. Sci. USA 107 (16) (2010) 7281–7286.
[37] J.K. Krueger, G.A. Olah, S.E. Rokop, G. Zhi, J.T. Stull, J. Trewhella, Structures of calmodulin and a functional myosin light chain kinase in the activated complex: a neutron scattering study, Biochemistry 36 (20) (1997) 6017–6023.
[38] R. Kitahara, K. Hata, A. Maeno, K. Akasaka, M.S. Chimenti, E.B. Garcia-Moreno, M.A. Schroer, C. Jeworrek, M. Tolan, R. Winter, et al., Structural plasticity of staphylococcal nuclease probed by perturbation with pressure and pH, Proteins 79 (4) (2011) 1293–1305.
[39] D. Neves, L.F. Estrozi, V. Job, F. Gabel, G. Schoehn, A. Dessen, Conformational states of a bacterial alpha2-macroglobulin resemble those of human complement C3, PloS One 7 (4) (2012) e35384.
[40] M. Hammel, Validation of macromolecular flexibility in solution by small-angle X-ray scattering (SAXS), Eur. Biophys. J.: EBJ 41 (10) (2012) 789–799.
[41] F.A. Carvalho, J.W. Carvalho, P.S. Santiago, M. Tabak, Urea-induced unfolding of Glossoscolex paulistus hemoglobin, in oxy- and cyanomet-forms: a dissociation model, Int. J. Biol. Macromol. 52 (2013) 340–348.
[42] J.W. Carvalho, F.A. Carvalho, P.S. Santiago, M. Tabak, Thermal stability of extracellular hemoglobin of Rhinodrilus alatus (HbRa): DLS and SAXS studies, European Biophysics Journal, EBJ, 2016.
[43] M. Kozlowska, A. Tarczewska, M. Jakob, K. Szpotkowski, M. Wojtas, G. Rymarczyk, A. Ozyhar, Calponin-like Chd64 is partly disordered, PloS One 9 (5) (2014) e96809.
[44] T. Yokouchi, Y. Izumi, T. Matsufuji, Y. Jinbo, H. Yoshino, Unfolding intermediate of a multidomain protein, calmodulin, in urea as revealed by small-angle X-ray scattering, FEBS Lett. 551 (1–3) (2003) 119–122.
[45] T. Uzawa, S. Akiyama, T. Kimura, S. Takahashi, K. Ishimori, I. Morishima, T. Fujisawa, Collapse and search dynamics of apomyoglobin folding revealed by submillisecond observations of alpha-helical content and compactness, Proc. Natl. Acad. Sci. USA 101 (5) (2004) 1171–1176.
[46] M. Brunori, Myoglobin strikes back, Protien Sci. 19 (2) (2010) 195–201.
[47] R.J. Carrico, W.E. Blumberg, J. Peisach, The reversible binding of oxygen to sulfhemoglobin, J. Biol. Chem. 253 (20) (1978) 7212–7215.